

XL CBRAVIC

**Brazilian Congress on Vacuum Applications
in Industry and Science**

Book of Extended Abstracts

edited by

Mauricio Antonio Algatti

and

Konstantin Georgiev Kostov

UNESP - Guaratinguetá, SP, Brazil
October 07-10, 2019

XL CBrAVIC

**Brazilian Congress on Vacuum Applications
in Industry and Science**

Realização:



Organização:



Apoio:



Patrocínio:





Preface

This year the “CBrAVIC – The Brazilian Congress on Vacuum Applications in Industry and Science”, celebrating its 40th edition will be hold at UNESP – Guaratinguetá's Campus of São Paulo State University in Guaratinguetá city, i.e., the land of the white herons in Tupi-Guarani, the Brazilian Indian language, localized in São Paulo State, Brazil.

This initiative makes evident the maturity and dynamism of national scientific community working in different areas of knowledge like Physics, Chemistry, Engineering, Biology, Medicine and so on.


Following the tradition of CBrAVIC's previous editions, the Organizing Committee made all the efforts to congregate national and foreign researchers working in different knowledge areas in order to improve the Congress's scientific level by means of several Plenary Invited Talks by outstanding scientists presenting the state of art in different fields of Science and Technology. The Organizing Committee hopes that this effort will strongly contribute for the personal and professional improvement of all conference's attendees.

The Organizing Committee decided to improve significantly the paper's poster presentation format, considerably reducing the number of short oral communications. This decision has the objective of promoting more profitable and deep discussions among the paper authors and the interested attendees. Therefore the “Poster Sections” loses their quite marginal role into the Conference's schedule being brought to the center of all attendee's attention.

The Organizing Committee hopes that this initiative will be appreciated by all XL CBrAVIC attendees and became a tradition that certainly will valorize all the efforts and care that authors spent in preparing their posters presentations.

The Organizing Committee decided to promote the “Best Paper Awards” in undergraduate and graduate levels for papers with student's authorship. The first author of the best poster will receive a money award and will have back the congress subscription fee as well as the other paper's authors. The authors of the papers ranked in 2nd to 5th will also receive the congress's subscription fee back. This initiative has the objective of enhancing the undergraduate and graduate student's participation.

The Organizing Committee hopes that all the congress's attendees have a profitable participation in XL CBrAVIC and enjoy their stay at this nice city and appreciate so much the Guaratingueta's people hospitality !

<p>Prof. Dr. Konstantin G. Kostov <i>Co-Chair of the Organizing Committee</i></p>	<p> Prof. Dr. Mauricio A. Algatti <i>Co-Chair of the Organizing Committee</i></p>	<p>Prof. Dr. Álvaro J. Damião <i>President of SBV</i></p>
--	--	---

A título de prefácio

Este ano o “CBrAVIC – Congresso Brasileiro de Aplicações de Vácuo na Indústria e na Ciência”, comemora sua quadragésima edição, nas dependências da UNESP - Universidade Estadual Paulista, Campus de Guaratinguetá entre os dias 07 a 10 de outubro de 2019.


Esta iniciativa evidencia a maturidade e o dinamismo da Comunidade Científica Nacional engajada nas diferentes áreas do conhecimento tais como Física, Química, Engenharia, Biologia, Medicina, etc.

Seguindo a tradição das edições anteriores, o Comitê Organizador procurou congregar pesquisadores Nacionais e Internacionais de diferentes áreas do conhecimento, objetivando o engrandecimento do evento através de Palestras Convidadas, da escolha de uma temática de ponta em Ciência e Tecnologia que viesse contribuir de forma significativa para o enriquecimento pessoal e profissional de todos os participantes.

O Comitê Organizador decidiu valorizar sobremaneira os trabalhos na forma de Pôster, reduzindo significativamente o número de apresentações orais de trabalhos. Esta decisão tem por finalidade resgatar a possibilidade de uma discussão mais profícua e aprofundada entre o apresentador e o congressista interessado. Desta feita, as “Seções de Pôsteres” deixa de ser algo praticamente “*marginal*” no Programa do Evento e passa a disputar em pé de igualdade o centro das atenções de todos os Congressistas.

O Comitê Organizador espera que esta iniciativa seja apreciada pelos participantes do XL CBrAVIC e que a mesma se torne uma tradição, fazendo jus ao esforço e capricho que todos os participantes tiveram na elaboração da apresentação de seus trabalhos. O Comitê Organizador decidiu ainda promover uma competição entre os trabalhos completos submetidos, cujo primeiro autor seja orientado de Doutorado ou Mestrado ou Iniciação Científica. O primeiro colocado em cada categoria receberá um prêmio em dinheiro e os cinco primeiros colocados, em cada categoria, terão a taxa de inscrição devolvida. Tal iniciativa tem por objetivo incentivar a participação maciça dos estudantes no Congresso.

Para finalizar, desejamos que todos os congressistas tenham uma profícua participação do *XL CBrAVIC* aproveitando a oportunidade para conhecer as belezas naturais de Guaratinguetá e cercanias bem como desfrutar da hospitalidade dos habitantes desta encantadora cidade.

<p>Prof. Dr. Konstantin G. Kostov <i>Co-Chair of the Organizing Committee</i></p>	<p> Prof. Dr. Mauricio A. Algatti <i>Co-Chair of the Organizing Committee</i></p>	<p>Prof. Dr. Álvaro J. Damião <i>President of SBV</i></p>
---	---	---

Os temas principais a serem discutidos no XL CBrAVIC são:

1. Vacuum Technology & Application
2. Materials Science and Technology
3. Plasma Science and Technology
4. Surfaces, Interfaces and Thin Films
5. Instrumentation and Metrology
6. Biomaterials
7. Treatment and Surface Modification
8. Nanoscience, Nanotechnology and Nanomaterials
9. Sensors and Devices

PALESTRANTES CONVIDADOS (Invited Speakers)

Invited Plenary Speakers:

1. **Prof. Dr. Thomas von Woedtke** - Plasma Medicine Program Manager - Leibniz Institute for Plasma Science and Technology - INP-Greifswald, Germany
2. **Prof. Dr. Holger Kersten** - Institute of Experimental and Applied Physics, University of Kiel, Germany
3. **Prof. Dr. Francesco Fracassi** - Department of Chemistry - University of Bari Aldo Moro, Bari, Italy

4. **Prof. Dr. Pietro Favia** - Department of Biosciences, Biotechnologies and Biopharmaceutics, University of Bari “Aldo Moro”, Italy
5. **Prof. Dr. Peter Bruggeman** - Department of Mechanical Engineering, University of Minnesota Twin Cities MN, USA
6. **Prof. Dr. Hiroshi Daimon** - President of the Japan Society of Vacuum and Surface Science, Professor at Nara Institute of Science and Technology, Ikoma, Japan
7. **Prof. Dr. Joseph E. Greene** - D. B. Willett Professor of Materials Science and Physics, University of Illinois, IL, USA
8. **Prof. Dr. Mario Ueda** - Plasma Associated Laboratory, National Institute for Space Research - INPE, São José dos Campos, SP, Brazil
9. **Prof. Dr. Carlos Roberto Grandini** - Institute of Biomaterials, Tribocorrosion and Nanomedicine - Brazilian Branch IBTN-Br Campus in Bauru, State University of São Paulo - UNESP Bauru, SP, Brazil

Invited Oral Presentations:

1. **Prof. Dr. Alexandre Zirpoli Simões** - Engineering Faculty - FEG, State University of São Paulo - UNESP, Campus de Guaratinguetá, SP, Brazil
2. **Profa. Dra. Cristiane Yumi Koga-Ito** Institute of Science and Technology - ICT State University of São Paulo - UNESP São José dos Campos, SP, Brazil
3. **Dr. Ruediger Hink** - Leibniz Institute for Plasma Science and Technology, INP - Greifswald, Germany
4. **Dra. Thalita Nishime** - Leibniz Institute for Plasma Science and Technology, INP-Greifswald, Germany

COMITÊ ORGANIZADOR (Organizing Committee):

Konstantin Georgiev Kostov – Co-Chair – UNESP-Guaratinguetá

Mauricio Antonio Algatti – Co-Chair – UNESP-Guaratinguetá

Rogério Pinto Mota – UNESP-Guaratinguetá

Milton Eiji Kayama – UNESP-Guaratinguetá

Carlos Roberto Grandini – UNESP-Bauru

Carlos Alberto Fonzar Pintão – UNESP-Bauru

Álvaro José Damião – IEAv-CTA-São José dos Campos

Pedro Augusto de Paula Nascente – UFSCar-São Carlos

Nazir Monteiro dos Santos – UNILA – Foz do Iguaçu

Cristiane Yumi Koga-Ito – UNESP-São José dos Campos

Leide Lili Gonçalves da Silva Kostov – FATEC-Pindamonhangaba

Cesar José Bonjuani Pagan - FEEC - UNICAMP, Campinas

COMITÊ ORGANIZADOR LOCAL (Local Organizing Committee):

Konstantin Georgiev Kostov – UNESP-Guaratinguetá

Mauricio Antonio Algatti – UNESP-Guaratinguetá

Rogério Pinto Mota – UNESP-Guaratinguetá

Milton Eiji Kayama – UNESP-Guaratinguetá

Roberto Yzumi Honda – UNESP-Guaratinguetá

Mauro Hugo Mathias – UNESP-Guaratinguetá

Edson Cocchieri Botelho – UNESP-Guaratinguetá

Ana Paula Rosifini Alves - UNESP-Guaratinguetá

Luis Rogério de Oliveira Hein – UNESP-Guaratinguetá

Olívia Maria Berengue – UNESP-Guaratinguetá

Teófilo Miguel de Souza – UNESP-Guaratinguetá

Leonardo Mesquita - UNESP-Guaratinguetá

COMITÊ LOCAL ESTUDANTIL (Local Student Committee):

Alonso Hernan Ricci Castro - UNESP-Guaratinguetá

Taiana She Mui Mir - UNESP-Guaratinguetá

Felipe Kodaira - UNESP-Guaratinguetá

Pedro Willian Moreira Jr - UNESP-Guaratinguetá

Kleber Petroski - UNESP-Guaratinguetá

Herick Emante da Silva Barros - UNESP-Guaratinguetá

COMITÊ CIENTÍFICO (Scientific Committee):

Konstantin Georgiev Kostov – UNESP-Guaratinguetá

Mauricio Antonio Algatti – UNESP-Guaratinguetá

Rogério Pinto Mota – UNESP-Guaratinguetá

Carlos Roberto Grandini – UNESP-Bauru

Álvaro José Damião – IEAv-CTA-São José dos Campos

Milton Eiji Kayama – UNESP-Guaratinguetá

Cristiane Yumi Koga-Ito – UNESP-São José dos Campos

Clodomiro Alves Júnior – UFERSA – Mosoró

Deborah Cristina Ribeiro dos Santos – SBV

Gilberto Petraconi Filho – ITA – São José dos Campos

Luís César Fontana – UDESC – Joinville

Júlio César Sagás – UDESC - Joinville

José Roberto Ribeiro Bortoleto – UNESP-Sorocaba

Antonio Renato Bigansolli – UFRRJ-Seropédica

Pedro Augusto de Paula Nascente – UFSCar-São Carlos

Nazir Monteiro dos Santos– UNILA - Foz do Iguaçu

Thalita Mayumi Castaldelli Nishime - INP - Greifswald

Mário Ueda – INPE-São José dos Campos

Francisco Tadeu Degasperi– FATEC-São Paulo

Rodrigo Sávio Pessoa – ITA – São José dos Campos

Leide Lili Gonçalves da Silva Kostov – FATEC-Pindamonhangaba

Evaldo José Corat – INPE – São José dos Campos

Vladimir Jesus Trava-Airoldi – INPE – São José dos Campos

Sociedade Brasileira de Vácuo **(Brazilian Vacuum Society)**

Biênio 2017-2019
(Biennium 2017-2019)

DIRETORIA EXECUTIVA (Executive Board)

Presidente: Prof. Álvaro José Damião (IEAv-CTA-São José dos Campos)

1º Vice Presidente: Profa Dra Maria Lucia Pereira da Silva (USP/FATEC-São Paulo)

2º Vice Presidente: Prof. Dr. Francisco Tadeu Degasperi (FATEC-São Paulo)

Diretoria Científica: Prof. Dr. Carlos Roberto Grandini (UNESP-Bauru)

Diretoria Cultural: Prof. Dr. Antonio Renato Bigansolli (UFRRJ-Seropédica)

1º Secretário: Pesq. Luciano Rugério Silva (Inertsolutions)

2º Secretário: Deborah Cristina Ribeiro dos Santos (FATEC-Pindamonhangaba)

1º Tesoureiro: Prof. Dr. Marcos Massi (Universidade Mackenzie - São Paulo)

2º Tesoureiro: Profa. Dra. Nazir Monteiro dos Santos (UNILA-Foz do Iguaçu-PR)

CONSELHO DELIBERATIVO (Deliberative Council)

A) Sócios Efetivos e/ou Honorários

Prof. Dr. Rogério Pinto Mota (UNESP-Guaratinguetá)

Prof. Dr. Leonardo Cabral Gontijo (IFES -Vitória)

Prof. Dr. Argemiro Soares da Silva Sobrinho (ITA-São José dos Campos)

Prof. Dr. Luis César Fontana (UDESC -Joinville)

Prof. Dr. Jair Scarminio (UEL-Londrina)

Prof. Dr. Carlos Fonzar Pintão (UNESP-Bauru)

B) Sócios Coletivos e/ou Mantenedores

Agilent

Edwards

Avaco

Leybold

IEAv

INPE

CONSELHO FISCAL (Fiscal Council)

Prof. Dr. Pedro Augusto de Paula Nascente (UFSCar)

MSc. Angelo Luiz. Gobbi (LNNano CNPEM)

Prof. Dr. Konstantin Georgiev Kostov (UNESP)

Prof. Dr. Mário Ueda (INPE)

Prof. Dr. Alfredo Gonçalves Cunha (UFES)

PROGRAMAÇÃO DAS PALESTRAS E APRESENTAÇÃO DE PÔSTERES

CONFERENCE'S TIMETABLE

	Monday 07/10/2019	Tuesday 08/10/2019	Wednesday 09/10/2019	Thursday 10/10/2019
Time	InovEE Building	InovEE Building	InovEE Building2	InovEE Building3
8:30-9:20	Minicourses	40 Years History of CBrAVIC Alvaro Damião In Memoriam of Prof. d'Agostino Pietro Favia	Plenary talk #3 Mario Ueda	Plenary talk #6 Carlos Grandini
9:20-10:10	Minicourses	Plenary talk #1 Pietro Favia	Plenary talk #4 Thomas Von Woedtke	Plenary talk #7 Francesco Fracassi
10:10-10:40		<i>Refreshment break</i>	<i>Refreshment break</i>	<i>Refreshment break</i>
10:40-11:30	Minicourses	Plenary talk #2 Peter Bruggeman	Plenary talk #5 Hiroshi Daimon	Plenary talk #8 Holger Kersten
11:30-12:00	Minicourses	Invited talk #1 Rüdiger Hink	Invited talk #2 Cristiane Koga-Ito	Invited talk #3 Thalita Nishime
12:00-13:30		<i>Lunch</i>	<i>Lunch</i>	<i>Lunch</i>
13:30-13:55	Minicourses	Oral contribution #1 Pedro Nascente	Keynote talk	Invited talk #4 Alexandre Simões
14:00-14:25	Minicourses	Oral contribution #2 Maria Lucia	Historical Overview of Material Science and Technology	Oral contribution #5 Fellype do Nascimento
14:30-14:55	Minicourses	Oral contribution #3 Clodomiro Alves Jr	Prof. Joseph Greene	Oral contribution #6 Julio Sagas
15:00-15:30	Minicourses	Oral contribution #4 Erica Antunes		Oral contribution #7 Rodrigo Savio
15:30-16:00		<i>Refreshment break</i>	<i>Refreshment break</i>	
16:00-17:30	Registration	Poster Session #1	Poster Session #2	
17:30-18:30	Opening Ceremony		Annual Meeting of the Brazilian Vacuum Society	
18:30-22:30	Welcome Reception			
19:30-23:30	<i>Conference Dinner</i>			

IN MEMORIAN OF PROFESSOR RICCARDO D'AGOSTINO**THE CONTRIBUTION OF PROF. D'AGOSTINO TO
PLASMA SCIENCE AND TECHNOLOGY**^{1,2}Pietro Favia, ^{2,3}Francesco Fracassi

1 Department of Biosciences, Biotechnology and Biopharmaceutics, University of Bari Aldo Moro, Bari, ITALY; 2 CNR Institute of Nanotechnology NANOTEC; 3 Department of Chemistry, University of Bari Aldo Moro, Bari, ITALY

Address: via Orabona 4, 70126 Bari, ITALY; mail: pietro.favia@uniba.it

Riccardo d'Agostino, Professor Emeritus of General Chemistry at the University of Bari (Italy), left us almost one year ago, at the age of 75, after five decades (1969-2018) of a bright career mostly devoted in investigating plasma deposition, treatment and etching processes, and in developing their applications in Material Science and Technology. With Prof. d'Agostino our community loses one of its pre-eminent members, a fine scientist, a committed organizer, a passionate communicator and a true gentleman. Author of about 300 papers, reviews, chapter of books and patents, co-editor of four books [1-4], in 2004 Prof. d'Agostino founded with Prof. M. R. Wertheimer, Dr. C. Oehr, and Prof. P. Favia *Plasma Processes and Polymers* (Wiley-VCH), one of the most impacting Journal today in the field of cold plasma processes.

Beside his scientific impact in Plasma Science and Technology, the contributions of Prof. d'Agostino include also the organization of several main events in the field, including the 9th (1989 Pugnochiuso, ITA) and the 16th (2003 Taormina, ITA) International Symposia on Plasma Chemistry, a NATO ASI School (1996, Acquafredda di Maratea, ITA), and several ISPC Summer Schools on Low Temperature Plasmas. A summary of his remarkable Curriculum Vitae can be found on *Plasma Processes and Polymers* [5].

Among his several prizes, Prof. d'Agostino was particularly proud of the Plasma Chemistry Award, presented to him at the 18th international Symposium on Plasma Chemistry (2007, Kyoto, JAP) by the Board of Directors of the International Plasma Chemistry Society “*in recognition of his longtime research contributions of consistently high quality in the areas of Plasma Chemistry and Plasma Processing Science, and for his exemplary service to the scientific community*”.

This talk is intended to offer to the audience a view of the scientific contributions of Prof. d'Agostino to Plasma Science and Technology in years, mainly in the fields of diagnostics of low pressure plasma processes, of kinetics of etching, PE-CVD and grafting surface-modification plasma processes, and of plasma-synthesized surfaces for various applications.

References

- [1] Plasma Deposition, Treatment and Etching of Polymers, R. d'Agostino ed., Plasma - Materials Interactions Series, Acad. Press., **1990**.
- [2] Plasma Processing of Polymers, R. d'Agostino, P. Favia, F. Fracassi ed., Kluwer Acad. Publ., NATO ASI Series E: Applied Sciences, Vol. 346, **1997**.
- [3] Plasma Processes & Polymers, R. d'Agostino, P. Favia, M.R. Wertheimer, C. Oehr ed., Wiley-VCH, **2005**.
- [4] Advanced Plasma Technology, R. d'Agostino, P. Favia, Y. Kawai, H. Ikegami, N. Sato, F Arefi-Khonsari ed., Wiley-VCH, **2008**.
- [5] P. Favia, M. R. Wertheimer, C. Oehr, D. Hegemann, R. Foerch, R. Hagen, Professor Riccardo d'Agostino (June 17, 1942 – April 21, 2018), Founding Editor of Plasma Processes and Polymers, Plasma Proc. and Polymers 15, 1815061, **2018**.

INVITED PLENARY LECTURE 1**PLASMA PROCESSES FOR LIFE SCIENCES:
FROM BIOMATERIAL SURFACES TO BIOLOGICAL SUBSTRATES**

^{1,2}Pietro Favia, ²Fabio Palumbo, ²Roberto Gristina, ²Eloisa Sardella

¹ *Department of Biosciences, Biotechnology and Biopharmaceutics University of Bari*

² *CNR Institute of Nanotechnology NANOTEC c/o Department of Chemistry, University of Bari, Italy*

pietro.favia@uniba.it

Plasma, ionized gas matter with equal density of positive and negative charges, is considered “the fourth state of the matter”, the most common form of visible matter in the Universe. Beside stars, lightnings and *Aurora Borealis*, natural examples of thermonuclear, thermal and cold plasmas respectively, men had to wait the 19th century to create plasmas in controlled environment. Plasma Science and Technology (PST) of non equilibrium “cold” plasmas started then and continue to develop today a steadily increasing number of researches and commercial products¹. Routinely applied for surface modification processes in Microelectronics, Solar Cells, Automotive, Polymers, Composite Materials and other fields, PST is one of the most pervasive, yet still promising technologies of our time. PST impacts nowadays three large areas of Life Sciences, namely:

SURFACE ENGINEERING OF BIOMEDICAL MATERIALS Cold plasmas can modify the surface of materials at room temperature with no bulk alterations, no use of solvents, in environment friendly way. In this particular field, many possible surface modification etching (ablation), deposition and grafting processes are optimized to develop tailored surfaces with pre-determined properties onto biomaterials, scaffolds and biomedical devices, to elicit the optimal response of biological entities (proteins, cells, bacteria, fluids, tissues) in contact with them, in vitro and in vivo.²

STERILIZATION OF BIOMEDICAL DEVICES The surface decontamination of biomedical materials from biological and organic molecules, as well as their sterilization, is one of the many applications of plasmas boosted by the diffusion of Atmospheric Pressure (AP) plasma discharges. Low Pressure plasma sterilizers indeed already exist on the market. Plasma decontamination/sterilization of materials is due to the lethal effects on bacteria and spores of reactive oxidant species (e.g., O atoms, OH radicals, etc) and UV photons generated in plasmas.

PLASMA MEDICINE This term defines the emerging discipline where living tissues are directly exposed to AP cold plasmas in air, for eliciting therapeutic effects such as wound sterilization and healing, tissue regeneration, blood clotting and killing of cancer cells. AP plasmas are also experimented for sterilization of dental cavities, teeth bleaching, treatments of acne and other therapies. Plasma Medicine combines plasma physics, plasma chemistry, life sciences and clinical medicine in what is probably today the most promising field of PST³.

The aim of this talk is to introduce the audience in a tutorial way to the field of Plasma Science and Technology for Life Sciences, with a stress on the recent developments and the interdisciplinary interconnections with the field of Biomaterials.

REFERENCES

1. K-D Weltmann, J F Kolb, M Holub, D Uhrlandt, M Simek, K Ostrikov, S Hamaguchi, U Cvelbar, M Cernak, B Locke, Al Fridman, P Favia, K Becker, The future in Plasma Science and Technology, Plasma Proc. Polym. 16, e1800118, 2019
2. I Trizio, M Garzia Trulli, C Lo Porto, D Pignatelli, G Camporeale, F Palumbo, E Sardella, R Gristina, P Favia, Plasma Processes for Life Sciences, In: Reedijk, J. (Ed.) Elsevier Reference Module in Chemistry, Molecular Sciences and Chemical Engineering. (2018).
3. S Bekeschus, P Favia, E Robert, T von Woedtke, White Paper on Plasma for Medicine and Hygiene: Future in Plasma Health Sciences, Plasma Proc. Polym. 16, e1800033, 2019.

INVITED PLENARY LECTURE 2**PLASMA-LIQUID INTERACTIONS: FUNDAMENTAL STUDIES ELUCIDATING BIOMEDICAL AND ENVIRONMENTAL APPLICATIONS**

Peter Bruggeman

*University of Minnesota, Department of Mechanical Engineering
111 Church Street SE, Minneapolis, MN 55455, U.S.A.
e-mail: pbruggem@umn.edu*

Non-equilibrium atmospheric pressure plasmas interacting with water offer a unique source of highly reactive chemistry beneficial for many applications. These include analytical chemistry, environmental remediation, material processing and synthesis, chemical synthesis, sterilization, disinfection and medical applications. This contribution provides an overview of the current state-of-the-art of plasma-liquid interactions and identifies key research challenges on the road to controlling plasma-liquid interactions in applications. I will show examples of fundamental studies that illustrate the importance of short-lived species in many of these applications and introduce an experiment that enables us to obtain quantitative data on reactive species in both the plasma and liquid phase. The results highlight the importance of the strong coupling of the plasma and liquid phase at the gas-liquid interface. The possible impact of the insights obtained from these investigations will be illustrated for biomedical and environmental applications.

This work is partially supported by the "Plasma Science Center on Control of Plasma Kinetics" of the United States Department of Energy, Office of Fusion Energy Science (DE-SC0001319), a Department of Energy Early Career Research Award (DE-SC0016053) and the National Science Foundation (PHY 1500135).

INVITED PLENARY LECTURE 3**MODERATE TO HIGH TEMPERATURE (270 TO 1100°C) PIII AND PIII&D PROCESSING BY CONTROLLING THE TREATMENT PARAMETERS AND CONFIGURATIONS IN DISCHARGES INSIDE METAL TUBES**

M. Ueda¹, C. Silva^{1,2}, S.F.M. Mariano¹, N. M. Santos¹, G.B. de Souza³, L. Pichon⁴, H. Reuther⁵

¹*Associated Laboratory of Plasma, National Institute for Space Research, S.J.Campos, SP, Brazil*

²*Associated Laboratory of Sensors and Materials, National Institute for Space Research, S.J.Campos, SP, Brazil*

³*Universidade Estadual de Ponta Grossa, Ponta Grossa, PR, Brazil*

⁴*Université de Poitiers, Poitiers, France*

⁵*HZDR, Rossendorf, Dresden, Germany*

To obtain sufficiently thick treated layer in the surface of materials by Plasma Immersion Ion Implantation (PIII) and PIII&D (Deposition) techniques aiming at the surface protection of components for many scientific and industrial applications, it is necessary to heat them (the components) to adequate maximum temperatures during those treatments. In that way, normally very thin modified layer obtained by those ion implantation methods in low temperatures, of order of few dozen *nanometers*, can reach *micron* sizes, due to high thermal diffusion. As for the deposition case, either of sputtered wall material or condensable gaseous carbonaceous films (DLC and DLC-Like), the success of the treatment may depend also on the used temperature. Therefore, in order to operate PIII and PIII&D in adequate temperatures, intensive parametrization studies combined with exploration of many different configurations, dimensions and set-ups of metal tubes were carried out in our laboratory, recently. Results of those experiments will be shown and discussed in terms of the range of temperatures used, spanning from 270 to 1100 °C, depending on the type of the material of the tubes (SS304 and Ti-6Al-4V) and on the pursued applications. Parameters as used power, current, voltage, total time of treatment, pulse repetition rate, pulse length, and temperature of the treatments were varied while different tube set-ups were tested. Results of the analysis of the modified surfaces of the treated samples monitoring the process as well as of the tube inner walls will be presented in this invited talk.

INVITED PLENARY LECTURE 4**PLASMA MEDICINE: INNOVATIVE PHYSICS FOR MEDICAL APPLICATIONS**Thomas von Woedtke^{1,2}¹*Leibniz Institute for Plasma Science and Technology (INP Greifswald),
Felix-Hausdorff-Str. 2, 17489 Greifswald, Germany*²*Greifswald University Medicine, 17475 Greifswald, Germany
e-mail: woedtke@inp-greifswald.de*

Plasma medicine means the direct application of physical plasma on or in the human body for therapeutic purposes. For a direct application on living tissue, cold atmospheric pressure plasma (CAP) is used, i.e. plasma generated in atmospheric air environment with temperatures lower than 40°C at the target site during plasma treatment. During recent years, mainly two basic concepts of CAP devices were tested and partially applied for medical purposes: dielectric barrier discharges (DBD) and plasma jets [1]. Because CAP chemistry is dominated by nitrogen and oxygen chemistry, biological plasma effects that are potentially useful for medical applications are mainly based on reactive (redox-active) oxygen and nitrogen species (ROS, RNS) [2,3].

Based on both the very effective inactivation of a broad spectrum of microorganisms by CAP and its ability to stimulate tissue regeneration, main focus of clinical application is in the field of wound healing, yet. For this field of application, a few CAP sources are CE-certified as medical devices now opening up the possibility of broad clinical use of CAP. Besides wound healing, several other indications for plasma application in dermatology are taken into consideration, mainly in treatment of pathogen-based and/or inflammatory skin irritations and diseases. Also in ophthalmology anti-infective plasma applications were tested. Several plasma applications in dentistry are under research for several years, too. Finally, because CAP is able to induce programmed cell death (apoptosis) also in cancer cells, plasma application for cancer treatment is now an important research field [4].

To consolidate medical plasma application and to open up further medical fields, a more in-depth knowledge of control and adaptation of plasma parameters and plasma geometries is needed to get suitable and reliable plasma sources for the different therapeutic requirements [5].

REFERENCES

- [1]- Th. von Woedtke, S. Reuter, K. Masur, K.-D. Weltmann. Plasmas for medicine. Phys. Rep. 530 (2013) 291-320
- [2]- D.B. Graves. The emerging role of reactive oxygen and nitrogen species in redox biology and some implications for plasma applications to medicine and biology. J. Phys. D: Appl. Phys. 45 (2012) 263001
- [3]- D.B. Graves. Oxy-nitroso shielding burst model of cold atmospheric plasma therapeutics. Clin. Plasma Med. 2 (2014) 38-49
- [4]- H.-R. Metelmann, Th. von Woedtke, K.-D. Weltmann (Eds.). Comprehensive Clinical Plasma Medicine. Cold Plasma for Medical Application. Springer International Publishing AG, part of Springer Nature 2018, 526 p.
- [5]- K.-D. Weltmann, Th. von Woedtke. Plasma Medicine – current state of research and medical application. Plasma Phys. Control. Fusion 59 (2017) 014031

INVITED PLENARY LECTURE 5**Atomic-resolution holographies to reveal structure around active functional atoms**

Hiroshi Daimon

Toyota Physical and Chemical Research Institute, 41-1, Yokomichi, Nagakute, Aichi 480-1192, Japan

3D local atomic structure around specific active-site atom plays crucial role in functional materials such as high temperature ferromagnetic semiconductors or superconductors. The 3D atomic structure around this kind of local specific atom, however, has not been able to be analyzed by a standard structure analysis method of x-ray diffraction (XRD) because this kind of active site has no translational symmetry. Recently several atomic-resolution holographies have been developed to investigate the 3D atomic structure around this kind of specific atoms with no translational symmetry. One method is the photoelectron holography, where the obtained angular distribution pattern includes the interference between the direct photoelectron wave and the scattered waves from surrounding atoms. Because the phase difference information between the direct wave and the scattered waves are recorded, the diffraction pattern is considered as a hologram [1], and the real-space atomic arrangement is easily obtained directly.

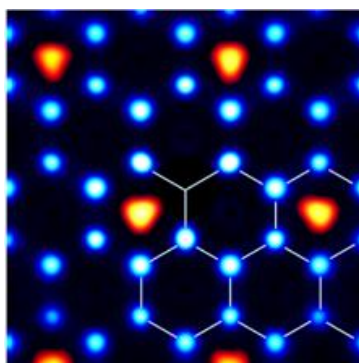


Fig. 1 Exemple of photoelectron holography [2]

Fig. 1 shows the reconstructed structure for K doped graphite intercalation superconductor [2]. A similar technique which uses fluorescent x-ray is called “x-ray fluorescence holography” [3]. Recently their accuracy improved dramatically by the development of new analysis code [4] and a sensitive detector [5]. A new technique of direct 3D atomic structure analysis method “stereography of atomic arrangement” has also been developed [6]. These techniques received renewed attention recently. Hence we started a project of “3D active-site science” [7] in order to open a new field of local 3D active-site science. The target materials in this project are ranging from inorganic materials to bio-materials. Recent results of dopant As in Si [8] and others are presented.

References

- [1] A. Szöke: AIP Conference Proceedings, No.147, AIP New York 1986.
- [2] F. Matsui, R. Eguchi, S. Nishiyama, M. Izumi, E. Uesugi, H. Goto, T. Matsushita, K. Sugita, H. Daimon, Y. Hamamoto, I. Hamada, Y. Morikawa, Y. Kubozono, Scientific Re-ports 6, 36258 (2016).
- [3] M. Tegze, G. Faigel: Europhys. Lett. 16, 41 (1991).
- [4] T. Matsushita, A. Yoshigoe, and A. Agui: Europhys. Lett. 71, 597 (2005).
- [5] K. Hayashi, N. Happo, S. Hosokawa, W. Hu, and T. Matsushita: J. Phys. Condens. Matter 24, 093201 (2012).
- [6] H. Daimon: Phys. Rev. Lett. 86, 2034 (2001).
- [7] URL: <http://www.en.3d-activesite.jp/>
- [8] K. Tsutsui, T. Matsushita, K. Natori, T. Muro, Y. Morikawa, T. Hoshii, K. Kakushima, H. Wakabayashi, K. Hayashi, F. Matsui, and T. Kinoshita, Nano Letters, 17, 7533 (2017).

INVITED PLENARY LECTURE 6

SURFACE MODIFICATIONS IN TI-BASED ALLOYS FOR BIOMEDICAL APPLICATIONS

Carlos Roberto Grandini, FBSE *

UNES –Univ. Estadual Paulista, Laboratório de Anelasticidade e Biomateriais, 17.033-360, Bauru, SP, Brazil
IBTN-Br – Institute of Biomaterials, Tribocorrosion and Nanomedicine – Brazilian Branch

Ti and its alloys are being used in biomedical field owing to their low elastic modulus, good fatigue strength and formability, and corrosion resistance (1). However, they are still not sufficient for long-term clinical usage as they are bio-inert and they cannot bond to living bone directly at the early stage after implantation into a human body. Their surfaces play an important role in response to the artificial devices in a biological environment; for these materials to meet the clinical demands, it is necessary to modify their surface (2). The corrosion resistance and biological properties of Ti and its alloys can be improved selectively by using the appropriate surface modification techniques while the desirable bulk attributes of the materials are retained. The proper surface treatment expands the use of these materials in the biomedical field. In this work, it will be presented the various surface modification techniques for Ti and its alloys including mechanical methods, chemical and electrochemical treatment, thermal spraying, sol-gel, and ion implantation towards the field of biomedical engineering (3-5).

Acknowledgments

The author would thanks Capes, CNPq and FAPESP for the financial support.

References

1. Kaur M, Singh K. Review on titanium and titanium based alloys as biomaterials for orthopaedic applications. *Materials Science and Engineering: C*. 2019;102:844-62.
2. Spriano S, Yamaguchi S, Baino F, Ferraris S. A critical review of multifunctional titanium surfaces: New frontiers for improving osseointegration and host response, avoiding bacteria contamination. *Acta Biomaterialia*. 2018;79:1-22.
3. Sasikumar Y, Indira K, Rajendran N. Surface Modification Methods for Titanium and Its Alloys and Their Corrosion Behavior in Biological Environment: A Review. *Journal of Bio- and Tribo-Corrosion*. 2019;5(2):36.
4. Luz AR, de Lima GG, Santos E, Pereira BL, Sato HH, Lepiensi CM, et al. Tribo-mechanical properties and cellular viability of electrochemically treated Ti-10Nb and Ti-20Nb alloys. *Journal of Alloys and Compounds*. 2019;779:129-39.
5. Chernozem RV, Surmeneva MA, Tkachev M, Ignatov VP, Timin AS, Tyurin AI, et al. A study of the nanotubes fabricated onto Titanium-Niobium substrates: structure, mechanical and cells behaviors. *Surface & Coatings Technology*. 2019.

INVITED PLENARY LECTURE 7**Innovative non equilibrium plasma processes for environmental applications**

Fracassi F^{1,2}, Armenise V¹, P. Bosso¹, Fanelli F,² A. Milella¹

¹*Department of Chemistry, University of Bari Aldo Moro, Italy*

²*Institute of Nanotechnology (NANOTEC), National Research Council (CNR), Bari, Italy*

E-mail francesco.fracassi@uniba.it

Non-equilibrium plasmas, both at low and atmospheric pressure, allow the preparation of functionalized structured and unstructured surfaces with interesting and unique properties. The processes permit the grafting of specific chemical functionalities and the deposition of organic, inorganic or hybrid organic-inorganic thin films. In this presentation some novel processes, currently studied in the plasma laboratory at University of Bari in Italy, with interesting potential applications in the environmental field, will be discussed. It will be shown that low pressure processes, such as PECVD and RF sputtering, allow to obtain innovative nanotextured materials with important catalytic properties also for photoelectrochemical water splitting, photochemical wastewater treatment and biodiesel production. With atmospheric pressure plasma in DBD configuration, the processing of porous 3D substrates, e.g., polyurethane foams and PET meshes can be performed. The ignition of the discharge inside the small pores and the efficient penetration of the plasma generated species in the substrate result in an efficient surface modification or thin film deposition [1]. Some examples of novel processes will be described, i.e., the preparation of hybrid organic/inorganic multifunctional nanostructured thin films [2], the deposition fluoropolymers [1], and the surface functionalization with carboxylic groups for oxygen treatment and deposition from acyclic acid containing feed [3]. Results will be presented on the utilization of the treated 3D substrates as photocatalysts for organic pollutant destruction, superhydrophobic and oleophilic material for water-oil separation and as adsorbent for the removal of heavy metals from polluted water.

References

- [1] F. Fanelli, F. Fracassi, *Plasma Processes and Polymers*, 13, 470 (2016).
- [2] F. Fanelli, A. Mastrangelo, F. Fracassi, *Langmuir*, 30, 857 (2014).
- [3] P. Bosso, F. Fanelli, F. Fracassi, *Plasma Process. Polym.* 13, 217 (2016).

INVITED PLENARY LECTURE 8**Determination of momentum and energy fluxes in plasma surface processing**

H. Kersten, T. Trottenberg, A. Spethmann, M. Klette, L. Hansen, M. Maas

Institute for Experimental and Applied Physics, Kiel University, Kiel, Germany

kersten@physik.uni-kiel.de

For an optimization of plasma-based processes as thin film deposition, suitable diagnostics are required. In addition to well-established plasma diagnostic methods (e.g. optical emission spectroscopy, mass spectrometry, Langmuir probes, etc.) we perform examples of “non-conventional” low-cost diagnostics, which are applicable in technological plasma processes. Examples are the determination of energy fluxes by calorimetric probes [1,2] and the measurement of momentum transfer due to sputtered particles or changes of plasma pressure by force probes [3].

The total energy influx from the plasma to a substrate can be measured by special calorimetric sensors. One method is the passive thermal probe (PTP) based on the determination of the temporal slope of the substrate surface temperature (heating, cooling) in the course of the plasma process. By knowing the calibrated heat capacity of the sensor, the difference of the time derivatives yields the integral energy influx to the surface. Simultaneously, the electrical current to the substrate can be obtained and by variation of the bias voltage the energetic contribution of charge carriers can be determined. By comparison with model assumptions on the involved plasma-surface mechanisms the different energetic contributions to the total energy influx can be separated.

Furthermore, for thin film deposition by sputtering it is essential to determine the sputtering yield as well as the angular distribution of sputtered atoms. In addition to model calculations (TRIM, TRIDYN etc.) an experimental determination of the related quantities is highly demanded. For this purpose, we developed interferometric force probes. Such a quite sensitive probe bends a few μm due to momentum transfer by the bombarding and released particles, i.e. sputtered target atoms and recoiled ions. By knowing the material properties of the cantilever and by measuring its deflection, the transferred momentum, e.g. the force in μN range, can be determined experimentally. In the present study, the measurements are compared with TRIM simulations for different experimental discharge conditions. Furthermore, the method of momentum transfer will be demonstrated also for small changes in pressure due to gas heating and charged species in the sheath of a low-pressure rf-plasma as well as for an atmospheric surface barrier discharge.

References

- [1] Kersten, H., Deutsch, H., Steffen, H., Kroesen G.M.W., Hippler, R., (2001) The energy balance at substrates during plasma processing, *Vacuum*, 63, 385-431.
- [2] Gauter, S., Haase, F., Kersten, H., (2019) Experimental unravelling the energy flux originating from a DC magnetron sputtering source, *Thin Solid Films*, 669, 8-18.
- [3] Trottenberg, T., Spethmann, A., Kersten, H., (2018) An interferometric force probe for beam diagnostics and the study of sputtering, *Eur. Phys. J. TI*, 5, 3.

KEYNOTE TALK**THE 14-BILLION YEAR HISTORY OF THE UNIVERSE
LEADING TO MODERN MATERIALS SCIENCE**

Joe Greene

D.B. Willett Professor of Materials Science and Physics, University of Illinois

The story begins approximately 13.8 billion years ago with the Big Bang. A brief introduction will trace the evolution of the universe to what we observe today. Many of the formative events occurred in the first tiny fractions of a second (our universe evolved from consisting entirely of a quark/gluon plasma to form the first hadrons: protons and neutrons) to minutes (free neutrons decay to electrons, neutrinos, and more protons) to a few tens of thousands of years (elementary particles react to form the first elements which leads, in turn, to the development of stars due to local density fluctuations). Planet Earth nucleated and began to accrete interstellar debris ~4.5 billion years ago. While the lighter metal elements on earth formed primarily due to stellar supernovae explosions, the primary mechanism leading to the formation of the heavier elements has only recently been demonstrated. The first known sophisticated stone tools used by hominids, found in northern Ethiopia, date to 2.6 million years ago

Gold is likely the first metal discovered by man, >11,000 years ago. However, unlike copper (Mesopotamia, ~9000 BC), bronze (Iran, ~5000 BC), and cast iron (China, ~600 BC), it was too soft for fabrication of tools and weapons. Instead, gold was used for decoration, religious artifacts, and commerce. Spectacular metal sculpting displaying very high levels of metallurgical and artistic craftsmanship have been found in Mesopotamia (S. Iraq). The earliest high-purity Au artifacts derive not from Egypt, as commonly thought, but from NE Bulgaria ~6500 y ago; however, the largest known concentration of ancient gold mines is in the Egyptian Eastern Desert. Metal extraction from ore, copper smelting, was already being carried out in the Balkans (E. Serbia and S. Bulgaria) ~7500 years ago.

Gold brazing of metal parts was first reported in ~3400 BC in Sumaria. The earliest documented thin metal films were gold layers, some less than 1000 Å thick, produced chemi-mechanically by Egyptians ~5000 years ago. Examples, gilded on copper and bronze statues and artifacts (requiring sophisticated compositionally-graded interfacial adhesion layers), were found in hewn-stone pyramids dating to ~2650 BC in Saqqara. Spectacular samples of embossed gold sheets date to at least 2600 BC. Electroless gold and silver plating was developed much later by the Moche Indians of Peru in ~100 BC. Early biomaterials used as human prosthetics following successful amputations date to 950 BC in Egypt, while the first recorded quantum-mechanical nano-based devices, exhibiting spectacular dichroic nanophotonic effects based on ~200-Å-diameter Au alloy quantum dots, were synthesized in Rome during the early third-century AD.

Vapor-phase deposition of thin metal and ceramic films on bulk substrates (as used in manufacturing of today's transistors, hard discs, LED TVs, etc.) had to wait for the invention of vacuum pumps (~1650 for mechanical pumps, through ~1865 for ballistic mercury momentum-transfer pumps). The fascinating development of crystallography (Plato [Greece], 360 BC; through Kepler [Germany], 1611; Haüy [France], 1780s; and Miller [UK, 1839]), is essential for describing crystal structure in modern materials science, mineralogy, and geology.

While an historical road map tracing the progress of materials technology is interesting in itself, the stories behind these developments are even more remarkable and provide insight into the evolution of scientific reasoning.

INVITED TALK 1

INFLUENCE OF DIELECTRIC THICKNESS AND STRUCTURE ON THE ION WIND GENERATION BY MICRO FABRICATED PLASMA ACTUATORS

R. Hink^{1*}, A. V. Pipa¹, J. Schäfer¹, A. Max², R. Caspari², R. Foest¹, R. Brandenburg¹

¹*Leibniz Institute for Plasma Science and Technology, Greifswald, 17489, Germany*

²*Airbus Defence and Space, Manching, 85077, Germany*

**Corresponding Author: R. Hink: ruediger.hink@inp-greifswald.de*

1. Introduction

The growing demand on passenger aircraft and the limitation of air transportation and finite fossil fuels require fuel-saving technologies. During the last decade, the flow control by non-thermal plasma with asymmetric dielectric barrier discharges (DBDs) were extensively investigated as drag reduction technology for the aerospace applications [1, 2, 3, 4].

These DBD's have typically two electrodes fixed on opposite sites of a dielectric. A discharge beginning from the edge of the high voltage electrode expands over the dielectric surface above the ground electrode and induce an air flow called ion wind. The induced flow can prevent a boundary layer separation at aircraft wings even at higher angles of attack [5] or damp Tollmien-Schlichting waves [6] and thus delay the boundary layer transition from laminar to turbulent, which lead to a remarkable reduction of the drag.

Different approaches are taken to increase the flow control effects by increasing the ion wind velocity. One way is to decrease the dielectric thickness, which leads to an increase of the electric field and thus the effect of such DBDs as Forte et al. showed [7].

Another way to increase the ion wind velocity is the use of a structured high voltage electrode, which increase the electric field at sharp edges. Thomas et al. [8] showed already that the thrust increases more than 40% at the same voltage amplitude of about 20 kV for structured electrodes in comparison to straight electrodes. In that study an equal sided triangle electrode structure was investigated with a base length of 3.18 mm and a height of 12.7 mm. However, to our knowledge micro fabricated electrodes were up to now not investigated and is therefore put in the focus of this study.

2. Experimental investigations

In this study both parameters – the dielectric thickness and a structured electrode - are investigated to increase the performance and lower the weight of DBDs. It is investigated if the positive effect of the structured high voltage electrode remains for smaller right-angled triangles with a hypotenuse lengths of 200 and 250 μm . A focus in this study is set on the comparison of the dynamic pressures for different DBDs. Furthermore, the efficiency of the different samples by the ratio of dynamic pressure to the consumed power is compared. Finally the surface degradation by the plasma operation was investigated by an optical and a scanning electron microscope (SEM), especially due to the fact that latest studies show a strong degradation of organic materials like the often used polyimides (e.g. Kapton®) [9].

3. Results and Discussion

The electrode structure demonstrated a higher ion wind generation as well as a slightly higher actuator efficiency. However, the discharge filaments are aligned to the peaks of the electrode structure. The preferable location of the filaments is well recognized by erosion channels in the dielectric. Further details will be presented on the conference.

4. References

- [1]- N. Benard and E. Moreau, *Exp Fluids* **55**, 1846, (2014).
- [2]- A. Masati and R. J. Sedwick, *J. Appl. Phys.*, **123**, (2018).
- [3]- J. Kriegseis, B. Simon and S. Grundmann, *Applied Mechanics Reviews*, **68**, (2015).
- [4]- M. Kotsonis, *Meas. Sci. Technol.*, **26**, (2015).
- [5]- M. L. Post and T. C. Corke, *AIAA Journal*, **42**, No. 11, 2177-2184, (2004).
- [6]- J. Kriegseis, S. Grundmann and C. Tropea, *J. Appl. Phys.*, **110**, (2011).
- [7]- M. Forte, J. Jolibois, J. Pons, E. Moreau, G. Touchard and M. Cazalens, *AIAA Flow Control Conference*, **3**, (2007).
- [8]- F. Thomas, T. Corke, M. Iqbal, A. Kozlov and D. Schatzman, *AIAA Journal*, **47**, (2009).
- [9]- D. Bian, Y. Wu, C. Long and B. Lin, *J. Appl. Phys.*, **124**, (2018).

INVITED TALK 2

NON-THERMAL ATMOSPHERIC PRESSURE PLASMA REDUCES *CANDIDA ALBICANS* VIRULENCE GENES EXPRESSION

Cristiane Yumi Koga-Ito^{1*}, Marcia Hiromi Tanaka^{1,2}, Aline Chiodi Borges¹,
Thalita Mayumi Castaldelli Nishime^{1,3}, Konstantin Georgiev Kostov¹

¹São Paulo State University (UNESP)

²Universidade Santo Amaro

³Leibniz Institute for Plasma Science and Technology

*Corresponding author: cristiane.koga-ito@unesp.br

1. Introduction

Candida species are fungal pathogens that can cause superficial to systemic diseases [1]. *C. albicans* is the most frequently isolated species. *Candida* spp. express a number of virulence factors that enable them to invade the host and cause diseases [2]. One of the most important virulence factor is the formation of biofilm, as this form is much more resistant to the antifungals than the planktonic cells [1]. Non-thermal atmospheric plasma showed promising antifungal activity against *C. albicans* both in vitro [3] as in vivo [4], however little is known about its effect on the expression of virulence genes. Thus, the aim of this study was to evaluate the effect of non-thermal atmospheric pressure plasma on *C. albicans* *ALS3*, *HWPI*, *SAP2*, *SAP4* and *SAP6* genes.

2. Experimental

Candida albicans ATCC 18804 standardized suspensions were obtained. Biofilms were formed in 96 wells microplates using yeast nitrogen base broth supplemented with 50mM glucose. After initial adherence for 90 min under shaking, plates were incubated for 24 h at 37°C, under aerobiosis, for biofilm formation. After, the biofilms were exposed to previously standardized sub-inhibitory period of exposure to non-thermal atmospheric pressure plasma (1 min). Plasma was generated with mean power of 1.8 W and the system was fluxed with helium at 2.0 SLM. Non-exposed biofilms were included for comparative purposes. Total RNA was extracted from the biofilms and purified. The expressions of the virulence genes *ALS3* (cell adhesion), *HWPI* (cell adhesion involved in biofilm formation), *SAP2*, *SAP4* and *SAP6* (protease secretion) were investigated. Positive control (of the amplification reaction) and negative control were included. The experiments were done in triplicate. Gene expression was analyzed by qPCR after normalized to an endogenous control (*ACT1*). The results were expressed as rate of gene expression of plasma treated biofilms in relation to non-exposed controls.

3. Results and Discussions

Gene expression of *ALS3* after exposition to non-thermal atmospheric pressure plasma was 0.75 times lower in relation to non-exposed control ($p < 0.0001$). For *HWPI*, the expression was 0.35 times lower in relation to control ($p < 0.0001$). *SAP2* was 0.59 times less expressed in relation to control ($p = 0.0005$), while *SAP4* gene expression was 0.27 times lower when compared to control ($p < 0.0001$). Gene *SAP6* was 0.21 times less expressed in relation to non-exposed control ($p < 0.0001$). It could be concluded that *C. albicans* exposed to plasma for 1 minute showed reduced virulence genes expression when compared to non-exposed control.

4. References

- [1]- M. Cavalheiro and M. C. Teixeira, *Front. Med.*, **13**, 5-28, (2018).
- [2]- S. Höfs, S. Mogavero and B. Hube, *J. Microbiol.*, **54**, 149-69, (2016).
- [3]- T.M.C. Nishime et al., *Surf. Coat. Technol.*, **312**, 19-24, (2017).
- [4]- A.C. Borges et al., *Plos One.*, **13**, e0199832, (2018).

Acknowledgments

The authors would like to thank MSc. Clelia Paiva for technical assistance.

INVITED TALK 3

A MEDIUM SCALE ATMOSPHERIC PRESSURE PLASMA SOURCE FOR PRE-HARVEST TREATMENTS

Nishime, T. M. C.^{1*}, Wannicke, N.¹, Mui, T. S. M.², Horn, S.¹, Weltmann, K.-D.¹, Brust, H.¹

¹Leibniz Institute for Plasma Science and Technology, Felix-Hausdorff-Str. 2, 17489 Greifswald, Germany

²São Paulo State University (Unesp), School of Engineering - Av. Dr. Ariberto Pereira da Cunha, 333; 12516-410, Guaratinguetá - SP, Brazil.

*Corresponding author: thalita.nishime@inp-greifswald.de

1. Introduction

For decades non-thermal atmospheric pressure plasmas have been studied as possible alternatives to conventional treatments, from material processing to medical therapies [1], [2]. Thereby, cold plasmas have recently drawn much attention to their potential usage in agriculture. Studies have shown that plasma can be used not just in post-harvesting processes, such as in decontamination of crops, but also in pre-harvest procedures. The last includes decontamination of seeds in storage, enhancement of seed germination and growth of plants and removal of volatile organic compounds [3]. In the present work, the development and characterization of a medium scale dielectric barrier discharge (DBD) for pre-harvest treatment is presented.

2. Experimental

A medium scale DBD with coaxial configuration and fed with pure Argon was developed for seed's treatment. The reactor contains a 2 liters compartment for seeds connected to the discharge quartz tube. The high voltage electrode is wrapped around the outer quartz tube. While a central metallic rod is connected to ground. The electrodes arrangement is presented in Fig. 1. During the treatment, the seeds are transported from the primary reservoir through the tube where plasma is produced.

The discharge was operated in burst mode with 30% of voltage duty cycle to avoid overheating. Power measurements and optical emission spectroscopy (OES) were carried out for different stages of treatment, that is, for different amount of seeds inside the discharge zone. To test the reactor efficiency for agricultural applications, seeds of barley and wheat were treated with different exposure times. Water contact angle of the seed's surface, water uptake and germination were investigated

3. Results and Discussions

Plasma treatments can be performed directly or indirectly and commonly, the direct case provides a much richer and active environment capable of quickly acting on the target. However, when the discharge is in direct contact with the samples, because it is placed inside the gap, the amount of treated material can affect the dissipated power. Thus, upscaling a reactor for seed's treatment can lead to some difficulties mainly concerning its homogeneity. However, as can be observed in Fig. 2, plasma treatment can effectively accelerate the germination of barley seeds for different exposure times. The small standard deviations indicate that plasma treatment by the medium scale DBD reactor is homogenous.

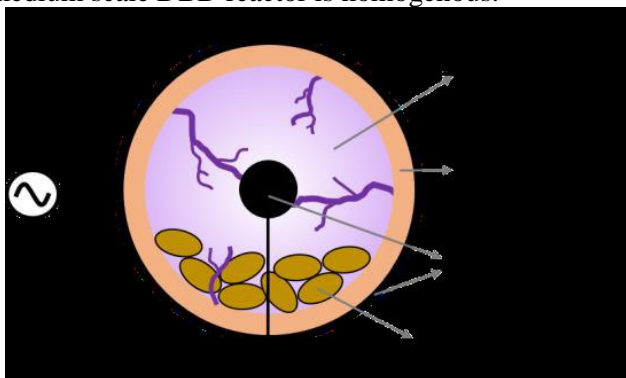


Fig. 1. Experimental arrangement of the DBD reactor used for seed's treatment and electrodes configuration.

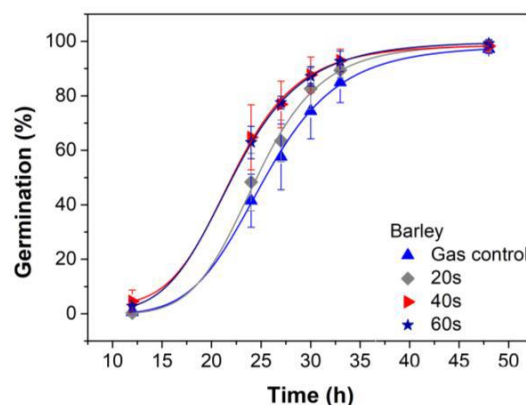


Fig. 2. Germination acceleration of barley seeds treated with different exposure times (control, 20s, 40s and 60s).

4. References

- [1] U. Kogelschatz, Plasma Phys. Control. Fusion, vol. 46, no. 12 B, pp. 63–75, 2004.
- [2] M. Laroussi, Plasma, vol. 1, no. 1, pp. 47–60, 2018.
- [3] M. Ito et al., Plasma Process. Polym., vol. 15, pp. 1–15, 2017.

INVITED TALK 4**SENSOR RESPONSE TOWARDS CO GAS: ROLE OF CeO₂ NANOPARTICLE MORPHOLOGIES AND THEIR CORRESPONDING CRYSTALLINE PLANES**

Rafael A. C. Amoresi^{1*}, Maria A. Zaghete⁴, Elson Longo³, Julio R. Sambrano², Alexandre Z. Simões¹.

¹*São Paulo State University – UNESP, 12516-410, Guaratinguetá, SP, Brazil*

²*Modeling and Molecular Simulations Group, São Paulo State University, UNESP, 17033-360, Bauru, SP, Brazil*

³*Interdisciplinary Laboratory of Electrochemistry and Ceramics, LIEC – Department of Chemistry, Universidade Federal de São Carlos – UFSCAR, 13565-905 São Carlos, SP, Brazil*

⁴*Interdisciplinary Laboratory of Electrochemistry and Ceramics, LIEC – Chemistry Institute, São Paulo State University – UNESP, 14800-060 Araraquara, SP, Brazil*

Currently, numerous properties of semiconducting oxides are correlated to their morphological characteristics resulting from their exposed surfaces. In the present work, the relationship between the following morphologies: rods, beans, hexagons, and rods/cubes of CeO₂, with the exposure of (111), (110), (100), and (311) surfaces and the main carriers was investigated related to the CO adsorption. Therefore, the active species were correlated to the computational simulations using the density functional theory (DFT). Accordingly, the relationships between the morphology, surface exposure in the particles, surface defects, sensor generated species, and preferential attack were shown. Specific surface area analyses demonstrate an effective relationship between gas sensors and the exposed surface of the particle. This will allow rationalization of the relation between the catalytic and electronic properties of semiconductor surfaces.

Keywords: CeO₂, surface, CO, Sensors, DFT

TI-MG ALLOY COATING SPUTTER-DEPOSITED ON AISI 316L STAINLESS STEEL FOR BIOMEDICAL APPLICATIONS

E.D. Gonzalez¹, A.L. Gobbi², N.K. Fukumasu³, V.R. Mastelaro⁴, C.R.M. Afonso^{1,5}, P.A.P. Nascente^{1,5*}

¹*Federal University of São Carlos, Graduation Program in Materials Science and Engineering, 13565-905, São Carlos, SP, Brazil.*

²*Brazilian Center for Research in Energy and Materials, Brazilian Nanotechnology National Laboratory, 13083-970, Campinas, SP, Brazil.*

³*University of São Paulo, Polytechnic School, Department of Mechanical Engineering, 05508-030, São Paulo, SP, Brazil.*

⁴*University of São Paulo, São Carlos Institute of Physics, 13566-590, São Carlos, SP, Brazil.*

⁵*Federal University of São Carlos, Department Materials Engineering, 13565-905, São Carlos, SP, Brazil.*

*Corresponding Author: nascente@ufscar.br

1. Introduction

Titanium and its alloys have been widely employed as biomedical devices, especially for the replacement of hard tissues. Two critical criteria for selecting a metallic material for manufacturing orthopedic and dental implants are the absence of toxic elements and a low modulus of elasticity. Since magnesium is a lightweight metal, it is expected that alloying Ti with Mg produces a useful metallic biomaterial [1]. Due to the lack of complete solubility in the Ti-Mg phase diagram, high Mg content Ti-Mg alloys cannot be obtained by conventional melting processes, and non-equilibrium processes, such as magnetron sputtering, have been employed for producing Ti-Mg alloys [2]. A Ti-Mg alloy coating was co-deposited on AISI 316L SS substrate by magnetron sputtering, and its composition, structure, and morphology were analyzed by energy dispersive X-ray spectroscopy (EDS), X-ray diffraction (XRD), atomic force microscopy (AFM), and X-ray photoelectron spectroscopy (XPS), while the mechanical properties were characterized by nanoindentation, scratch, and nanowear tests.

2. Experimental

A Ti-Mg coating was deposited on AISI 316L substrate by co-sputtering pure Ti and Mg targets. The magnetron sputtering system was an AJA Orion 8 Phase II J, and the deposition conditions were: base pressure of 1.0×10^{-5} Pa, working pressure of 0.67 Pa, and argon flux of 20 sccm. The substrate was cut in the form of 15 mm diameter disk, and the targets were Ti and Mg disks (50.8 mm diameter and 3 mm thick) with a purity of 99.95 %. The target-sample distance was 20 cm, and it was applied a DC power of 300 and 34 W to the Ti and Mg targets, respectively. XRD analysis was carried out using a Bruker diffractometer in Bragg-Brentano grazing incidence mode (GIXRD), the AFM images were acquired with a Bruker nanoscope V multimode microscope, using the tapping mode, and the XPS spectra were obtained by a V Omicron Nanotechnology spectrometer. The mechanical properties were evaluated using nanoindentation test with a Berkovich diamond indenter having a maximum applied load of 1000 μ N, using the Oliver-Pharr method; the scratch tests were carried out using a CETR-UMT-2 equipment, with a Rockwel C 200 μ m radius indenter; and nanowear tests were performed with a TI-950 Bruker Triboindenter.

3. Results and Discussions

The coating thickness is estimated to be 1.0 μ m, and its composition that was evaluated by EDS is Ti₈₃Mg₁₇ (Ti-9.4 wt% Mo). The XRD diffractograms present peaks corresponding to the α (hexagonal close packed – hcp) and β (body centered cubic – bcc) phases. AFM analysis for the coating yields a mean grain size of 99 ± 14 nm and roughness of 8.2 nm. XPS results reveal that the coating surface is oxidized and enriched by Mg. The addition of Mg in the coating causes an increase in the hardness and a decrease in the elastic modulus. The scratch test for the Ti₈₃Mg₁₇ coating deposited on SS shows that there is no sign of coating detachment, demonstrating its integrity and indicating a good adhesion of the coating to the substrate. These results indicate the application potential of the Ti-Mg alloy coatings in medical implant devices.

4. References

- [1] J. Hieda *et al.*, Mater. Sci. Eng. C 54 (2015) 1-7.
- [2] G. L. Song, D. Haddad, Mater. Chem. Phys. 125 (2011) 548-552.

Acknowledgments

FAPESP (process 2017/25983-8), CNPq (process 302450/2017-2), CAPES (fellowship for E.D.G.), and LNNano-CNPEN/MCTIC (proposal LMF-23110).

PRODUCTION OF PLASMA-ACTIVATED SALT FLOWER CRYSTAL

Clodomiro Alves Junior^{1,2*}, Jairo B.F.O. Barauna², Kristy³, Liliane. F.A. Almada⁴,
Jussier de Oliveira Vitoriano²

¹Federal Rural University of Semiárid, PPGCEM, Mossoró, RN, Brazil

²Federal University of Rio Grande do Norte, PPGEM, Natal, RN, Brazil

³State University of Campinas, Mechanical Engineering Department, Campinas, SP, Brazil

*Corresponding Author: Clodomiro.jr@ufersa.edu.br

1. Introduction

Crystallization from saturated solutions is driven by changes in the free energy. Strong electrical field applied in liquids containing solvated ions induce or assist crystallization due polarization on solvation layer. Plasma-liquid interactions have potential to be useful in that area, since the electric discharge transfers charge as a solid electrode, but without any surface to adsorption. It means that is possible to produce compounds in the liquid surface just above the discharge, and they will not be adhered to any solid surface as a film. Thus, this work is the first effort to better understand which differences an electric discharge would produce in the crystallization of salts from a saturated solution.

2. Experimental

Brine samples, obtained at Salina F. Souto Ind, Grossos-RN at 28 ° Bé (1,28 g / cm³) were used as starting material for the present work. Saturation was achieved by heating 150 ml of the brine in beakers, laterally isolated with styrofoam to avoid radial temperature variations. The beaker was placed on a plate heated to 40 ° C to maintain the mean water temperature constant and equal to 35 ° C (Figure 1A). A stainless steel, with a electrical discharge of 10 kV and 990 Hz was applied over brine sample. The discharge was produced with a thin tip of 2mm and 5 mm away from the solution, during time enough to induce a crystallization. The solution was weighted before and after the discharge and the solids obtained were filtered using an 8 µm paper filter, and then dried in the drying oven (60° C) (Figure 1C).

3. Results and Discussions

Immediately after the beginning of the discharge, it was observed that crystals start to form under the plasma, spreading across the liquid on the electrode's surroundings, as the time passes (Figure 2). There was no significant temperature increment, however, it was registered crystals denser near discharge than another region (Figure 1B). This result can be explained because the generated discharge can be assumed as cold atmospheric discharge, where the electrons have high temperature but do not transfer that temperature to the heavier species. In addition, strong electric fields can induce crystallization out of equilibrium on the surface, whose crystals remain on the surface with the aid of air bubbles produced during the evaporation of the brine. It can also be justified by a nonequilibrium evaporation is happening, which was already visualized in the interaction between electric discharges and aqueous solutions [2]. It is caused mainly by the impact of ions coming from the plasma, hitting the liquid surface driven by the electric field. That sputtering effect can eject atoms and molecules from the liquid into the gaseous phase and can also be helped by the transport of water attached to ions attracted by the electric field. So, to explain that, it is proposed that a nonequilibrium evaporation is happening, which was already visualized in the interaction between electric discharges and aqueous solutions.

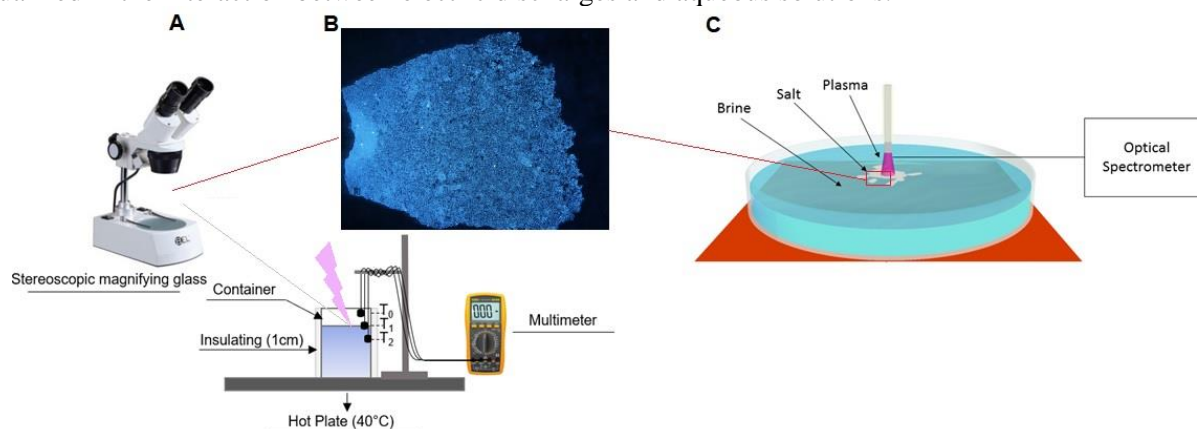


Figure 1. (A) Experimental apparatus, (B) Salt flower denser details formed by plasma and (C) Discharge applications illustration.

4. References

- [1]-S.W. Lee, D. Liang, X.P.A Gao and R.M. Sankaran Adv Funct Mater., 21(11), 2155-2160, (2011).
- [2]- A. Fedorets et al. . 14th Int. Conf. on Heat Transfer, Fluid Mech. and Thermodyn. (HEFAT-2019)

THE ROTATIONAL AND VIBRATIONAL TEMPERATURES FOR DIFFERENT REACTIVE SPECIES IN DBD PLASMA JETS

Fellype do Nascimento^{1,2*}, Konstantin Kostov³, Munemasa Machida¹, Stanislav Moshkalev²

¹*Institute of Physics “Gleb Wataghin”, UNICAMP, Campinas, SP, Brazil*

²*Center for Semiconductor Components and Nanotechnologies, UNICAMP, Campinas, SP, Brazil*

³*Faculty of Engineering, UNESP, Guaratinguetá, SP, Brazil*

*Corresponding Author: fellype@gmail.com

1. Introduction

A large number of applications for plasmas produced at atmospheric pressure and in open environment (APP) have been developed in the last years due to their versatility, easiness of operation and low cost of implementation compared to plasmas in vacuum environment, and Dielectric Barrier Discharge (DBD) is a kind of configuration commonly used to produce APP jets. One of the most promising applications is the use of APP jets in medical procedures, specially for treatment of cancerous tissues. Recent studies reported that reactive oxygen and nitrogen species (RONs) present in APP jets play an important role when these kind of plasmas are applied to cancerous tissues by reacting with the free radicals present in those tissues, destroying its diseased cells, but preserving the healthy ones [1]. In this context, it is important to know the values of rotational and vibrational temperatures (T_{rot} and T_{vib} , respectively) of the RONs present in a plasma jet, since such parameters, specially T_{vib} , can influence the results of plasma treatment. In this work we present results of T_{rot} and T_{vib} values obtained for OH and NO molecules that are compared to those obtained for N_2 , which is the most used molecule for temperature calculations in APP jets.

2. Experimental

A sinusoidal voltage of 20 kV peak-to-peak and frequency of 10 kHz was applied to a four-electrodes DBD plasma device, whose details can be obtained in [2], in order to produce plasma jets using Ar, He and Ne, separately, as working gases. A gas flow rate of 1.5 l/min was used in all cases. Temperature values were obtained through comparisons between measured and simulated spectra, using molecular band emissions from N_2 , OH, and NO in the wavelength ranges 360-385 nm, 305-310 nm and 260-274 nm, respectively. The spectroscopic measurements were performed using a multi-channel spectrometer from Avantes (model AvaSpec-ULS2048X64T), with spectral resolution of (0.678 ± 0.022) nm.

3. Results and Discussions

Table 1 shows the temperatures for N_2 , OH, and NO obtained when Ar, He and Ne were used as working gases. It was considered an average uncertainty of $\sim 5\%$ on both T_{rot} and T_{vib} values, unless otherwise indicated. T_{vib} values for OH could not be measured. From the data in Table 1, it can be seen that there are variations in both T_{rot} and T_{vib} values obtained for different species, with T_{rot} having higher values for OH than for N_2 and NO in all cases. It is interesting to note that the T_{rot} values for OH and NO are about 600 K and 400 K, respectively, and that the T_{vib} value for NO is ~ 3200 K regardless of the working gas used to produce the plasma jets. The T_{vib} values for N_2 are almost the same for He and Ne plasma jets, being twice the value observed for Ar. This last finding is an indication that the metastables present in He and Ne, that have higher energies than the Ar metastables, have a strong influence on the vibrational excitation of N_2 , and it is expected that the N_2^+ ions follow this same behavior.

Table 1: Summarized results for temperature measurements. ^{***}Uncertainties of ^{*}10% and ^{**}25%.

Working gas	Argon			Helium			Neon		
	N_2	OH	NO	N_2	OH	NO	N_2	OH	NO
T_{rot} (K)	550	625	375*	375	575	450	375	625	375
T_{vib} (K)	2100	–	3100**	4300	–	3100	4500	–	3400

We can conclude that the use of He and Ne may produce better results in plasma treatment of cancerous tissues due to the higher T_{vib} values observed for N_2 and NO, if we consider that the N_2^+ ions follow the same tendency of N_2 . Further measurements are required to obtain T_{vib} for OH molecules.

4. References

- [1]-J. Duan, X. Lu and G. He, Phys. Plasmas, **24**, 073506, (2017)
 [2]-F. Nascimento, M. Machida, K. Kostov, S. Moshkalev *et al*, Eur. Phys. J. D, **71**, 274, (2017)

Acknowledgments

This work was supported by CNPq and FAPESP.

BALANCE ENERGY EQUATION FOR GLOBAL MODEL OF HIPIMS DISCHARGES

Júlia Karnopp^{1,2}, Julio César Sagás^{1*}

¹Laboratório de Plasmas, Filmes e Superfícies, Universidade do Estado de Santa Catarina, Joinville - SC

²Instituto Federal de Santa Catarina, Jaraguá do Sul - SC

*Corresponding Author: julio.sagas@udesc.br

1. Introduction

The advent of high power impulse magnetron sputtering (HiPIMS) caused a renewed interesting in magnetron modeling, and recently, an approach based on global model has been proposed [1]. However, there is an intensive discussion about how to write the balance energy equation in such models. In particular, there is several questions about how to account the effect of electron and ion diffusion outwards the ionization region (IR). In this work, six different approaches for the energy balance equation were considered to modeling HiPIMS discharges and used to fit experimental current-voltage curves [2].

2. Methodology

The model was developed for argon plasma and titanium target. Plasma electrons and secondary electrons emitted from the cathode were considered as two different populations. Three different populations of neutral argon (cold, warm and hot) were included, as well as, argon ions, metastable argon, titanium in the ground state, singly ionized metal ions and doubly ionized metal ions. Six different models for energy balance equation were used: (1) considering only the power absorbed by electrons; (2) including explicitly the electron diffusion in model 1; (3) considering all the power absorbed in the IR and Bohm velocity for ions; (4) including the electron diffusion in model 3; (5) similar to model 3, but considering the effect of potential fall across the IR in ion velocity; and (6) based on model 4, but considering the effect of potential fall across the IR in ion velocity. In all cases, a maxwellian electron energy distribution function was assumed.

3. Results and Discussions

As the model is not self-consistent, two fitting parameters are necessary: the fraction of total discharge voltage across IR (f) and the back-attraction probability of ions (β). The comparison of simulated and experimental curves indicates that the parameters f and β can change during the pulse (fig. 1).

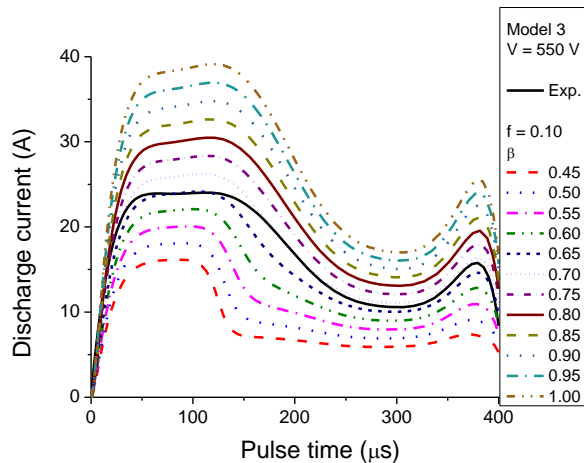


Fig. 1. Simulated curves using model 3 compared to experimental one.

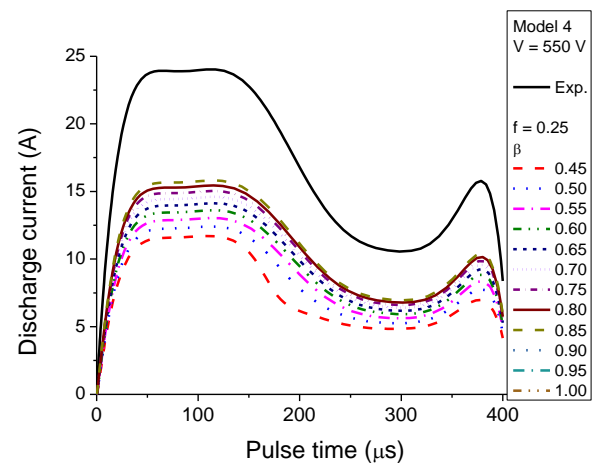


Fig. 2. Simulated curves using model 4 compared to experimental one.

The fact that all the energy balance equations used give reasonable values of the fitting parameters shows that is a difficult task to find the “correct” equation. But, for some cases, in particular using model 4, there is no reasonable values for f and β that fits the experimental curve (fig. 2). By this way is possible to exclude such energy balance equation from the possibilities.

4. References

- [1] C. Huo, et al., J. Phys. D: Appl. Phys., **50**, 354003, (2017).
 [2] A. Anders, J. Andersson, A. Ehasarian, J. Appl. Phys., **102**, 113303, (2007).

Acknowledgments

This project has been funded by FAPESC through the program PAP in association with UDESC under contract PAP-TR 655. Júlia Karnopp also thanks FAPESC and CAPES by the scholarship.

IMAGE PROCESSING ON THERMAL CAMERA EVALUATION

Alvaro José Damião*, Hingrid Spirlandeli Nunes da Silva, Raphael Eféisio da Silva
 PPGAO/CTE-S - Instituto Tecnológico de Aeronáutica
 *Corresponding Author: damiao@ieav.cta.br

1. Introduction

The employment of Unmanned Aerial Vehicles or drones in activities such urbanization control, agriculture and military operations is rapidly increasing. The reasons for expansion are due to the current ability to integrate high-resolution cameras to these aircrafts and the possibility of quickly over-fly and efficiently collect surface information. Those capabilities are essential in remote sensing activities, for example. In Search and Rescue (SAR) activities, this can mean the difference between life and death. At which altitude should a SAR team should fly, at night, in order to detect a cast away?

Considering the image quality, it is important that those images comply with the technical specifications intended for any particular application. Spatial resolution and sensitivity are essential criteria for evaluating the performance of a thermal electro-optical device. The former represents how the camera can distinguish the smallest details in a scene, and the latter deals with the smallest signal that can be detected. Parameters as Minimum Resolvable Temperature Differential (MRTD) can be obtained from the Modulation Transfer Function (MTF) of a commercial thermal camera, using specific images processing software. The Spatial resolution and sensitivity data can be obtained from special (non-complex) target images. Information as camera ageing and calibration data can be obtained. Even it is possible to analyze satellite images in order to know if they were previously treated or not.

2. Experimental

A case study of the FLIR Star Safire III sensor, which operates in the mid-infrared range, as do a large part of the imaging sensors shipped on aircraft and used militarily was made. Considering that similar equipment is used in the accomplishment of SAR missions of the Brazilian Air Force, the process described in this work takes the determination of parameters such as the Modulation Transfer Function (MTF) of the thermal camera are relevant. Then, one will be able to estimate a maximum distance to the target at which detection is possible, knowing previously the target size and the background temperature, in order to contribute to the planning SAR aerial operations.

3. Results and Discussions

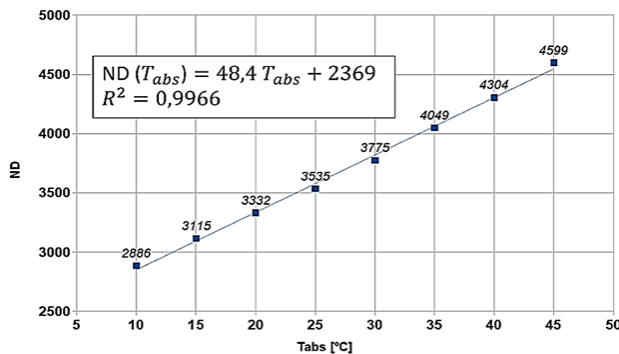


Fig. 1. FLIR Star Safire camera Responsivity

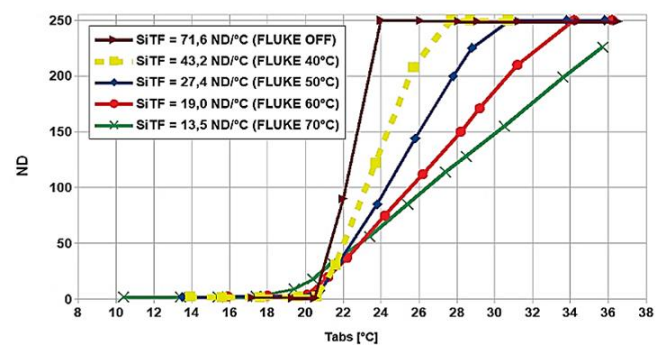


Fig. 2. FLIR Star Safire camera SiTF

Using international standards to establish the maximum distance of SAR operations, the results obtained in this work showed figures around 2 km. The temperature target/background difference was 2°K and the target size 2.3 m x 2.3 m.

Acknowledgments

To the Brazilian Air Force (FAB) and Brazilian Army (EB) for authorizing the use of the equipment used in this work.

STUDY OF THE LASER ABLATION PROCESS USED CVD-DIAMOND FILM OBTAINED VIA THE HFCVD TECHNIQUE FOR BIOMEDICAL APPLICATIONS

Cristiane da Costa Wachesk^{1,4*}, Carolina Ramos Hurtado^{1,2}, Rebeca Falcão Borja de Oliveira
Correia^{1,4}, Dayane Batista Tada¹, Getúlio Vasconcelos³,
Evaldo José Corat⁴, Vladimir Jesus Trava-Airoldi⁴

¹ *Laboratory of Nanomaterials and Nanotoxicology - Institute of Science and Technology, Federal University of São Paulo (UNIFESP), Talim Street, 330 - Vila Nair, São José dos Campos – SP, Brazil, 12231-280*

² *Federal Institute of São Paulo (IFSP), Rod. Pres. Dutra, km 145 - Jardim Diamante, São José dos Campos - SP, 12223-201*

³ *Laboratory of Lasers and Optical Applications Development - Dedalo, Institute of Advanced Studies (IEAv), Coronel Aviador José Alberto Albano do Amarante, 01 - Putim, São José dos Campos - SP, Brazil, 12228-001*

⁴ *Associated Laboratory of Sensors and Materials - National Institute for Space Research (INPE) – Astronautas Avenue, 1.758 - Jardim da Granja, São José dos Campos – SP, Brazil, 12227-010*

*Corresponding Author: cris_cw@hotmail.com

1. Introduction

The diamond-like carbon film, who has been the focus of extensive research in recent years due to its potential in applications such as surface coatings [1] and biomedical devices [2][3]. Moreover, Diamond films, in particular, have become a focus of interest [4], and has been strongly continued in order to develop new understandings and approaches for the growth and processing of this attractive material to the scientific community [5]. Furthermore, Diamond Nanoparticles (NDs) are a class of carbon-based nanomaterials of increasing interest in science and technology [6]. NDs are inert, optically transparent, photoluminescent, biocompatible, effective novel drug delivery and can also be functionalized in many ways depending on their final application [7][8]. In this work, the synthetic CVD-diamond by CVDVale company was used, to investigate the effect of laser ablation on the morphology and particle size of DIAMANTE CVD, which makes them suitable for industrial and applications medical. The results used CVD diamond production from pulsed laser ablation, where we obtained nanometric sizes (10-20 nm) after centrifuged.

2. Experimental

The process of synthesis CVD diamond film thick (30 μm) was macerated agate mortar and pestle, and sifted in granulometry sieve of 200 mesh (0,074 mm of mesh opening). CVD-diamond 5mg/mL aqueous suspensions (40mL volume) were prepared and irradiated by pulsed laser ablation of ytterbium doped fiber (Yb) ($\lambda=1062\text{nm}$) PRO Marking (Pulsed Fiber-Yb laser). In order to reduce the size of CVD-NDs, at 30 and 60 min time, the colloidal solution was centrifuged for 0 and 60 min, respectively. Hydrodynamic diameter, size distribution values were obtained through the dynamic light scattering (DLS) technique. The equipment used for this analysis was the DelsaTM Nano C by Beckman Coulter, belonging to ICT-UNIFESP multi-user NAPCEM laboratory. The micrographs were obtained using the Transmission Electron Microscope MET Tecnai G2 Spirit BioTWIN 120 kV (FEI) through a digitally controlled system, CompuStage Single-Tilt tilt support, Olympus-SIS Veleta CCD 120/200 kV digital camera, tungsten emitter (W), TIA (TEM Imaging and Analysis) program for image visualization. In collaboration with the Institute of Advanced Studies of the Sea (IEAMar), UNESP.

3. Results and Discussions

The results show a reduction in particle size due to the laser ablation and centrifuging time. This size is very close to the size of a single diamond nanocrystallite [9]. This can be seen by the left dislocating curves at 30-60 min ablation time and 0-60 min centrifugation time, the medium hydrodynamic radius was 54 ± 5 and $57\pm 6\text{nm}$ (Fig. 1a-b), while in the non centrifuged CVD-NDs, the medium was 72 ± 6 and $82\pm 7\text{nm}$ (Fig. 1c-d), respectively. Furthermore, a wider distribution curve is shown with laser ablation time and centrifugation. Figure 2 shows the particle average size, morphology and dispersion of CVD-NDs After ablation obtained by transmission electron microscopy (TEM), after centrifugation (Fig. 2a). Note there was a morphological difference, the synthesized CVD-NDs are agglomerated with rounded shape due to the performed process. Figure (2b) shows the image analyzed with the imageJ software to estimate de size distribution, the diameters found were between 10 e 20 nm. According to the results, laser ablation time and the centrifugation process produces a little particle, with diamond nanoparticles having the size of nanometric [10].

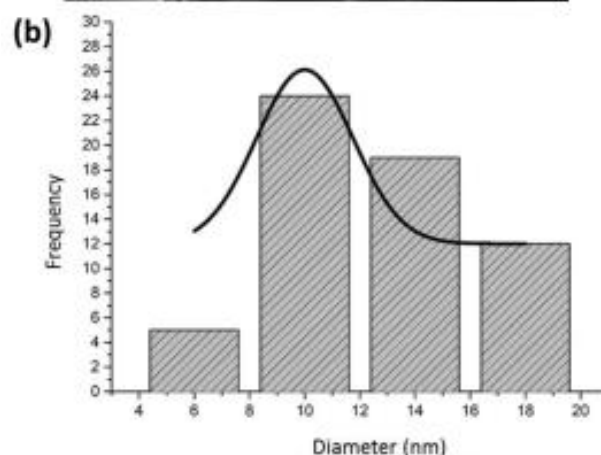
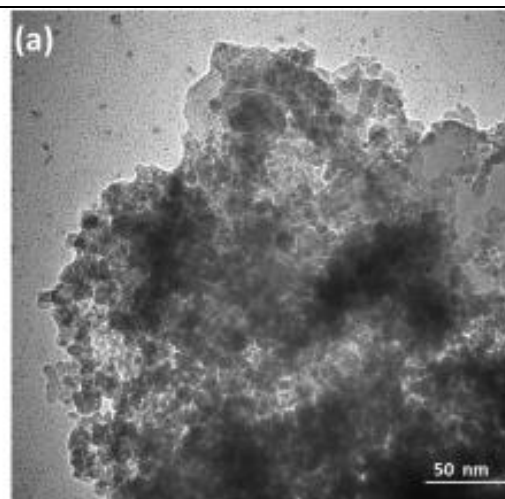
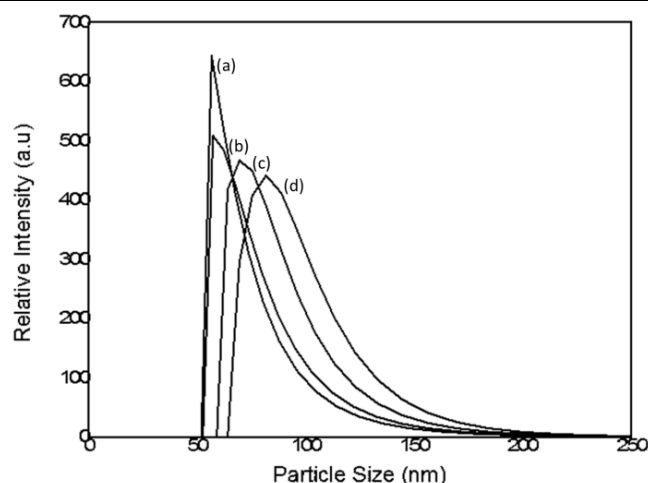


Fig. 1. Particle size distribution of the (a) 60 min laser ablation and 60 min centrifugation, (b) 30 min laser ablation and 60 min centrifugation (c) 60 min laser ablation (d) 30 min laser ablation without the centrifugation process.

Fig. 2. TEM images of the particles (a) Sample after 60 min of laser ablation with 60 min centrifugation (20 Kx) and (b) Image granulometric distribution, with average size of $20,50 \pm 6,19$ nm.

Acknowledgments

The authors want to acknowledge support from FAPESP (grant number 2012/15857-1; 2017/01697-6), National Council for Scientific and Technological Development (CNPq) (grant number 380402/2019-0) Coordination for the Improvement of Higher Education Personnel (CAPES), Ministry of Science, Technology and Innovation (MCTI) and PRO marking company, for the use of ytterbium doped pulsed fiber laser.

4. References

- [1]-V.J.T. Airoidi, L.V. Santos, L.F. Bonetti, G. Capote, P.A. Radi, E.J. Corat, , Int. J. Surf. Sci. Eng. 1 (2008) 417.
- [2]-C.C. Wachesk, C.A.F. Pires, B.C. Ramos, V.J. Trava-Airoidi, A.O. Lobo, C. Pacheco-Soares, F.R. Marciano, N.S. Da-Silva. Appl. Surf. Sci. 266 (2013).
- [3]-C.C. Wachesk, V.J. Trava-Airoidi, N.S. Da-Silva, A.O. Lobo, F.R. Marciano, J. Nanomater. (2016).
- [4]-A. Krueger, Chem. - A Eur. J. 14 (2008) 1382–1390.
- [5]-R.J. Nemanich, J.A. Carlisle, A. Hirata, K. Haenen, MRS Bull. 39 (2014) 490–494.
- [6]-B. Engineering, C. Cha, S.R. Shin, N. Annabi, M.R. Dokmeci, Carbon-Based Nanomaterials : Multifunctional Materials for, (n.d.).
- [7]-A. Barras, F.A. Martin, O. Bande, J.S. Baumann, J.M. Ghigo, R. Boukherroub, C. Beloin, A. Siriwardena, S. Szunerits, Nanoscale. 5 (2013) 2307–2316.
- [8]-S. Szunerits, R. Boukherroub, F. Teodorescu, J.G. Croissant, O. Hocine, M. Seric, L. Raehm, V. Stojanovic, D. Aggad, Materials Chemistry B, (2016) 5803–5808.
- [9]-A.T. Dideikin, A.E. Aleksenskii, et. al. Carbon N. Y. 122 (2017) 737–745.
- [10]-S.R.J. Pearce, S.J. Henley, F. Claeysens, P.W. May, K.R. Hallam, J.A. Smith, K.N. Rosser, 13 (2004) 661–665.

SILICA FILMS DEPOSITION ASSISTED BY COLD PLASMA USING HYBRID CORONA-DBD REACTOR

Alonso H. Ricci Castro*, André Petraconi, Larissa Nascimento, Rodrigo Pessoa, Gilberto Petraconi Filho.

Technological Institute of Aeronautics, ITA, São Jose dos Campos, SP-Brazil.

**Corresponding Author: alonso_elfisico@yahoo.com*

1. Introduction

On the last years there were reports of several results about atmospheric pressure plasma applications, such as, surface modification, film deposition and ion implantations. It was developed and tested different depositions systems. Those deposition systems are based on plasma jet and dielectric barrier discharge (DBD). They can operate by using different geometrical configuration type, primary gas and monomers (aerosol or gas). The molecules of monomer (gas) are dissociated and excited as result to interaction with the plasma. However, the interaction of plasma with small drops of liquids is more complex. The plasma can dissociate and ionize the molecular chains on the surface and vaporize some drops [1]. The use of deposition systems based on DBD can produce inhomogeneous films and generate powder on polymerization to one step. The plasma jet system can deposit films in small areas. It is reported that different configurations were tested to increase the area of film deposition, these configurations consist on the addition of movement system (of substrate or plasma jet) and/or matrix of plasma jets [2]. On this work we use a hybrid configuration Corona-DBD to deposition films on fabrics substrate.

2. Experimental Setup

The cold plasma was generated in atmospheric pressure using a hybrid Corona-DBD system. The reactor consists in two cylindrical electrodes with variable gap. The high voltage electrode is made from a metallic tube with 6.5 mm of external diameter and has a hole for entrance to different gases and liquids. The second electrode is grounded made from metallic tube (steel) with 140 mm of external diameter and covered by dielectric layer of alumina with 5.5 mm of thickness. This system can work with different pressure or gas type. The power supply can operate with different voltage amplitudes (1-35 kV), frequencies (1- 40 kHz) and wave signals. In this work, the system configuration was set as follow, a duty cycle with 300 μ s of period, 5 cycles, voltage 22 kV_{p-p}, frequency of 23 kHz and gap of 2 mm between the two electrodes. The silicic acid (0.5 mol) was used like precursor monomer and was introduced on the plasma reactor using a commercial ultrasonic nebulizer. The size of atomized acid has 5 μ m at a flow rate about 0,7 ml/min.

3. Results and Discussions

The polyamide fabric was treated several times (5-10 times) using deposition assisted by plasma. After plasma treatment, the FTIR analysis shows a presence of silica film on the substrate. The figure 1 shows the spectrum IR of samples before/after treatment. After treatment it can be observed two new peaks, 800 cm^{-1} corresponds to O-Si-O (bend) and 1080 cm^{-1} to Si-O-Si (asymmetric vibration).

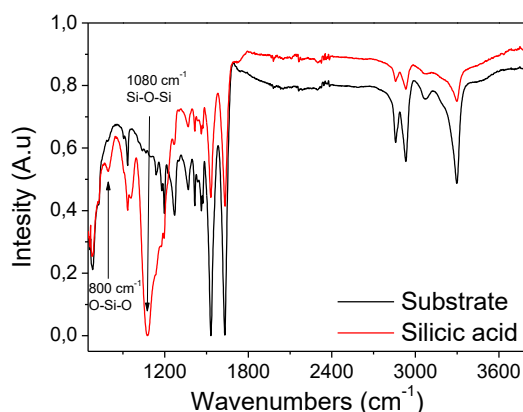


Fig. 1. FTIR spectrum on fabrics of polyamide 6.6 after and before film deposition.

4. References

[1] Fanelli, Fiorenza, et al. "Insights into the Atmospheric Pressure Plasma-Enhanced Chemical Vapor Deposition of Thin Films from Methylsiloxane Precursors" *Plasma Processes and Polymers* 9.11-12 (2012): 1132-1143.

[2] Fanelli, F., & Fracassi, F. "Atmospheric pressure non-equilibrium plasma jet technology: general features, specificities and applications in surface processing of materials" *Surface and Coatings Technology*, (2017): 322, 174-201.

Acknowledgments

The authors acknowledgement CNPq and FAPESP by the financial support.

AGING EFFECT OF BRAGG MIRRORS MADE WITH POROUS SILICON

Ana Carolina Fernandes da Silva^{1*}, Luiz Ângelo Berni^{2*}

¹Universidade Federal de São Paulo, Engenharia de Materiais

²Instituto Nacional de Pesquisas Espaciais, Laboratório Associado de Sensores e Materiais /SJC

*Corresponding Author: fanasilva2@gmail.com

1. Introduction

Porous Silicon (PSi) is a material with defective (pores) on surface. Some of its properties, like luminescence, may degrade over time if exposed to high temperatures, gases or reactive solvents, since the material presents in very small-scale structures (nanometer), leaving it fragile. [1]. With PSi it is possible to fabricate Bragg Mirrors. These mirrors are structures produced with superposition of multiple layers with alternating refractive index to get the maximum reflectance for a certain wavelength. It is necessary that the ratio of the thickness of each layer with the refractive index must be 1/4 of the desired wavelength. This relationship was given by the equation $\lambda = 4nL$, which λ is the desired wavelength, n is the refractive index chosen and the L is the thickness of layer. Their properties are also affected over time and it is of great importance to study this degradation. [2,3].

2. Experimental

The PSi was produced by electrochemical etching from a p-type crystalline silicon wafer (100) of low resistivity (0.01 – 0.02 Ω .cm) in hydrofluoric acid (40%) and ethanol (99.5%) solution (1:1). The etching time was varied from 10 to 900 seconds and the current density from 10 to 200 mA/cm². For characterization of each layer of PSi it was used the Spectroscopy Liquid Infiltration Method (SLIM) [4]. From this, ones can determinate the refractive index, porosity and the thickness of each sample. For manufacturing Bragg Mirrors, the same conditions were used but with two alternating currents in repetitive cycles. For current density were used 50 mA/cm², with time of 1,15 s, and 150 mA/cm², with time of 0,76 s, and the total time of one layers was 1.91 s, producing 40 layers. The reflectance of the samples of Bragg Mirrors was measure weekly for the knowledge of degradation.

3. Results and Discussions

For this work, three Bragg Mirror's samples were produced with maximum reflectance in 500nm. Each sample was stored in different ways, one was stored in alcohol, another in vacuum and the last in air. The Reflectance of the samples stored in air and alcohol were measured weekly, while the sample stored in vacuum was measured monthly. The results are shown in the figure 1 below and in the figure 2 is possible to note the superposition of multiple layers of the Bragg Mirror.

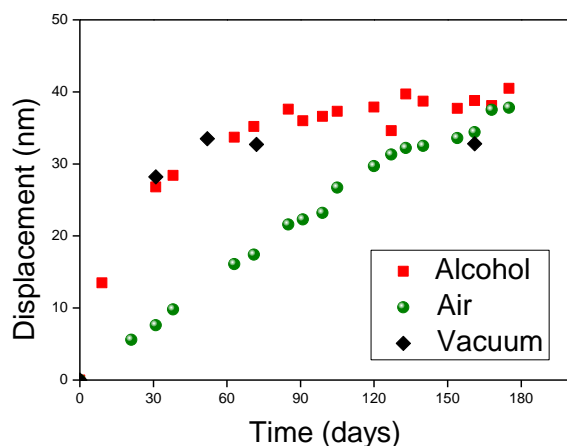


Fig. 1. Degradation of the samples 081118p1 (stored in alcohol), 081118p2 (stored in vacuum) and 081118p3 (stored in air)

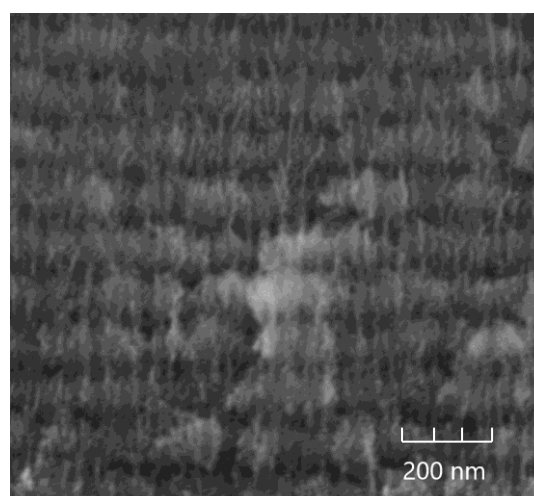


Fig. 2. FEG image of the sample 081118p4 (stored in alcohol) with magnification 150kx.

From figure 1, it was analyzed that for 081118p1 sample, a large displacement occurred from the initial reflectance in the first 30 days and then shows a tendency of stabilization. The behavior of the reflectance in the sample stored

in air (081118p3) is almost linear, having a continuous degradation over time. For sample stored in vacuum (081118p2) initially occurred a great displacement and after the first month the displacement was estabilized.

4. References

- [1]. AMARAL Jr, M. A. *Produção de Silício Poroso por processo eletroquímico e estudos da evolução morfológica e do tamanho dos cristalitos*. Tese de mestrado – INPE, São Jose dos Campos (2014).
- [2]. FILHO, D. O. T. et al. *Refletividade em Espelhos de Bragg de AlGaAsSb/AlAsSb sobre InP*. Semina: Ciências Exatas e Tecnológicas, Londrina, v. 24, p. 69-84 (2003).
- [3]. BERNI, L. A. GALVÃO, E. C. S. *Bragg reflectors fabricated from multilayered porous silicon*. Rev. Bras. Apl. Vac., Campinas, Vol. 37, N°3, pp. 129-133 (2018).
- [4]. PAIS, T. F., BELOTO, A. F., DE SOUZA GALVÃO, E. C., & BERNI, L. A. *Simple method for measuring the porosity, thickness and refractive index of porous silicon, based on the Fabry-Pérot interference spectrum*. Revista Brasileira de Aplicações de Vácuo, 35(3), 117-122. (2017).

Acknowledgments

Ana Carolina F. da Silva is grateful to CNPq for the financial support.

NEW SUBSTRATE HEATING FOR SPUTTERING DEPOSITION SYSTEM

Angel Fidel Vilche Peña^{1*}, Gleyson Tadeu de Almeida Santos, Camilla Martins Ruiz,
 Silvio Rainho Teixeira and Agda Eunice de Souza Albas
Departamento de Física, Faculdade de Ciências e Tecnologia
Universidade Estadual Paulista UNESP
 *Corresponding Author: *angel.pena@unesp.br*

1. Introduction

In order to obtain crystalline films some parameters are fundamental: deposition rate, substrate choice and temperature are the most relevant. The heating of the substrate is important among others, to promote chemical reactions or to facilitate the crystallization of the film. Usually in the Systems of deposition, whether thermal or by Sputtering the heating system[1] of substrate and optional (and very expensive); so our aim of this work is to provide a minimal configuration to obtain a substrate heating required to obtain strontium titanate films. Initially we had prepared a thermal heating system [1] but it was impractical for the source used (greater than 80A). It has been suggested to use halogen lamps to heat the substrate, capable of reaching temperatures above 300°C required to obtain a crystalline film.

2. Experimental

The sputtering deposition system Orion 5, has a removable blind cap, used when acquiring a substrate exchange system under high vacuum conditions. This cover has been replaced by another one with two electric passers for high vacuum. As heating element we used four quartz lamps of 127V, 100 W connected to a source of 220V. A K-type thermocouple placed on a metal conductor through a mechanical bypass. The temperature of the substrate was kept constant using a temperature controller. At the end of the desired heating the thermocouple is removed from the substrate holder, the final temperature of the controller is readjusted and film deposition is started.

3. Results and Discussions

A substrate, glass slide with a Cu coating, was used for testing. Cu deposition was placed to support a deposition of strontium titanate (200W RF, 30min).

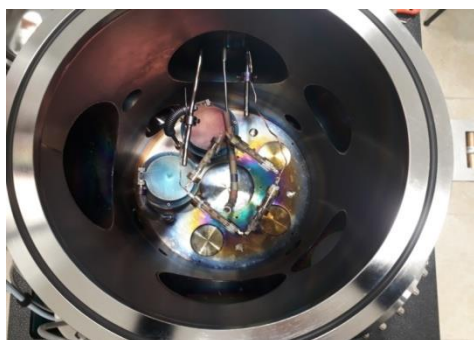


Fig. 1. Frontal view of the heating system. The lamps had a Cu deposition to increase the reflectivity. Glass rings were placed in each corner of the lamps joints to prevent short circuit when metal deposition occurs.

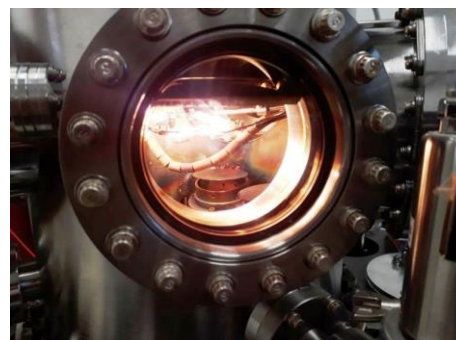


Fig. 2. Lateral view of the heating system.

The heating system is being tested by successfully passing these tests and we are preparing to deposit the desired barium titanate films and other ceramics materials like ZnO.

4. References

[1] F. Paulo Rouxinol; B. Cláudio Trasferetti; Richard Landers; Mário A. Bica de Moraes, J. Braz. Chem. Soc. vol.15 no.2 São Paulo Mar./Apr. 2004.

Acknowledgments

FAPESP 2013/07296-2 - CEPID - Centros de Pesquisa, Inovação e Difusão.

CHARACTERIZATION OF HYBRID WELDED JOINTS MADE OF DUAL PHASE STEEL AND ALUMINIUM ALLOY

Antonio dos Reis Faria Neto ^{1*}, Francisco Henrique Cappi de Freitas¹, Cristina Sayuri Fukugauchi², Antonio Jorge Abdalla³, Marcelo dos Santos Pereira¹

¹Universidade Estadual Paulista - Faculdade de Engenharia de Guaratinguetá

²Instituto Federal de Educação, Ciência e Tecnologia de São Paulo – São José dos Campos

³Instituto de Estudos Avançados – Departamento de Ciência e Tecnologia Aeroespacial – São José dos Campos

*Corresponding Author: antonio.fariant@gmail.com

1. Introduction

The application of more resistant materials (steels) welded to lower density materials (aluminum) has a great application potential. Several advantages of this process result from reduced weight, fewer parts, simplified assembly process and significant cost savings [1]. There are a large number of studies on the application of different welding technologies to join these alloys, but the problem of loss of strength in welding areas is always a major challenge which, up to now, because of the formation of fragile intermetallic compounds, has not been sorted out. Therefore, this work aims to analyze laser welded biphasic steel and aluminum alloy joints by macroscopic and microhardness characterization.

2. Experimental

Three samples of DP980 and AA6013-T4 sheet steel of 200 x 100 x 1.2 mm was taken with surfaces in a 600 mesh sandpaper. The samples were placed in an overlapped configuration. The equipment used was a fiber laser based on ytterbium-doped silica fiber, model IPG-YLR-2000, operative at 1070 nm wavelength and 2000 W of maximum power. Argon gas was used for weld pool protection with a flow rate of 10 L/min and the focal position aimed at 2.4 mm down and the welding speed was 25 mm/s. The main variable investigated was the power (set at 800, 900 and 1000 W). After welding the specimens, a metallographic (ASTM E3-11-2017) and microhardness (ASTM E384-2017) analysis of the samples was performed.

3. Results and Discussions

The results show that the power of 800W was insufficient to weld the sample while that of 1000W was excessive. It can also be observed that for the powers of 800 and 900W there are defects inside the weld bead, such as pores and cracks. The power of 900W proved efficient for steel and aluminum welding, as there is no evidence of defects and sufficient penetration of the aluminum alloy sheet. It can also be observed that the microhardness values increase as the weld gets closer. In the 800W sample, there is no decrease in microhardness, as there was no mixing of steel and aluminum due to lack of penetration. The decrease in microhardness in the central region of samples 2 and 3 may be due to the fusion of steel and aluminum.

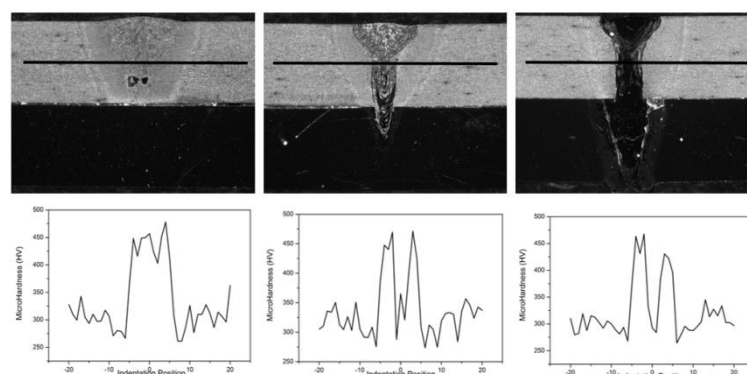


Fig. 1. Macrograph of the welded regions and the respective microhardness values of the central region of the DP980 Steel. a) 800W b) 900W and c) 1000W.

4. References

- [1]- P. Favia and R. D'Agostino, Surf. & Coat. Tech., **98**, 1102-1106, (1998). R. Shakeri *et al*, Journal of Light Metals, **2**, 95-110, (2002).
- [2]- ASTM E3-11: Standard Guide for Preparation of Metallographic Specimens, (2017).
- [3]-ASTM E384: Standard Test Method for Microindentation Hardness of Materials, (2017).

Acknowledgments

To UNESP PROPG and funding agency CAPES for supporting the activities.

EFFECT OF LASER CARBURIZING IN FATIGUE LIFE OF 300M STEEL

Abdalla, A. J.^{1*}, Santos, D.², Lima, E. S.^{1,3}, Vasconcelos, G.¹

¹Instituto de Estudos Avançados – IEAv

²Instituto de Aeronáutica e Espaço – IAE

³Instituto Tecnológico de Aeronáutica – ITA

*Corresponding Author: ajorgeabdalla@gmail.com

1. Introduction

300M steel used in this work is a high-strength steel and is used in aeronautic and aerospace industry. Thermochemical surface treatments are commonly applied to improve wear and corrosion properties. In this work laser carburizing was used [1, 2].

2. Experimental

Initially a heat treatment was performed to formation of the bainitic structure in 300 M steel. After that a specific surface treatments, using CO₂ laser, have been employed on fatigue specimens' surface of the steel, to introduce carbon into it. After the initial tests, a new heat treatment of quenching was applied. The analysis was made by optical and electronic microscopy. The mechanical properties were analyzed using microhardness, tensile and fatigue tests.

3. Results and Discussions

The coating showed an increase in the hardness of the layer formed on the surface, mainly, after de quenching treatment. The increase has reached 150 HV. The thickness of the compound layer was around 20 μm and the heat affected zone was around 45 μm for de laser carburizing (Fig. 1).

The tensile strength increase of 1490 MPa in 300 M steel as received to 1620 MPa in condition bainitic and to 1780 MPa in condition quenched and tempered. The steel that received a quenching showed better fatigue behavior as can seen in Fig.2.

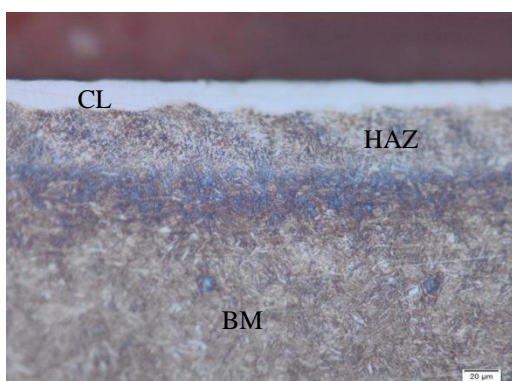


Fig. 1. Microstructure of 300 M steel laser carburized. (CL-compound layer; HAZ-heat affected zone; BM-basic material)

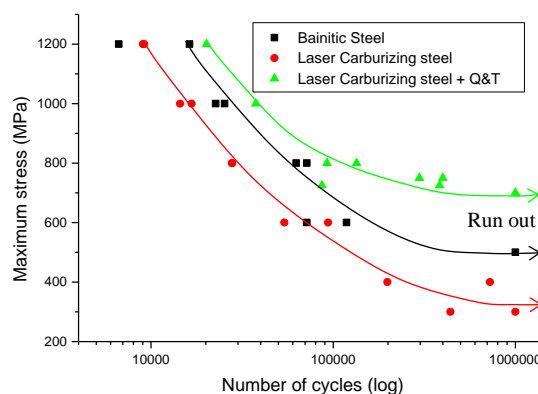


Fig. 2. Fatigue life of 300 M steel as received, after laser carburizing and laser carburizing and quenched and tempered (Q&T).

4. Conclusions

The treatment combined of laser carburizing an quenching and tempering heat treatment showed better properties in hardness of surface, tensile and fatigue.

4. References

- [1]. SANTOS, D.; VASCONCELOS, G.; ABDALLA, A. J.; LIMA, M.S.F.; SOUZA NETO, F. Surf. Characterization in a 300 M Bainitic Steel Laser Carburizing. *Procedia Engineering.*, v.114 (2015).
- [2]. CARDOSO, A. S.M.; ABDALLA, A.J.; LIMA, M.S.F.; SCHEID, VLADIMIR H. B.; BAPTISTA, C.A.R.P. *Trat.térm. e superfície dos aços 4340 e 300M após sold. laser. Ver.Bras.Vácuo on Line.*(2015).

Acknowledgments

The authors acknowledge the IEAv/DCTA and IAE/DCTA by the support for this research.

LOW TEMPERATURE ATMOSPHERIC PRESSURE PLASMA CAN REDUCE THE VIABILITY OF METHICILLIN-RESISTANT *Staphylococcus aureus* and *Enterococcus faecalis* BIOFILMS

Carvalho, R.C.R.¹, Oliveira, M.A.C.¹, Paiva C. A. ¹, Kostov, K.G.², Koga-Ito C.Y.^{1*}.

¹Institute of Science and Technology, São Paulo State University UNESP, São José dos Campos, Brazil.

²Department of Physics and Chemistry, São Paulo State University UNESP, Guaratinguetá, Brazil.

*Corresponding Author: cristiane.koga-ito@unesp.br

1. Introduction

Staphylococcus aureus and *Enterococcus faecalis* are the most prevalent bacterial species in chronic wound infections. The presence of biofilm in wounds affects negatively the healing process, increasing significantly the duration of treatment. Low temperature atmospheric pressure plasma (LTAPP) has been considered promising for medical applications due to antimicrobial activity. The aim was to evaluate in vitro the antimicrobial effects of LTAPP on mono-species biofilms formed by methicillin-resistant *Staphylococcus aureus* (MRSA) and *Enterococcus faecalis*.

2. Experimental

Mono-species biofilms were formed by methicillin-resistant *Staphylococcus aureus* (ATCC 33591) and *Enterococcus faecalis* (ATCC 29212). To obtain the biofilms, the strains were incubated at 37°C in triptic soy agar for 24 hours. Standardized suspensions with a concentration of 10⁶ cells per milliliter were prepared in sterile 0.9% NaCl solution with the aid of a spectrophotometer. Then, bacterial suspensions in triptic soy broth (TSB) were transferred to 96-well plates. The plates were incubated at 37°C for 90 minutes for pre-adhesion in a 120 rpm rotary shaker. The medium was then removed, and the biofilm washed with 200 µl of sterile 0.9% NaCl solution to remove non-adherent cells. After washing, 200 µl TSB was added to each well. The plates were incubated at 37°C for 48 hours. Culture medium was refreshed after 24 hours of incubation. After 48 h incubation, the culture medium was removed and the biofilms were washed with sterile 0.9% NaCl solution. Then, biofilms were exposed to LTAPP for 5 minutes. Helium (99.5% purity) was used as working gas (2.0 SLM) and the adopted parameters were 32 kHz frequency and 1.0 W potency. The distance between nozzle and biofilm surface was kept fixed at 1.5 cm. The number of colony forming units was determined by plating method. Non-exposed control was included. Results were compared by unpaired t test. The level of significance was set at 5%.

3. Results and Discussions

The exposition for 5 min was able to reduce significantly the number of MRSA (p=0.0203) (Figure 1) and *E. faecalis* (p<0.001) (Figure 2) viable cells in the mono-species biofilm when compared to non-exposed control.

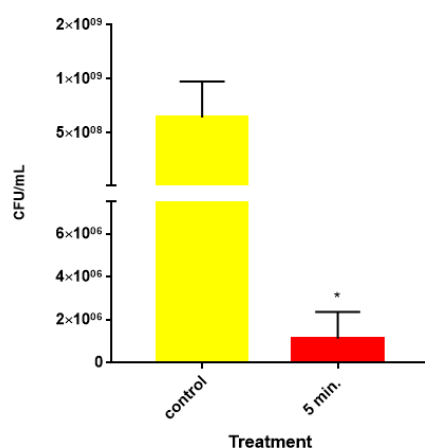


Fig. 1. Mean of colony forming units per milliliter (CFU/ml) of resistant methicillin-resistant *S. aureus* biofilm. *p<0.05

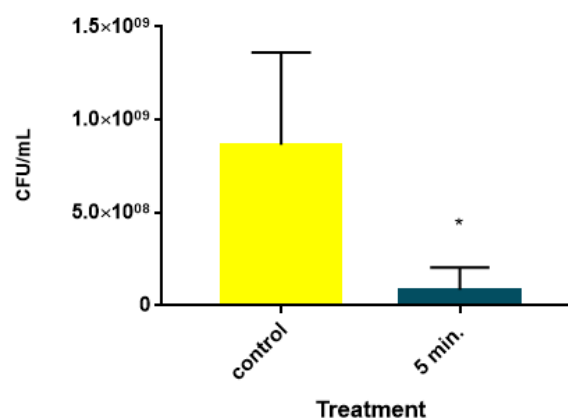


Fig. 2. Mean of colony forming units per milliliter (CFU/ml) of resistant *E. faecalis* biofilm. *p<0.05

Acknowledgments

Funding by CNPQ (National Council for Scientific and Technological Development).

CHARACTERISTICS OF AN ATMOSPHERIC PLASMA VAPOR DEPOSITION DEVICE FOR COATING IN DIELECTRIC SURFACES

Thiago J Michelin*, Mauricio A. Algatti, Renata Angelovska, Stella Sochan and Milton E. Kayama
*Laboratory of Plasma and Applications, São Paulo State University, Campus of Guaratinguetá,
 12516-410, Guaratinguetá, SP, Brazil*

*Corresponding Author: thiago.michelin@unesp.br

1. Introduction

Non-thermal atmospheric plasmas carry the intrinsic feature of operating in low applied voltage and high power density in its media. They are very suitable for applications in medical area and in local material surface treatment as well. An extended application in deposition of thin films in dielectric surfaces is presented in this work using vapor of the monomer dragged by an inert gas prior to the plasma formation.

2. Experimental

Figure 1 illustrates the experimental scheme of the device, which is an arrangement of two electrodes in the form of a needle and a thin disk. The disk can be placed at any position along the capillary's length. There are two gas inputs. The first one (right most input in Figure 1) directs the gas to flow through the needle, whereas the second input directs the gas to flow around the outside the needle while still inside the tube of glass. Electrical discharges take place in the small gap between the needle and the disk, with the tube of glass acting as the insulating dielectric barrier. The input source applies a sinusoidal, 37 kHz, signal to the needle electrode. Different voltage values were applied to the electrodes. In order to measure power, the monitor capacitor method was employed, where the capacitor has a capacitance of 3.3 nF.

3. Results and Discussions

Figure 2 illustrates the power measured for the electrical discharge with varying values for the applied voltage. Each curve represents power characteristics at a given flow rate. The mass monomer collected by the gas can be controlled by the flow rate and the temperature in the monomer reservoir. We used HMDSO at 25°C. The gas was industrial argon with flow rate in the range of 0.5-1.0 L/min and the substrate was glass. The structure of the transparent films had the same structure as the original monomer according to the Fourier infrared spectroscopy. Static contact angle measurement indicated the typical rise of the hydrophobicity on the surface. The achieved results have shown a wide range of application of the device in deposition of films at atmospheric pressure.

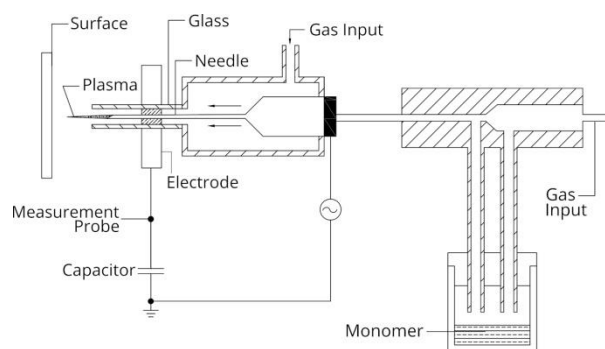


Fig. 1. Experimental scheme of the plasma device.

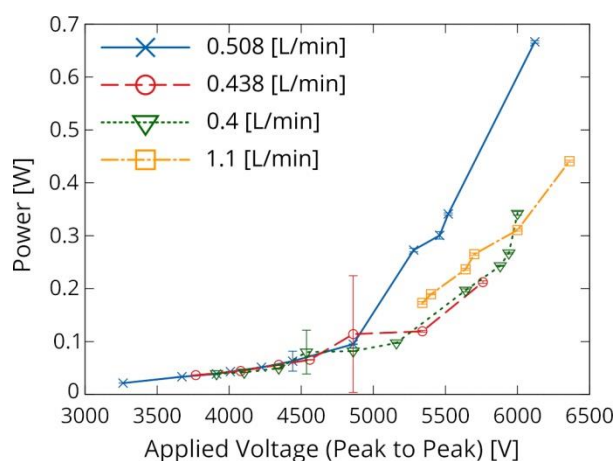


Fig. 2 Power measured from the discharge with varying applied voltage at different gas flow conditions.

References

- [1]- XinPei Lu, Stephan Reuter, Mounir Laroussi, DaWei Liu; *"Nonequilibrium Atmospheric Pressure Plasma Jets Fundamentals, Diagnostics, and Medical Applications"*, CRC Press, Taylor & Francis Group, New York, (2019).
- [2]- Hans-Robert Metelmann, Thomas von Woedtke, Klaus-Dieter Weltmann; *"Comprehensive Clinical Plasma Medicine - Cold Physical Plasma for Medical Application"*, Springer Verlag, Berlin, (2016).

DEVELOPMENT AND MECHANICAL CHARACTERIZATION OF IMPLANTS FOR OSTEOSYNTHESIS, BASED ON LDPE/GO NANOCOMPOSITES

Silva M. M. B*, Tegon C. C., Melo M., Oliveira A., Massi M.

Mackenzie Presbyterian University, School of Engineering-PPGEMN, Rua da Consolação, 896 - 01302-907 - São Paulo / SP - Brazil

1. Introduction

Nowadays, for the production of osteosynthesis materials and prostheses expensive materials have been used, such as titanium, which has an expensive cost, due to the large material waste [1]. Besides that, there are different options in the market that are difficult to develop and manufactured [2]. Thus, the use of complex three-dimensional structures in polymeric materials can have advantages over titanium materials, like reduced surgery time, greater precision and adaptation of the material to bone tissue, and better results in reconstruction prostheses [3]. The main objective of this work was the development and the analysis of mechanical properties of low-density polyethylene (LDPE)/graphene oxide nanocomposite, as well as the study of finite elements with complex geometries, for 3D printing implants. This study has become relevant for the development of new alternative materials with similar or better mechanical properties than the existing materials.

2. Experimental

The nanocomposite (LDPE + GO) was processed in double screw extruder and characterized by the techniques of infrared absorption spectroscopy, x-ray diffraction, scanning optical microscopy, thermogravimetric analysis and differential exploratory calorimetry. For the mechanical tests, specimens were made by 3D printing process, according to ASTM standards and two (2) prototypes with complex geometries were printed.

3. Results and Discussions

Through formulations with different concentrations of GO (0.5% wt, 1.0% wt and 1.5% wt) and through processing techniques of pre-mixing, milling and extrusion of LDPE + GO, crystallinity and chemical structure has been modified. These modifications allowed changes in the mechanical resistance that were shown in the mechanical tests such as tensile strength and impact resistance.

4. References

- [1]- Philippe, B. (2013). Custom-made prefabricated titanium miniplates in le Fort i osteotomies: Principles, procedure and clinical insights. *International Journal of Oral and Maxillofacial Surgery*, 42(8), 1001–1006. <http://doi.org/10.1016/j.ijom.2012.12.013>
- [2]- Qassemyar, Q., Assouly, N., Temam, S., & Kolb, F. (2017). Use of a three-dimensional custom-made porous titanium prosthesis for mandibular body reconstruction. *International Journal of Oral and Maxillofacial Surgery*, 46(10), 1248–1251. <http://doi.org/10.1016/j.ijom.2017.06.001>
- [3]- Luo, M., Yang, X., Wang, Q., Li, C., Yin, Y., & Han, X. (2018). Skeletal stability following bioresorbable versus titanium fixation in orthognathic surgery: a systematic review and meta-analysis. *International Journal of Oral and Maxillofacial Surgery*, 47(2), 141–151. <http://doi.org/10.1016/j.ijom.2017.09.013>

Acknowledgments

The authors thank to Mackpesquisa-Mackenzie Presbyterian University and the Brazilian agency CAPES for financial support.

EFFECT OF DLC FILM IN THE WEAR RESISTANCE OF THE 7050-T7451 ALUMINUM ALLOYCésar A. A. Júnior.^{1*}, Larissa S. de Almeida², Marcos D. Manfrinato^{1,2} Luciana S. Rossino^{1,2}¹Sorocaba Technology College FATEC²São Carlos Federal University UFSCAR – Sorocaba Campus**1. Introduction**

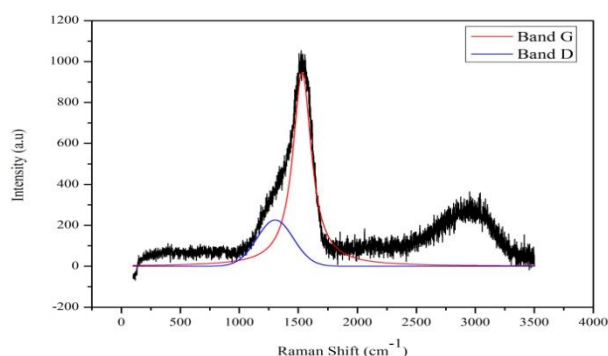
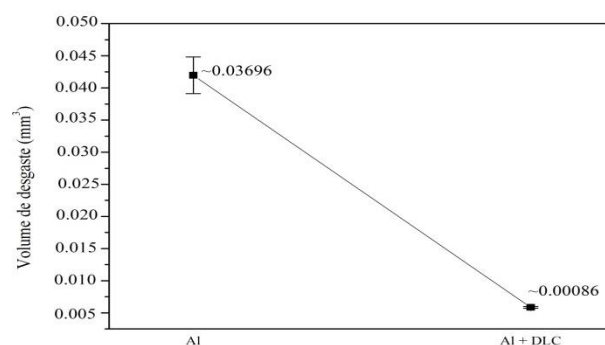
Aluminum alloys have high mechanical strength and high ductility when subjected to aging treatment, but their low hardness may compromise the wear resistance of this material. DLC films have properties such as chemical inertness, low friction coefficient, high hardness and very high wear resistance [1]. This work aims to study the deposition and wear resistance of DLC film on the surface of AL7050-T7451 alloy.

2. Experimental

The Al7050-T7451 samples, polished and washed with isopropyl alcohol, were subjected to film deposition by PECVD using DC-pulsed source. Plasma ablation cleaning was performed under two conditions: 50% Ar and 50% H₂ with 1 Torr pressure for 30 min., and 50% Ar with 50% H₂ at a pressure of 2 Torr for 30 min. After ablation, a hydrogenated amorphous silicon deposition was performed using 70% HMDSO as precursor with 30% Ar for 15 min. with pressure of 1×10^{-1} Torr. Then the DLC treatment was performed using 90% methane gas and 10% Ar at a working pressure of 3.5×10^{-1} Torr for 2 hours. The treatment was characterized by Raman spectrometry and microabrasive wear test by fixed ball. The hydrogen percentage of the film was calculated taking into account Casiragha's work [2].

3. Results and Discussions

For the ablation treatment performed with 1 Torr it was possible to obtain the cleaning without changing the sample surface, being the most appropriate this process. For the ablation treatment using 2 Torr, the maximum deposition time was 4 minutes, having to interrupt the treatment due to the high luminescence and heating of the sample leaving it with reliefs and porous point. The deposited DLC film demonstrated homogeneous and good adhesion on the material surface. The results investigated by Raman spectroscopy, shown in Fig. 1, demonstrated characteristics of the formation of the DLC film by the presence of the G band at 1530 cm^{-1} and the D band at 1304 cm^{-1} . The ID/IG relationship with G band demonstrated a topological disorder of the graphite layer and loss of aromatic bonds, weakening the bonds compared to perfect graphite, classified as a-C. The theoretical hydrogen percentage of the film was 43% H and is classified as a-C:H [3]. Fig. 2 show that the sample with DLC film considerably increased the wear resistance of the material studied, proving that this treatment is effective in increasing the wear resistance of studied material.

**Fig. 1.** Raman spectrum of substrate**Fig. 2.** Wear volume studied samples**4. References**

- [1]-Grill, A. Diamond-like carbon: state of the art. *Diamond and Related Materials*, v. 8, n.2-5, p. 428-434, 1999.
- [2] Casiraghi, C.; Ferrari, A.; Robertson, J. Raman spectroscopy of hydrogenated amorphous carbons. *Physical Review B*, v. 72, n. 8, p. 085401.1-085401.14, 2005.
- [3] Robertson, J. Diamond-like amorphous carbon. *Materials Science and Engineering*, v. 37, n. 4-6, p. 129-281, 2002.

Acknowledgments

We would like to thank the Fatec Sorocaba and the LabTES for the infrastructure.

SPRINGBACK OF HIGH STRENGTH STEEL DP 800

Christyane Oliveira Leão Almeida^{1*}, Luís Henrique Lopes Lima², Dayane Oliveira Leão Almeida³ and Marcelo dos Santos Pereira¹

¹São Paulo State University "Júlio de Mesquita Filho" UNESP

²Federal University of Juiz de Fora UFJF

³São Paulo State University UNESP

*Corresponding Author: christyaneleao@gmail.com

1. Introduction

Modern car feature lighter, more comfortable and safer building solutions, while meeting the requirements for stiffness, shock resistance and energy absorption. The increasingly thin steel sheets used in vehicle structures, because having lower density and better absorb impact when compared to conventional materials [ref. number 1].

2. Experimental

To analyze the microstructure of the high strength steel DP 800 (dual phase), the standard procedure was performed in the metallography steps (ASTME3-10). The tensile and U bending test was based on the E8 / E8M and E290 standards respectively. They were subjected to conformation until the internal bending angle reached 30° and 90° (Fig. 1). The desired angle was achieved by controlling the y-axis punch displacement with a descent velocity of 4 and 8 mm / min, along with a digital inclinometer, magnetic base. The punch was removed from the material 20 seconds after reaching the desired angle bending, where the angles shown in figure 1 are in relation to the horizontal axis and the angle under study is the internal angle of the plates, or between the ends of the plate. Then, the new bending angle was measured to check for elastic return. These measurements continued to be made for the 24, 48, 72, 96 and 120 hours post-conformation periods using an angle meter or better known as a professional digital ruler.

3. Results and Discussions

The values of the elastic return change with the variation of the punching speeds, with the predetermined angles and the observation time of this effect. It can be seen from Fig. 2 that, for the predetermined angle of 30 degrees, the springback values are higher, between 16,5 and 17,5 degrees, but for the angles of 90 degrees, the elastic return is smaller, between 7 and 9 degrees. Springback values increased with increasing punching speed (4 to 8 mm / min) for both predetermined angles (30 and 90 degrees). Through statistical data, hypothesis test "A Nova" and "Tukey", it is concluded that there is a significant difference between each observation day (5 days).



Fig. 1. U bending test for predetermined angles of 30° and 90° respectively. Predetermined angles that appear in the image refer to the x axis.

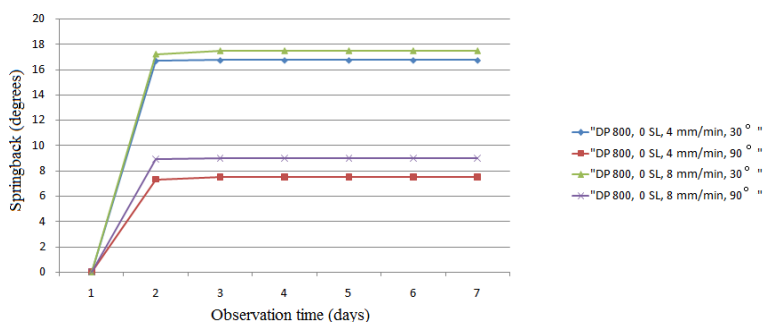


Fig. 2. Springback (degrees) x Time (days) Comparison of return elastic values with variation of punch speed and predetermined angle.

4. References

[1]- Ximenes Dias, E.; Horimoto, L. Y. R.; Pereira, M. S., 2014. Análise metalográfica de um aço de fases complexas por microscopia óptica. Revista Brasileira de Aplicações de Vácuo, [s. l.], v. 33, n. 1–2, p. 7, 2014.

Acknowledgments

Prof. Dr. Marcelo dos Santos Pereira, CAPES, Prof. Dr. Luis Rogério de Oliveira Hein, Flávio Felício da Silva, Fatec's technician from Pindamonhangaba, the educational institutions UNESP and UFJF.

OPTICAL CHANGES IN CARBON FIBER COATED WITH TiO₂ THIN FILMS BY ATOMIC LAYER DEPOSITION TECHNIQUE

Dias, V. M. *, Pessoa, R. S., Maciel, H. S.

*Laboratório de Plasmas e Processos - LPP - Instituto Tecnológico de Aeronáutica***Corresponding Author: vanny@ita.br*

1. Introduction

The carbon fiber is used due to excellent properties such as mechanical, thermal conductivity and high thermal resistance, but a problem for new applications is its black color [1]. The atomic layer deposition (ALD) stands out in relation to other technologies namely reactive sputtering, electrochemical deposition and chemical vapor deposition (CVD), since it allows depositing more conformal layers in complex 3D substrates such as fibers and textiles [2]. Among the materials synthesized by the ALD technique, Titanium dioxide (TiO_2) is often used due to improved photocatalytic, chemical and optical properties [3]. This work focused in change the color of carbon fiber by using TiO_2 thin films aiming applications in the military, automotive, chemical and energy processes.

2. Experimental

Carbon fibers samples were coated with TiO_2 thin film by ALD with different reaction cycles (500, 1000, 2000 and 3000 cycles) and substrate temperature of 100°C . Subsequently, the TiO_2 -covered carbon fibers were analyzed for its morphology and chemistry by Field Emission Gun (FEG) Scanning Electron Microscopy technique coupled with energy dispersive spectroscopy (EDS) and for optical properties by using spectrophotometry technique with method color scale L^* (lightness), a^* axis points the red (positive) to green (negative) and b^* points the yellow (positive) to blue (negative) and the points is positioned on the center (a^*, b^*)=(0,0) on the coordinate plan.

3. Results and Discussions

Results indicated that ALD technique for coatings promoted a considerable modification in the color and the surface. The Fig. 1 indicated that carbon fiber samples coated with TiO_2 thin films showed different colors on the coordinate plan where can be seen for 500 cycles the color blue, 1000 green, 2000 almost yellow going to the red and for 3000 cycles blue, however each sample within four-square. The FEG image shown the surface looked smooth, uniform and compact particles were deposited on the surface of fiber carbon. Finally is possible to confirm that the colors can be adjusted and controlled by the thickness on ALD.

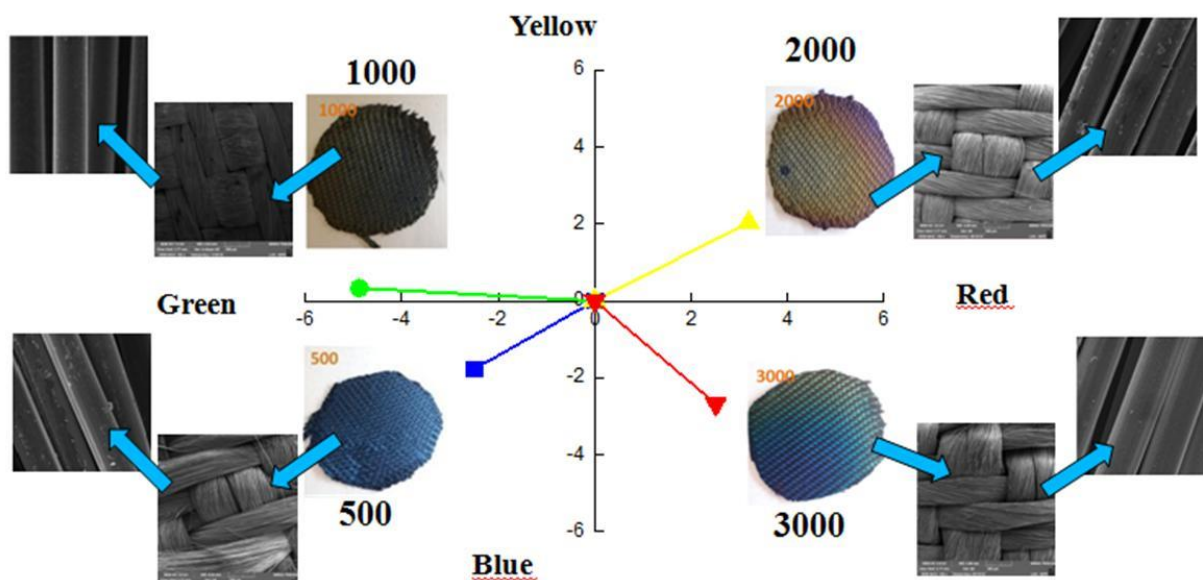


Fig. 1 Distribution of chromaticity indices, a^* and b^* for: a) 500, b)1000, c) 2000 and d) 3000 cycles

4. References

- [1]- Chen, F. et al, ACS Nano-American Chemical Society, **11**, 10330-10336, (2017).
- [2]- Marin, E. et al, Surface & Coatings Technology, **211**, 84-88 (2012).
- [3]- Shan, C. et al, Surface & Coatings Technology, **202**, 2399-2402 (2008).

Acknowledgments

Capes (Finance Code 001), FAPESP, .CNPQ, FINESP, LAS-INPE and Golden Technology.

SURFACE CHARACTERIZATION OF MAO-TREATED Ti-15Zr-15Mo-(1,3)Ag ALLOYS FOR USE AS BIOMEDICAL IMPLANTS

Torrento, J.E.¹, Grandini, C.R.¹, Sousa, T.S.P.²; Rocha, L.A.²; Sottovia, L.⁴; Cruz, N.C.⁴; Correa, D.R.N.^{1,2,3,*}

¹UNESP – Univ. Estadual Paulista, Laboratório de Anelasticidade e Biomateriais, Bauru (SP), Brazil

²IBTN/Br – Brazilian Branch Inst. of Biomaterials, Tribocorrosion and Nanomedicine, Bauru (SP), Brazil

³IFSP – Grupo de Pesquisa em Materiais Metálicos Avançados, Sorocaba (SP), Brazil

⁴UNESP – Univ. Estadual Paulista, Laboratório de Plasmas Tecnológicos, Sorocaba (SP), Brazil

*Corresponding Author: diego.correa@ifsp.edu.br

1. Introduction

Ti and its alloys are mainly employed as biomaterials due to their well-known favorable properties. Ti-15Zr-Mo-xAg alloys have been recently developed for use as biomaterials, combining low Young's modulus, high specific strength, verified biocompatibility, and potential antibacterial effects [1]. Surface modifications have been applied on titanium surfaces to enhance wear and corrosion resistance against the biological host. Micro-arc oxidation (MAO) is a low-cost and versatile treatment, which tend to grow a thick and hard TiO₂ oxide layer along the titanium surface [2]. This study aims to analyze the surface characteristics of MAO-treated Ti-15Zr-15Mo-xAg (1 and 3 wt.%) alloys for potential use as biomaterials.

2. Experimental

Ti-15Zr-15Mo-(1,3)Ag (wt.%) alloys were produced by argon arc melting from commercially pure metals. After that, the samples were homogenized (vacuum of 10⁻⁵ Torr, 1273 K and furnace cooling), hot-forged (1273 K and air-cooling), and solution treated (vacuum of 10⁻⁵ Torr, 1123 K and water-cooling). MAO treatment were carried out in a DC power source at room temperature, 300 V, 2.5 A, and during 60 s. The electrolyte was composed by 0.35M calcium acetate monohydrate, 0.02M β-glycerol phosphate and 0.1M magnesium acetate tetrahydrate. Chemical and phase composition was evaluated by XRD, EDS, XPS and FTIR analyses. Topographical, morphological and cross-sectional analyses were performed by SEM imaging. Surface properties were analyzed by profilometry and contact angle measurements.

3. Results and Discussions

The samples exhibited some anatase phase peaks (TiO₂) in the XRD patterns, with a porous morphology (Fig. 1). EDS results indicated the predominance of elements Ti and Zr and the successful incorporation of Ca, P and Mg ions into the oxide layers (Fig. 2). XPS and FTIR analyses corroborated the EDS results. The profilometry and contact angle measurements indicated that the samples possessed high potential to be applied as biomedical implants.

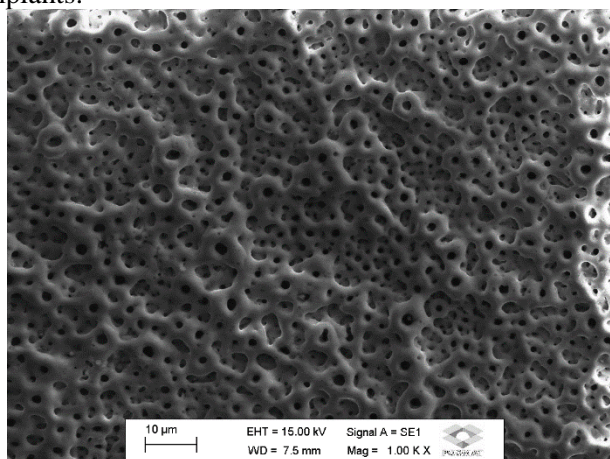


Fig. 1. SEM image of the MAO-treated Ti-15Zr-15Mo-1Ag sample.

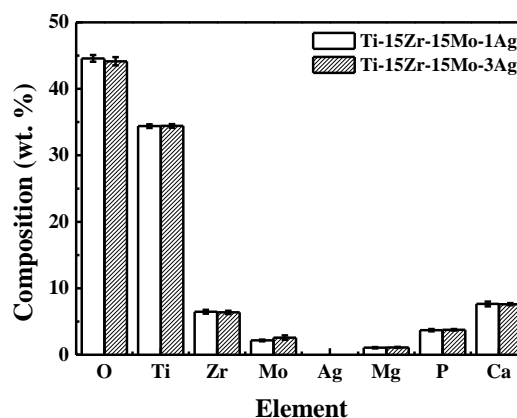


Fig. 2. Semi-quantitative EDS analysis of the MAO-treated surfaces.

4. References

- [1] D.R.N. Correa et al., Journal of Alloys and Compounds, **749**, 163-171, (2018).
 [2] D.R.N. Correa et al., Surface and Coatings Technology, **344**, 373-382, (2018).

Acknowledgments

The authors acknowledge the Brazilian funding agencies CNPq and FAPESP for the financial support.

OPTICAL PROPERTIES OF HIGHLY TEXTURED GALLIUM NITRIDE FILMS ELUCIDATED BY SPECTROSCOPIC ELLIPSOMETRY

D. M. G. Leite^{1*}, I. M. Horta¹, R. S. de Oliveira¹, H. A. Folli¹, C. Stegemann¹,

¹Technological Institute of Aeronautics, Plasmas and Processes Laboratory, São José dos Campos, SP, Brazil.

²Universidade Federal da Grande Dourados, Grupo de Pesquisa em Materiais Fotônicos e Energia Renovável (MaFER), Dourados, MS, Brazil.

³Mackenzie Presbyterian University, School of Engineering-PPGEMN, São Paulo, SP, Brazil.

*Corresponding Author: leite@ita.br

1. Introduction

Low temperature reactive sputtering is known to produce amorphous or nanocrystalline films with columnar microstructure aligned with the growth direction [1,2]. In the special case of wurtzite GaN, it is common to observe the coincidence of the crystallographic c-axis with the columns direction [3]. In this scenario, sputtered GaN films are likely to show interesting anisotropic behaviors, mainly those related to mechanical, electronic and optical properties. In this work, optical properties of highly textured sputtered GaN films are studied by Spectroscopic Ellipsometry (SE). By varying the angle of incidence (AOI) from 30° to 80° it is expected to separate the in plane and out of plane contributions from the refractive index, optical gap and other optical constants, in order to introduce a methodology of studying the texture of the films directly by SE.

2. Experimental

Representative GaN films, with different degrees of crystallographic texture, were grown by planar reactive sputtering technique onto Si (100) substrates. The films have wurtzite nanostructure highly textured with c-axis perpendicular to substrate surface as demonstrated by XRD experiments. These films were then submitted to SE experiments in a HORIBA Uvisel II ellipsometer. The spectra were obtained in the spectroscopic mode in the 0.6 to 6.0 eV energy range with fixed AOI ranging from 35° to 80°. The outputs were then modeled by the DeltaPsi® software in order to calculate the refractive index dispersion and the optical gap in each situation.

3. Results and Discussions

As preliminary results, Fig. 1 and Fig. 2 show, respectively, the n and k dispersions for a set of GaN samples obtained by SE with AOI = 70°. These and further results are discussed in terms of the intrinsic and extrinsic anisotropic responses of the wurtzite nanocolumns.

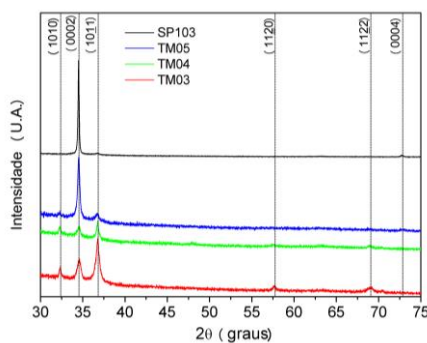


Fig. 1. XRD patterns of GaN samples

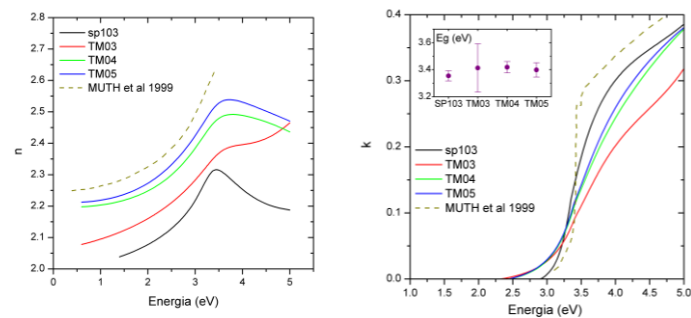


Fig. 2. Refractive index (left) and extension coefficient (right) dispersions of different GaN samples obtained by SE.

4. References

- [1] D. L. Smith, *Thin Film Deposition: Principles and Practice*. Boston: McGraw-Hill Inc., 1995.
- [2] D. Depla, *Magnetrons, reactive gases and sputtering*. Diederik Depla, 2013.
- [3] D. M. G. Leite, et. al., *J. Cryst. Growth*, vol. 327, no. 1, pp. 209–214, 2011.

Acknowledgments

Fapesp (2015/06241-5, 2011/05772-0), CAPES (PG-FIS/ITA, 88881.122156/2016-01, 8887.157419/2017-00), CNPq (143273/2018-3, 159754/2018-6), FINEP

EFFECT OF LASER CEMENTATION PROCESS ON HARDNESS PROPERTIES AND WEAR RATE SAE 8620 STEEL

Santos, E. L.^{1,2,3*}, Abdalla, A. J.², Siqueira, R. H. M.², Rodrigues, H. L.³, Volu, R. M.²

¹Instituto de Tecnológico de Aeronáutica (ITA)

²*Instituto de Estudos Avançados (IEAv)*³*Universidade Estadual Paulista (FEG-UNESP)***Corresponding Author: dudasantosl@outlook.com*

1. Introduction

The SAE 8620 steel is considered a high strength material, generally applied to gears, being usually heat treated to alter the mechanical properties thereof. Laser carburizing is studied with the purpose of improving the conventional process by having a greater precision on the application site, be fast application and more uniform result over the entire length of the treated material. To evaluate the wear rate, the volume of material removed during the wear test is measured, considering a certain force, the distance traveled and the speed of the test.

2. Theory

This work was used from SAE 8620 steel in the shape of disks with a diameter of 35 mm in annealed state. The unit's surface fumone black was deposited as a carbon source, and the surface irradiation CO₂ laser was applied as a 50W current output, as a nitrogen to an irradiated phase protector, avoiding oxidation, velocity 50 mm / sec at 600 and 800 dpi, respectively corresponding to a sample I and II.

The Vickers hardness test was performed on the samples and the disc pin was released, with a 5N load and forming a 4mm track, which caused the roughness and volume consolidation test to be removed from the image analysis given by optical profilometry.

3. Results and Discussions

Hardness test was performed on both samples, I, II and S / T (untreated), with results shown in table 1. It is observed that the average hardness measurements of sample II are higher than the average of sample I, because the laser parameters were more intense, with quenching of the region near the surface, thus forming martensite phase in the structure. The S / T sample exhibited a lower hardness result because of its structure having the ferrite and perlite phase. Table 1 shows the volume of material removed during the wear test and the wear rate, with sample II removing material less than I due to hardness, but the S / T sample showed a reduction in wear rate. and in the volume of material removed. This phenomenon indicates that the carburizing layer was removed during the wear test.

Table 1 – Hardness and wear results

Test	Hardness (Kgf/mm ²)	Volume (mm ³)	Wear Rate K (mm ³ /Nm)
I	706,58	0,034640	7,328 e-4
II	827,83	0,013414	2,6828 e-4
S/T	218,15	0,0005486	1,097 e-5

4. References

- [1]- ABDALLA, A. J.; Scheid, V. H. B. Tratamentos termoquímicos a plasma em aços carbono. Revista Corrosão e Proteção de Materiais, Vol. 25, No. 3, p. 92 – 96. 2006.
- [2]- BARROSO, E. A. Influência da carbonetação a laser e nitretação a plasma nas propriedades tribológicas do par aço AISI/SAE 4340 e liga bronzalumínio 630. Tese (Doutorado em Engenharia de Materiais e Tecnologia) - Universidade Estadual Paulista – Guaratinguetá, 2017.
- [3]- OLIVEIRA, R.J.B.; Siqueira, R.H.M.; Lima, M.S.F. Microstructure and wear behaviour of laser hardened SAE 4130 steels. Int. J. Surface Science and Engineering, Vol. 12, No. 2, 2018.

Acknowledgments

One of us, i.e., E. L. S., would like to thank Feg / UNESP, ITA and IEAv for the opportunity to conduct this research.

PROPERTIES ANALYSIS OF HARDNESS AND METALLOGRAPHIC OF SAE 8620 STEEL CARBONIZED BY LASER

Santos, E. L.^{1,2,3*}, Abdalla, A. J.², Siqueira, R. H. M.², Rodrigues, H. L.³, Hein, L. R. O.³

¹*Instituto de Tecnológico de Aeronáutica (ITA)*

²*Instituto de Estudos Avançados (IEAv)*³*Universidade Estadual Paulista (FEG-UNESP)**Corresponding Author: *dudasantosl@outlook.com*

1. Introduction

The carburizing process consists of increasing the carbon content of the material surface to obtain an increase in hardness and changes in tribological properties. Laser carburizing modifies the microstructure by self-quenching, making further heat treatment unnecessary. AISI 8620 steel is characterized by its composition of chromium, nickel, molybdenum and about 0.20% by weight of carbon, has good machinability and temperability, being applied to shafts and gears.

2. Experimental

The AISI 8620 steel, based on table 1, was laser carburized by applying 4 passes using a 50 W power laser, 600 dots per inch (dpi) resolution, 50 mm / s speed.

Table 1 – Chemical Composition of SAE 8620 Steel

Element	C	Cr	Mn	Mo	Ni	Si
Wt %	0,18-0,23	0,40-0,60	0,70-0,90	0,15-0,25	0,40-0,7	0,15-0,35

3. Results and Discussions

The carbon content was increased by adding carbon black powder to the surface of the sample to be treated by modifying the microstructure composition, forming a hardened layer about 20µm deep (region I), having an interface (region II) between the formed layer and the base material (MB), as can be observed in figure 1. Having the interface composed of slats of martensite, having a hardness higher than the base material, which is about 180 HV, and lower than the hardened and tempered layer of the surface, which presented about 710 HV hardness as shown in the graph. Figure 2 showing the hardness difference between these three regions.

Figure 1- Metallography 8620 Steel
TT

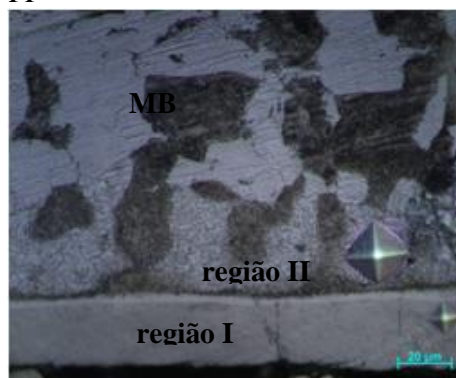
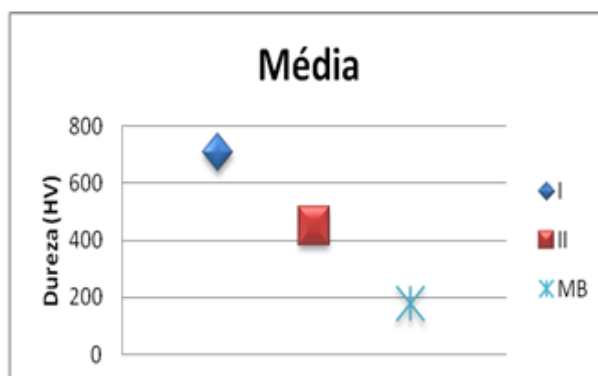


Figure 2 – Analysis of hardness



4. References

- [1]- Barroso, E. A. Influência da carbonetação a laser e nitretação a plasma nas propriedades tribológicas do par aço AISI/SAE 4340 e liga bronzalúminio 630. Tes (doutorado)- FEG/UNESP. 169 p. 2017.
- [2]- Da Silva, D. L. G. A. Da Silva, L. S. Análise das propriedades mecânicas do aço sae/aisi 8620 quando submetidos aos tratamentos térmicos de cementação e têmpera. Revista Perspectivas Online: Exatas e Engenharias – Anais do VI CICC V. 08, Nº 22, Suplemento, 2018.
- [3]- Oliveira, R.J.B., Siqueira, R.H.M. and Lima, M.S.F. Microstructure and wear behaviour of laser hardened SAE 4130 steels, Int. J. Surface Science and Engineering, Vol. 12, No. 2, 161–170 p. 2018.

Acknowledgments

One of us, i.e., E. L. S., would like to thank Feg / UNESP, ITA and IEAv for the opportunity to conduct this research.

EFFECT OF INTERCRITICAL HEAT TREATMENT AFTER LASER WELDING OF DISSIMILAR STEELS: DP600 AND 300M

Zanni E. G. S.^{1,2}, Ferreira C. C. A.¹, Harada A. T.^{1,2}, Abdalla A. J.^{1*}
¹*Instituto de Estudos Avançados (IEAv),*

²Instituto Tecnológico de Aeronáutica (ITA)
 *Corresponding Author: *ajorgeabdalla@gmail.com*

1. Introduction

In this work, adequate parameters were studied to weld the DP600 and 300M steels with a fiber laser. The integrity of the weld and the mechanical properties of the welded joint were analyzed such as: hardness and tensile strength. The micro structural characterization allows us to understand the structural changes that occur due to the welding process. It was possible to identify, through analysis, the phases present in the material and the fusion between them, proving the effectiveness of the weld [1]. Through the hardness profile, it was observed that in the region of the weld and the HAZ (thermally affected zone) there was a significant increase in the hardness values in relation to the hardness of the base material. The efficiency of the weld can also be proven through the tensile test, since there was no rupture of the material in the welded region, but in the DP600 steel that has less mechanical strength [2].

2. Experimental

The materials used were 300M steel and DP 600 steel, these steels were received in sheet form with the following thicknesses: DP 600 with 2.19 mm and 300 M with 3.29 mm, which were cut, machined and ground, subsequently these plates were welded with a continuous CO2 laser. The parameters used were taken based on previous work, such as that studied by Cardoso (2011). The welding parameters shown in Table 1 were adopted.

Table 1: Welding parameters

Power	1800 W
Speed	50 mm / s
Laser Pass	2 passes (one on each side)
Gas Flow	Argon gas 10 l / min
Focus	2.2 mm (on the surface of the thinner sheet)

After welding, the plates received a surface treatment (Intercritical heat treatment), that was realizing at 760°C, with oil cooling. After, they were tested and compared in hardness and tensile tests were performed to analyze their properties.

3. Results and Discussions

The two conditions (base material and treated material) was compared in hardness test and tension test. How show the figure 1, the hardness test produced a beneficial effect in treated material, because occurred smooth transition from to steel the lowest hardness to higher hardness, which improved compatibility between lower and higher hardness phases.

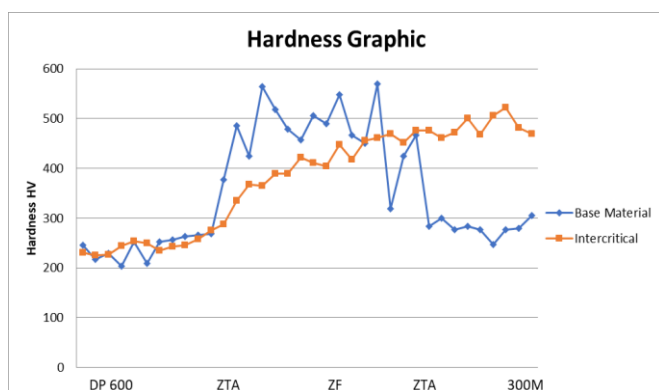


Figure 1: Hardness graphic

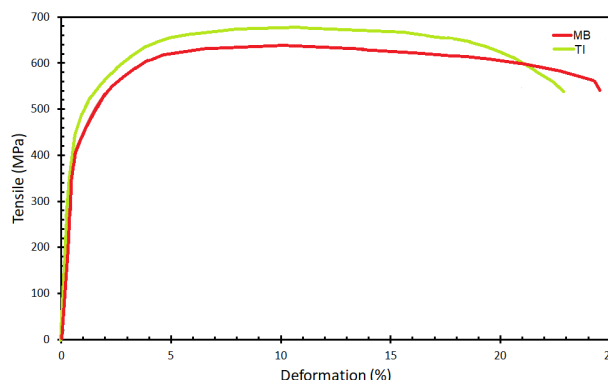


Figure 2: Tensile graphic

As can be seen in figure 2, the intercritical heat treatment improved the strength and flow limit, maintaining basically the same ductility, with approximately 25% deformation in both situations.

4. References

[1]-CARDOSO, A. S. M. Mechanical and microstructural characterization of SAE 4340 and 300M steels after laser welding and surface treatment of plasma nitriding. Dissertation (Master of Science - Postgraduate Program in Materials Engineering) - Lorena School of Engineering University of São Paulo, 2011.

- [2]- ANDRADE, S.L.; TAISS, J.M.; ROSA, L.K. Steel in the automobile of the future. (in CD-Rom) In: 57th Congress of the Brazilian Association of Metallurgy and Materials, São Paulo, Brazil, 2002 July, Anais São Paulo, Brazilian Association of Metallurgy and Materials, 2002.

Acknowledgments

The present authors thank Dr. Antonio Jorge Abdalla, IEAv researcher, for their support and guidance during the development of the works presented here and Dr. Rafael Siqueira for their collaboration in the development of the work. They also thank IEAv for the opportunity to conduct this research.

MECHANICAL CHARACTERIZATION OF COMPOSITE EPOXY RESIN REINFORCED WITH FIBERGLASS TYPE-E FOR APPLICATION IN STRUCTURES

Philipe Henrique Mendes¹, Matheus José da Silva², Mauricio Eduardo Lopes¹, Lidiane Gomes da Silva¹

¹University Center of Itajubá - FEPI

²University Federal of Itajubá - UNIFEI

Corresponding Author: *philipe.mendes@gmail.com*

1. Introduction

Civilization entered a new era, causing society to evolve creating materials from existing ones, satisfying their needs. Through the advancement of materials science, resin and fiber composites of different types emerged, where, for engineering is the combination of two or more materials resulting in a material whose property is superior. Thus, a new distinct class of materials has been identified and can be used in several industrial areas.

2. Experimental

The samples were subjected to mechanical traction and compression assays, and investigated the structural characteristics of the test specimens using optical micrography (OM) and scanning electron microscopy (SEM), both to evaluate the state to Initial and final fibre matrix. Standards such as ASTM D3039 (traction test) and ASTM D3410 (compression test) were used for the tests.

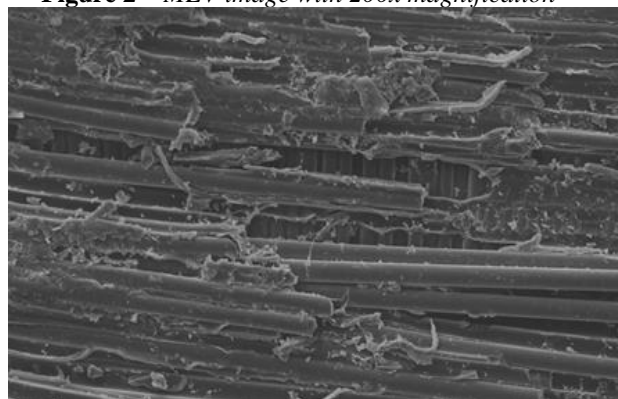
3. Results and Discussions

The results of the mechanical assays were compared with those of the researched literature. Mechanical analysis of compression and traction that the epoxy resin reinforced with glass fiber type E, features characteristic of fragile material for traction voltages and ductile for compressive forces. The assay values were higher in what the literature found as shown in Figure 1, being that this material still has two-way braided fibers, represented in Figure 2, which ensured such high properties.

Figure 1 – Results and comparisons

Traction Test				
	Traction Voltage (Mpa)	Modulus of elasticity (Gpa)	Deformation	
	Fiberglass-E	393,86	23,03	17,1
1	Carbon Fiber	200	13,34	32
2	Jute Fiber	43	15,87	44,69
3	Coconut Fiber	16	0,07	21,9
Compression Test				
	Traction Voltage (Mpa)	Modulus of elasticity (Gpa)	Deformation	
	Fiberglass-E	2560	122	0,25
1	Carbon Fiber	247,13	3,59	87,7
2	Polyester Fiber	204,65	22,25	58,1
3	Kevlar Fiber	43,9	6,68	18,5

Figure 2 – MEV image with 200x magnification



4. References

- [1]- Callister, William d, Rethwisch, David g. Materials Science and engineering. (2016).
- [2]- Lima, José Eduardo Salgueiro. Preliminary study of reinforcement of Polymeric Material by means of carbon fibers. (2017).
- [3]- Gonçalves, Jorge Antônio. Composites based on epoxy resin reinforced with coconut fiber. (2010).
- [4]- Pires, Eduardo N. Effect of alkaline treatment of jute fibers on the mechanical behavior of epoxy matrix composites. (2009).
- [5]- Gama, J. P. F. Hybrid polymeric composites based on carbon fiber/glass: uniaxial traction and compression. (2018).
- [6]- Reis, Ligia Reghin. Obtaining and characterization of unsaturated polyester resin composites molded by the infusion process. (2016).
- [7]- Santos, Jayna Kátia Dionisio dos. Residual resistance after impact on hybrid composites of vinylic matrix reinforced by glass fibre and Kevlar. (2018).

Acknowledgments

I thank God first, my mother Ana, my father Carlos and my advisor Lidiane.

A LASER BEAM WELDING EXPERIENCE IN AN OVERLAP JOINT CONFIGURATION BETWEEN A DP980 AND TRIP 780 STEEL

Francisco Henrique Cappi de Freitas^{1*}, Marcelo dos Santos Pereira²,
Antonio dos Reis Faria Neto³, Cristina Sayuri Fukugauchi³

^{1,2,3} São Paulo State University “Júlio de Mesquita Filho”, Guaratinguetá’s Campus

⁴Federal Institute of Education, Science and Technology, São José dos Campos’ Campus

*Corresponding Author: francapp@gmail.com

1. Introduction

The automotive industry motivated by the need for reduction of vehicle weight and increase fuel efficiency, push up the steel mills to go forward to advance technologically. According to WorldAutoSteel FutureSteelVehicle Program (FSV), the main achievements will reach up to 31.3% for dual-phase (DP) steels and up to 9.5% for transformation-induced plasticity (TRIP) steels in a Battery Electric Vehicle (BEV) body structure until 2020 [1, 2]. The laser beam welding (LBW) has shown a high cost-efficient in various joining applications in the automotive industry, such as body-in-white and passenger safety [1]. This paper consists to experience eight different welding conditions in an overlapped joint configuration of DP980 and TRIP780 steels and investigate if could exist a correlation between the joint efficiency and wide of HAZ.

2. Experimental

Eight samples of DP980 and TRIP780 sheet steel of 200 x 100 x 1.2 mm was taken with surfaces in a 600 mesh sandpaper. The samples were placed in an overlapped configuration without a gap on a CNC-driven table. The welding was performed autogenously in a plan position at sheets rolling direction. The equipment used was a fiber laser based on ytterbium-doped silica fiber, model IPG-YLR-2000, operative at 1070 nm wavelength and 2000 W of maximum power. Argon gas was used for weld pool protection with a flow rate of 8.4 L/min and the focal position aimed at the surface. The main variables investigated were the power (set at 1200 and 1300 W), the welding speed (set at 2000 and 3000 mm/min) and face side material (DP980 and TRIP780). Sub size specimens according to ASTM E8M-16 [3] for tensile tests were taken in a cross-section of bead welding direction, and metallography samples were taken in adjacent place of tensile tests specimens. The analysis magnification was 1.25x and HAZ wide measured.

3. Results and Discussions

According to Souza [4], the welded materials tensile test specimen which includes the weld seam in midway point shall have as acceptance criteria the rupture load, once the consequence is a heterogeneous microstructure and is not possible find out the yield point elongation. Therefore the joint efficiency may be determined using as reference the rupture load, calculating the quotient through the base material and joint values. The condition of 1200 W, 2000 min per min and DP980 in face side have shown the best efficiency, with values of 87.90 %. The HAZ wide has reached 874 and 1212 μm . Although the bead weld exhibit pores inside, the tensile test verified a satisfactory efficiency.

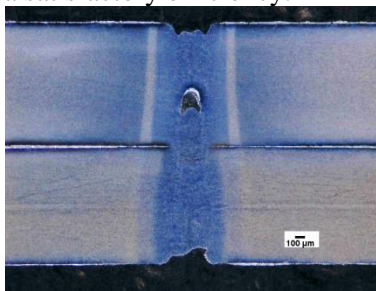


Fig. 1. Weld bead metallography analysis; 1200 W, 2000 mm/min, DP980 face side material.

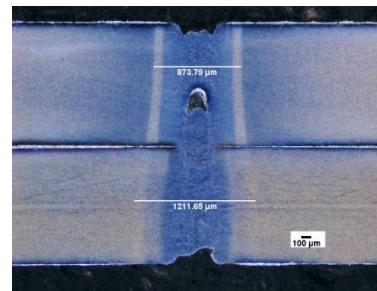


Fig. 2. HAZ wide measurement: 154 μm DP980 side; 209 μm TRIP780 side.

4. References

- [1]- Auto Steel Partnership, 2005, “Advanced High Strength Steel Application Guidelines”, Arlington, Virginia, USA, IISI, 2005, 123p.
- [2]- S. Keeler, and M. Kimchi, Advanced High Strength Steels Application and Guidelines, version 6, Worldautosteel, 2017.
- [3]- ASTM E8M. Standard Test Methods for Tension Testing of Metallic Materials. 2016
- [4]- Souza, S. A. Ensaios Mecânicos de Materiais Metálicos. 5ª Edição. Editora Edgar Blücher Ltda, 1982

Acknowledgments

To UNESP PROPG and funding agency CAPES for supporting the activities.

ON THE INFLUENCE OF POLYMER COMPOSITE PROCESS IN VOID FORMATION: POROSITY FRACTION AND MORPHOLOGY ANALYSIS

Francisco Maciel Monticeli^{1*}, Heitor L. Ornaghi Jr.¹, Herman J. C. Voorwald¹, Maria Odila H. Cioffi¹
¹*Fatigue and Aeronautical Materials Research Group, Department of Materials and technology, Sao Paulo State University (Unesp), School of Engineering, Guaratingueta. 12516-410. Sao Paulo, Brazil*
 *Corresponding Author: f.monticeli@unesp.br

1. Introduction

Polymer composites reinforced with continuous carbon fiber are attractive to aeronautical industries due to respective low specific mass combined with appropriated mechanical resistance [1]. A significant difficulty is to control defects formation during processing, such as porosity, which are stress concentrators and decreases the mechanical property of the material [2]. In the search for improvements in composite processing, several techniques have been devised to ensure impregnation homogeneity of polymer composites for primary structural application [3]. The most commonly used processes in aeronautic industries are resin transfer molding (RTM), resin film infusion (RFI) and vacuum-assisted resin transfer molding (VARTM) considering process control, reproducibility and cost [3–5]. The present work aims to evaluate the influence of different types of processing in void formation and their respective morphology, using the acid digestion and mercury porosimetry techniques.

2. Experimental

The composites were processed into the following compositions: 8 layers of carbon fibers IM10 NCF $[(0^\circ/+45^\circ/-45^\circ/90^\circ)_2]_s$, epoxy resin RTM6 from Hexcel processed via RTM, VARTM, and RFI according to references procedure [1,3]. Porosity characterization was performed using acid digestion (ASTM 3171 - proc. B) and through mercury porosimeter (POROMASTER® GT 33 from Quantachrome Instruments®) to determine the fraction of open voids as well as the void size distribution.

3. Results and Discussions

The results obtained by each analysis reveals that composite processed by RTM presented higher porosity fraction and higher standard deviation when compared to the void results of laminates processed by VARTM and RFI (Fig. 1a). VARTM processing has a relatively higher vacuum than RTM processing, which facilitates porosity removal. For the RFI system, resin is inserted as films between each layer, ensuring better impregnation at each fabric interface and maintaining the same porosity variation. On the other hand, RTM and VARTM are infusion processes and ensures a smaller amount of surface-connected porosity (Fig. 1b), compared to the RFI system, which has the same distribution between open and closed voids. Open pores facilitate crack initiation and growth during load application [1]. In addition, RFI is the most proper processing in this first analysis.

Regarding pore diameter distribution, all processing had a similar influence. The highest frequency of smaller pores (<5 - 15 μm) and pores larger than 50 μm was found for all processing type. As a matter of fact, diameter distribution is influenced by polymer matrix and reinforcement compared to the type of processing used.

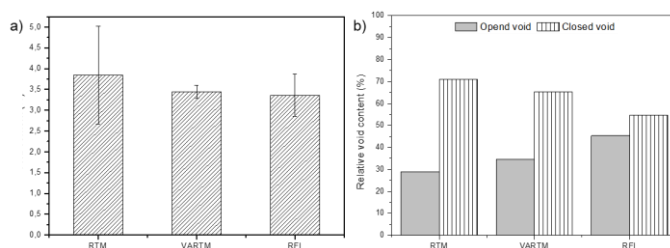


Fig. 1. Porosity results: a) void content and b) relative open and closed porosity

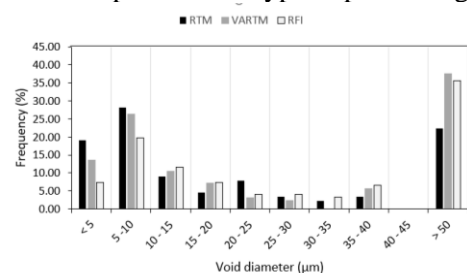


Fig. 2. Pore size distribution

4. References

- [1]- F. Monticeli, D. Daou, M. Dinulović, H. Voorwald, M. Cioffi. *Polym. Polym. Comp.*, **27**, 66-75, (2019).
- [2]- Y. Hamidi, S. Dharmavaram, L. Aktas, M. Altan. *J. Eng. Mater. Technol.*, **131**, 021014, (2009).
- [3]- M. Li, S. Wang, Y. Gu, Y. Li, K. Potter, Z. Zhang. *Compos. Sci. Technol.*, **72**, 873-878, (2012).
- [4]- Y. Hamidi, L. Aktas, M. Altan. *Polym. Compos.*, **26**, 614-627, (2005).
- [5]- C. Xia, S. Shi, L. Cai, J. Hua. *Holzforchung*, **69**, 307-312, (2015).

Acknowledgments

This study was funded in part by CAPES Brazil – Financing Code 001 and CNPq (process 153335/2018-1).

RESISTIVITY OF TITANIUM NITRIDE THIN FILMS WITH AND WITHOUT NITROGEN GRADIENT

Gabriel Cardoso Grime^{1*}, Thais Macedo Vieira¹, and Julio César Sagás¹

¹Laboratório de Plasmas, Filmes e Superfícies, Universidade do Estado de Santa Catarina. Joinville, Brazil

*Corresponding Author: gabrielgrime@gmail.com

1. Introduction

Titanium nitride (TiN) thin films have been employed in many applications due to their mechanical characteristics, resistance to friction and corrosion [1]. The electrical properties and the good adhesion of these films on silicon substrates also enable them to be used in microelectronics [2]. A gradient of N concentration along the film thickness can be used to reduce residual stress. In this work the effects of this gradient on electrical resistivity of TiN films are evaluated by comparing the results with homogeneous TiN films.

2. Experimental

The films were deposited in a grid-assisted magnetron sputtering system [3], with a titanium target in an Ar/N₂ atmosphere. The working pressure was fixed in 3.0 mTorr. The discharge current was 2.00 A. Two modes of N₂ injection were employed to grown the films: (i) constant (6.4 sccm), labeled TiN-H (homogeneous), and (ii) variable, 0 – 6.5 sccm, with steps of 0.4 sccm at each minute (Fig. 1), labeled TiN-G (graded). To improve adhesion, before the TiN deposition, a pure titanium film was deposited in both samples with a thickness about 0.11 μm. To obtain the films thicknesses a profilometer was used, making 12 measurements in each sample. The electrical characterization was made using a Hall effect measurement system and the van de Pauw method. The input current was fixed at 20 mA. Measurements of electrical resistivity of the films were obtained varying the temperature in a range of 90 K – 600K.

3. Results and Discussions

The homogeneous sample get a thickness of 0.72 ± 0.02 μm, and the graded, 1.35 ± 0.04 μm. The resistivities as a function of temperature are shown in Figure 2. The linear behavior of resistivity is clear in both films. In a certain temperature (about 350 K for TiN-H and 500 K for TiN-G) the dispersion of the points increases considerably. The resistivity of TiN-G is higher than for TiN-H, for all temperatures. This is consequence of different resistivities of Ti and TiN (more conductive). The fraction of Ti is greater in the graded film, causing an increase in effective resistivity.

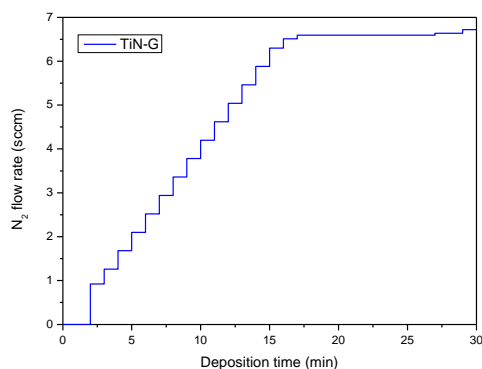


Fig. 1. N₂ flow rate during the deposition of sample TiN-G.

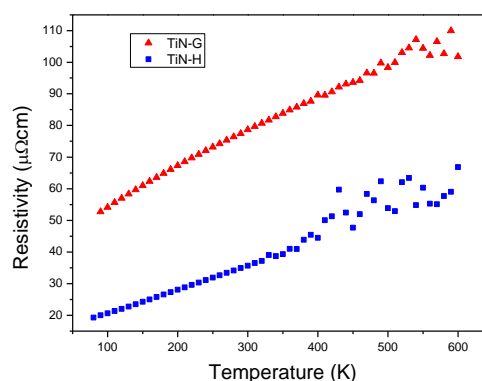


Fig. 2. Resistivity of TiN-H and TiN-G samples as a function of temperature.

4. References

- [1]- VAZ, F. et al. Surface and Coatings Technology, **191**, 2-3, 317-323 (2005).
- [2]- WITTMER, M. et al. Journal of Applied Physics, **52**, 9, 5722-5726, (1981).
- [3]- Fontana, L. C., & Muzart, J. L. R. Surface and Coatings Technology, **114**, 7–12 (1999).

Acknowledgments

This project has been funded by the Santa Catarina state research funding agency (FAPESC) through the program PAP in association with the Santa Catarina State University (UDESC) under contract PAP-TR 655. Gabriel Cardoso Grime also thanks UDESC by the financial support through PROBIC grant.

SURFACE STRUCTURING OF SAE 4340 STEEL BY LASER FIBER

H. P. Vicente^{1*}, R. M. S. Custódio¹, A. S. Paula², G. Vasconcelos³

¹*Instituto Tecnológico de Aeronáutica, São José dos Campos-SP*

²*Instituto Militar de Engenharia-Seção de Engenharia Mecânica e de Materiais, Rio de Janeiro – RJ*

³*Institute of Advanced Studies – EFO-L, São José dos Campos-SP*

*Corresponding Author: *helder.10@hotmail.com*

1. Introduction

Research on surface modifications through laser texturing has been performed by several researchers, aiming at applications in mechanical parts that require low coefficient of friction and wear [1]. Dunn used a laser fiber pulsed 50W and wavelength 1.064 μm to generate microcavities in the samples surfaces of 316L stainless steel and observed if the coefficient of friction between the mechanical parts was reduced. Based on this research, we intended to treat by the same process, SAE 4340 steel which is a material widely used in critical structural components in the aeronautics and aerospace industry, for example in landing gear. The process of structuring by laser comprises to apply pulses of time and power controlled in the surface of the steel with objective to create microcavities [2]. In this work, we intend to evaluate the dimensional variation of microcavities as a function of pulse frequency and power. Since these microcavities act as a lubricant (liquid or solid) reservoir on the contact surfaces of mechanical components, the volume of lubricant stored in the cavities is a key parameter.

2. Experimental

Samples of SAE 4340 steel, with 25mm diameter and a 5 mm thickness, were sanded with abrasive sandpaper of 80 to 1200. After sanding, it was cleaned with ethyl alcohol. These samples were placed in the focal region of an ytterbium fiber laser (1,064 μm) of 50W and 100 nanoseconds pulse time. The experiments of micro surface drilling on the samples were performed by changing the laser power from 10 to 50W, with a 10W interval and two pulse frequency values (50kHz and 100kHz), generating two process charts. This experiment aims to evaluate possible variations in the diameter of the microcavities as a function of power and pulse frequency. All experiments were performed according to the percussion drilling process with three consecutive pulses of 100 nanoseconds. After the irradiation step, it was done the analysis using an optical microscope Mark Zeiss. In order to minimize possible dimensional uncertainties, the remelted material inside the cavities and solidified at the edges were removed using 600 to 1200 sandpaper. After this step, ultrasonic cleaning was performed to remove the particles that lodged inside the holes.

3. Results and Discussions

The general appearance of the surface after laser irradiation can be observed in figure 1. According to the dimensional evaluations obtained by an optical microscopy, it was possible to plot figure 2 which correlates hole diameter as a function of power and frequency. In this figure we can be observed that with the increase of the power, the linear increase of the hole diameter occurs. It is also noted that by reducing the frequency to the same power value the hole diameter is increased. This observation is supported by the relationship:

$$P_k = P_m / f \cdot t_p$$

Where:

P_k is the peak power (W)

P_m is the average power (W)

t_p is the pulse time (s)

f is the frequency (Hz)

From this equation, it is observed that the reduction of the frequency causes an increase of the peak power, resulting in the increase of the microcavities diameter, corroborating with the obtained results.

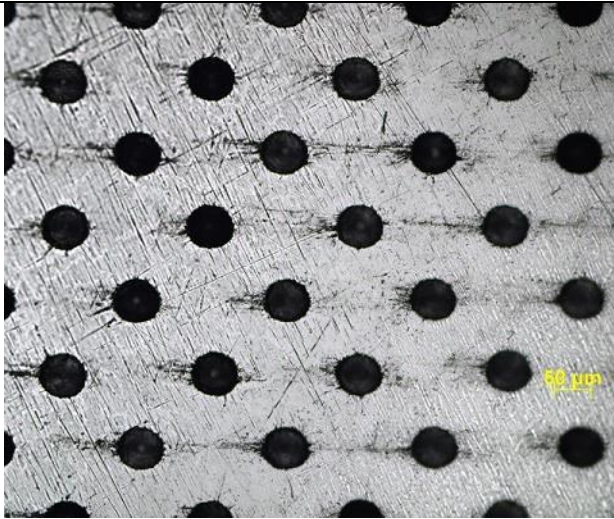


Fig. 1. Image of micro-cavities obtained by optical microscopy from the structured surface steel SAE 4340 obtained with a laser 50W ytterbium fiber with wavelength of $1.064 \mu\text{m}$

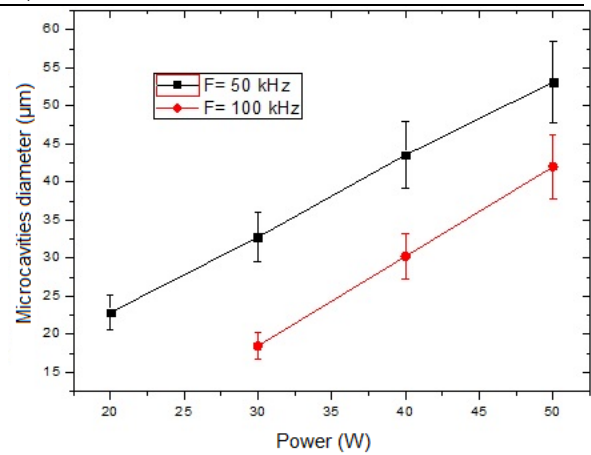


Fig. 2. Influence of power and frequency variation on dimensional variations of microcavities.

4. References

- [1]- A.Dunn, K.L.Wlodarczyk, J.V.Carstensen, E.B.Hansen, J.Gabzdyl, P.M.Harrison, J.D.Shephard, D.P.Hand “*Laser surface texturing for high friction contacts*”, Institute of Photonics and Quantum Sciences, Heriot-Watt University, Edinburgh EH14 4AS, UK, (2015).
- [2]-M. Scaraggi, F. P.Mezzapesa, G. Carbone, A. Ancona, D. Sorgente, P. M. Lugarà “*Minimize friction of lubricated laser-microtextured-surfaces by tuning microholes depth*”, DII, Università del Salento, 73100 Monteroni-Lecce, Italy, (2014).
- [3]- Y. Xing, J. Deng, X. Wang, R. Meng “*Effect of laser surface textures combined with multi-solid lubricant coatings on the tribological properties of Al₂O₃/TiC ceramic*”, Key Laboratory of High Efficiency and Clean Mechanical Manufacture of MOE, Department of Mechanical Engineering, Shandong University, Jinan 250061, PR China, (2015).

Acknowledgments

Processo CAPES – Pró Defesa IV
 Instituto de Estudos Avançados – DCTA.

SYNTHESIS AND CHARACTERIZATION OF Sb₂O₄ BY THERMAL OXIATION

Herick Ematne¹, Rosana Alves Gonçalves¹, Olívia Maria Berengue¹, Maurício Ribeiro Baldan²

¹São Paulo State University (UNESP) School of Engineering of Guaratinguetá – Brazil

²National Institute of Space Research (INPE) São José dos Campos - Brazil

*Corresponding Author: hematne@yahoo.com.br

1. Introduction

Antimony oxides (AO) are known to be widely used as flame-retardants, gas sensors and catalytic agents. The most stable AO is Sb₂O₄, which has two allotropic phases: orthorhombic (α -phase) and monoclinic (β -phase). Sb₂O₄ is widely used together with other oxides as catalytic agent and present properties that make it a promising material for the fabrication rechargeable sodium batteries [1, 2].

In this work, Sb₂O₄ nanobelts were synthesized by thermal oxidation of a vapor solid source process. The samples structure, composition and morphology were characterized by XRD, Raman and FEG-SEM measurements

2. Experimental

The as-grown Sb₂O₄ nanostructures were synthesized in a tubular furnace by thermal oxidation of metallic Sb source. The temperature was set to 950°C in order to generate a saturated Sb vapor that is driven to the growth region (750°C – 580°C) where Au covered Si/SiO₂ substrate are satted up. The chamber (alumina tube) was sealed and purged with argon flux (60sccm) for the entire synthesis. At 950 ° C, the O₂ flux was inserted and maintained for one hour, after that time the furnace was allowed cool down to room temperature.

3. Results and Discussions

From FEG-SEM images, it was possible to verify two different morphologies presented in the samples: a zigzag microbelt structure with lengths ranging between tens and hundreds of microns and width ranging from 0.76 to 9.7 μm and smooth and flexible micro- and nanowires with a width ranging from 0.165 and 2.85 μm and an estimated thickness between 17 and 285 nm. From the XRD data, we found Sb₂O₄ α -phase main structure presented in our sample and presence of strong and sharped peaks indicate high crystalline quality of the samples. Raman spectrum revealed the Sb₂O₄ main vibrational modes for this structure and the presence of sharped peaks confirming the high crystalline quality of the samples.

4. References

- [1]-SUN, Qian et al. "High capacity Sb₂O₄ thin film electrodes for rechargeable sodium battery". Electrochemistry Communications, v. 13, n. 12, p. 1462-1464, 2011.
- [2]-REN, Guangping et al. "Synthesis of α -Sb₂O₄ nanorods by a facile hydrothermal route". Materials Letters, v. 63, n. 6-7, p. 605-607, 2009.

Acknowledgments

This study was financed in part by the Coordenação de Aperfeiçoamento de Pessoal de Nível Superior - Brasil (CAPES) - Finance Code 001 and FAPESP (grant 2015/21816-4).

MICROSTRUCTURE EVOLUTION IN GUM METAL Ti-23Nb-0.7Ta-2Zr-O ALLOY PROCESSED BY POWDER METALLURGY

João Guilherme Jacon de Salvo^{1*}, Daniela Gomes Silva², Vinícius André Rodrigues Henriques¹

¹*Divisão de Materiais do Instituto de Aeronáutica e Espaço - IAE*

²*Universidade Federal de São Paulo - UNIFESP*

*Corresponding Author: joaodesalvo@gmail.com

1. Introduction

Gum metal alloy Ti-23Nb-0.7Ta-2Zr-O (%at.) was developed by Saito et al. (2003) based on theoretical calculations [1]. Their aim was to reduce titanium elastic modulus by the addition of β stabilizing elements, such as V, Nb, Ta e Mo. Additionally, the addition of group IV elements provide increased strength without unduly increase in elastic modulus. Gum metal alloy presents unique properties, differing significantly from β traditional alloys; main attributes are: extremely low elastic modulus (40-60 GPa); elastic deformation further than 2.5%; 1200-1600 MPa tensile strength; highly cold workable without work hardening. This investigation aimed to fabricate the alloy by powder metallurgy and to evaluate the microstructure after sintering.

2. Experimental

Elemental powders of Ti, Nb, Ta e Zr were produced by hydriding followed by milling, and blended for 1h according to alloy composition. Compaction of samples was carried out by uniaxial followed by isostatic cold pressing at 400 MPa. High vacuum (10^{-5} torr) sintering was realized at 1200°C for 1h and 3h for comparison.

3. Results and Discussion

Results are presented in Figures 1-4. Sintering at 1200°C promoted the stabilization of a predominantly β phase matrix, although remaining α phase was observed. Increasing sintering time from 1h to 3h resulted in reduction of α phase volume fraction and higher densification; from 93.7% to 95.1%. However, higher temperatures may be required to complete the dissolution of Nb and Ta nuclei.



Fig. 1. Microstructure after sintering for 1h.

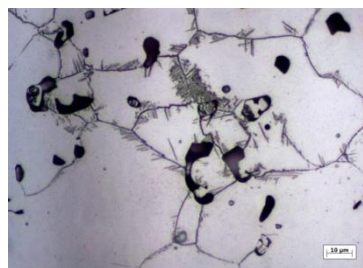


Fig. 2. Microstructure after sintering for 3h.

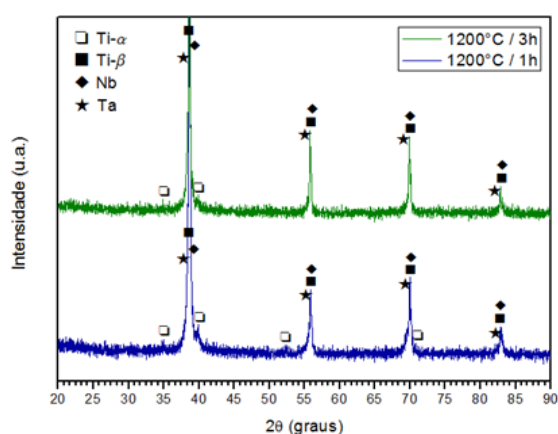


Fig. 3. XRD results for the investigated conditions.

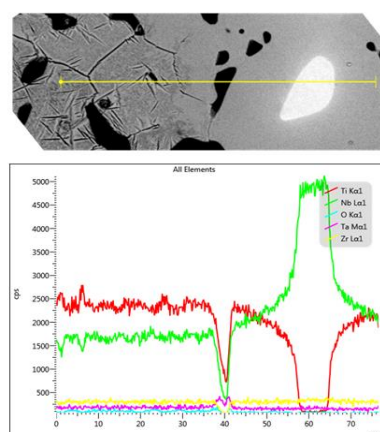


Fig. 4. EDS analysis showing undissolved Nb nuclei.

4. References

- [1]- Saito T. et al., Science, 80, (5618), 464–7, (2003).
- [2]- Furuta T, Kuramoto S, Hwang J, Nishino K, Saito T., Mater Trans., 46(12), 3001-7 (2005).

Acknowledgments

The authors are thankful to IAE and CNPq for support.

MODELLING THE MAGNETRON SPUTTERING DISCHARGE USING GLOBAL MODEL

Júlia Karnopp^{1,2*}, Julio César Sagás¹

¹Laboratório de Plasmas, Filmes e Superfícies, Universidade do Estado de Santa Catarina, Joinville -SC

²Instituto Federal de Santa Catarina, Jaraguá do Sul - SC

*Corresponding Author: julia_karnopp@outlook.com

1. Introduction

Magnetron sputtering is one of the main methods used for thin film deposition. However, the presence of a non-homogeneous magnetic field becomes the modelling of this discharge a difficult task. Recently, an approach based on global model has been proposed [1]. In this kind of model, an electron energy distribution function (EEDF) must be informed. A general distribution function can be expressed as

$$f(\varepsilon) = c_1 \varepsilon^{1/2} \exp(-c_2 \varepsilon^x) \quad (1)$$

where the parameter x defines the shape of the distribution. It represents a Maxwellian distribution for $x = 1.0$ and the Druyvesteyn distribution for $x = 2.0$. The parameters c_1 and c_2 are presented by Toneli *et al* [2]. Usually, a Maxwellian EEDF is considered, but it is not always valid for magnetron sputtering discharges. In this work, different EEDFs were considered to modelling the ionization region of such systems.

2. Methodology

The model was developed for argon plasma and titanium target. Two electron populations were considered, cold and hot (secondary electrons emitted from the cathode), three populations of argon in ground state (cold, warm and hot), argon ions, metastable argon atoms, titanium atoms in the ground state, singly ionized metal ions and doubly ionized metal ions. With this model is possible simulate the typical I-V (current – voltage) curve of magnetron discharge. The factor x in eq. (1) was varied between 1.0 and 2.0.

3. Results and Discussions

Increasing the current, the electron density grows up, consequently more ionizations of the argon and the metal atoms occur, as can be seen in figure 1. With the increase in the ion density, there is also an increase in metal production (by sputtering) and in the generation of hot electrons.

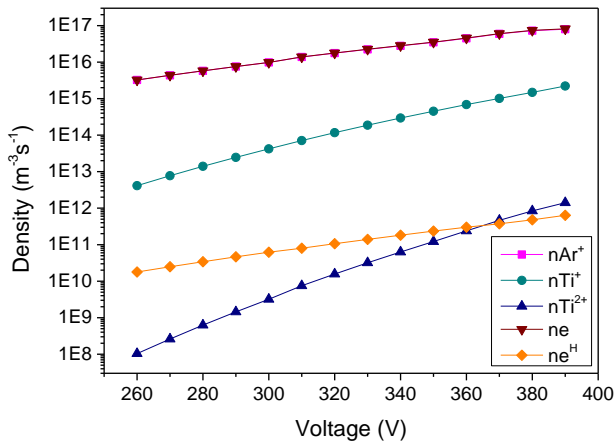


Fig. 1. Density of charged particles for Maxwell-Boltzmann distribution ($x=1.0$).

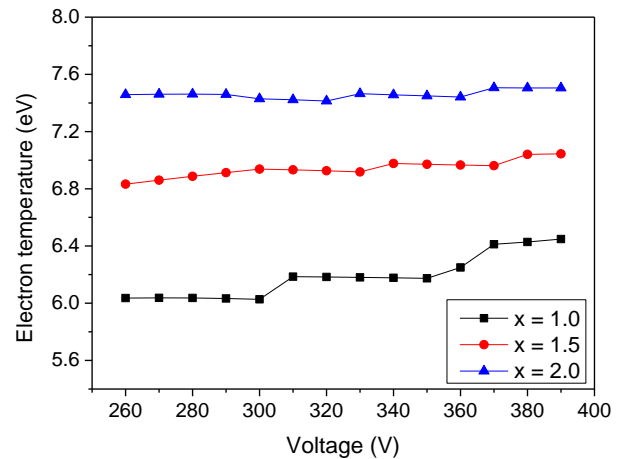


Fig. 2. Electron temperature for different electron energy distribution function.

For a Maxwellian distribution the electron temperature is lower (fig. 2), and the electron density is higher than for a Druyvesteyn distribution at the same I-V condition. The Druyvesteyn EEDF has a smaller population of high energy electrons, which results in high values of collisional energy loss per electron-ion pair created. As consequence a higher temperature is necessary to sustain the discharge at a given I-V condition.

4. References

- [1] C. Huo, et al., J. Phys. D: Appl. Phys., **50**, 354003, (2017).
- [2] D. A. Toneli, et al., J. Phys. D: Appl. Phys., **48**, 495203, (2015).

Acknowledgments

This project has been funded by FAPESC through the program PAP in association with UDESC under contract PAP-TR 655. Júlia Karnopp also thanks FAPESC by the scholarship.

ANODE EFFECTS ON A MAGNETRON SPUTTERING DISCHARGE: CHANGES IN

CURRENT-VOLTAGE CURVES

Kleber Alexandre Petroski^{1*}, Julio César Sagás²

¹ São Paulo State University (UNESP), School of Engineering, Guaratinguetá - SP

²Laboratory of Plasmas, Films and Surfaces, Santa Catarina State University (UDESC), Joinville -SC

*Corresponding Author: kleber.a.petroski@gmail.com

1. Introduction

Conventional magnetron sputtering is a deposition system widely known in the area of thin films. However, for a wide range of gas and target combinations there is a hysteresis region for process curves in the system as a function of gas flow rate. Therefore, the grid-assisted magnetron sputtering (GAMS) was proposed in which a grid is added between the two electrodes of the conventional magnetron sputtering aiming to decrease or even eliminate the hysteresis. Despite this effect be achieved, an undesirable consequence arises, the reduction of the deposition rate on the substrate because part of the material is deposited on the grid. When grounded, the grid becomes the main anode of the discharge. In addition, it also modifies the current-voltage relation by increasing magnetron efficiency. In this work, it is proposed to change the grid commonly used in GAMS by ring anodes with external diameter of 110 mm and internal diameters of 20, 40, 60, 80 and 100 mm.

2. Experimental

Measurements were made using a homemade magnetron sputtering system. Two types of targets were used: Al and Ti, both 100 mm in diameter and 60 mm away from the substrate. The current-voltage curve measurements were made in pure argon and constant pressure of 0.40 Pa. The power supply operated in direct current mode. The anode was kept 20 mm away from the target. The experiments were not made in order of increasing or decreasing internal diameter, to avoid superposition with the effects of target erosion. In addition to the measurements with the rings, measurements were made without extra anode (the discharge anode is the chamber walls and substrate) and with the commonly used GAMS grid for the Al target.

3. Results and Discussions

Figure 1 shows the current-voltage curves with Ti target. The magnetron efficiency increases in the following order: 20 mm of internal diameter, with grid, 40, 60, without grid, 80 and 100 mm; that is, considering only the rings, the larger the ring area, the lower its efficiency. Figure 2 presents the measurements with the Al target. The increasing order of magnetron efficiency is 60, 20, 40, 80 and 100 mm. With exception of the 60 mm ring, a smaller area ring again provides higher magnetron efficiency.

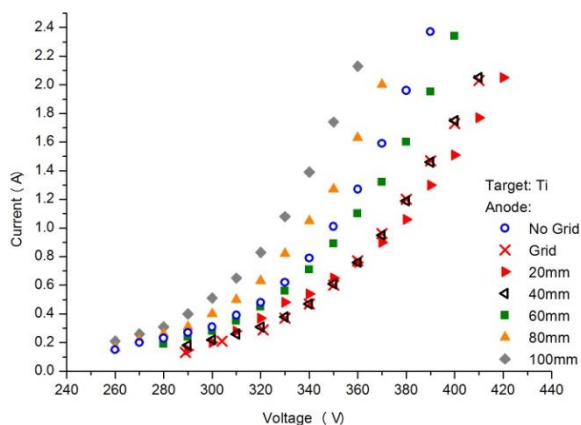


Fig. 1. Current-voltage curves for Ti target.

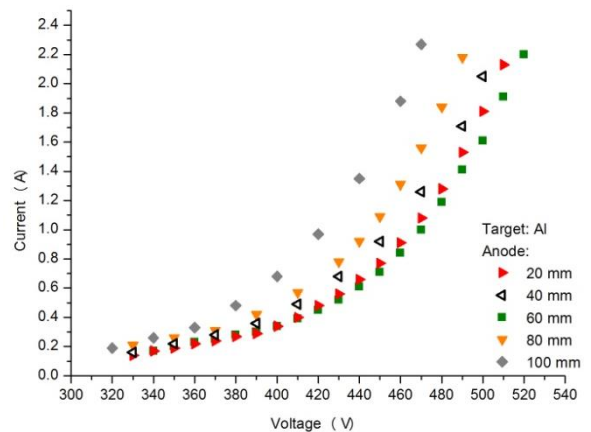


Fig. 2. Current-voltage curves for Al target.

The data obtained for both targets indicate that electrons are being captured with enough energy to cause more ionization. Increasing the ring area, this capture of high energy electrons grows. It is also noted that the anode presence alters the electric field lines, field lines ending on the wall is now ending on the rings. This change can be seen by comparing the 100 mm ring with the no grid case for Ti target, despite its small area, the effect is easily identified on the graph, for example, for a voltage of 320 V the current obtained is 73% higher.

Acknowledgments

The authors would like to thank Brazilian agency CAPES for their financial support.

ATMOSPHERIC PRESSURE PLASMA POLYMERIZATION OF HEMA:DEAEMA MIXTURE FOR DRUG DELIVERY

F. V. P. Kodaira^{1,2*}, I. Amin², E. Makhneva², R. P. Mota¹, K.-D. Weltmann², K. Fricke²

¹São Paulo State University (UNESP), School of Engineering, Guaratinguetá, SP, Brazil

²Junior Research Group Biosensing Surfaces, Leibniz Institute for Plasma Science and Technology e.V. (INP), Greifswald, Germany

*Corresponding Author: Kodaira.felipe@gmail.com

1. Introduction

Plasma polymerization is an alternative to conventional processes, and it has some advantages, it generates no chemical wastes, have enough energy to polymerize compounds wet chemistry can't, and can be easily tuned to obtain plasma polymers with different properties. The plasma polymers have unique properties, usually have a high crosslinked structure and are very adherent to any substrates. In this work, the plasma polymerization was achieved by using an Atmospheric Pressure Plasma Jet (APPJ), unlikely the usual low-pressure plasma polymerization, it does not need a huge and expensive vacuum system, saving money and time. Depending on the monomers and plasma parameters used in the polymerization, it is possible to obtain biocompatible coatings. That kind of coatings have a wide range of applications, one of them is for drug delivery. The coating can be incorporated with a drug which is released for a period right on the desired target, reducing the amount of drug taken and the side effects it could have. Also, the coating can be tuned to control the time of the releasing. In this work the plasma polymerization using an APPJ was performed aiming for biocompatible hydrogel-like coatings for drug delivery application.

2. Experimental

For the polymerization process, an APPJ fed by 5W@27.12MHz. As the precursor, a mixture of (Hydroxyethyl)methacrylate (HEMA) and 2-(Diethylamino)ethyl methacrylate (DEAEMA) in the proportion 1:1 was used. Methylene Blue (MB) was used as a model drug for it is easy to detect. Double side polished silicon of 10 x 10 mm was used as substrate.

The mixture HEMA:DEAEMA (HD11) deposited on top of substrates using the APPJ 5 mm distant. For higher homogeneity, the jet was moving in circles of 5 mm during the process. The total time of polymerization was 1 min. After that, the covered silicon substrate was immersed in a solution of MB 1 mM for 6 hours and let dry overnight. A multilayer composition of the film was also studied, to prepare the additional layers, the overnight dried sample received another layer of HD11 and the polymerization process repeated.

The plasma polymer molecular structure was evaluated by FTIR, the incorporation process was also assessed by FTIR, looking for the presence of MB bands, and the releasing of MB was measured by UV/Vis Spectroscopy.

3. Results and Discussions

In the FTIR spectra of the polymerized HD11, peaks relative to their nitrogen groups were present, which is be important for the aiming application as biocompatible cover. In the FTIR spectra is also possible to observe peaks referent to both monomers of the mixture and some new groups, due to the characteristic of the plasma polymerization and interaction with air, since it was deposited in a open system. The peak referent to MB (1600 cm⁻¹) was observed after the incorporation.

The release of the drug was delayed when using multilayers and went from few minutes, when using only a single layer, to up to 3 hours. However, it was not possible to control the total amount of the drug loaded into the film, only the ratio of releasing.

Acknowledgments

The authors would like to acknowledge CAPES for the financial support in Brazil, and DAAD and CNPq (process Nr. 290317/2017-7) for the financial support abroad.

SENSOR BASED PROGNOSTIC SOFTWARE TOOLS

Leandro Colevati dos Santos^{1,2*}, Eliphaz Wagner Simões², Sebastião Gomes dos Santos Fo.² and Maria Lúcia Pereira da Silva^{1,2}

¹Faculty of Technology of São Paulo, Centro Paula Souza, Brazil

²School of Engineering, University of São Paulo, Brazil

*Corresponding Author: lecolevati@gmail.com

1. Introduction

On the last decades the amount of different low cost sensors available elsewhere was astonishing. These sensors encompass a huge range of utilities, some of them also present specificity, i.e., solve well known problems. However, this easiness of acquiring and maintaining such instruments also implies in an extensive amount of data to be analyzed, or, in other words, the needing for data mining tools. Therefore, the aim of this work is the proposal of a low cost broad band use analysis sensor data [1].

2. Experimental

This work followed the software engineering recommendations with Case Study Methodology. The chosen case study is in Healthcare Sector due to the amount of data freely disposed on the net.

3. Results and Discussions

This section shows the Case Study properties and, after that, the developed solution for such problems. **Case Study Properties:** Brazil Healthcare sector shows some trends: telemetry – i.e. wireless tools; telemedicine, which implies in patient and doctor not necessarily at the same place; due to the amount of different computer analysis it is advisable some artificial intelligence, classifiers and archetypes are also need. Therefore, the needs of the developed data mining tools are: a) up to 50 different data base to be analyzed, which requires structuring the data; b) georeferenced database is unavailable but is useful for comparison among district, states and the whole country; c) IoT is a need in any technological decision support tool. **Proposed Solution:** It was considered two types of sources of data. The first source is distributed on webpages of public or private medical departments, with any type of structure and disseminate this data in files of various types and needs the development of a Web Scraping service, accessing the pages, checking the possibility of extracting the data or locating files that can be downloaded. The second source comes from microelectronic sensors that can be attached directly to people or indirectly, such as sensors on personal devices such as smartphones. The developed system structure, Fig. 1, is based on an Enterprise Service Bus that has arbitration as REST service receiving the data from the various sources, identifies the source of the data and sends to one of the services, which uses FaaS technology, coupled to the bus that will persist in a NoSQL database. **Conclusion:** The main advantage is the choice for the unstructured database, which is due to the fact since the same medical entity may have only some measured characteristics, not necessarily creating a defined structure. The last service associated with the bus utilizes NoSQL database extraction technologies, analysis with technologies such as Artificial Intelligence and the creation of medical archetypes that can aid in making real-time decisions or future studies. Testing in FaaS services file types generated a mass of more than 30 million of JSON documents on Apache Spark® environment and returned data in about 30 milliseconds. Although tested on Healthcare sector, this tool can be adapted for several fields, not only agricultural but also industrial, from environmental analysis to vacuum technology.

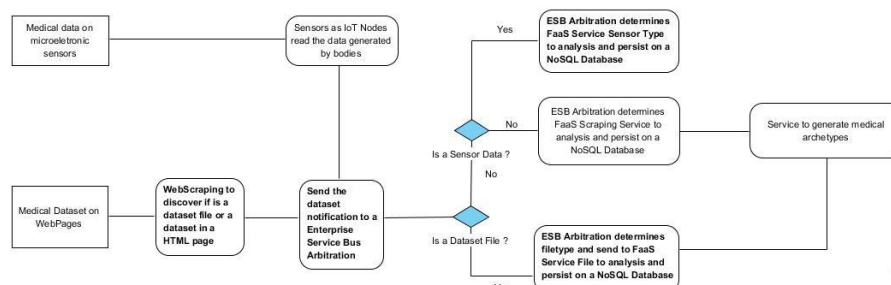


Fig. 1 – Diagram of activities for the development of the system

4. References

[1]- W. Hersh, J. A. Jacko, R. Greenes, J.Tan, D. Janies, P. J. Embi, P. R. Payne, Nature, **470**, 327-329, (2011).

Acknowledgments

FAPESP and CNPq for financial support.

STRUCTURAL, MORPHOLOGICAL AND ELECTRICAL CHARACTERIZATION OF GLASSY CARBON FOR USE AS ANTISTATIC AGENT IN POLYMERIC MATRICES

Leonardo de Souza Vieira ^{1*}, Larissa Stieven Montagna¹, Fábio Roberto Passador¹

¹*Polymer and Biopolymer Technology Laboratory (TecPBio), Universidade Federal de São Paulo (UNIFESP), 330, Talim, São José dos Campos, São Paulo, Brazil, 12231-280*

**Corresponding Author: leonardhovieira@gmail.com*

1. Introduction

Carbon black (CB) is one of the most commonly used antistatic agents in the industry to provide dissipative properties in antistatic packages produced with insulating polymeric matrices. However, its use is associated with the generation of respiratory problems and the deterioration of the mechanical and rheological properties of the final composite. Thus, it is suggested as an alternative to CB the use of glassy carbon (GC), which consists of a disordered carbonaceous material little used up to now in thermoplastic matrices and that has good gas impermeability, high elastic modulus and high electrical and thermal conductivity [1]. GC is obtained from the carbonization of thermosetting resins at temperatures above 1000 °C and has a reduced amount of functional groups on its surface and therefore has a hydrophobic character [2]. In this work, chemical and physical characterization of glassy carbon was performed to validate its use as an antistatic agent in polymeric matrices.

2. Experimental

The GC was produced using a poly(furfuryl alcohol) resin (PFA). The compound para-toluene sulfonic acid (3 wt %) was used as the resin catalyst. The PFA resin was cured in two steps: 60 °C for 2 h and then 80 °C for another 2 h. In the next step, the cured PFA was heat-treated from room temperature up to 1000 °C, at 1.0 °C min⁻¹ under an N₂ flow of 1 L h⁻¹. The sample was kept at the final temperature for 30 min and then left to cool at room temperature. The GC was milled at room temperature in an IKA mini mill, model A11. The milling time was approximately 3 min. GC powder was separated by sieving to obtain particles smaller than 45 µm. GC was characterized by X-ray diffraction (XRD, Rigaku Ultima IV diffractometer, PANalytical, X'pert Powder model), operating at 40 kV and 30 mA with CuK α radiation ($\lambda = 1.54056 \text{ \AA}$) at a scan rate of 5 °/min. The morphology of the GC powder was analyzed by a scanning electron microscope (FEG-SEM) MIRA3 operating at 5 keV. The particle size distribution curves were obtained using a CILAS particle analyzer (model 1190 L). Water content determination by titration was performed on Metrohm Ion Analysis, 870 KF Titrino model. The sheet resistance of the film was measured using a four-point probe meter Jandel, RM3000 model.

3. Results and Discussions

The XRD results show that the GC presents a characteristic band at 23.7° that corresponds to the reflection (002). Using Bragg's Law, it is verified that the distance between the graphite planes (d_{002}) is 0.3754 nm, which is within the d_{002} characteristic range of disordered carbonaceous materials, allowing to conclude the effectiveness of carbonization [3]. The particle size distribution results show that 10%, 50% and 90% of the particles has a diameter smaller than 3.56 µm, 20.86 µm and 40.71 µm respectively. The average Fraunhofer diameter of particulate material is 21.65 µm. The values obtained are within the expected diameter range. The FEG-SEM micrograph of the GC powder showed that the GC particle has a smooth surface and narrow edges, which are characteristic of fragile materials. The average moisture content of 9.89 + -0.11 was obtained on the surface of the sample, evidencing the need for prior drying in its use in melt processing. The sheet resistance value measured was $5.51 \times 10^{-2} \Omega \text{ sq}^{-1}$, and the correspondent bulk resistivity was $1.34 \times 10^{-4} \Omega \text{ m}$, which is relatively higher than the value of resistivity found in the literature for CB ($\sim 1,0 \times 10^{-2} \Omega \text{ m}$) [4]. Considering the properties and conductive character of GC it can be concluded that this material can be used as an antistatic agent for thermoplastic and thermoset polymeric matrices.

4. References

- [1]-M. S. Santos; L.S. Montagna; M. C. Rezende and F. R. Passador. Journal of Applied Polymer Science, p.47204-8, (2018).
- [2]-E.S. Gonçalves; M. C. Rezende; M. R. Baldan and N. G. Ferreira. Quim. Nova, 32, 158-164 (2009).
- [3]-S. Oishi; E. C. Botelho; M. C. Rezende and N. G. Ferreira. Appl. Surf. Sci. 394, 87 (2017).
- [4]-S. S. Pinto and M. C. Rezende. Polímeros, 22, 325-331 (2012).

Acknowledgments

This study was financed in part by the Coordenação de Aperfeiçoamento de Pessoal de Nível Superior-Brazil (Capes)- Finance Code-001).

EVALUATION OF WEAR AND CORROSION PROPERTIES OF DLC FILMS

DEPOSITED ON THE AISI 4340 STEEL

Lucas A. P. de Campos^{1*}, Larissa S. de Almeida¹, Marcos D. Manfrinato^{1,2}, Luciana S. Rossino^{1,2}

¹Federal University of São Carlos (UFSCar), Sorocaba Campi, Sorocaba, SP, Brazil

²Sorocaba Technological College- FATEC, Sorocaba, SP, Brazil

*Corresponding Author: lucasalmeidamk@gmail.com

1. Introduction

Properties as high hardness, low friction coefficient and chemical inertia can be attributed to DLC films. In this way, the properties of wear and corrosion resistance of DLC film coated on the AISI 4340 steel were studied in this work [1].

2. Experimental

The AISI 4340 steel was used as substrates. To plasma treatment, the cleaning by plasma ablation process was carried out with 80% Ar + 20% H₂ for 30 minutes. After that, the silicon interlayer was carried out with 70% HMDSO + 30% Ar for 15 minutes, followed by deposition of the DLC film, carried out with 90% CH₄ + 10% Ar at 200 ° C for 2 hours by PECVD method using a Pulsed-DC power supply, at 500V deposition voltage. The characterization of the DLC film was performed by Raman spectroscopy. The wear resistance was verified by micro-abrasive wear tests by fixed ball with 600 seconds and a load of 8N. The corrosion resistance was carried out by potention-dynamic polarization (PP) curves, obtained in aerated 0.6 mol L⁻¹ sodium chloride (NaCl).

3. Results and Discussions

The results of Raman spectra and potention-dynamic polarization curves obtained for DLC films are shown in Figure 1 and Figure 2, respectively.

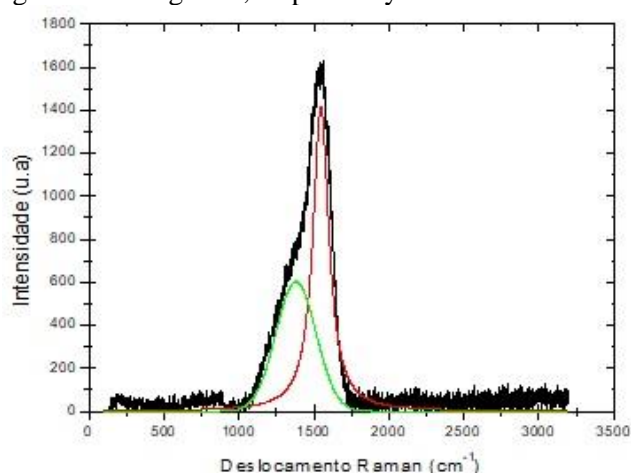


Fig. 1. The typical Raman spectra of DLC film.

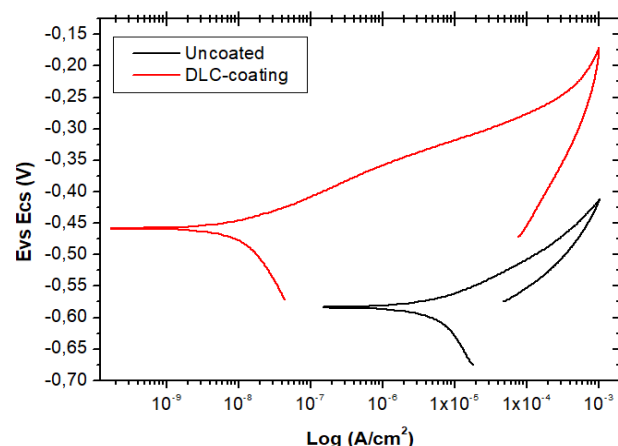


Fig. 2. Potention-dynamic polarization curves of uncoated and DLC coated.

The Raman spectra of the DLC presents the region of 1380 cm⁻¹ and 1549 cm⁻¹, which are called D and G band, refers to chemical bonds sp³ and sp², respectively, and according to the amount of hydrogen (29,06%) found in the film, it's indicated the presence of DLC a-C:H film on the surface of AISI 4340 steel. The wear volume of untreated material was of 4.52x10⁻³ mm³, and the material with DLC coating presented a wear volume of 9.231x10⁻⁵ mm³, showing that the wear volume has significantly decreased with DLC a-C:H film coatings. To corrosion experiments, the material with and without treatment did not show the passive region, although the corrosion potential of the material with DLC film was more positive, presented 457.9 mV value, while uncoated material presented -583.2 mV corrosion potential. According to Robertson (2002), the DLC film act as a good barrier to corrosion, which can promote more positive corrosion potentials to material [1]. Thus, it was verified the DLC coating improved the wear and corrosion resistance of AISI 4340 steel.

4. References

- [1]- ROBERTSON, J. Diamond-like amorphous carbon. *Materials Science And Engineering: R*, [s.l.], v. 37, n. 4-6, p.129-281, 24 maio 2002. Elsevier BV. [http://dx.doi.org/10.1016/s0927-796x\(02\)00005-0](http://dx.doi.org/10.1016/s0927-796x(02)00005-0).

Acknowledgements

We would like to thank CAPES (code 0001) to financial support.

EFFECT OF THE CLEANING PARAMETERS BY PLASMA ABLATION ON ADHESION OF DLC FILM IN THE Ti6Al4V ALLOY

Luciana S. Rossino^{1,2*}, Larissa S. de Almeida², Alan R. M. Souza², Marcos D. Manfrinato^{1,2}

¹Faculdade de Tecnologia José Crespo Gonzales – Fatec Sorocaba, Sorocaba/SP, Brazil

²Universidade Federal de São Carlos – UFSCAR Campus Sorocaba, Sorocaba/SP, Brazil

*Corresponding Author: lu.sgarbi@yahoo.com

1. Introduction

In metals, plasma treatment can be performed to chemically and structurally alter the surface of the material by thermochemical treatment and coating or thin film deposition. But, to efficacy of the treatment, the surface must be free of impurities, which can be removed by plasma ablation process [1]. The aim of this work is to determine the effect of the treatment parameters of the plasma ablation process on surface cleaning and adhesion of DLC films in the Ti6Al4V alloy.

2. Experimental

The study of the ablation process by the PECVD technique was carried out with the pressure range of 0.39 to 2.0 torr and proportion of gases of 100% Ar, 80% Ar - 20% H₂, 50% Ar - 50% H₂ and 20% Ar - 80% H₂, at fixed time of 30 min, and the temperature of $\pm 300^\circ$ C. The analysis of metal surface after ablation process were obtained by the techniques of visual analysis and Energy Dispersive Spectroscopy (EDS) by Scanning Electron Microscopy (SEM). The DLC film was deposited with CH₄ and Ar flow at 27 and 3 sccm respectively, power 120W and by 2 h. To determine the influence of surface cleaning on adhesion of the DLC film to the substrate, the Rockwell C hardness test was carried out.

3. Results and Discussions

The increase of the pressure causes an increase in the intensity of the luminescence, besides making it thinner, uniform and concentrated on the sample, being more efficient in surface cleaning, show in Fig. 1. The sample treated at pressure of 1,8 torr does not show purple coloration as in the sample treated at 0.39 torr, presenting a uniform treatment. The hydrogen also has influence in surface cleaning, assisting in oxygen removing, as observed in Fig. 2. Then, not only the pressure but also the kind and proportion of the gases used for the cleaning are factors that contribute to the removal of impurities from the samples. The best surface cleaning cause smaller film delamination around the indentation impression, as shown in Fig. 3, pointing the influence of the surface impurities of the substrate in the adhesion of the DLC films.

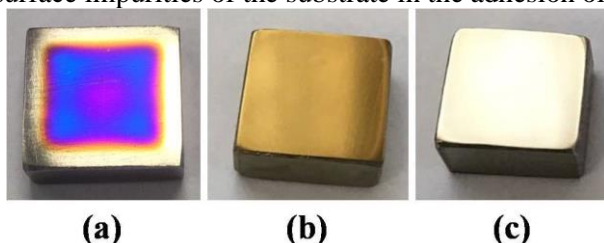


Fig. 1. Sample treated at (a) 0.39 torr with 100% Ar, (b) 1,8 torr with 100% Ar and (c) 1,8 torr with 80% Ar - 20%H₂.

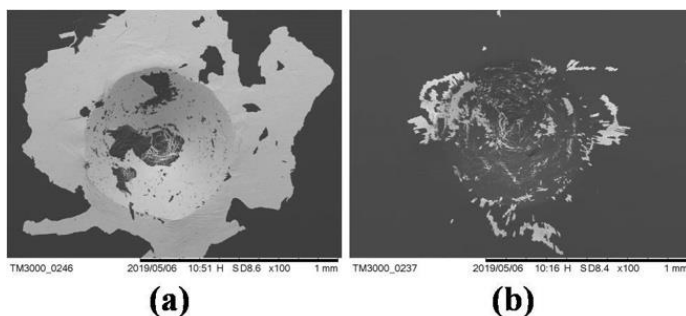


Fig. 3. Indentation in DLC film on sample cleaned at (a) 1,8 torr with 100% Ar and (b) 1,8 torr with 80% Ar - 20%H₂.

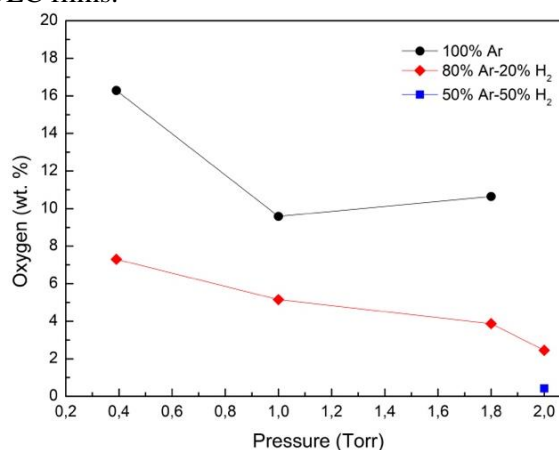


Fig. 2. Influence of the gases proportion and pressure ablation treatment parameters in the oxygen presence (wt. %) on the cleaned surface.

4. References

[1]- D'AGOSTINO, R., et al. Advanced Plasma Technology. 1^a. ed. Mörlenbach: Wiley-VCH, 2008.

Acknowledgements

We would like to thanks Fapesp and Capes (Code 001).

A DICTACTIC EXPERIMENT TO DEMONSTRATE THE BEHAVIOUR OF DIFFERENT PRESSURE GAUGES USING DISTINCT GASES

Nilberto Heder Medina¹, Bruno Amado Rodrigues Filho², Luiz Marcos Ferreira Fagundes^{1*}

¹Instituto de Física da Universidade de São Paulo

²Instituto Nacional de Metrologia, Qualidade e Tecnológica

*Corresponding Author: MarcosfagLL@hotmail.com

1. Introduction

Vacuum measurement is an important quantity in several highly technological industries such as micro and nanotechnologies, aerospace, petrochemical, and pharmaceutical industries [1]. Consequently, metrological aspects involving vacuum measurement shall be taken into account for proper measurement. Vacuum gauges are usually adjusted to measure in a nitrogen environment and when submitted to different gases, a correction must be applied, due to the variation of physical properties of the gauge when working different gases [2]. Proper training is a vital component for specialists working in the pressure measurement field, and the students must be aware of the influence quantities. In order to provide a proper understanding in vacuum measurement, this study presents the experiment regarding the behavior of different pressure gauges when submitted to distinct gases, conducted at the Physics Institute of the University of São Paulo.

2. Experimental Setup

The experimental setup comprises a thermistor GT 340-A and a Pirani Edwards PRE 10K pressure gauge connected to a vacuum chamber, as well as a connector to an external gas source. The system is connected to an Edwards n° 8 mechanical rotary pump and a Veeco diffusion pump. Additionally, a liquid nitrogen trap set up between the system and the Leybold mercury McLeod mercury-based gauge, which is used as the reference. A needle valve is also used to adjust the pressure inside the system. Nitrogen, helium and argon were flushed into the system to obtain the curves for the tested gauges and three measurements were taken for each value.

3. Results and Discussions

Results show that the indicated pressure in both thermistor and Pirani gauges are dependent on the gas inside the vacuum chamber. Figure 2 shows the indication of tested pressure gauges as a function of the McLeod reference gauge. A linear behavior is observed for nitrogen whilst a sensibility loss is observed for argon for pressures higher than 50 Pa and after 10 Pa for helium. Differences between the gauges for the same gas are attribute to physical principles which measurement is based on, as well as systematic differences from calibration, once they are devices used for educational purposes.

Finally, the results allow undergraduate students to visualize the influence of different gases in vacuum measurement, as well as the differences from different pressure gauges.



Fig. 1. Overview of vacuum chamber, pressure gauges, both mechanical and diffusion pump and nitrogen trap.

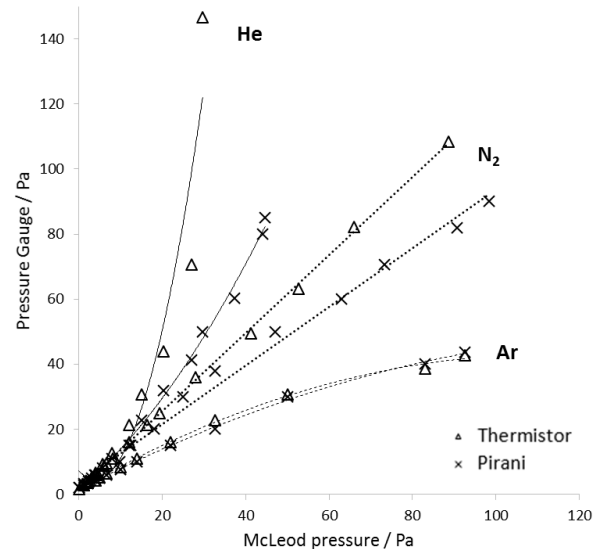


Fig. 2. Feature curves for the thermistor and Pirani pressure gauges for helium, nitrogen and argon.

4. References

- [1]-Kumar A, Thakur VN, Zafer A, et al. Contributions of National Standards on the growth of Barometric Pressure and Vacuum Industries. MAPAN 2019; 34: 13–17.
- [2]-Grinham R, Chew A. Gas Correction Factors for Vacuum Pressure Gauges. Vakuuum in Forschung und Praxis 2017; 29: 25–30.

EFFECT OF THE TEMPERATURE ON THE FORMED LAYER BY SOLID BORONIZATION ON THE AISI 321H STAINLESS STEEL

Marcos D. Manfrinato^{1,2*}, Rogério K. Nishimoto¹, Kevin L. S. Ferreira¹, Luciana S. Rossino^{1,2}

¹Sorocaba Technological College- FATEC, Sorocaba, SP, Brazil

²Federal University of São Carlos (UFSCar), Sorocaba Campi, Sorocaba, SP, Brazil

*Corresponding Author: marcos.manfrinato@fatec.sp.gov.br

1. Introduction

The boronizing process is a thermochemical treatment in which the boron atomic diffusion occurs to the material surface, and the stable phases, as FeB e Fe₂B, are formed. These formed layers improve the tribological properties of the materials, as decreased in friction coefficient and increased in the wear and corrosion resistance [1,2,3]. The aim of this work is to evaluate the influence of the temperature in the formation of a borated layer and wear resistance of the AISI 321H stainless steel.

2. Experimental

The solid boretation in the AISI 321H stainless steel is carried out using EKABOR® 2 dust in muffle furnace keeping the time of 5 hours, varying the temperature at 850°C, 950°C e 1050°C. The material characterization with and without treatment was carried out by metallography and microhardness Vickers. The microabrasive wear by fixed ball was carried out with a load of 2N, time test of 10 min. and 75 RPM, using abrasive paste consisting of F-1200 SiC (4-5µm) particles dissolved at 20% (80 g / 100 ml of deionized water). The solution was constantly stirred with a magnetic stirrer to avoid the particle precipitation.

3. Results and Discussions

The transversal section of boride layer in the different temperatures present two kinds of distinctly regions [1,2], the upper clear phase of FeB, and a dark phase of Fe₂B, as presented in Figure 1. The layer thickness increased with an increase in the treatment temperature.

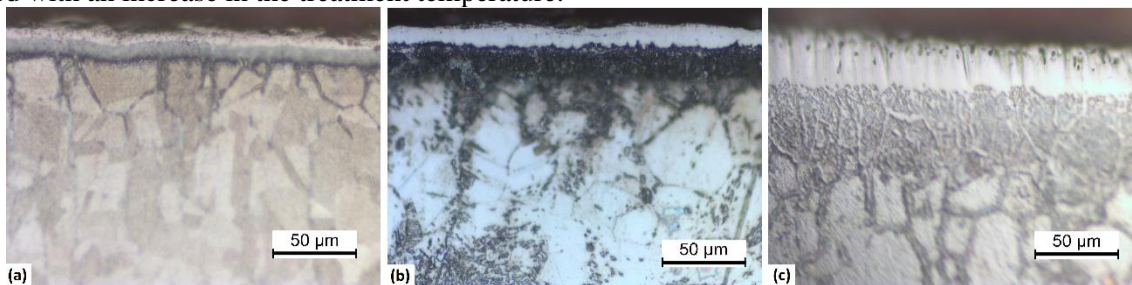


Figure 1. Optical cross-section view of borided AISI 321H steel (a) 850°C, (b) 950°C and (c) 1050°C

It is observed, in Figure 2 and Figure 3, the increase in the hardness and wear resistance with the increase in the treatment temperature. The wear volume was smaller to the treated materials, showing treatment effectiveness.

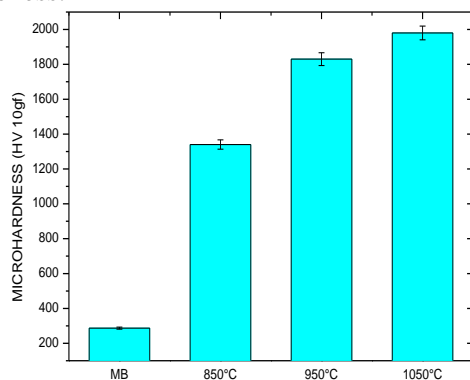


Figure 2. Microhardness of the AISI 321H stainless steel untreated and boronized.

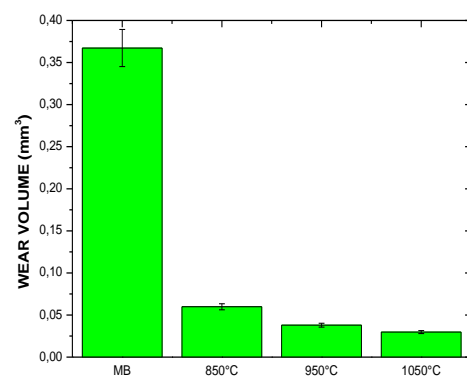


Figure 3. Influence of temperature on the wear volume of AISI 321H stainless steel.

4. References

- [1]- Y. Kayalli, I. Gunes and S. Ulu, *Vaccum*, **86**, 1428-1434, (2012).
- [2]- C.D.R. Calderon, G.A.R. Castro, A.M. Amador, I.E.C. Silva, J.A. Adame, M.E.P. Pardavé, E.A.G. Hernández. *Journal .Mat. Eng. Perf.*, **26(11)**, 5599-5609, (2017).
- [3]- I.C. Silva, M.E.P. Pardavé, R.P.P. Borja, O.K. Feridum, D.B. Bárcenas, C.L. García, R.R. Helguera. *Surf. Coat. Tech.*, **349**, 986-997, (2018).

MECHANICAL STRENGTH OF CEMENT BLOCKS WITH SCRAP TIRES

Maria Gabriela A. Ranieri^{1*}, Maria Auxiliadora de Barros Martins², Mirian de Lourdes Noronha Motta Melo³
and Adilson da Silva Mello¹

¹Instituto de Engenharia de Produção e Gestão, Universidade Federal de Itajubá, campus de Itajubá, MG.

²Instituto de Física e Química, Universidade Federal de Itajubá, campus de Itajubá, MG.

³Instituto de Engenharia Mecânica, Universidade Federal de Itajubá, campus de Itajubá, MG.

*Corresponding Author: gabirani77@gmail.com

1. Introduction

Encouraging sustainable development has put pressure on all industrial areas, including construction, to implement appropriate methods to protect the environment. Due to current global concerns that have arisen from extensive environmental problems such as climate change and resource impoverishment, coupled with rapid technological advancement in the construction sector, interest in alternative building materials has developed as the concept of sustainability is gaining ground. An alternative found is to reuse waste materials from waste materials as raw material to compose materials for construction. That in this case, waste from waste tires was used instead of natural raw material.

2. Experimental

In this research were studied compositions for the manufacture of blocks with incorporation of residues for the civil construction. For the composition of concrete block compositions with waste incorporation, the following materials were used: soil, sand, cement (CPV), water, waste granulate of waste tires. For the production of concrete blocks with tire waste incorporation (RP), four traits were hereinafter referred to as Ref, T10, T15 and T20, that is, with 0, 10, 15 and 20% of sand replacement by mass RP.

3. Results and Discussions

By analyzing the results of the mechanical resistance to compression, it can be observed that the greater the addition of tire residue, the lower the resistance. Figure 1 shows this behaviour of the samples. Resistance only increases with the reference sample after the aging process, whereas with RP samples the difference in resistance after aging is not relevant.

	7 days	28 days	after wetting and drying
Reference	5.17	6.70	7.90
10 %	3.20	3.48	3.77
15 %	1.92	2.08	2.13
20 %	1.43	1.99	1.67

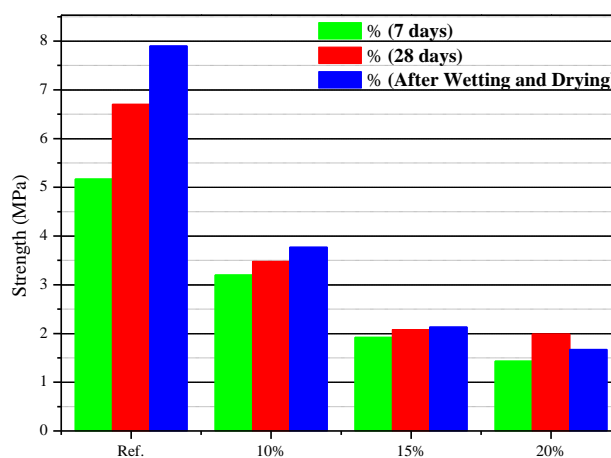


Table 1 Compressive strength values in MPa, after 7 days, 28 days and after wetting and drying.

Fig. 1. Mechanical strength after wetting and drying.

4. References

- [1]- N. V.Boltkova et al. Waste Management, **60**, 230–246 (2017).
- [2]- F. M. da Silva et al. Construction and Building Materials, **91**, 71–79 (2015).
- [3]- B.S.Thomas et al. Journal of Cleaner Production, **112**, 504–513 (2016).
- [4]- P. Zak et al. Construction and Building Materials, **106**, 179–188 (2016).

Acknowledgements

The authors would like to thank Coordenação de Aperfeiçoamento de Pessoal de nível Superior (CAPES) for financial support.

LOW TEMPERATURE ATMOSPHERIC PRESSURE PLASMA CAN REDUCE THE VIABILITY OF WOUND-RELATED MULTISPECIES BIOFILMS

Oliveira, M.A.C^{1*}, Lima G. M. G. ^{1.}, Sampaio, A.G. ^{1.}, Carvalho, R.C.R. ^{1.}, Kostov, K.G.², Koga-Ito C.Y.^{1.}

¹Institute of Science and Technology, São Paulo State University UNESP, São José dos Campos, Brazil.

²Department of Physics and Chemistry, São Paulo State University UNESP, Guaratinguetá, Brazil.

*Corresponding Author: cristiane.koga-ito@unesp.br

1. Introduction

Clinical treatment of chronic wounds is considered one of the main challenges in the medical area. Low temperature atmospheric pressure plasma (LTAPP) is generated by subjecting a gas to an electromagnetic field and has been considered promising for medical applications due to simultaneous antimicrobial, anti-inflammatory and tissue repair activities. The aims were to establish the effective parameters of LTAPP against wound-related multispecies biofilms, and to evaluate the cytotoxicity of the protocol to fibroblasts.

2. Experimental

Multispecies biofilms were formed by methicillin-resistant *Staphylococcus aureus* (ATCC 33591), *Pseudomonas aeruginosa* (ATCC 27853) and *Enterococcus faecalis* (ATCC 29212) on collagen membranes. The membranes were positioned on the surface of tryptic soy agar supplemented by SWF solution (50% fetal bovine serum and 50% NaCl 0.9% solution) 1:1. After 24 h incubation, biofilms were exposed to LTAPP for 1, 3, 5 and 7 min. Helium (99.5% purity) was used as working gas (2.0 SLM) and the adopted parameters were 32 kHz frequency and 1.0 W potency. The distance between nozzle and biofilm surface was kept fixed at 1.5 cm. Non-exposed control was included. Cytotoxicity of the effective protocol to fibroblasts 3T3 was tested. The experiments were performed in triplicate in three separate occasions.

3. Results and Discussions

The exposition for 5 min was able to reduce significantly the number of *S. aureus* ($p=0.019$), (Figure 1) *E. faecalis* ($p=0.000$), (Figure 2) and *P. aeruginosa* ($p=0.010$) (Figure 3) viable cells in the multispecies biofilm when compared to non-exposed control. The expositions for 1 and 3 min were not able to inhibit all the species. LTAPP showed low cytotoxicity to fibroblasts with 90% of cell viability after 24 h (Figure 4). LTAPP was able to reduce the viability of wound-related multispecies biofilms in 5 min, with low cytotoxicity to fibroblasts.

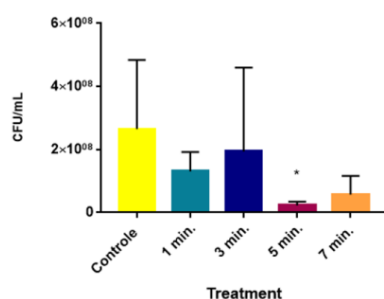


Fig. 1. Mean of the values of colony forming units per milliliter (CFU/ml) of resistant *S. aureus* methicillin isolated from multispecies biofilm.

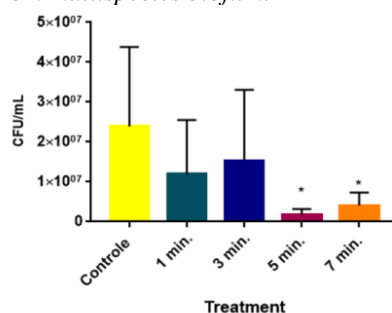


Fig. 3 Mean of the values of colony forming units per milliliter (CFU/ml) of resistant *P. aeruginosa* isolated from multispecies biofilm.

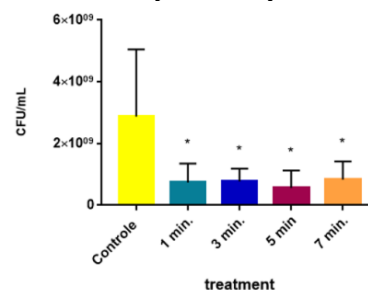


Fig. 2. Mean of the values of colony forming units per milliliter (CFU/ml) of resistant *E. faecalis* isolated from multispecies biofilm.

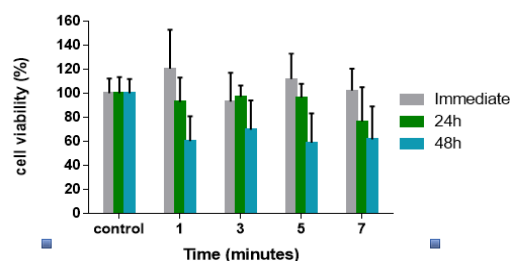


Fig. 4 Cytotoxicity analysis of low temperature plasma at atmospheric pressure expressed by percent cell viability.

Acknowledgements

Funding by CNPq (National Council for Scientific and Technological Development).

MINIATURIZATION, PROCESS INTENSIFICATION AND FIBERS: A PROPOSAL FOR LOW COST EQUIPMENT

Walter Pichi Jr¹, Roberto da Rocha Lima² and Maria Lúcia Pereira da Silva^{1,2*}

¹Faculty of Technology of São Paulo, Centro Paula Souza, Brazil

²School of Engineering, University of São Paulo, Brazil

*Corresponding Author: malu@lsi.usp.br

1. Introduction

Due to the huge development of microelectronics area, miniaturization becomes a reality for several different technological fields and one in particular has strongly emerged on the last decade: Process Intensification (PI). In order to speed this area development, some assets are required, in special portable, low cost equipment – with a set of functions that ranges from reactants admission to detection, and miniaturized unit operations [1]. Therefore, the aim of this work is the development and tests of a small low cost equipment useful for PI.

2. Experimental

This work followed the engineering recommendations for the development of electrical and mechanic instruments. It also relies on Sustainable Criteria, which means, among other issues, that only safety reactants were used. Commercial oxidized PAN fibres were used as packed on fluidized beds.

3. Results and Discussions

Figure 1a shows the main parts of the PI equipment. This instrument was project to receive 10 micro-reactors simultaneously and be heated up to 200°C, useful range for mainly organic reactions. The admission was manufactured to manipulate reactants on gaseous state, which means liquid ones should be inserted using a septum. The recommended amount of liquid is proportional to reactants vapour pressure but it is usually up to 10 μ liters. Detection is provided by TGS® sensors, which means that volatile organic compounds are easily detected. Reactors are made of copper and own 100 μ m channels. Fulfilled channels can be obtained using a felt of fibres, which surface are quickly modified by tetraethoxysilane hydrolysis, using not only acids but also basic reactants. Figure 1b shows such fibres (1mmX1mm sample) and the red circle points out the formation of a small amount of silicon oxide like structure. On this particular case, basic hydrolysis was carried out, which required a long time and favoured the formation this kind of structure. Finally, Figure 1c depicts a typical answer, obtained by the injection of 2-propanol on a sequence of 10 μ liters samples, in order to test adsorption. A reproducible response is clearly observed, with each step on the graph corresponding to one insertion. It is also possible to observe some transients, especially at the end of the graph; this is probably due to the saturation of the surface, whereas the last step shows an even more acute transient, probably owing to clogging. Moreover, desorption can be easily done (not shown on the figure) by micro-reactors heating. Thus, this low cost instrument can help on definition of several unit operations for PI.

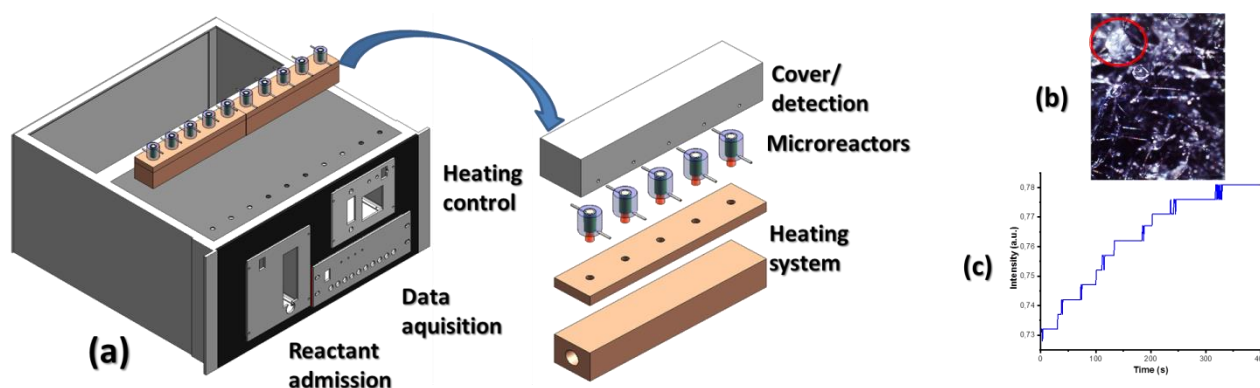


Fig. 1. PI instrument schematics (a) Fibre felt for micro-reactors (b) and (c) measurement of 2-propanol injection

4. References

- [1]- A. R. Leite. Equipamento versátil para teste de mini-estruturas utilizadas como mini-lab, 2016, <http://www.teses.usp.br/teses/disponiveis/3/3140/tde-19122016-153121/pt-br.php>

Acknowledgements

FAPESP and CNPq for financial support.

INFLUENCE OF SHOT PEENING ON THE FATIGUE BEHAVIOR OF AA 7050-T451

ALUMINUM ALLOY

Martin F. Fernandes^{1*}, Yara C. Bastos¹, Verônica M. O. Velloso¹ and Herman J. C. Voorwald¹
¹Department of Materials and Technology, Sao Paulo State University (Unesp), School of Engineering,
 Guaratinguetá. 12516-410. Sao Paulo, Brazil

*Corresponding Author: martin.fernandes@unesp.br

1. Introduction

AA 7050-T451 aluminum alloy is applied in aerospace applications due to a high strength-to-weight ratio. Strengthened aluminum alloys exhibit, despite high tensile strength values, a relatively low fatigue resistance [1]. As a result, aluminum alloys are frequently subjected to surface treatments [1]. Shot peening (SP) is a cold working process widely used to increase the fatigue strength that consists in impacting the surface of a component with round ceramic, glass or metallic particles [2]. The present work aimed at investigating the fatigue behaviour of AA 7050-T451 aluminum alloy treated with SP surface treatment.

2. Experimental

The material studied in this work is AA 7050-T451 aluminum alloy. Rotating bending fatigue tests (stress ratio $R=-1$) were carried out for the base material and SP treated specimens. The SP parameters were an Almen intensity of 0.41-0.49 mm A and coverage of 100%. The shot was made of S 230 with a hardness of 57 HRC. The treatment was carried out according to AMS 2430, and the granulometry was defined according to SAE J444. Scanning electron microscopy was used to observe the fracture surfaces. The residual stresses at the surface layer were measured using the X-ray diffraction method.

3. Results and Discussions

The fatigue test results for the base material and the SP treated condition are shown in Fig. 1, where only the average points are presented for each stress level. The results show that the shot peening treatment was capable of increasing the fatigue strength for all stress levels analyzed. The residual stress measurements showed that the SP modified the residual stress condition at the surface of the base material from -62 MPa to -130 MPa after the SP treatment. The fatigue behaviour results show that the compressive residual stress field created by the SP process was able to supplant the negative effect of the increased surface roughness after the process. The typical fracture surfaces for both conditions are displayed in Fig. 2. For the base material, the crack nucleation sources are indicated by arrows at the surface (Fig. 2a). For the material treated with SP, there were several crack nucleation sources around the specimen and the main fatigue crack propagation front originates from the region indicated by the arrow. The more compressive residual stress condition created by SP was capable of increasing the fatigue crack nucleation life and slow down the propagation of short fatigue cracks around the surface of the specimen. Therefore, the SP treatment with the parameters tested in this work was efficient in increasing the fatigue life of AA 7050-T451.

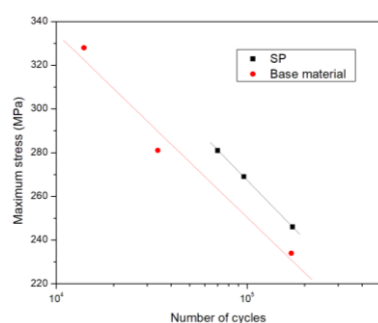


Fig. 1. S-N curves of the base material and after shot peening.

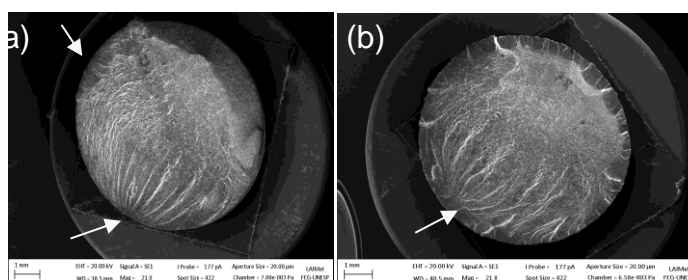


Fig. 2. Fracture surfaces of (a) base material tested at maximum stress of 281 MPa, (b) shot peened material condition tested at maximum stress of 269 MPa.

4. References

- [1]-M. Benedetti, V. Fontanari, P. Scardi et al., Int. J. Fatigue, **31**, 1225-1236, 2009.
- [2]-M.A.S. Torres and H.J.C. Voorwald, Int. J. Fatigue, **24**, 877-886, 2002.

Acknowledgments

This study was financed in part by the Coordenação de Aperfeiçoamento de Pessoal de Nível Superior - Brasil (CAPES) and São Paulo Research Foundation (FAPESP), grant # 2019/02125-1.

PROPRIEDADES MECÂNICAS DE NANOCOMPÓSITOS A BASE DE POLIETILENO LINEAR DE BAIXA DENSIDADE UTILIZANDO ÓXIDO DE GRAFENO E GRAFENO COMO CARGAS

Mayara C. de Araujo*, Natalia Lira, Guilhermino J. M. Fechine

Centro de Pesquisas Avançadas em Grafeno, Nanomateriais e Nanotecnologias - Mackgraphpe;

Universidade Presbiteriana Mackenzie, São Paulo, SP, Brasil

*Autor Correspondente: mayara.c.araujoo@gmail.com

1. Introdução

Nanocompósitos poliméricos obtidos pela inserção de cargas bidimensionais (2D) via mistura no estado fundido tem sido objeto de estudo de diversos pesquisadores devido ao aumento nas propriedades mecânicas, térmicas e elétricas que estas partículas podem proporcionar ao polímero mesmo em percentuais muito baixos [1]. O aumento nas propriedades mecânicas está relacionado com a capacidade de transferência de tensão da matriz para a nanopartícula e depende da dispersão das nanopartículas na matriz e da qualidade da interface gerada [2,3]. Este trabalho refere-se à preparação e caracterização de nanocompósitos a base de polietileno linear de baixa densidade – PELBD com óxido de grafeno (GO) e grafeno (G), a fim de se obter nanocompósitos poliméricos baseados em materiais 2D com diferentes possibilidades de interface.

2. Experimental

O óxido de grafeno foi obtido pelo método de Hummers modificado com posterior esfoliação líquida em meio aquoso e o grafeno previamente liofilizado foi igualmente esfoliado. As nanopartículas foram caracterizadas por espectroscopia Raman, difração de raios-X, análise termogravimétrica e microscopia de força atômica com o objetivo de comprovar a qualidade do material. Os nanocompósitos foram obtidos via mistura no estado fundido através do método Solid Solid Deposition – SSD [4] em extrusora dupla rosca, utilizando-se concentrações de carga entre 0% e 0,3% em massa e analisados por ensaios mecânicos para verificar de forma indireta a interação das nanopartículas com a matriz.

3. Resultados e Discussões

Através dos ensaios mecânicos observou-se que os nanocompósitos de PELBD/G apresentaram melhorias consideráveis em suas propriedades para as composições de 0,05% e 0,1%. De maneira análoga, os nanocompósitos de PELBD/GO também exibiram aumento em suas propriedades mecânicas para as mesmas concentrações, contudo, de maneira menos acentuada. Como esperado, o sistema PELBD/G apresentou melhores resultados, indicando que os nanocompósitos que possuem semelhança na polaridade de seus componentes, apresentam melhor interação carga/matriz.

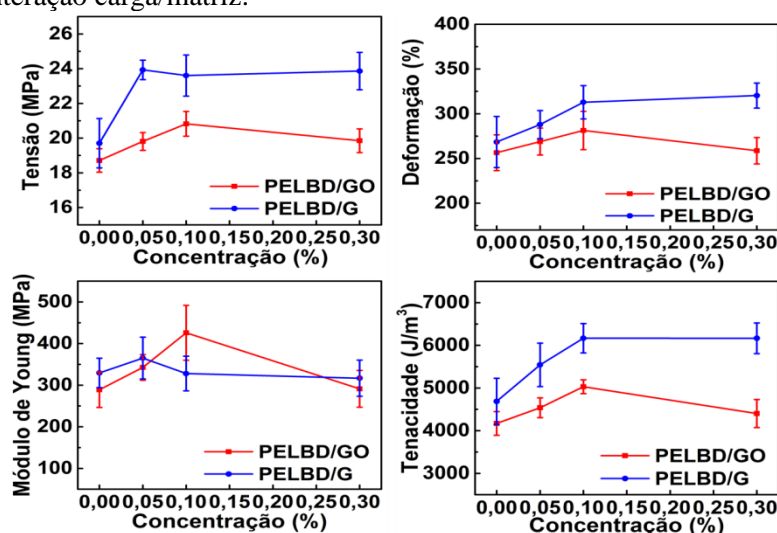


Fig. 1. Propriedades mecânicas dos nanocompósitos de PELBD.

4. Referências

- [1]-D. G. Papageorgiou, I. A. Kinloch & R. J. Young, Prog. Mater. Sci., **90**, 75–127, (2017).
- [2]-J. Phiri, P. Gane, & T. C. Maloney, Mater. Sci. Eng. B, **215**, 9–28, (2017).
- [3]-R. J. Young, et al, Compos. Sci. Technol., **154**, 110–116, (2018).
- [4]-P. A. R. Muñoz, et al, Express Polym. Lett., **12**, 930–945, (2018).

Agradecimentos

Ao Mackgraphpe e à CBrAVIC pela oportunidade de realização e apresentação deste trabalho.

STUDY OF THIN FILMS POLYMERIZATION PROCESSES OBTAINED BY 2-METHYL-2-OXAZOLINE PLASMAS UNDER LOW PRESSURE CONDITION

Rogério Pinto Mota*, Pedro William Paiva Moreira Júnior

UNESP – Univ. Estadual Paulista, Av. Dr. Ariberto Pereira da Cunha, 333 - Guaratinguetá, SP, Brazil.

*Corresponding Author: rogerio.mota@unesp.br

1. Introduction

Poly(2-oxazoline) are polymers that has similar structure to Poly(ethylene oxide) (PEO), however, instead of an oxygen on the repetition structure there is a nitrogen bonded to an acetyl group. These polymers might substitute PEO material in biomedical applications since they have the same properties of this material and new functionalities. As covering materials they present surface properties as resistance against protein attachment (bioinert or *non-fouling*), *non-cytotoxic*, biocompatibility and resistant to biological degradation [1]. These properties lead to applications like biosensors, *drug-delivery*, implants surface covering among others.

The plasma polymerization of this kind of materials includes advantages that are: one-step process where there is no requirement to solvents or catalytic substances, do not generate chemical waste and the minimum amount of monomer is utilized [2].

2. Experimental

Thin films were generated in a stainless-steel plasma reactor chamber. The discharges were excited by an rf-power supply, RF-300 model – Tokyo Hy-Power, at 13.56 MHz and the applied power was varied from 5 to 25 W. The chamber was evacuated by a mechanical pump, M-18 model – Edwards, while the pressure was monitored by Penning™ and Pirani™ gauges. The discharges were performed at 80, 120, 160 and 200 mTorr of total pressure. The 2-methyl-2-oxazoline monomer was utilized as precursor of plasma discharges.

The plasmas were investigated using optical emission spectroscopy in actinometric method (A-OES), using argon as diagnostic gas, and electrostatic measurements with RF-compensated Langmuir probe technique (electronic temperature). To perform A-OES a Horiba spectrometer (model MicroHR) with 1200 lines/mm grating and focal length of 140mm was used providing a spectral resolution up to 0.30 nm. The LP was designed with a retractable protective glass shell and a probe tip degassing system to avoid material deposition on the tip. It still has a choke system to avoid RF effects on the probe *I vs. V* signal. The thin films were studied by Fourier transform infrared spectroscopy (FTIR), where the Perking Elmer FTIR Spectrometer Spectrum 100™ was utilized. The water contact angle (WCA) technique was carried out by a Ramé-Hart 300-F1™ goniometer. A Shimadzu atomic force microscope (AFM) model SPM 9600 was used to measure the thin films roughness. The thickness of thin films was evaluated by confocal microscopy using a Leica DCM 3D microscope.

3. Results and Discussions

The electrons temperatures were observed between 0.2 and 0.4 eV. The electronic temperature behaviour was analyzed as a function of operating pressure and applied power. This behaviour was linked to production of CH, CN, CO and NH in 2-methyl-2-oxazoline plasmas. The mean roughness investigation, the bonds observed by FTIR technique and the deposition rates revealed the role of these species on polymerization processes. There were no species in the plasma phase related to volatile compounds production. High deposition rates, decreasing of closed oxazoline rings amounts in plasma polymers and at least three kinds of oxygen bonds were observed, showing that the plasma polymerization process was able to perform the ring opening process and fragmentation of monomer molecules. The cross-link structures and amount of polar groups on the plasma polymers surface were assigned to the thin films hydrophilic character. High concentrations of polar groups in 2-methyl-2-oxazoline plasma polymers were responsible to low contact angle values, around 10°.

4. References

- [1]-XIANG, L. N. et. al. Chinese chemical letters. v. 24, p. 597 – 600, 2013.
- [2]-RAMIASA, M. N. et al. Chem Commun. v. 51, p. 4279 – 4282, 2015.

Acknowledgements

The authors would like to acknowledge CAPES and FAPESP for the financial support.

D'ávila, N. I. C.^{1*}, Leme, L. C.¹, Campos, M. A. M. C.², Borille, A. V.¹

¹*Instituto Tecnológico de Aeronáutica - ITA, São José dos Campos, Brazil*

²*Escola Técnica Everardo Passos – ETEP, São José dos Campos, Brazil*

**Corresponding Author: davila@ita.br*

1. Introduction

According to Association for Manufacturing Technology (AMT) research, the gear production has grown in last years. However, the professional qualification is insufficient to meeting demand of this industrial sector. [1] The search for optimization of gear manufacturing process and performance are then continuous investigation objectives. The gear research is a major industrial challenge because involves many critical factors such as noise reduction, gain of power efficiency and reduction of weight in gearbox. [2]

A research project has been developed in a test center for gears designed in Competence Center in Manufacturing (CCM-ITA). This project has the purpose of controlling loading, temperature and rotation conditions in the gears, in order to evaluate and compare their state after test. In the initial analysis of the test center, some problems occurred during the durability test and one of the most important complication was torque relaxation, which the group judged as a possible cause was the wear of spacer bushings and the action plan decided to solve this problem is to perform heat treatment on bushings.

The bushings, located inside of gearboxes, have the function of delimiting the position of the gear in the axis and, therefore, guarantee their alignment. Therefore, the minimal wear of bushings allowed the axial displacement of the gear. The bushing material (1045 steel) has hardness lower than the axle stop and the gear, which they are in contact. Thus, the group suggested to execute a surface treatment, as plasma nitriding, in the bushings with the intention of the material surface acquiring similar mechanical proprieties of the adjacent surfaces in contact.

The concept of plasma also understood as "electric discharge" or "discharge luminescent" is applied to the definition of an ionized gas, which contains in total neutral species and electrically charged species such as electrons, positive ions, negative ions, molecules and atoms [3]. Ion nitriding is a glow discharge surface modification technique, which is used to increase the fatigue strength, wear, corrosion resistance and surface hardness of steels [4].

2. Experimental

The mechanical component is a bushing forged in 1045 steel with dimension of 45 mm in diameter external, 34 mm in diameter internal and 4 mm thickness in and it is used in a test bench of gear. This element presented an unpredicted wear failure during performance. With the intention of reducing wear failures, we propose to investigate the influence of surface treatment by plasma nitriding process as a driver of growth of nitrite layers on the material surface. Consequently, this process provides the increase of abrasive wear resistance. The bushing was exposed in plasma atmosphere with Nitrogen (80%), Hydrogen (10%) and Argon (10%), at a pressure of 3 Torr. The temperature controlled throughout the PVD (Plasma Vapor Deposition) process was 540 °C and the nitriding process lasted 3 hours. The nitrided samples were analyzed by the techniques of chromatic aberration microscopy (Cyber), scanning electron microscopy (SEM) and X-Ray Diffraction (XDR). In the final, all the analyzes were reproduced with the untreated bushes and the results were compared between nitrided and untreated samples.

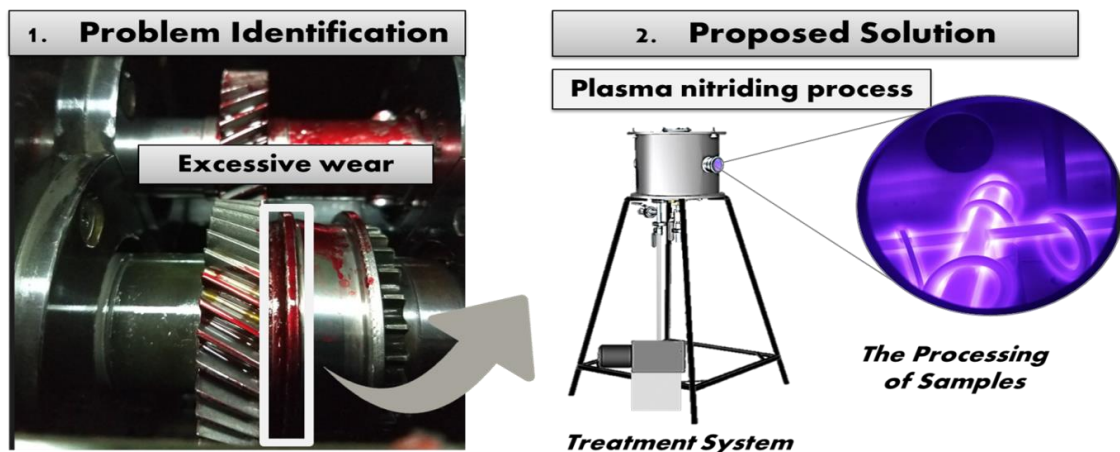


Fig. 1. Methodology Process.

3. Results and Discussions

The results demonstrate that the ion nitriding surface treatment improves to the evaluated mechanic component proprieties. The analysis results from Cyber show the removed wear volume in mm^3 and overview 3D images analysis. In the figure 2, the results demonstrate that the nitrided bushing presented better performance, than untreated bushing, when they were applied in the test bench gear. The sample T01 (untreated component) showed a wear of almost 95% more in volume lost in abrasive wear, than the component with nitriding (T01 - Nitriding Process). The sample T02 (untreated component) results presented the same behavioural pattern, which the component demonstrate a wear almost 82% more in volume lost in abrasive wear, than the component with nitriding (T02- Nitriding Process).

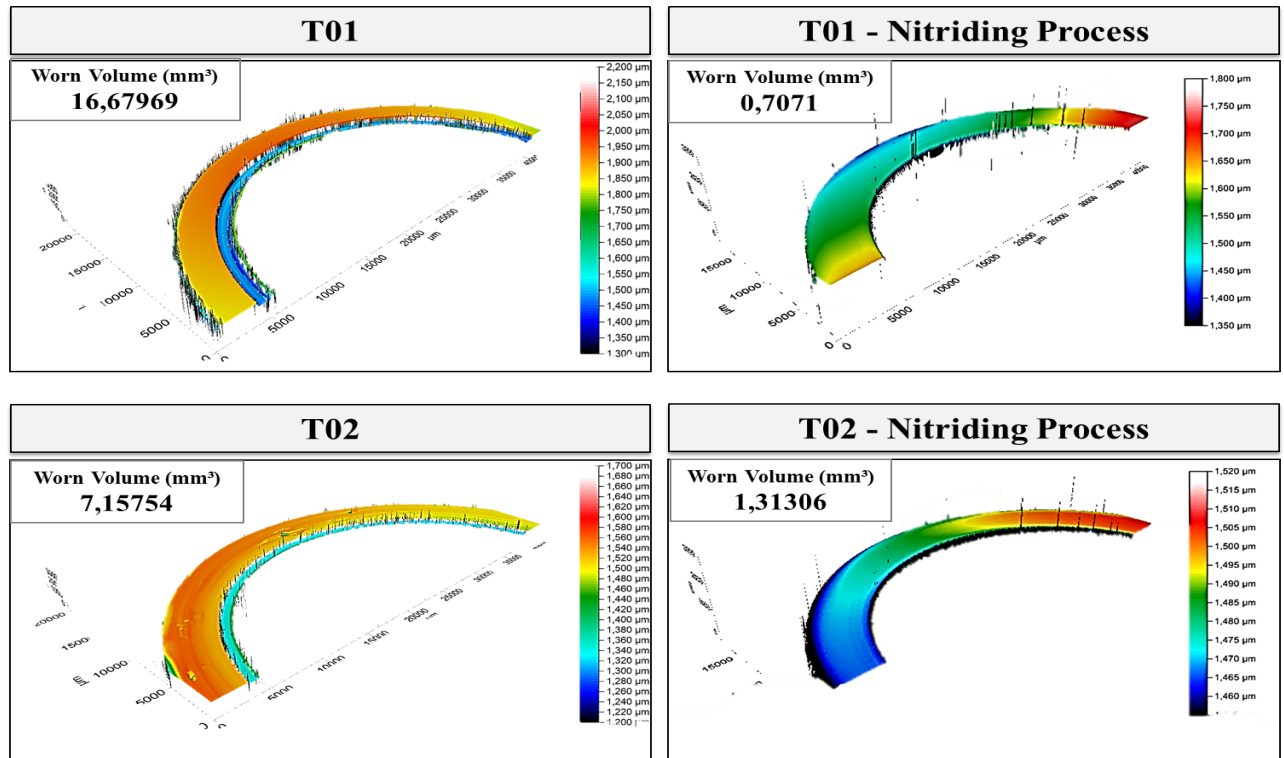


Fig. 2. Comparison of component wear - (Volume in mm^3)

These results suggest that the proposed surface treatment remarkably increased surface hardness and increased wear resistance. In application, the bushings improved in their live cycle, reducing at approximately 2,5 Nm/h in relation of the torque relaxation rate. In conclusion, the nitriding plasma is a kind of surface treatment that increases the wear resistance and consequently, improve the spacer bushing performances.

4. References

- [1]-Golden, M., "We'd Grow Faster If We Could", Magazine Gear Technology, January 2018.
- [2]-Capitalmind 2016, "Drive Technology – Gears", Capitalmind Corporate Finance Advisory Sector Repot, Summer 2016.
- [3]-CHAPMAN, B. N. Glow Discharge Process: Sputtering and Plasma Etching. New York, John Wiley & Sons, 1980.
- [4]-ALVES JR., C. Nitretação a plasma: Fundamentos e Aplicações. Natal/RN: Brasil, 2001.
- [5]-STOETERAU, R.L. ; L.C. Leal. "Apostilas de Tribologia". Departamento de Engenharia Mecânica – UFSC, 2004.

COMPARATIVE STUDY BETWEEN SAMPLES OF TI-TA ALLOYS PRODUCED BY LASER DEPOSITION AND ARC MELTING

Odila Florêncio^{1,2*}, Cícero Junior Rodrigues Lustosa¹, Yonaikel Josuhe Contreras Acosta¹, Marco Antonio Tito Patrício², Amélia Almeida³, Rui Vilar³

¹Universidade Presbiteriana Mackenzie, São Paulo, Brasil

²Universidade Federal de São Carlos, São Paulo, Brasil

³Instituto Superior Técnico, Universidade de Lisboa, Lisboa, Portugal

*Corresponding Author: odila.florencio@mackenzie.br

1. Introduction

Titanium and its alloys are of great interest in the biomedical area as structural materials due the good resistance to corrosion, low density and excellent chemical and mechanical biocompatibility presented [1]. Ti alloys can be found in the α or β phases, according to the type and amount of stabilizing element used [2]. The phase transition may occur as the concentration of β -stabilizing is increased, causing the martensitic structure α' (acicular martensite) to be replaced by α'' (orthorhombic martensite). The α'' phase can be considered a transition from the α' to the β phase [3]. In this work, Ti-Ta alloys fabricated by laser deposition and arc melting were studied. Their mechanical properties and microstructure were evaluated and compared.

2. Experimental

A combinatorial method was used for alloy synthesis that is based on the laser deposition technique with a gradient of compositions along the tracks. The alloys were deposited from mixtures of Ti and Ta powders, using a Nd-YAG laser. The Ti-40Ta ingots were fabricated using tantalum with 99,9% purity and titanium grade 2 in an arc melting furnace. The composition and microstructure of the alloys produced by both methods were characterized by XRD and SEM, while the mechanical properties were assessed using depth-sensing ultramicroindentation tests.

3. Results and Discussion

Fig. 1 shows a biphasic microstructure of the Ti-40Ta alloy produced by arc melting, where the lighter regions are rich in Ta (matrix-grain interior) and the darker regions (grain boundary) are rich in Ti (α'' phase with transition to α). The alloy presented a microhardness of 3.4 GPa and an elastic modulus of 71 GPa. Fig. 2 presents the microstructure of the Ti-36Ta produced by laser deposition, showing a very fine grain structure with predominance of the α'' phase and a low content of β . The Young's modulus of the alloys produced by laser decreases from 120 GPa to about 45 GPa with increasing the Ta content to 35% (wt.), corresponding to the region with the predominant α'' (orthorhombic) phase. The lowest value of Young's modulus (45 GPa) was obtained for the Ta-36Ti (wt%) alloy, that has a microhardness of 2.3 GPa. Due to the high fraction of the orthorhombic phase and the fine grain structure the laser deposited alloys are less stiff and softer than those produced by arc melting.

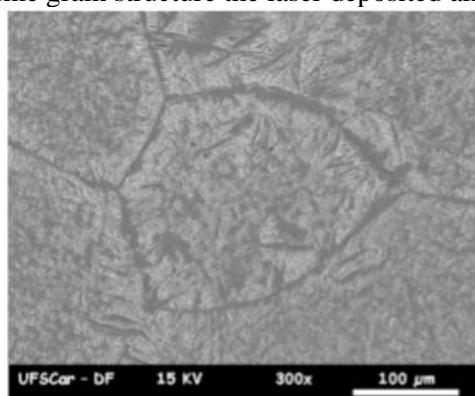


Fig. 1. Microstructure of the Ti-40Ta alloy produced by arc melting showing a biphasic region with presence of α'' phase (grain boundary) and β phase (inside the grain).

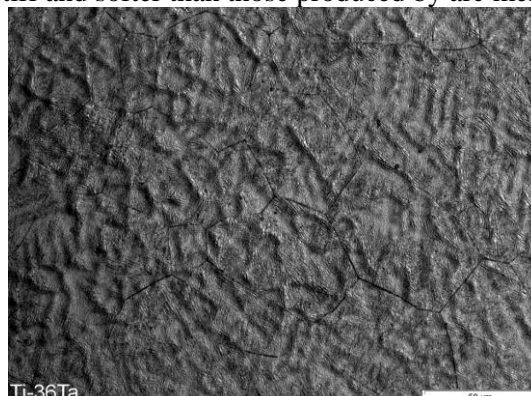


Fig. 2. Microstructure of Ti-36Ta alloy produced by laser deposition showing the predominance of the α'' phase (orthorhombic martensite).

4. References

- [1]- M. Geetha, A. K. Singh, R. Asokamani and A. K. Gogia, Progress in Materials Science, **54**, 397 (2009).
- [2]- M. Long, H. J. Rack, Biomaterials, 19 (18), 1621 (1998).
- [3]- G. Lütjering and J. C. Williams "Titanium", 1st edition, Springer, USA, (2003).

Acknowledgments

FAPESP (2011/20151-8)/Br, CAPES/Br, MackPesquisa/Br and FCT (PTDC/CTM/09811/2008)/Pt.

INFLUENCE OF PARAMETERS IN THE FABRICATION OF TiO₂

NANOTUBES FOR BIOMEDICAL APPLICATIONS

Patrícia Capellato^{1*}, Gilbert Silva¹, Daniela Sachs¹, Lucas V Vasconcelos¹, and Ana P. R. Alves Claro²

¹UNIFEI- Federal University of Itajubá, Av. BPS; 1303. Itajubá, Minas Gerais, Brazil

²UNESP- Uni. Estadual Paulista, Faculty of Mechanical Engineering, Guaratinguetá, São Paulo, Brazil

*Corresponding Author: pat_capellato@yahoo.com.br

1. Introduction

The ideal biomaterial specifically used for dental implants must exhibit biocompatibility, elastic modulus similar to natural bone, high strength, corrosion and wear resistance, high fatigue and ductility[1]. Current approaches for enhancing biomaterial osteo integration include topographical and biofunctional surface modifications[2]. Several studies have shown that by modifying the surface at a nanoscale or a microscale it can alter cellular response[3]. In this study, the self-ordered formation of nanotubular oxide layers on Ti–30Ta alloy was investigated.

2. Experimental

The Ti-30Ta alloy was fabricated by mixing Ti and Ta. These metals were combined using a melting process in a high purity argon atmosphere. The resulting ingots were homogenized and then cold -worked by a rotary swaging process. The anodization process was performed using a electrolyte solution containing HF +H₂SO₄ (1:9) + 5% DMSO on group A)12V for 20 min and group B) 35V for 40 min. The nanotube layer was annealed in an oxygen ambient furnace at 530 °C (5° C/min) for 3 hours. The Ti-30Ta alloy surface were investigated using scanning electron microscopy (SEM), contact angle measurement and X-ray diffractometer (XRD).

3. Results and Discussions

The results indicated that the anodization process on Ti-30Ta alloy was highly influenced by time duration and voltage. SEM images confirm results of a parameter-driven surface topography. Figure 1 A) shows the surface whitout nanotube and Figure 1B) we can see nanotube formation. The crystalline phase of TiO₂ nanotube array was the same for all conditions. The water-drop method identified a hydrophilic interface, which is preferable for eliciting a favourable environment for cellular interaction

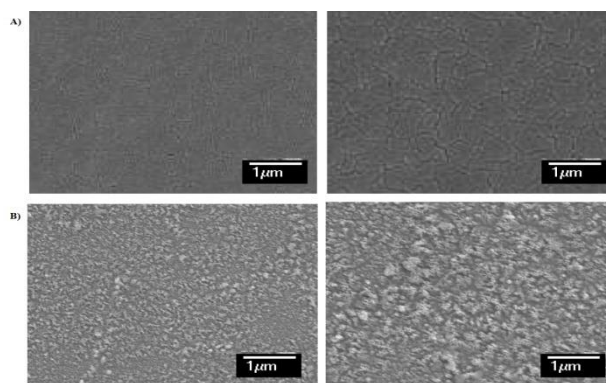


Fig. 1. SEM images of Ti-30Ta alloy substrate surfaces after anodization in HF +H₂SO₄ (1:9) + 5% DMSO A) 12V/20 min and B) 35V/40 min. The samples annealed in an oxygen ambient furnace at 530 °C for 3 hours.

4. References

- [1]-M. Geetha et al. Ti based biomaterials, the ultimate choice for orthopaedic implants - A review. Progress in Materials Science, **54**, 397-425,(2009).
- [2]-P. Capellato et al. Interaction between mesenchymal stem cells and Ti-30Ta alloy after surface treatment. Journal of Biomedical Materials Research Part A, **102**, 2147-2156, (2014).
- [3]-P. Capellato et al. Fibroblast functionality on novel Ti30Ta nanotube array. Materials Science and Engineering: C , **32**, 2060- 2067,(2012).

Acknowledgments

Partial funding support for this work was provided by the Brazilian federal government and the National Council for Scientific and Technological Development (CNPq).

PLASMA POLYMERS PRODUCED UNDER LOW PRESSURE CONDITIONS OF ETHYLENEDIAMINE AND ACETYLENE MIXTURE

Pedro William Paiva Moreira Júnior*, Rogério Pinto Mota

UNESP – Univ. Estadual Paulista, Av. Dr. Ariberto Pereira da Cunha, 333 - Guaratinguetá, SP, Brazil.

*Corresponding Author:

1. Introduction

Functionalized amine-containing coatings are of interest in biomedical applications by its capacity to improve human cells attachment, hydrophilicity and non-fouling characteristics [1]. They can present applications as implant coatings, drug delivery and enzyme electrodes production. The plasma polymerization of these materials is advantageous since it is a one-step dry process, solvents free, do not generate dangerous waste and the thin films can be deposited in a wide range of substrates [2]. There are many nitrogen-containing precursors of these coatings as allylamine, cyclopropylamine, oxazoline, ethylenediamine (EDA) among others. The EDA is a monomer that presents a 1:1 N/C ratio in its structure, being an excellent candidate to produce those films; however it was observed that the films produced by only EDA discharges are very soluble in water. In this work, the mixture EDA / acetylene (C_2H_2) was utilized with 3:7 ratio to produce low solubility amine-rich coatings.

2. Experimental

The thin films were generated in a stainless-steel plasma reactor chamber. The discharges were excited by an rf-power supply, RF-300 model – Tokyo Hy-Power, at 13.56 MHz and the applied power was varied from 5 to 30 W. The chamber was evacuated by a mechanical pump, M-18 model – Edwards, while the pressure was monitored by Penning™ and Pirani™ gauges. The discharges were performed at 100 and 200 mTorr of total pressure. It was utilized the EDA/ C_2H_2 ratio of 3:7 to produce the thin films

The plasmas were investigated using optical emission spectroscopy in actinometric method (A-OES), using argon as diagnostic gas, and electrostatic measurements with RF-compensated Langmuir probe technique (electronic temperature). To perform A-OES a Multichannel Avantes spectrometer (model AvaSpec-ULS2048X64) with 600 lines/mm grating and focal length of 75mm was used providing a spectral resolution up to 0.70 nm. The LP was designed with a retractable protective glass shell and a probe tip degassing system to avoid material deposition on the tip. It still has a choke system to avoid RF effects on the probe I vs. V signal. The thin films were studied by Fourier transform infrared spectroscopy (FTIR), where the Perking Elmer FTIR Spectrometer Spectrum 100™ was utilized. The water contact angle (WCA) technique was carried out by a Ramé-Hart 300-F1™ goniometer. A Shimatzu atomic force microscope (AFM) model SPM 9600 was used to measure the thin films roughness. The thickness of thin films was evaluated by confocal microscopy using a Leica DCM 3D microscope.

3. Results and Discussions

The electrons temperatures were observed between 0.4 and 1.2 eV and the plasmas electron densities were about $10^{-15} m^{-3}$. The electronic temperature behavior was analyzed as a function of operating pressure and applied power. This behaviour was linked to production of CN, CH and NH species in plasmas of EDA and C_2H_2 mixture. The mean roughness investigation, the bonds observed by FTIR technique and the deposition rates revealed the role of these species on polymerization processes. The CN species in plasmas were responsible for production of volatile groups both in the growing polymers surface and in suspension. The cross-link structures and amount of polar groups on the plasma polymers surface were assigned to the thin films hydrophilic character. The amount of nitrogen groups (amines) in plasmas polymers of EDA and C_2H_2 mixture were closely related to contact angle behaviour. Plasma polymers with higher amounts of amine groups were obtained under conditions in which low CN concentrations was observed on plasmas of EDA and C_2H_2 mixture. The nitrogen-rich films, produced by plasma polymerization of EDA and C_2H_2 mixture, presented low solubility in water.

4. References

- [1]-GRIESSER, H. et al. J. Biomater. Sci. Polymer. v. 3 (6), p. 531 – 554, (1995).
- [2]-H. Testrich, H. Rebl, B. Finke, F. Hempel, B. Nebe and J. Meichsner, Mat. Sci. and Eng. C, **33**, 3875-3880, (2013).

Acknowledgments

The authors would like to acknowledge CAPES and FAPESP for the financial support.

ELECTRICAL CHARACTERIZATION OF α -Sb₂O₄ ZIGZAG NANOBELTS

Rosana A. Gonçalves^{1*}, Maurício R. Baldan², Adenilson J. Chiquito³, Olivia M. Berengue¹

1. Introduction

Antimony tetroxide (Sb_2O_4) is a wide gap semiconductor with two allotropes phases: orthorhombic (α -phase) and monoclinic (β -phase), being the first most stable even at high temperatures [1]. α - Sb_2O_4 presents important optical properties and it have been used for applications as flame retardants, catalytic agents, ceramic enamels, batteries, dyes degradation, etc. [2] However, despite the variety of applications, little attention has been paid to the electronic properties of this material in its nanostructural form. In this work, α - Sb_2O_4 nanostructures studied by using two-terminal devices measurements and data on electron conduction mechanisms. Results confirm the Sb_2O_4 has obtained semiconductor character and also that thermionic emission is the dominant conduction mechanism at a high temperatures range (300-490K).

2. Experimental

The α - Sb_2O_4 zigzag nanostructures used in this work were grown on Si/SiO₂ substrates with the aid of Au nanoparticles through the vapor-solid (VS) growth mechanism driven by a thermal evaporation process. The two-terminal devices were fabricated by evaporation of Au metal contacts (100 nm) on the as-grown Sb_2O_4 nanobelts by using shadow masks. Figure 1 (insert) shows the schematic drawing of the obtained electronic device. Electrical characterization was performed and current-voltage ($I \times V$) curves and temperature-dependent resistance measurements were obtained by using an electrometer (Keithley 6517) and a closed cycle helium cryostat (Janis CCD 400H) working at ambient pressure.

3. Results and Discussions

The current-voltage curves ($I \times V$) presented in the Figure 1 shows that the current in the device increases linearly with the applied voltage confirming the formation of ohmic contacts. Moreover, as the temperature increases the slope of the curves decreases indicating that the material resistance is reduced with temperature as expected in intrinsic semiconductor materials. Temperature-dependent resistance measurement is depicted in Figure 2 and also shows the expected dependence of resistance with temperature for an intrinsic semiconductor: as the temperature increases, the conductivity increases. Furthermore, the curve is similar to the characteristic pattern for thermal emission indicating that this is the dominant conduction mechanism in the sample. This is the first direct experimental confirmation, so far as we know, of the semiconductor character of nanostructured α - Sb_2O_4 .

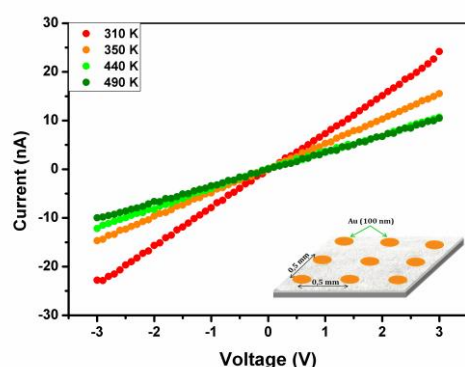


Fig. 1. $I \times V$ curves for Sb_2O_4 based device in different temperatures.

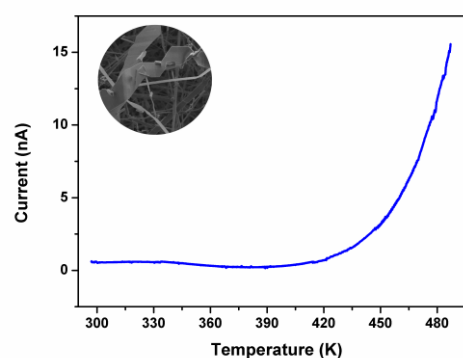


Fig. 2. Temperature-dependent resistance measurements taken from Sb_2O_4 nanobelts.

4. References

- [1]- T. Cebriano, B. Méndez and J. Piqueras, Cryst. Eng. Comm., **18**, 2541-2545, (2016).
- [2]- H. W. Kim et al, Electrochem. Solid State Lett., **15**, K49-K52, (2012).

Acknowledgments

This work was supported by Coordenação de Aperfeiçoamento de Pessoal de Nível Superior - Brasil (CAPES) - Finance Code 001 and by the Brazilian funding agencies FAPESP (grant number 2015/21816-4) and CNPq.

GERMINATION RATE OF SUNFLOWER SEEDS TREATED BY PLASMA

T. S. M. Mui, R. P. Mota, K. G. Kostov
Faculty of Engineering – FEG, Universidade Estadual Paulista – UNESP, Guaratinguetá, SP, Brazil
**Corresponding Author: taiana_mui@yahoo.com.br*

1. Introduction

In the last two decades, atmospheric pressure plasma (APP) has received significant attention in agriculture and food industry [1]. Plasma is being employed in many different sub-groups process of agriculture, from decontamination of seeds, plants or soil to controlling insect pests in the field [2,3]. It is known that reactive nitrogen species (RNS) and reactive oxygen species (ROS) participate in plant developmental processes such as seeds germination and roots growth [1,2]. However, the mechanisms of how it can affect directly the seeds and later the seedlings treated by plasma are still unclear. Due to vast differences between plants species and plasmas setups, the effects of plasma on seeds are not fully comprehended, yet [2]. Therefore, in this study the effect of an atmospheric pressure plasma jet treatment on sunflower seeds were investigated. Seeds surface were characterized and the seeds germination rate were documented.

2. Experimental

A plasma jet with a funnel nozzle, reported in previous work [4] was applied to treat sunflower seeds. Argon plasma was excited by an AC power supply generating an amplitude-modulated sinewave with 25 kHz frequency and 24.0 kVp-p amplitude.

Sunflower seeds germination was performed in two different ways: on petri-dish with filter paper and on commercial soil substrate, which were placed inside a greenhouse with controlled light, water and temperature.

Leaves area, shoots and roots length were collected after 4 week of germination. A qualitative experiment was also performed to verify the absorption of water on sunflower seeds with bromophenol blue ink.

3. Results and Discussions

Germination rate of the petri-dishes seeds versus the ones sown in commercial soil presented a significantly delay in the first 48 h.

Results of ink absorption showed that in plasma treated seeds the ink penetrated deeply inside the seeds coating and hulk, while on untreated seeds the ink did not permeate as much as on plasma treated seeds. As water plays an important role in germination of the seeds, this could be an indication of how plasma is affecting the seeds.

The obtained results can elucidate a little further on how plasma affects the sunflower seeds germination and later the seedlings growth.

4. References

- [1]-A.G. Volkov et al. *Bioelectrochemistry* 128, 175–185, (2019).
- [2]-D.H. Kwon, H-S Kimb, M-R Park, *Journal of Asia-Pacific Entomology* 22, 868–873, (2019).
- [3]-J. Lee et al. *Food Chemistry* 240, 430–436, (2018).
- [4]-T.S.M. Mui, R.P. Mota, A. Quade, L.R.O. Hein, K.G. Kostov. *Surf. Coat. Technol.* 352 (2018).

Acknowledgements

This research was supported by FAPESP under grant 2015/21989-6 and was financed in part by the Coordenação de Aperfeiçoamento de Pessoal de Nível Superior - Brasil (CAPES) - Finance Code 001.

THE CARBON NANOTUBE/MALEIC ANHYDRIDE PREMIX INFLUENCE ON PLASMA FUNCTIONALIZATION

Teresa Tromm Steffen^{1*}, Luis César Fontana¹, Daniela Becker¹, Peter Hammer²
¹Center for Technological Sciences, UDESC, Joinville, Santa Catarina, Brazil
²São Paulo State University (UNESP), Institute of Chemistry, Araraquara, Brazil
 *Corresponding Author: teretromm@hotmail.com

1. Introduction

Carbon nanotubes (CNT) have emerged recently as an interesting nanomaterial for water purification and desalination [1]. However, to they act efficiently at this propose it is first necessary to provide their functionalization, which can be reached by plasma treatment [2]. At this work, the CNT were functionalized by plasma with maleic anhydride (MA) in solid form, against to the traditional method involving the monomer insertion in gaseous form. CNT and MA were mixed by two different ways before the functionalization process and characterized to analyze the premix influence in CNT functionalization.

2. Experimental

CNT (purity > 95%) and MA (purity > 98,5%) were mixture at proportion 90:10 in mass proportion through two methods: 1) in a planetary mill by 10 minutes at 300 rpm; 2) with mortar and pestle assistance, manually. Samples were treated through ICP-RF plasma at 35 W, 1 Torr, by 15 and 30 minutes. Argon (12.2 sccm) was utilized as working gas. Samples treated were washed three times with methanol before characterization. To only evaluate the effect of mixture method on CNT's properties, samples obtained after premixing were submitted to the same washing procedure.

3. Results and Discussions

FTIR spectra (Fig. 1) indicates the CNT plasma functionalization and the MA opening ring at the plasma process [3, 4]. XPS (Fig. 2) indicates that the mortar-assisted premix is more favorable for posterior plasma treatment O-C=O insertion than the planetary mixing. Regarding to H₂O molecules, for samples premixed using the planetary method, only a small reduction in water percentage relative to the pristine CNT was observed, while, for those premixed with mortar assistance, the water was completely removed from the samples. The selective adsorption of methanol in CNT functionalized with MA may find applications in carbon nanotube drying and methanol/water separation.

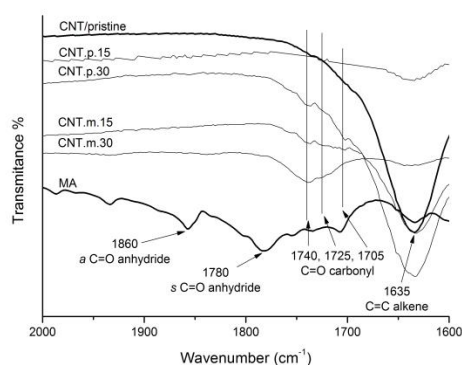


Fig 1. FTIR spectra showing new bands at 1740, 1725 and 1705 cm^{-1} , assigned to C=O stretching vibrations from carbonyl groups, pointing the CNT functionalization. MA opening ring is suggested in the plasma process by the absence of bands at 1780 and 1860 cm^{-1} in samples treated., related to C=O stretching vibrations of cyclic anhydride.

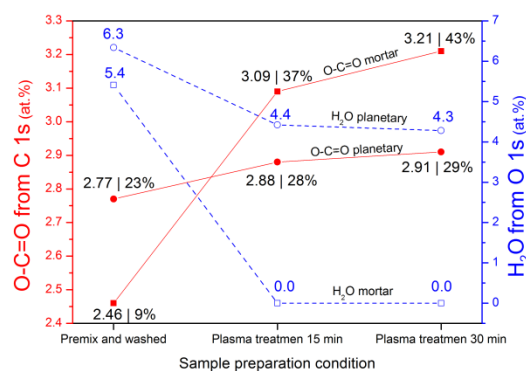


Fig. 2. Atomic percentage (at.%) of O-C=O groups (red) and H₂O molecules (blue), extracted respectively from the fitted C 1s and O 1s spectra, for samples premixed and washed or plasma-treated using different preparing methods: mortar (square) and planetary mixer (circle). The numbers presented after de vertical bar indicate the percentage increase in respect to the pristine CNT sample. The lines are guides for the eyes.

4. References

- [1]-Ihsanullah, Sep. Purif. Technol., **209**, 307–337, (2019).
- [2]-M.U. Farid, et al., Chem. Eng. J., **325**, 239–248, (2017).
- [3]-E. Guinter, L.C. Fontana, D. Becker, Bull. Mater. Sci., **42**, 23, (2019).
- [4]-T.T. Steffen, et al., Polym. Compos., **40**, E1162–E1171, (2018).

Acknowledgments

This work was supported in part by the Coordenação de Aperfeiçoamento de Pessoal de Nível Superior - Brasil (CAPES) [Finance Code 001] and CNPq [project Universal/445242/2014-0].

SURFACE ENERGY OF TITANIUM NITRIDE THIN FILMS WITH NITROGEN GRADIENT ALONG FILM THICKNESS

Thais Macedo Vieira*, Gabriel Cardoso Grime and Julio César Sagás

¹Laboratory of Plasmas, Films and Surfaces, Universidade do Estado de Santa Catarina, Joinville, Brazil

*Corresponding Author: vieira.thaism@gmail.com

1. Introduction

Titanium nitride (TiN) thin films have diverse applications in different areas due their mechanical, optical and electrical properties. This material is a ceramic with some metallic properties. In particular, TiN has higher electrical conductivity than Ti [1]. Functional coatings can be obtained through compositional gradients. In this work, the N concentration in TiN films was varied along film thickness and the effects of this procedure in surface energy were evaluated in comparison with homogeneous TiN and Ti films.

2. Experimental

The films were deposited onto Si substrates by grid-assisted magnetron sputtering. Working pressure was fixed at 0.40 Pa and all depositions were carried out with a constant discharge current of 2.00 A in Ar/N₂ atmosphere. The grid-target distance was 2.0 cm and the target-substrate distance 7.5 cm. The substrates were biased at -30 V and heated up to 300°C. Three samples were deposited for each condition. TiN films were deposited with constant N₂ flow rate (TiN H) and with progressive increase of N₂ flow rate during deposition (TiN G). Prior all TiN depositions a Ti interlayer was grown to improve adhesion. Contact angle hysteresis was measured for deionized water by tilting base method. The surface energy was evaluated by the multi-liquid method [2] using glycerol, deionized water, ethyleneglycol and dimethyl sulfoxide.

3. Results and Discussions

The hysteresis contact angle (Fig. 1) has no significant difference between homogeneous and graded TiN. It denotes a homogeneous surface in both cases. An increase (decrease) of dispersive (polar) component of surface energy is observed when comparing TiN and Ti (Fig. 2). However, the N gradient has no effect on total surface energy.

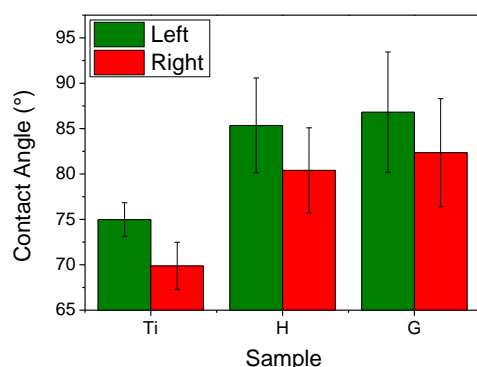


Fig. 1. Hysteresis contact angle in 90° of the sample groups Ti, H and G.

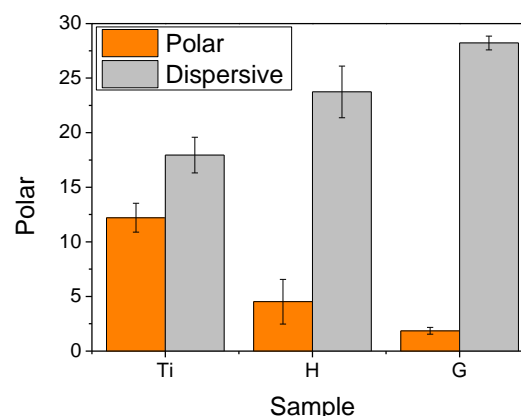


Fig. 2. Polar and dispersive components of the surface energy of the sample groups Ti, H and G.

4. References

- [1]-T. Oyama "The Chemistry of Transition Metal Carbides and Nitrides", 1st edition, Blackie Academic & Professional, USA, (1996).
- [2]-P. Favia and R. D'Agostino, Surf. & Coat. Tech., **98**, 1102-1106, (1998).
- [3]-S. Siboni, C. Della Volpe, D. Maniglio, M. Brugnara, The solid surface free energy calculation: II. The limits of the Zisman and of the "equation-of-state" approaches, J. Colloid Interface Sci. 271 (2004) 454-472.

Acknowledgments

This project has been funded by FAPESC through the program PAP in association with UDESC under contract PAP-TR 655. Thais Macedo Vieira also thanks UDESC by the financial support through PROMOP grant.

PORTLAND CEMENT MORTAR WITH ADDITION OF BARYTE (BaSO_4)

Yonaikel Josuhe Contreras Acosta*, Antônio Hortêncio Munhoz, Odila Florêncio
Universidade Presbiteriana Mackenzie, Rua Consolação, 930 – São Paulo – SP – Brazil
 *Corresponding Author: josuhecontreras@gmail.com

1. Introduction

Cementitious materials have been used historically in the society for their important properties of strength, low cost and convenience in production. The use of additives can become fundamental in the production of composite materials with innovative physical and chemical properties. In this work was prepared Portland cement mortar with addition of baryte, studying the rheological, mechanical and attenuation properties of ionizing radiation, trying to reduce in the future the volume and cost of barriers with cementitious material, decrease the use of lead in equipment and workrooms further harmful contact with the human body. In this work the preliminary tests of this project will be presented.

2. Experimental

Mortars were prepared using a mechanical mixer, water/cement ratio of 0.7 with addition of 0; 15; 20 and 25wt% of baryte. Then, cylindrical specimens with dimensions of 5 cm in diameter and 10 cm in height were molded and transferred to a humid chamber, demolded after 24 hours and remained under conditions of temperature ($23 \pm 2^\circ\text{C}$) and humidity $\geq 95\%$ by defined period for curing and performing the other tests (3, 7, 14 and 28 days). *Characterization of the samples:* The baryte used was supplied by the company Necipa and characterized in the laboratories of Mackenzie Presbyterian University by several techniques. The X-ray dispersive energy spectroscopy (EDS) test was performed on the Jeol JSM-6510 scanning electron microscope. Material density was determined following by pycnometer. Thermal analyses: thermogravimetric analysis (TG) and differential thermal analysis (DTA) were performed in a Netzsch-Jupiter STA449F3 equipment heating from room temperature to 1300°C at 10 K/min and $50 \text{ cm}^3/\text{min}$ N_2 flow. The mortar was characterized in the fluid state by the table test for slump test [1]. In the compressive strength test specimens with and without baryte at different curing ages have been tested on the Universal Testing Machine.

3. Results and Discussions

The specific gravity calculated in the pycnometer test is 4.2. Thermal analysis shows an initial mass loss due to dehydration and a total loss of 1.47%. (Figure 1) The material presents at the temperature of 1188°C the endothermic transition. The mortar slump test shows an approximate 10% decrease in the formulation with the addition of 20% baryte. Barium weight percentage is 38.30% registered in the analysis by EDS. In the compression tests, the 25 wt% baryte mortar registers the highest resistance values and wave propagation speed for 28 days of cure. (Figure 2) and ultrasound tests showed similar behavior.

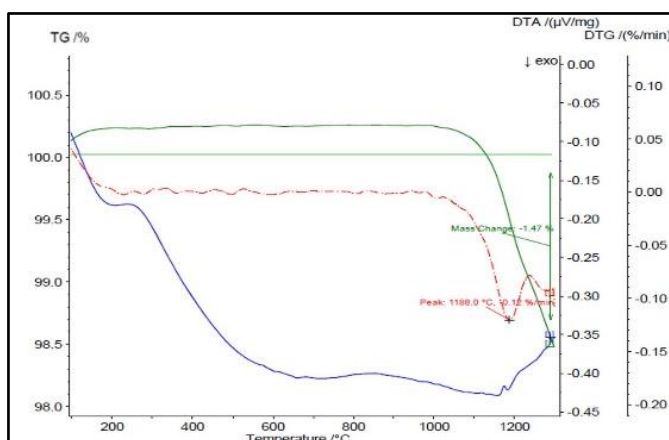


Fig. 1. Thermal Analysis

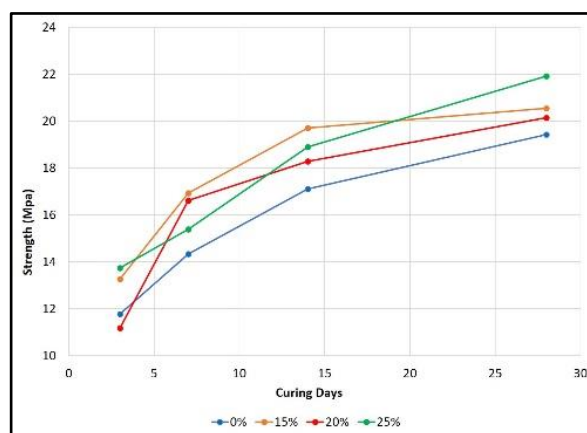


Fig. 2. Compressive Strength

4. Reference

[1]- ABNT NBR 7215 Cimento Portland - Determinação da resistência à compressão 1996.

Acknowledgments

This work was supported by Capes, Fapesp and MackPesquisa

THE INFLUENCE OF THE THICKNESS OF SULPHUR-DOPED TiO₂ FILMS ON THE METHYL ORANGE DYE DEGRADATION UNDER VISIBLE LIGHT

Rodrigo Teixeira Bento^{1,2}, Olandir Vercino Correa¹, Thiago Fernando dos Santos¹, Marina Fuser Pillis^{1*}

¹Materials Science and Technology Center, Nuclear and Energy Research Institute (IPEN–CNEN/SP)

²São Judas Tadeu University

*Corresponding Author: mfpillis@ipen.br

1. Introduction

Sulphur-doped titanium dioxide (TiO₂) films are promising photocatalysts for water treatment by heterogeneous photo catalysis under visible light [1]. However, their photocatalytic behavior is influenced by several parameters, such as the pH of the reaction medium, the luminous intensity of the radiation source, and the structural and morphological characteristics of the films [2]. In this way, in order to ensure an efficient photo catalytic activity, the present work evaluated the influence of the sulfur-doped TiO₂ film thickness on the methyl orange (MO) dye degradation under visible light.

2. Experimental

280 nm and 470 nm-thick TiO₂ films were grown on borosilicate substrates (25x76x1 mm) at 400 °C by metal organic chemical vapour deposition (MOCVD) process. Subsequently, the catalysts obtained were sulphur-doped in a horizontal tubular furnace for 60 min at 50 °C under a 0.2 slm flux of the mixture H₂-2v.% H₂S. The photo degradation tests of the MO dye was carried out in a homemade reactor setup previously described by Bento and Pillis [2], and the dye concentration was measured in a UV-vis spectrophotometer.

3. Results and Discussion

The cross-sectional FE-SEM analyses revealed the formation of a dense columnar anatase-TiO₂ films characteristic of the growths by MOCVD [2]. The films grow perpendicular to the substrate surface, and exhibit good uniformity of thickness and good adhesion to the substrate. The results indicated that the film thickness was preserved after the sulphur-doping process. XPS depth profile revealed the formation of SO₄²⁻ groups on the catalysts surface, and indicated the cationic diffusion of the S⁶⁺ ions, forming a Ti-O-S bond, probably replacing the Ti⁴⁺ cations [1]. Photo degradation tests showed that the 470 nm-thick sulphur-doped TiO₂ film exhibited the best photo catalytic behaviour (Fig. 1), with 72.1 % of the MO dye degradation in 300 min., 87.7 % more efficient than the 280 nm-thick film. The less thick films have a higher electron recombination rate than thicker films [3].

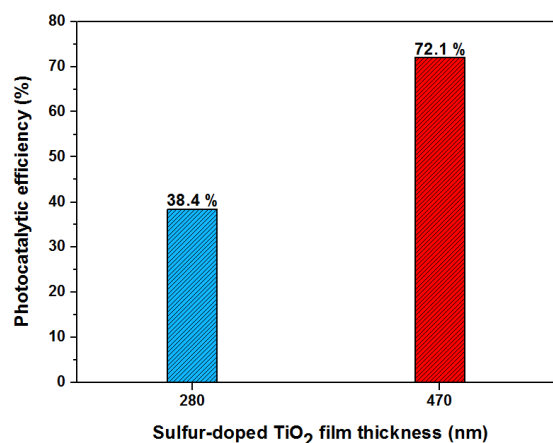


Fig. 1. Influence of the sulfur-doped TiO₂ film thickness on the methyl orange dye degradation under visible light.

4. References

- [1]-R. T. Bento, O. V. Correa and M. F. Pillis, *J. Eur. Ceram. Soc.*, **39**, 3498-3504, (2019).
- [2]-R. T. Bento and M. F. Pillis “*Titanium dioxide films for photocatalytic degradation of methyl Orange dye*”, 1st edition, InTech, London, (2018).
- [3]-H.A.J.L. Mourão, et al. *Quim. Nova*, **32**,8, 2181-2190, (2009).

Acknowledgments

The authors are grateful to the Brazilian agencies CAPES, CNPq (Proc. 168935/2018-0), and FAPESP (Proc. 05/55861-4) for the financial support.

INVESTIGATING THE AGING OF WATER TREATED BY COLD ATMOSPHERIC PLASMA

Rayanne Cássia de Sousa Freitas¹, Jussier de Oliveira Vitoriano², Clodomiro Alves Junior^{1,2*}

¹Federal Rural University of Semiárid, Mossoró, RN, Brazil

²Federal University of Rio Grande do Norte, Natal, RN, Brazil

*Corresponding Author: Clodomiro.jr@ufersa.edu.br

1. Introduction

Cold atmospheric plasma applied in liquid has attracted considerable attention in recent years due to its potential for application in agriculture, health and other living tissue [1,2]. Since in living tissues water is always present, the study of plasma - liquid interaction is fundamental in these applications. When discharge is produced over water in atmospheric air, different species as ions, excited and neutral energetic particles are formed on surface, reacting with water. Depending of plasma polarity, voltage and duration time of the discharge, different products can be formed during and after plasma treatment [3]. In this work, aging of plasma activated water was investigated through the change in pH, electrical conductivity, NO₃ and NO₂ concentration.

2. Experimental

Electric discharge produced by a voltage of 15 kV and 500 Hz was applied at a distance of 5 mm from the surface of distilled water contained in a 15 ml beaker (Fig. 1). After application for 15 min, the samples were stored in an open or closed container. Monitoring of pH, electrical conductivity in addition to NO₂ and NO₃ concentrations were performed. Cathodic and anodic polarization of the discharge were used. Each condition was repeated 3 times.

3. Results and Discussions

It was found that the pH was reduced from 6.5 to 5.8 on cathodic polarization. For anodic polarization this reduction was lower. After the treatment, the acidification process continued for times greater than 8h, when it stabilized at a pH around 4. For samples exposed in closed containers, the decay rate was higher. With respect to the electrical conductivity, there was an increase of 14 $\mu\text{S/cm}$ (untreated), to approximately 20 $\mu\text{S/cm}$ (treated sample) and progressive increase over time to around 350 $\mu\text{S/cm}$ (open system) or 200 $\mu\text{S/cm}$ (closed system). The concentration of nitrite tends to remain constant after treatment, while nitrate has a slight increase from 6 to 8 mg/L. We concluded from these results that plasma change permanently distilled water. Even with the plasma turned off, the concentrations of reactive components in the aqueous solution vary continuously over several hours, thereby maintaining a final state different from the untreated water. This change depends on the polarity of the plasma and the surrounding atmosphere.

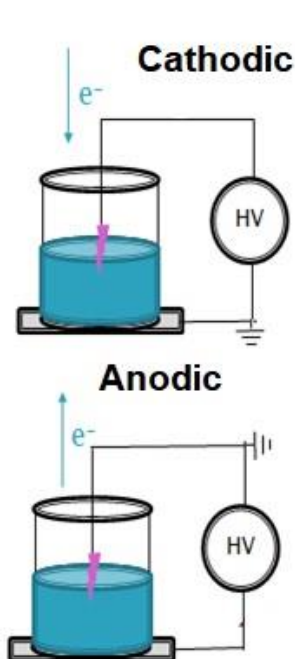


Fig. 1. Experimental apparatus used in this work

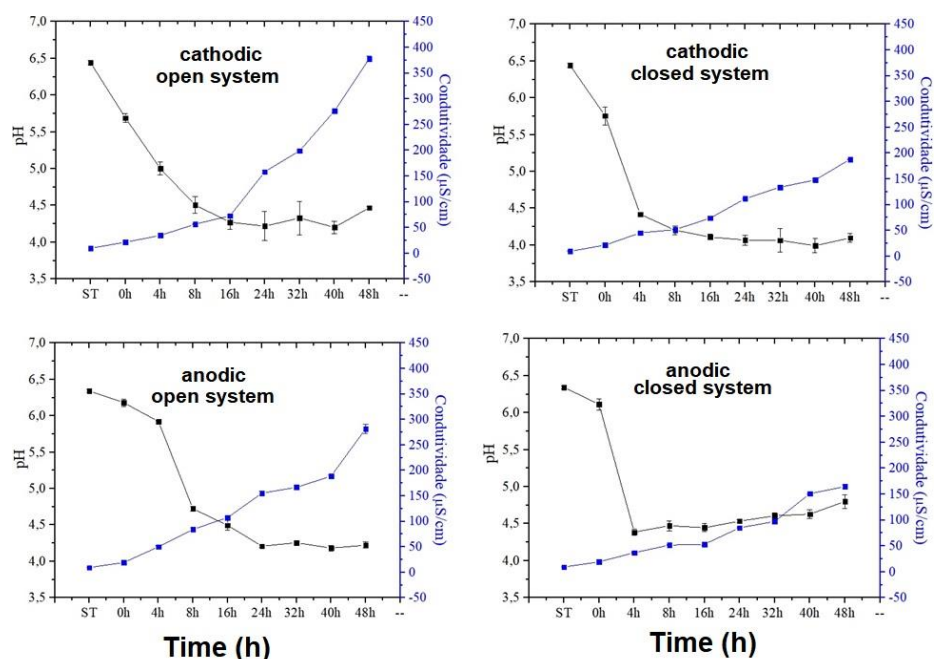


Fig. 2. Values of pH and electrical conductivity for different conditions of treatment or plasma configuration.

4. References

- [1]-S. Jung et al., *Meat Science*, **108**, 132-137 (2015).
 [2]-P.J. Bruggeman et al., *Plasma Sources Sci. Technol.* **25** (2016) 053002

STUDY OF THE MODIFICATION OF POLYIMIDE FILM TREATED BY PLASMA IMMERSION ION IMPLANTATION USING X-RAY PHOTOELECTRON SPECTROSCOPY

Marcondes, A. R.^{1*}, Ueda, M.¹, Santos, N. M.²

¹*National Institute of Space Research, São José dos Campos – São Paulo – Brazil*

²*Universidade Federal da Integração Latino-Americana, Foz do Iguaçu – Paraná – Brazil*

*Corresponding Author: *andre.marcondes@inpe.br*

1. Introduction

Aluminized polyimide film (Kapton™) has been used for decades in the passive thermal control systems of spacecraft. But, as other polymers, Kapton undergoes degradation due to the exposition to the aggressive space agents such as atomic oxygen, solar UV radiation, high vacuum, microparticle environment and charging [1,2]. In this way, a lot of researches have been conducted to extend the Kapton's life in the space environment. In this study we evaluate the chemical modifications on the Kapton surface when implanted with nitrogen ions using plasma immersion ion implantation (PIII) technique. The chemical modifications were evaluated using X-ray photoelectron spectroscopy (XPS).

2. Experimental

Kapton film type HN (1 mil in thickness) was cut in samples of two different dimensions. The samples were treated in two PIII experimental systems (3IP-LAP and 3IP-CE) reported elsewhere [2]. The samples were put in the treatment chambers using an aluminum cylinder as a sample holder in one case and a stainless steel tube in the other case. The samples were placed around the cylinder or in the interior of the tube, which was pulsed by a high voltage pulser to produce the high-voltage glow discharge. In some treatments, a stainless steel metallic grid was placed over the samples to avoid the charge accumulation on the polymer surface.

3. Results and Discussions

The extended XPS spectra of untreated and treated samples using cylindrical sample holder can be seen in Figure 1. In Figure 2 one can see the extended XPS spectra of untreated and treated samples using stainless steel tube as the sample holder. In this work we present all high resolution spectra of all samples in the region of the C1s, O1s and N1s. The results show that the treatment inside metallic tube (hollow cathode) is more suitable to promote chemical modifications in the Kapton surface and that the treatment with metallic grid is useful to avoid the damage of the aluminum layer present in the pristine polymer when subjected to the high voltage pulses. An extensive discussion of the high resolution spectra is presented.

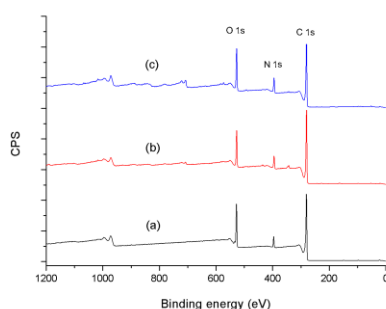


Fig. 1 – Extended XPS spectra of (a) untreated sample, and treated samples using cylindrical holder: (b) without metallic grid (c) with metallic grid

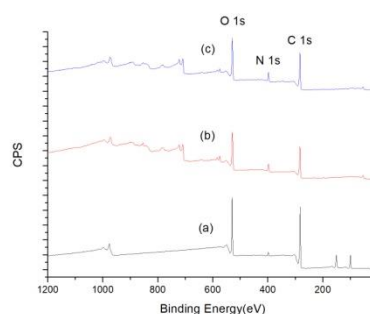


Fig. 2 - Extended XPS spectra of (a) untreated sample, and treated samples using metallic tube holder: (b) without metallic grid (c) with metallic grid

4. References

- [1]-GROSSMAN, E.; GOUZMAN, I. Space environment effects on polymers in low earth orbit. *Nuclear Instruments and Methods in Physics Research Section B: Beam Interactions with Materials and Atoms*, v. 208, p. 48-57, 2003.
 [2]-MARCONDES, André Ricardo; UEDA, Mario; ROSSI, José Oswaldo. Effect of nitrogen plasma immersion ion implantation on surface electrical breakdown strength of the aluminized polyimide. *Revista Brasileira de Aplicações de Vácuo*, v. 36, n. 3, p. 122-130, 2018.

Acknowledgments

We would like to thanks to the Brazilian Ministry of Science, Technology, Innovation and Communication that has supported this work.

ELECTRICAL CHARACTERISTICS OF LARGE-AREA NITROGEN-DOPED HFCVD DIAMOND FILMS

Evaldo Chagas Gouvêa^{1*}, Júlia Corrêa Reis¹, Pedro Magalhães Sobrinho¹, Teófilo Miguel de Souza¹

¹Engineering College, UNESP - Univ Estadual Paulista, Guaratinguetá campus, Avenida Ariberto Pereira da Cunha, 333, CEP 12.516-410, Guaratinguetá, São Paulo State, Brazil

*Corresponding Author: evaldo.gouvea@unesp.br

1. Introduction

Diamond is known for its unique physical and chemical properties, that allows it to be used in industrial applications such as semiconductors, cutting tools, and sensors. Hot Filament Chemical Vapour Deposition (HFCVD) and Microwave-Plasma Chemical Vapour Deposition (MPCVD) are the two main techniques being used to grow diamond thin films over several substrates materials [1]. The HFCVD is relatively cheap and easy to operate when compared to MPCVD; it is able to produce large area polycrystalline diamond thin films [2]. Nitrogen is an important impurity in both natural and synthetic diamond. It has been proven that nitrogen impurities can strongly affect the structure, physical, thermal and electrical properties of diamond films [3]. In this study we analyze large-area nitrogen-doped polycrystalline diamond films grown over boron-doped silicon substrates to verify how nitrogen affects the electrical characteristics of the films.

2. Experimental

Polycrystalline diamond films have been grown on p-type boron-doped Si (100) substrates using a HFCVD reactor. A gas mixture of 1.5% methane, 0.5% nitrogen and 98% of hydrogen were used. The gas mixture flow was 200 sccm and the chamber pressure was kept at 20 torr. Tungsten filaments were employed to heat the substrates to 800 °C for 4 hours. A thermocouple was used to monitor the substrate temperature. Electrical characterization of the diamond films were done using high-precision voltage sources, voltmeters and ammeters.

3. Results and Discussions

The larger samples have an area up to 40 cm² and are about 5 μm thick, presenting a homogeneous surface thin film. As shown in the green curve of Figure 1, the undoped diamond acts as an electric insulator material, presenting a very small current when voltage is applied to the film. This is the common behaviour of diamond. However, the red curve on Figure 1 reveals that the addition of nitrogen to the gas mixture has created a n-type semiconducting diamond film, which interacts with the p-type boron-doped Si substrate. The exponential growth of current for voltages greater than 4 V indicates that a PN junction was formed between the diamond film and the substrate. This study showed that the addition of nitrogen creates a semiconducting diamond thin film. The use of large-area semiconducting diamond films can lead to electronic devices that could exhibit high current densities. Further investigations are needed to better understand the electrical properties of nitrogen-doped diamond films.

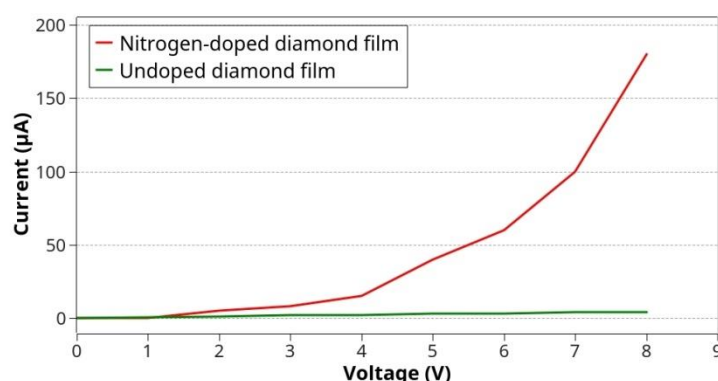


Fig. 1. Electrical characteristic curves of undoped and nitrogen-doped diamond films.

4. References

- [1]- E. M. A. Fuentes-Fernandez et al., *Thin Solid Films*, **603**, 62-68, (2016).
- [2]- A. Amorim et al., *Vacuum*, **83**, 1054-1056, (2009).
- [3]- M. K. Kuntumalla et al., *Thin Solid Films*, **653**, 284-292, (2018).

Acknowledgments

MAGNETIZATION OF Gd/GdN MULTILAYERS

Francisco Alfaro*, Julio César Sagás and Luís César Fontana.

Laboratory of Plasmas, Films and Surfaces, Universidade do Estado de Santa Catarina Joinville, SC, Brazil.

*Corresponding Author: francisco.alfaro@udesc.br

1. Introduction

Multilayers with different material combinations have been studied to develop new magnetic semiconductors for spintronic area [1-2]. The present work reports the deposition of different Gd/GdN multilayers by DC grid-assisted magnetron sputtering. The magnetization of the samples was measured to investigate how the presence of GdN affects the magnetic phase transitions.

2. Experimental

Gd/GdN multilayer were grown on Si (100) with constant current (0.40 A), cathode power (~130 W), working gas pressure (~0.40 Pa) and without external heating. Ar and N₂ mass flow rate were set at 2.6 sccm and 1.3 sccm, respectively. Total film thickness is around 200 nm. In addition to a pure Gd film, eight samples with different multilayer structure were deposited. The samples were analyzed by X-ray diffraction (XRD), X-ray photoelectron spectroscopy (XPS) in depth profile mode and a physical property measurement system (PPMS) for magnetization measurements as a function of temperature in constant magnetic fields (B).

3. Results and Discussions

The evolution of the Gd 4d peak along the depth of the sample [Gd(20nm)/GdN(20nm)]₄ is shown in Fig. 1. In the first 40 nm, the change in the spectrum is caused by the decrease of oxygen contamination. After that, it is possible to identify the periodicity of the Gd concentration due to the attenuation of the peak at 147 eV. The normalized magnetization as a function of temperature is shown in Fig. 2 for a 2 T magnetic induction. It is noticed that samples with lower GdN percentage present behaviour closer to the Gd film.

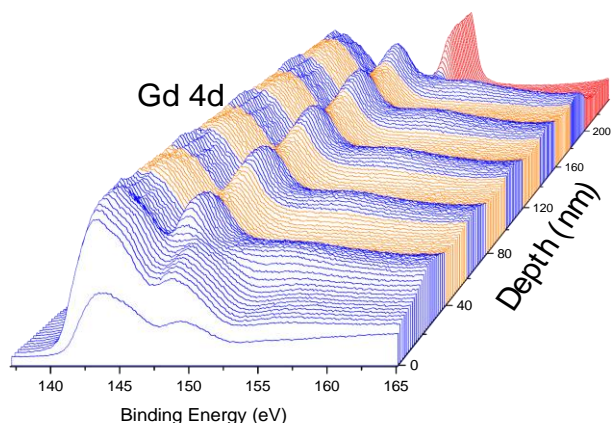


Fig. 1. Evolution of the Gd 4d photopeak along the depth of the sample [Gd(20nm)/GdN(20nm)]₄.

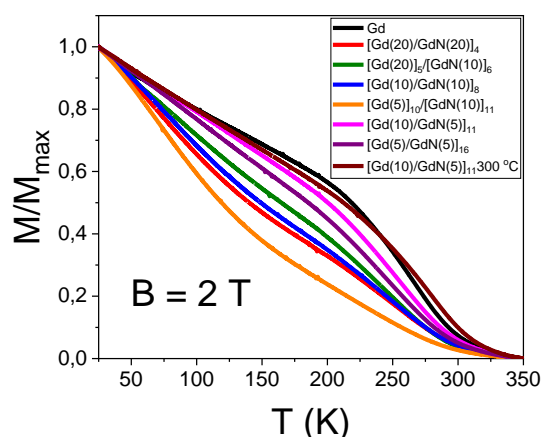


Fig. 2. Normalized magnetization as a function of temperature for $B = 2$ T and temperature ranging from 350 K to 25 K for all samples.

When the GdN layers have thickness of 10 nm and 20 nm, there is no sharp magnetic phase transition observed, in opposition with pure Gd film. When cooling from 350 K to 25 K, a pure Gd film has 50% of its magnetic domains aligned at approximately 225 K, while multilayer achieve the same level between approximately 150 K and 100 K, depending on the layer architecture.

4. References

- [1]- R. Vidyasagar, T. Kita, T. Sakurai, T. Shimokawa, H. Ohta. Phys. Lett. A, **381**, 1905–1909, 2017.
- [2]- A.V. Svalov, S.V. Andreev, A. Larrañaga, I. Orue, G.V. Kurlyandskaya. J. Magn. Magn. Mater., **490**, 165529, 2019.

Acknowledgments

The authors thank LabCAM of UFSC by magnetization measurements. This project has been funded by FAPESC and UDESC through the program PAP under contract PAP-TR 655.

DEVELOPMENT AND CHARACTERIZATION OF CVD DIAMOND CUTTING TOOLS FOR PRECISION MICRO-TURNING OF MOLYBDENUM

Silva Neto, J. V.^{1*}, Andrade, A. E. N.², Trava-Airoldi, V.J.¹, Corat, E.J.¹

¹National Institute for Space Research, São José dos Campos, SP, Brazil

²ETEP Faculty of Technology, São José dos Campos, SP, Brazil

*Corresponding Author: jvneto.ifsp@gmail.com

1. Introduction

The machining of molybdenum is unconventional, usually performed by electrocorrosion or laser methods (1,2). However, one desirable use is the precision turning of thin Mo rods for posterior CVD diamond coating for application as dental tools (3,4). This process yield per tool insert is substantially impaired by the wear process by metal carbide particles formation (5). In order to obtain better results in turning procedures of Mo, we developed a modified insert geometry and coated these tools with a CVD diamond thin layer. Film quality was studied by FEG-SEM, EDS, Raman spectroscopy and turning tests.

2. Experimental

Tool inserts were cut to appropriate geometry by grinding wheel, sanded with sandpaper then polished with diamond abrasive paste with sequential grain sizes of 6, 3 and 1 μm . After this process samples were cleaned in isopropanol ultrasonic bath. Then took to the chemical corrosion of surface Cobalt by a two step chemical etching. After these preparation steps, samples were seeded with diamond nanoparticles, CVD diamond layer was applied in a HFCVD reactor, with the following set up: gas mixture of 2% methane in 98% hydrogen, 800 ± 5 °C process temperature, chamber pressure of 50 Torr. After etching and deposition steps samples were characterized by FEG-SEM and EDX. Film structured was studied by Raman spectroscopy. The machining performance was evaluated by turning of molybdenum rods with 2 mm diameter, cutting parameters were cutting depth 0.2 mm, cutting speed 2500 rpm and feed 11 mm/min.

3. Results and Discussions

The characterization by FEG-SEM can be seen at Figure 1 it was possible to obtain a homogenous and continuous CVD diamond coating over the entire surface. Figure 2 brings the Raman spectroscopy showing the diamond peak centered at 1339 cm^{-1} and the presence of G band, D band and a considerable luminescence.

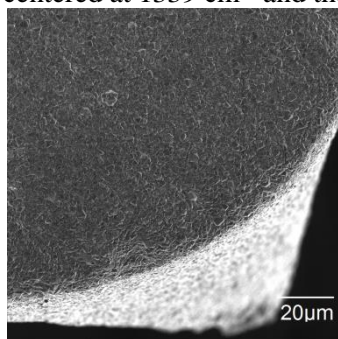


Fig. 1. (figure number in bold face times new roman 10 pt) Cutting tool tip with homogenous and continuous CVD diamond film.

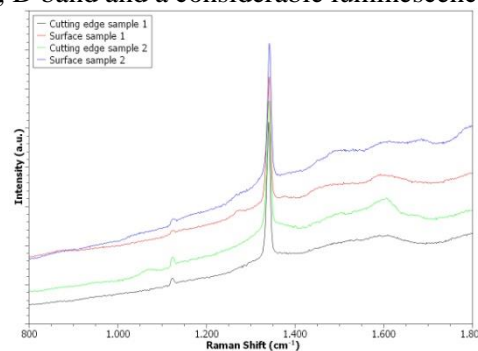


Fig. 2. Raman spectroscopy performed in 2 points of each sample, at rake surface lines in red and black for samples 1 and 2, and at cutting edges lines in blue and green for samples 1 and 2.

4. References

- [1]- Demellayer R, Richard J. High precision electro discharge machining of Molybdenum and Tungsten. *Procedia CIRP* [Internet]. 2013;6:89–94. Available from: <http://dx.doi.org/10.1016/j.procir.2013.03.030>
- [2]- Torres R, Kaempfe T, Delaigue M, Parriaux O, Hönninger C, Lopez J, et al. Influence of laser beam polarization on laser micro-machining of molybdenum. *J Laser Micro Nanoeng.* 2013;8(3):188–91.
- [3]- Trava-Airoldi VJ, Corat EJ, Del Bosco E, Leite NF. Hot filament scaling-up for CVD diamond burr manufacturing. *Surf Coatings Technol.* 1995;76–77(PART 2):797–802.
- [4]- Sein H, Ahmed W, Rego C. Application of diamond coatings onto small dental tools. *Diam Relat Mater.* 2002;11(3–6):731–5.
- [5]- Poulachon G, Moisan A, Jawahir IS. Tool-wear mechanisms in hard turning with polycrystalline cubic boron nitride tools. *Wear.* 2001;250–251(1–12):576–86.

Acknowledgments

This work was supported by FAPESP (process number 2012/15875-1) and CAPES.

TORSION MODULUS OF PTFE USING THE DEFORMATION ENERGY METHOD

Carlos Alberto Fonzar Pintão*, Lucas Pereira Piedade, Edgar Borali
¹Departamento de Física-FC-UNESP-17033-360, Bauru, SP, Brazil
 *Corresponding Author: carlos.fonzar@unesp.br

1. Introduction

It is necessary to know polymers mechanical characteristics, such as rigidity (elastic modulus) to predict the behavior of materials when subjected to stresses or loads. This work uses a specially designed system to determine the torsion modulus (G) of polymers. We have chosen the polymer polytetrafluoroethylene (PTFE). The properties of this polymer make it suitable for use in aerospace applications[1] and the biomedical industry, for implants[2-3], making it essential to know its elastic properties, such as the torsion modulus.

2. Experimental

The system used to apply the torque (Mt) on one of the pendulum arms is in Fig. 1. It consists of a coordinated table attached to a plate, which is fixe with the structure of the torsion pendulum (Fig. 1(a) and (b)). The sample is attached to the system for measuring G and previously positioned at the desired practical length L. Using an inextensible wire attached at one end to the upper pendulum rod and the other to the force sensor (FS), it is possible to apply and measure the force. We used a 12V Stepper motor to move the coordinated table in the two required directions: one for approximation and the other to draw it away from the pendulum (Fig. 1(c)), twisting the sample at a rate of $3 \times 10^{-4} \text{ s}^{-1}$. Using a rotational movement sensor (RMS) capable of recording the torsion angle of the axis (θ) that holds one end of the sample, then the force curves (F_s) versus torsion angle (θ) are obtained. Using the software PASCO, the experimental points for F (N) and θ (rad) were earned simultaneously in real-time. We can thus adjust the straight line and get the slope of B. Eq. (1) was deduced considering the work of Mt and the internal energy of the sample in the torsional deformation, resulting

$$\text{in: } G = \frac{BLa}{J} f \quad (1)$$

3. Results and Discussions

Knowing the values of the polar moment of the cross-sectional area of sample J, the slope B, the calibration factor (f) of the FS, the pendulum arm length a (Fig. 1(c)), and the practical length L, we can calculate the torsion modulus G by using the Eq. (1). Fig. 2 shows the result for a cylindrical sample with 6.50 mm of diameter and 69.20 mm of length, whose found value was $354 \pm 11 \text{ MPa}$.

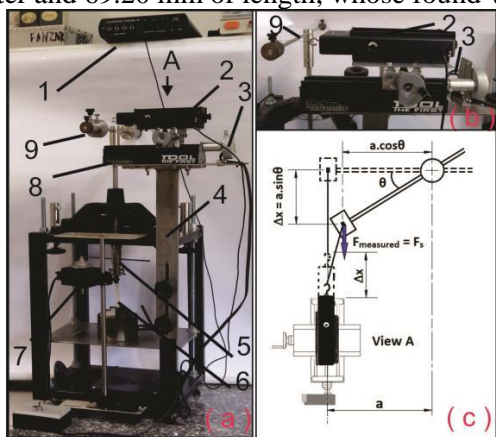


Fig. 1. (a) – System for measuring G: (1)- Interface (PASCO: CI7650-750); (2)- Force sensor (FS-PASCO: CI6537); (3) Motor for moving XY table; (4) Torsion pendulum structure for table fixation XY; (5) Pendulum axis attached to the sample; (6) Samples: PTFE; (7)- Rotational movement sensor (RMS-PASCO: CI6538); (8) XY table; (9) Torsion pendulum. **(b)** – Foto da vista A; **(c)** – Desenho esquemático.

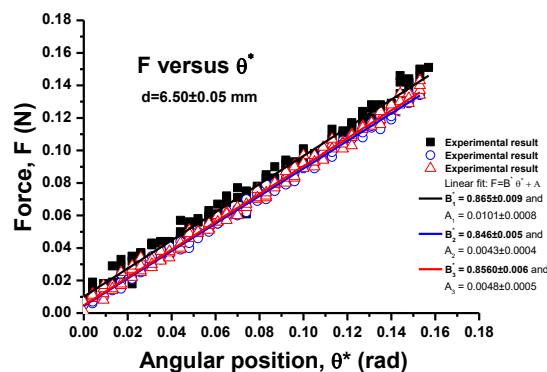


Fig. 2. Typical curves of force F (N) as a function of the angular position θ^* (rad). Sample of PTFE: $L = (69.20 \pm 0.05) \text{ mm}$; $d_2 = (6.50 \pm 0.05) \text{ mm}$; $B^* = 0.856 \pm 0.007 \text{ N/rad}$; $G = (354 \pm 11) \text{ MPa}$. It should be noted that the ratio θ/θ^* is 0.222 ± 0.001 , so that B is calculated as $B^*/0.222$.

4. References

[1]- J. L. Jordan, C. R. Silviour, J. R. Foley & E. N. Brown. Polymer, **48**, 4184-4195, (2007).
 [2]- E.N. Brown, P.J. Rae, E. Bruce Orler, G.T. Gray & D, M. Dattelbaum. Materials Science and Engineering: C, **26**(8), 1338-1343, (2006).
 [3]- K. Messner & J. Gillquist. Biomaterials, **14**(7), 513-521, (1993).

Acknowledgments

The authors thank FAPESP, proc. 2007/04094-9.

ELETROMAGNETIC PROPERTIES OF THE SUPERCONDUCTOR MATERIAL

Gonçalves H. P.^{1*}, Coelho L. S.², Bittar E. M.², and Bigansolli A. R.³.

¹IME – Instituto Militar de Engenharia, Rio de Janeiro, RJ, Brazil.

²CBPF – Centro Brasileiro de Pesquisas Físicas, Rio de Janeiro, RJ, Brazil.

³UFRRJ – Universidade Federal Rural do Rio de Janeiro, Seropédica, RJ, Brazil.

*Corresponding Author: hugopedra4@gmail.com

1. Introduction

The materials superconductors have electromagnetic properties different than normal conductors because of their ability of expelling the external magnetic field from inside of the material and resistance zero when cooled into critical temperature (T_c) [1]. Actually, superconductors materials Type II are studied not only due their applications and capability to transport high current density and support magnetic field, but also because they permit partial penetration of the magnetic field without losing superconductor properties [2]. Then this work studied the electromagnetic properties of superconductors tapes of second generation (2G) using the Y-Ba-Cu-O' system (YBCO).

2. Experimental

Were used electric resistance and magnetic susceptibility test in the superconductors tapes donated from the SuperOx Company. The resistance electric test used heating rate of 0.5 Kelvin (K)/min and cooling rate of 2 K/min in Janis equipment (Janis Research Company Inc.), applying the four points' method. The magnetic susceptibility test used DynaCool™ (Quantum Design Company) with rate of 4 K/min and magnetic field of 100 Oersted. Both tests used temperature between 10 and 300 K, helium gas and were realized at the Superconductor and Magnetometry Laboratory of the Centro Brasileiro de Pesquisas Físicas.

3. Results and Discussion

Through the magnetic susceptibility and electric resistance tests, the critical temperature measure was approximately 93 K, as shown in figures 1 and 2. This value found were accepted because, according to the literature, YBCO' superconductor has this same T_c [1]. From these results, it was possible to affirm the superconductor sample is Type II and, consequently, has incomplete shielding. Additionally, the magnetic field permits partial penetration in the sample without losing superconductors properties, differently from superconductors Type I that do not allow this effect [1-2]. Therefore, these donated tapes demonstrated that they were in a good work condition because the electromagnetic properties of the superconductor material was preserved.

Fig. 1. Susceptibility magnetic curve of the YBCO' superconductor tape.

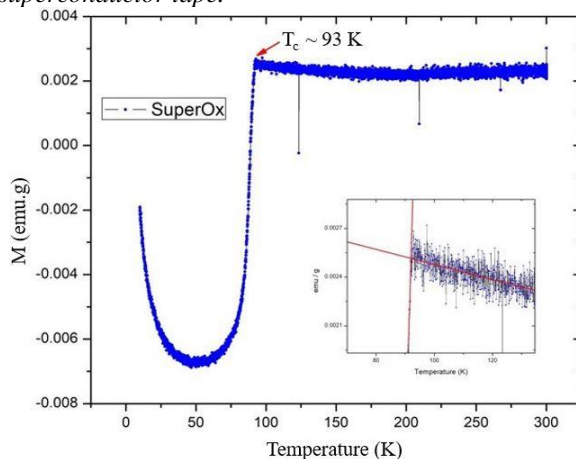
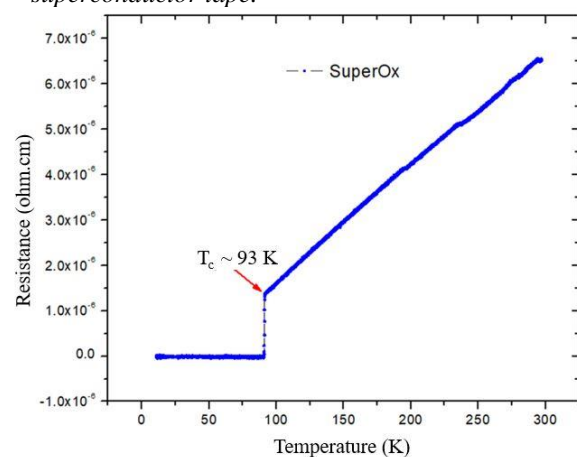


Fig. 2. Electric resistance curve of the YBCO' superconductor tape.



4. References

- [1]- M.J. Patel et al., Review on Superconductivity: The Phenomenon occurred at Low Temperature. National Conference on Recent Trends in Engineering & Technology, n. May, (2011).
- [2]- S. Yildiz et al., Physica C: Superconductivity and its Applications, v. 470, n. 13–14, p. 575–581, (2010).

Acknowledgments

H. P. G thanks the SuperOx Company and the CBPF for all the materials.

STRUCTURAL CHARACTERIZATION IN POROUS CERAMICS

Jônatas de O. Sousa¹, Belmira B. de Lima Kuhn¹, Antonio R. Bigansolli^{1*}, Daniel F. de Carvalho²

¹Departamento de Engenharia Química, Instituto de Tecnologia, UFRRJ, Seropédica,

²Departamento de Engenharia, Instituto de Tecnologia, UFRRJ, Seropédica.

*Corresponding Author: bigansolliarb@gmail.com

1. Introduction

Safe drinking water is one of the most important health indicators in the country. Domestic water treatment is of great health benefit, although it is not a substitute for a sustainable drinking water infrastructure. Therefore, candle filters have become a very useful means of filtering drinking water. Usually, the candles are made of a mix of clay and alumina arranged to have pores and filter production has been continuously studied [1]. The aim of the present work is to compare filter candle features by their results from DRX and FTIR.

2. Experimental

The experiments were made in two samples. Sample A was obtained from the candle filter produced by Stefani Company, while sample B of tensiometric capsules produced by the Feltre group. The samples were crushed in an agate mortar. After comminution, the samples were separated to particle size using a 150 # and 200 # sieve set and a sieve shaker. The particles retained in the 200 # sieve were analysed by DRX and FTIR. FTIR spectra were recorded with a BRUKER VERTEX 70 spectrometer by applying the ATR PLATINUM. Powdered samples were recorded for the 4000 cm^{-1} to 400 cm^{-1} region. For the XRD experiments, the measurements were carried out at room temperature using Ni-filtered Cu-K α radiation in a diffractometer (Rigaku, Miniflex II) and the measurement conditions were $5^\circ < 2\theta < 70^\circ$, 0.05° step. The phases were identified based on Villars and Calvert crystallographic data [2] and the Powder Cell software [3].

3. Results and Discussions

The FTIR spectra of sample A and sample B are shown in Fig. 1 and Fig. 2, respectively. The FTIR results of samples A and B showed traces of hydroxyl group in the structure of Aluminates and Silicates in the regions that permeate 3000 cm^{-1} as well as the hydroxyls present in the water molecules. There was variation in the absorption bands of the samples in the region between 1000 and 1100 cm^{-1} . The sample of filter candle (A) showed vibration between (Si-O-Si) while the sample of tensiometer capsules (B) showed vibration between (Si-O). Both samples showed the exchange of Silicon by Aluminum (Si-O-Al) in the 810 cm^{-1} region band. Below 600 cm^{-1} sample A presented silicon at the tetrahedral site and aluminum at the octahedral and vibration of sample B in flexion between Silicon and oxygen [4]. The XRD results showed, in both samples, characteristic peaks associated with traces of cristobalite and quartzo [5].

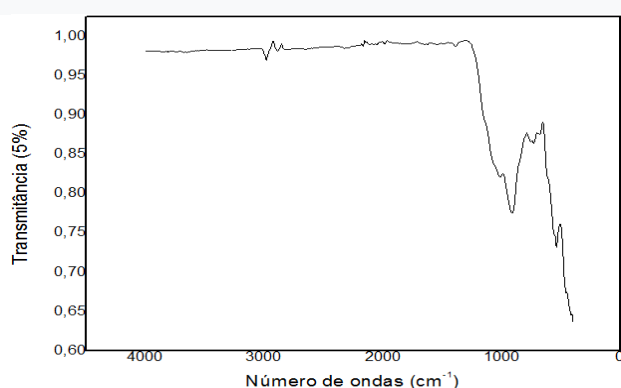


Fig. 1. FTIR spectra of the sample 1.

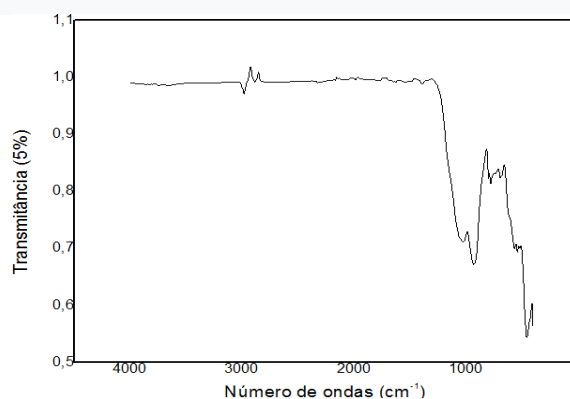


Fig. 2. FTIR spectra of the sample 2.

References

- [1]- J. C. Bellingieri, Anais do Museu Paulista. São Paulo. **12**, 161-191. jan/dez. (2004).
- [2]- P. Villars and L.D. Calvert, "Pearson's Handbook of Crystallographic Data for Intermetallic Phases", **2**^o, ASM International, Materials Park, OH. (1991).
- [3]- W. Kraus and G. Nolze, PowderCell for Windows (version 2.3). Berlin: Federal Institute for Materials Research and Testing. (1999).
- [4]- J. A. de Azevedo and E. M. da Silva, EMBRAPA-CPAC, 1-33, (1999).
- [5]- C. R. Alves and O. B. G. Assis, EMBRAPA-CNPDI, 1-13, (1999).

CHEMICAL ACTIVATION OF THE NATURAL BENTONITE BY HCl E H₂SO₄

Almeida L.S., Bigansolli A. R.* and Lima-Khün B. B.

UFRRJ – Universidade Federal Rural do Rio de Janeiro, Seropédica, RJ, Brazil.

**Corresponding Author: bigansolli.arb@gmail.com*

1. Introduction

Clay is a natural mineral of fine granulation, formed essentially by clay minerals. Bentonite is a clay belonging to the group of the smectites, being constituted mainly by montmorillonite, like predominant argilomineral. Bentonites have a wide industrial application, due to their properties and low cost. When these clays are subjected to acid activation treatments, they acquire adsorptive and catalytic properties and are therefore industrially employed as adsorbents and catalysts. The aim of this work is activate clay using HCl and H₂SO₄, at 90 °C under magnetic stirring in different times reaction and to characterize clay before and after chemical activation by infrared spectroscopy (FTIR).

2. Experimental

In this study the natural clay from “Schumacher Insumos” (Rio Grande do Sul, Brazil) was modified by acids. The bentonite sample was modified with acid treatment using sulphuric acid (H₂SO₄) or hydrochloric acid (HCl). Ten grams of bentonite were dispersed in 100 mL of 6 M acid solutions and stirred at 90°C for 30 min. or 1 h. Then, the bentonite was washed to remove the mineral acid until a 5<pH<6 range was reached. Finally, the bentonites treated with acid solutions were dried at 80°C for 36 h. After drying, they were disaggregated with mortar and subjected to characterization by FTIR.

3. Results and Discussions

The FTIR spectra of natural clay (sample A) and chemical activation clay (sample B) are shown in Fig. 1 and Fig. 2, respectively. The intensities of the OH elongation bands at 3626 cm⁻¹ and the hydroxyl flexural vibrations at 915 cm⁻¹ (Al₂OH), 885 cm⁻¹ (AlFeOH) and 840 cm⁻¹ (AlMgOH) from sample A (Fig. 1) ^{1,2} partially decrease due to the release of Al, Fe and Mg atoms from sample B (Fig. 2). Fig. 2 shows that the flexible AlFeOH band completely disappears while the AlMgOH and Al₂OH curvature bands are hardly distinguishable and the emergence of a 794 cm⁻¹ quartz band. Fig. 1 shows that the Si-O-Si elongation band of the tetrahedral sheet is located at 992 cm⁻¹. However, Fig. 2 shows the weakening and shifting the Si-O-Si elongation band to a wavelength greater than 40 cm⁻¹, 1033 cm⁻¹. This change occurs due to the dissolution of the structure smectite by the proton attack on the clay layers.

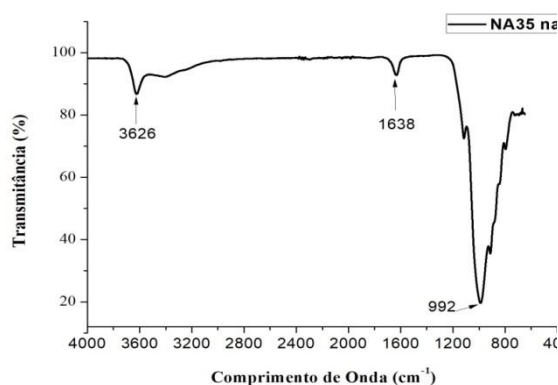


Fig. 1. FTIR spectra of the natural clay

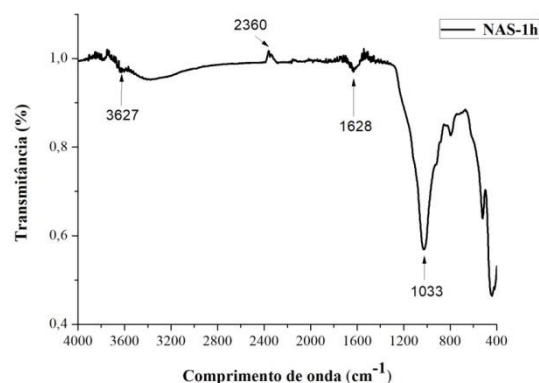


Fig. 2. FTIR spectra of the chemical activation clay

4. References

- [1]- M. A. V. Rodriguez, M. S Barrios, J. D. L. Gonzalez, M. A. B. Munoz, *Clays Clay Miner*, **42**, 724, (1994).
- [2]- G. E. Christidis, P. W. Scott, A. C. Dunham, *Appl. Clay Sci.*, **12**, 329, (1997).

EFFECT OF MILLING TIME ON GRANULOMETRIC DISTRIBUTION ON SODA-LIME GLASS

Jônatas de Oliveira Sousa, Belmira Benedita de Lima-Kuhn, Antonio Renato Bigansolli*

¹*Departamento de Engenharia Química, Instituto de Tecnologia, UFRRJ, Seropédica, RJ, Brazil.*

*Corresponding Author: bigansolliarb@gmail.com

1. Introduction

The high-energy milling gained visibility at 1960s as it was effective and simple method of obtaining fine particles. However, despite simple, many are the variables involved to reach the desired granulometry. Milling time is one of the most important parameters responsible for control the fracture and cold welding of the powder [1]. Currently, a large volume of waste glass is recycled. One of the process used in glass recycling is the milling, where it can used the high-energy planetary mill. Based on this, glass bottles were processed at the high-energy mill in order to analyze the relation between milling time and particle size.

2. Experimental

The glass used in this study comes from the fragmentation of amber bottles, commonly used in beverage industries. An early fragmentation was made and particles between 1.7 and 2.2 mm were obtained. From this material, five samples were separated and taken to the Restch's high-energy mill model PM 100. In this mill, each sample has undergone a different milling time: 10, 30 and 60 minutes. Then, the samples' particles were analyzed by laser diffraction using a analyzer Malvern model Mastersizer 2000. The parameters inserted in the equipment were refracting index of the particles of 1.513, light absorption index of 0.1 and obscurity varying between 12% and 16%. Two minutes of ultrasound were applied at the sample with the intention of disaggregating the particles.

3. Results and Discussion

According to the granulometric distribution of figures 1 and 2, it is observed that increasing milling time led to a decrease of particle size followed by a reduction of Sauter Mean Diameter (dmsauter). Nevertheless, when analyzing figures 2 and 3, it is noted he particle size increased and the variation of Sauter Mean Diameter expanded from 2,984 μm to 3,135 μm . Particles with reduced sizes hamper nucleation and propagation of comminution cracks and longer milling time lead to welding of particles. At figure 3 is observed the formation of a bimodal composition of granulometric distribution, this occurs influenced by the mean particle friction coefficient generated in glass milling process [3].

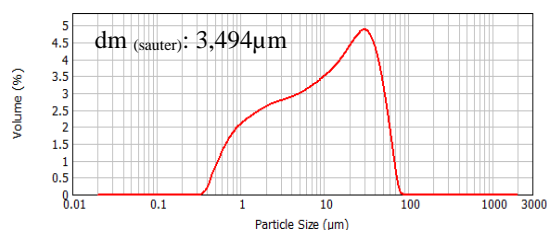


Fig. 1. Particle size distribution – milling by 10 minutes

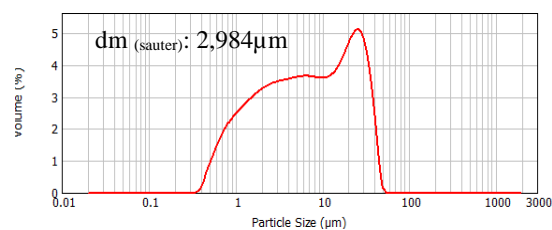


Fig. 2. Particle size distribution – milling by 30 minutes

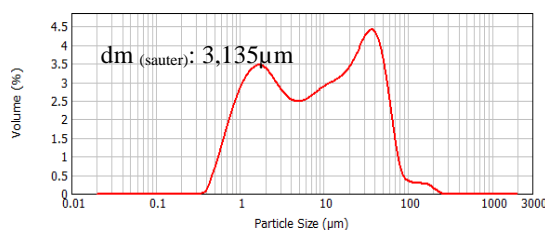


Fig. 3. Particle size distribution – milling by 60 minutes

4. References

- [1]- C. Suryanarayana, Progress in Materials Science, 46, 23, (2001).
- [2]- O. L. Alves, I. F. Gimenez and I. O. Mazili, "Vidros", Química Nova na Escola, Special Edition, 9-20, (2001).
- [3]- T. M. Mendes "Influência do coeficiente de atrito entre os agregados e da viscosidade da matriz no comportamento reológico de suspensões concentradas heterogêneas", Dissertação, Escola Politécnica, USP, BR, (2008).

EFFECTS OF MILLING ROTATION SPEED ON SODA-LIME GLASS

Jônatas de Oliveira Sousa, Belmira Benedita de Lima-Kuhn, Antonio Renato Bigansolli*
 UFRRJ – Universidade Federal Rural do Rio de Janeiro, Seropédica, RJ, Brazil.
 *Corresponding Author: bigansolliarb@gmail.com

1. Introduction

The glasses are inserted in almost all society routines, being widely used from floating glasses to optical fibers. Thus, a large volume of waste glass is recycled [1]. One of the processes used in glass recycling is the milling, where it can be used the high-energy planetary mill. In this equipment, speed of rotation is directly related to the particle size distribution of the material, which is a fundamental for its application in several areas [2]. Therefore, the present work aims to study the effect of rotation speed variation on particle size distribution of the glass milled.

2. Experimental

The glass used in this study comes from the fragmentation of amber bottles, commonly used in beverage industries. An early fragmentation was made and particles between 1.7 and 2.2 mm were obtained. From this material, five samples were separated and taken to the Restch's high-energy mill model PM 100. In this mill, each sample, for 10 minutes, has undergone a different rotation speed: 100 rpm, 200 rpm, 300 rpm, 400 rpm and 500 rpm. Then, the samples's particles were analyzed by laser diffraction using a analyzer Malvern model Mastersizer 2000 analyser. The parameters inserted in the equipment were refracting index of the particles of 1.513, light absorption index of 0.1 and obscurity varying between 12% and 15%. Two minutes of ultrasound were applied at the sample with the intention of disaggregating the particles.

3. Results and Discussion

At 100 rpm, particles larger than 1.7 mm in diameter were observed, showing that this rotation speed is not sufficient to reduce their size. Figures 1 to 4 show the results of the particle size distribution after milling of the samples in different rotation speed: 200 rpm, 300 rpm, 400 rpm and 500 rpm. Fig. 1 has a monomodal distribution with average diameter of 110 μm . A significant reduction of the particle size is associated with the increased speed of rotation and a formation of one granulometric distribution with asymmetrical trimodal distribution is observed in Figures 2, 3 and 4. We believe this occurs due to the influence of the coefficient of friction of the average particles generated in the glass processing [3]. There was a significant variation at the Sauter Mean Diameter ($d_{m,sauter}$), which at 200 rpm corresponded to 18,286 μm , while at 500 rpm reduced to

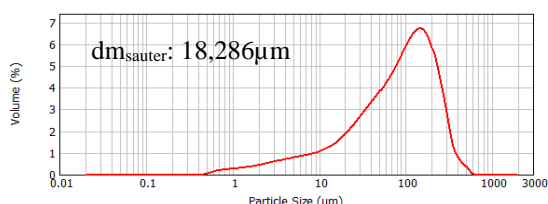


Fig. 1. Particle size distribution – milling at 200 rpm

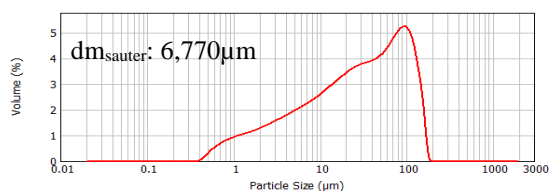


Fig. 2. Particle size distribution – milling at 300 rpm

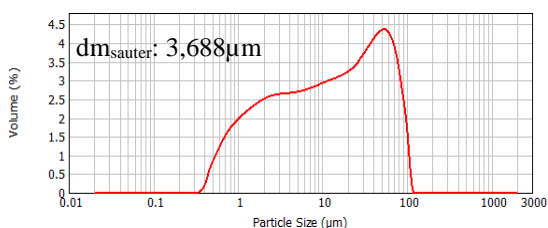


Fig. 3. Particle size distribution – milling at 400 rpm

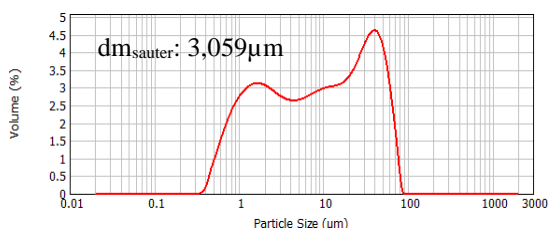


Fig. 4. Particle size distribution – milling at 500 rpm

3,059 μm .

4. References

- [1]- E. B. Araújo, Revista Brasileira de Ensino de Física, **19**, 3, 325 (1997).
- [2]- A. P. Spanholi “Projeto de um moinho de alta energia”, Trabalho de Conclusão de Curso, UTFPR, Pato Branco, BR, (2016).
- [3]- T. M. Mendes “Influência do coeficiente de atrito entre os agregados e da viscosidade da matriz no comportamento reológico de suspensões concentradas heterogêneas”, Dissertação, Escola Politécnica, USP, BR, (2008).

BIOACTIVE SURFACE CHEMISTRY OF TI GRADE 4 PREPARED BY CHEMICAL AND THERMAL TREATMENT

Marcelo Gabriel de Oliveira¹, Polyana Alves Radi², Danieli Aparecida Reis², Adriano Gonçalves dos Reis^{1*}
¹Universidade Estadual Paulista (Unesp), Instituto de Ciência e Tecnologia, São José dos Campos-SP Brazil
²Universidade Federal de São Paulo (UNIFESP), São José dos Campos-SP, Brazil
 *Corresponding Author: adriano.reis@unesp.br

1. Introduction

Several studies have been carried out to improve the osseous integration properties of the materials used in dental implants. However, some processes require complicated and expensive equipment and techniques. On the other hand, chemical and thermal treatment techniques are easily accessible, but more studies must be carried out in terms of their structural surface. This work shows the effect of the modification of the surface of titanium Grade 4 by chemical and thermal treatments, aiming the formation of a bioactive surface that improve the osseous integration [1-2].

2. Experimental

A Grade 4 titanium ingot was machined into disks (12.7 mm in diameter and 3 mm thick) and used as substrate (Control). The samples were cleaned with acetone in ultrasonic cleaner for a period of 20 min, and dried at 40°C. The samples were then soaked in an aqueous 5M NaOH solution at 60°C under agitation for a period of 24 h (CT). After being removed from the solution, the samples were gently rinsed with demineralised water and dried at 40°C. The samples were subsequently heated to different conditions: 600°C (CTT600) and 900°C (CTT900), both for a period of 1 h, at a heating rate of 5°C/min, followed by natural cooling in the furnace. The surface chemistry was analyzed by using thin-film X-ray diffraction (Rigaku Ultima IV) and Raman spectroscopy (Horiba LabRam HR Evolution).

3. Results and Discussions

Figures 1 and 2 show TF-XRD and Raman profiles of the surface of Ti-Grade 4 (Control) and samples subjected to NaOH (CT) and thermal treatments (CTT600 and CTT900).

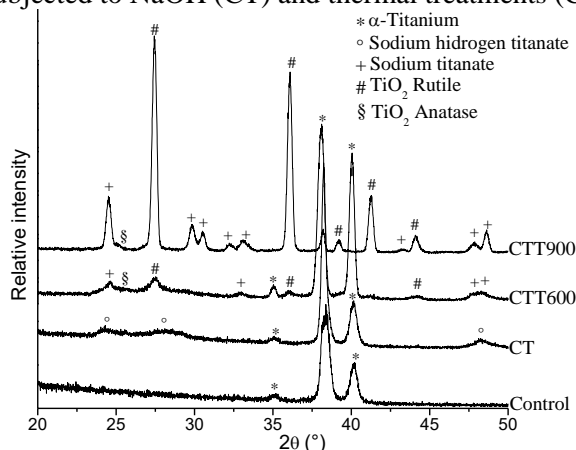


Fig. 1. TF-XRD profile of the surface of control and treated samples.

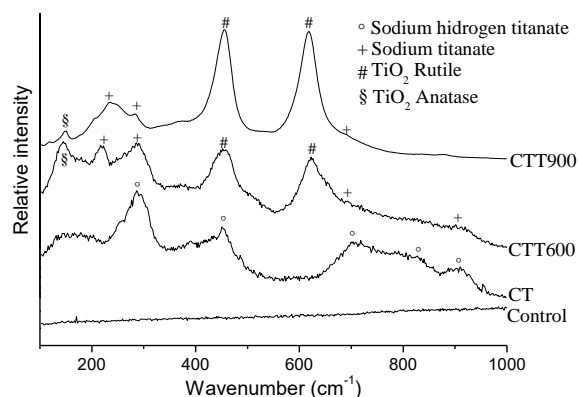


Fig. 2. Raman profile of the surface of control and treated samples.

From Figures 1 and 2, it can be noticed that sodium hydrogen titanate ($\text{Na}_x\text{H}_{2-x}\text{Ti}_3\text{O}_7$) was formed on the surface of Ti Grade 4 by the initial NaOH treatment, and then, this was transformed to sodium titanate ($\text{Na}_2\text{Ti}_6\text{O}_{13}$), rutile and anatase by the subsequent heat treatment. The rutile phase was more intense with increasing the temperature from 600 °C to 900 °C. The phases formed are according to the literature and are assigned to be bioactive since the Ti-OH groups formed on the sodium titanate are negatively charged, and combine with positively charged calcium ions and then the negatively charged phosphate ions. As a result, the osseointegration can be accelerated by this bioactive surface formed [1-2].

4. References

- [1]- S. Yamaguchi, H. Takadama, T. Matsushita, T. Nakamura and T. Kokubo, *J. Ceram. Soc. Jpn.*, **117(10)**, 1126-1130, (2009).
- [2]- N. Li, W. Xu, J. Zhao, G. Xiao, Y. Lu, *Thin Solid Films*, 646, 163-172, (2018).

Acknowledgments

This work was supported by CNPq (Proc.n° 403070/2016-3) and FAPESP.

MICROSTRUCTURE STUDY OF NiCrAlY OXIDATION BY VACUUM TREATMENT

Renata Jesuina Takahashi^{1*}, João Marcos Kruszynski de Assis², Danieli Aparecida Pereira Reis¹¹Federal University of Sao Paulo, São José dos Campos – SP²Institute of Aeronautics and Space, São José dos Campos – SP

*Corresponding Author: renata.takahashi@unifesp.br

1. Introduction

The protection against high temperature oxidation of the Thermal Barrier Coating (TBC) is associated with the NiCrAlY layer and the TGO layer (Thermally Grown Oxide composed especially of α -Al₂O₃) [1]. The TGO is an essential layer to the TBC system for protection against oxidation and adhesion between TBC layers, but it is one of the main sources of generators of strain and failures in the system [2]. Previous growth of the TGO layer is one method to pre form an exclusive α -Al₂O₃ scale before using samples in an oxidation and corrosive environment to improve the performance of the TBC protection [3]. This work aims to study the prior formation of the TGO layer by vacuum heat treatment and the microstructural characterization of the oxide formed on the NiCrAlY substrate.

2. Experimental

The NiCrAlY powder (Praxair Surface Technologies, USA) with 57.35 Ni – 31.00 Cr – 11.00 Al - 0.65 Y, wt.%, was used to make samples by uniaxial pressing at 200 MPa with binder (polyvinylalcohol) and isostatical pressing at 300 MPa. The sintering was performed in hot uniaxial pressing (HUP) at 10 MPa in temperature of 1150 °C for one hour [4]. The samples were polishing and submitted by thermal treatment in vacuum (10⁻⁵ Pa) in temperatures of 800, 1100 and 1150 °C for four hours.

The analyzes of the microstructure were used the scanning electron microscopy (SEM, Tescan, VEGA 3 XMU) equipped with an Energy Dispersive Spectroscopy (EDS, Oxford Instrument, x-act) and the X-ray diffraction (XRD, Philips Panalytical - X'Pert Pro).

3. Results and Discussions

With the increase of the temperature of the thermal treatment, the growth and homogenization of the structures formed with Ni + Al + O rich phases and the Cr + O rich phases were observed in the EDS analysis. In the XRD diffractograms shown in Fig. 1, the phases formed can be observed as well as the highest intensity peaks of α -Al₂O₃ at 1100 °C. The thermal treatment at 1100 °C suggests an improvement in the performance of TBC protection by growth of the TGO layer enriched with α -Al₂O₃ and by the microstructure and EDS analysis presented in Fig. 2.

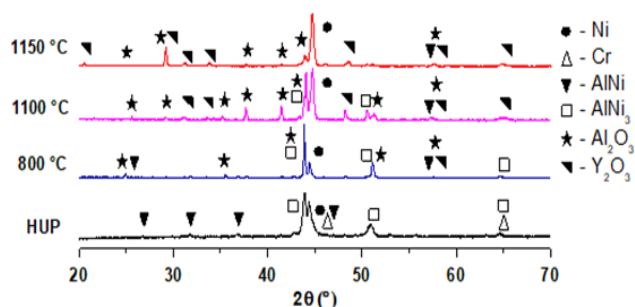
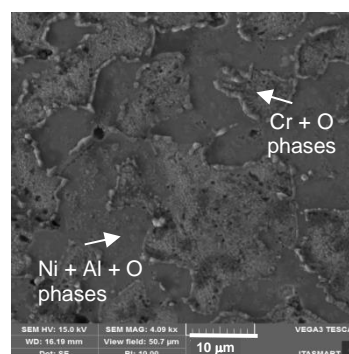


Fig. 1. The XRD result of the NiCrAlY substrate after vacuum thermal treatment at 800, 1100 and 1150 °C.



	wt %	σ
Ni	47,9	0.1
Cr	24,5	0.0
Al	14,2	0.0
O	12,9	0.0
Y	0,5	0.0

Fig. 2. Microstructure of the NiCrAlY substrate after vacuum thermal treatment at 1100 °C by scanning electron microscopy with EDS element map percent.

4. References

- [1]- A.G. Evans, D.R. Clarke, C.G. Levi, J. Eur. Ceram. Soc. 28 (2008) 1405–1419.
- [2]- W. Zhu, M. Cai, L. Yang, J.W. Guo, Y.C. Zhou, C. Lu, Surf. Coatings Technol. 276 (2015) 160–167.
- [3]- C. Zhu, P. Li, X.Y. Wu, Ceram. Int. 42 (2015) 7708–7716.
- [4]- R.J. Takahashi, J.M.K. Assis, F.P. Neto, A.M. Mello, D.A.P. Reis, Mater. Sci. Forum 899 (2017) 478–482.

Acknowledgments

This study was financed in part by the Coordenação de Aperfeiçoamento de Pessoal de Nível Superior - Brazil (CAPES) - Finance Code 001.

FABRICATION AND EVALUATION OF DIFFERENT DLC THIN-FILM RESISTOR GEOMETRIES FOR MEMS PRESSURE SENSORS

Gabriela Leal¹, Luiz Antônio Rasia², Humber Furlan³, Mariana Amorim Fraga^{1*}, Marcos Massi⁴

¹Universidade Federal de São Paulo, São José dos Campos, Brasil

²Universidade Regional do Noroeste do Estado do Rio Grande do Sul, Ijuí, Brasil

³Faculdade de Tecnologia de São Paulo, São Paulo, Brasil

⁴Universidade Presbiteriana Mackenzie, São Paulo, Brasil

*Corresponding Author: mafraga@ieee.org

1. Introduction

Diamond-like carbon (DLC) thin films exhibit outstanding properties, merged between diamond and graphite properties, such as high mechanical hardness, chemical inertness, optical transparency and wide bandgap [1-3]. These properties are attractive for the development of MEMS (micro-electrical-mechanical systems) devices, particularly piezoresistive pressure sensors. Here we report the fabrication and test of different DLC thin-film resistor geometries (Fig.1). The resistors were fabricated by reactive ion etching (RIE) with Ti/Au pads formed by lift-off process. The sensing properties of the thin-films resistors were evaluated from the gauge factor (GF) measurements using cantilever beam method.

2. Fabrication of the DLC Thin-Film Resistors

Tungsten-doped DLC thin films were deposited by a magnetron co-sputtering system on thermally oxidized (100) Si substrates, using C and W targets. The carbon target was sputtered by a DC power supply fixed at 150W whereas a HiPIMS power supply of 25W was applied to W target. The argon flow was maintained at 20 sccm, the work pressure at 5 mTorr and the target-substrate distance at 180 mm. Morphology, thickness and electrical resistivity of the W-DLC films have been studied by scanning electron microscopy (SEM) four points probe, respectively. Different resistor structures were fabricated using photolithography, metallization lift-off and RIE (reactive ion etching) processes and their sensing properties were evaluated.

3. Results and Discussions

W-DLC films have thickness of 400 nm and low resistivity (0.02 Ohm.cm). Figure 2 (a) shows the SEM images of the serpentine resistors fabricated, which exhibited the highest GF value among the types of resistors fabricated. As can be observed in Fig. 2(b), the GF of this resistor type is around 10 at room temperature. Overall, the characterization results indicate that W-DLC thin films have good characteristics for MEMS pressure sensor applications.

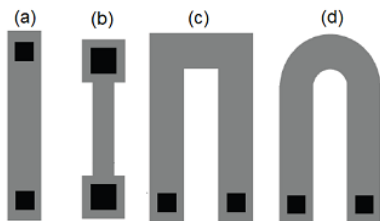


Fig. 1. Schematic representation of the resistors designed: (a) Strip, (b) Dogbone, (c) and (d) Serpentine or meander.

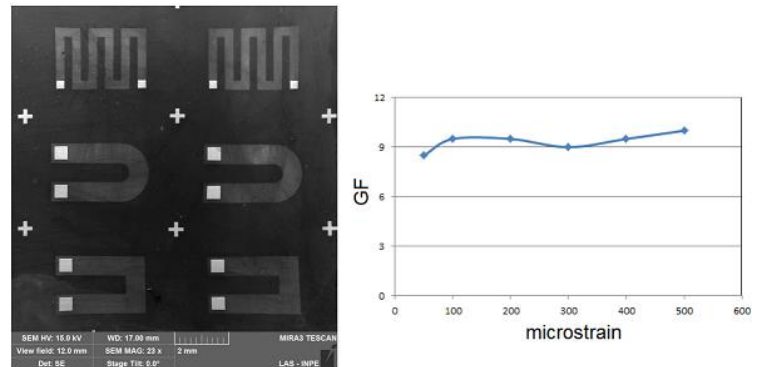


Fig. 2. (a) FEG-SEM images of the serpentine resistors fabricated and (b) GF of the serpentine resistor as a function of μ strain.

4. References

- [1]- M. A. Fraga, H. Furlan, R. S. Pessoa, M. Massi. *Microsyst. Technol.* 20, 9–21, (2014).
- [2]- Š. Meškiniš, A. Vasiliauskas, K. Šlapikas, R. Gudaitis, S. Tamulevičius, G. Niaura, *Surf Coat Technol.* 211, 172–175, (2012).
- [3]- M. Petersen, U. Heckmann, R. Bandorf, V. Gwozdz, S. Schnabel, G. Bräuer, C.P. Klages. *Diam Relat Mater.* 20(5-6), 814–818, (2011).

Acknowledgments

São Paulo Research Foundation – FAPESP (processes number 14/18139-8 and 13/17045-7) and CNPq.

DIAMOND-LIKE CARBON FILMS WITH INCORPORATED CVD-DIAMOND NANOPARTICLES VIA CONTROLLED PULSED VALVE

Rebeca Falcão Borja de Oliveira Correia^{1,2*}, Cristiane C. Wachesk^{1,2}, Thalita Sani Taiariol^{1,2}, G. Vasconcelos³,
Dayane B. Tada¹, Evaldo J. Corat², Vladimir J. Trava-Airoldi²

¹Federal University of Sao Paulo

²National Institute for Space Research

³Institute of Advanced Studies

*Corresponding Author: rebeca.correia@inpe.br

1. Introduction

Diamond-like carbon (DLC) films have been studied due to their attractive mechanical, chemical and tribological properties. Characteristics such as low friction coefficient, high hardness and high adherence on different substrates make this film been extensively applied in a wide range of fields [1][2]. The properties of the DLC film can be significantly enhanced by the presence of diamond nanoparticles (NPs) in their structure [3]. Therefore, the innovative aspect of this work is the growth of DLC films with incorporated CVD diamond NPs using a pulsed valve. In this study, CVD NPs were obtained by high energy ball milling technique and centrifugation process with controlled sizes. The DLC with incorporated CVD diamond NPs were obtained via PECVD technique with an additional cathode. The film properties were evaluated as a function of nanoparticles presence.

2. Experimental

CVD diamond NPs were obtained via milling a freestanding HFCVD diamond film. The milling time was 24 h, then the particles underwent a purification and centrifugation process. Then, a colloidal solution of NPs in methanol was prepared. CVD NPs size particle distribution in methanol was analyzed using Dynamic Light Scattering (DLS) technique. Afterwards, the colloid was deposited during the film growth using a pulsed valve. The film deposition was performed on a metallic substrate via PECVD technique with an additional cathode, in a high vacuum atmosphere. Then, characterization techniques such as Raman, Scanning Electronic Microscopy-Field Emission Gun (SEM-FEG), and X-ray diffraction were carried out in order to analyze the influence of the NPs presence in the film properties.

3. Results and Discussions

Figure 1 shows that it was possible to incorporate NPs during DLC film growth. The use of the controlled pulsed valve allows better control of the pressure variation in the growth chamber. However, the formation of clusters is observed. Figure 2 shows that the particles were agglomerated in the solution, indicating that functionalization processes are necessary.

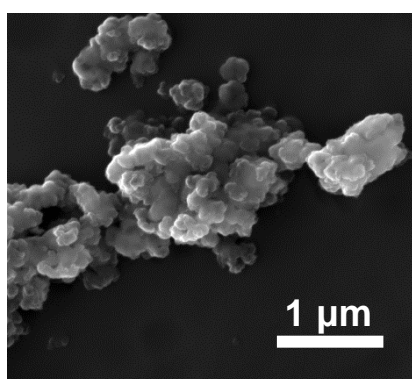


Fig. 1. SEM-FEG image of DLC film with CVD diamond NPs.

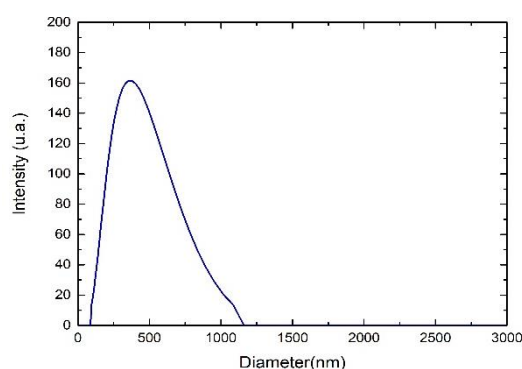


Fig. 2. Size particle distribution of the CVD diamond NPs in methanol.

4. References

- [1]-F.R. Marciano, L.F. Bonetti, R.S. Pessoa, J.S. Marcuzzo, M. Massi, L. V Santos, V.J. Trava-airoldi, *Diam. Relat. Mater.*,**17**,1674-1679, (2008).
- [2]-R. Hauert, *Diam. Relat. Mater.*,**12**,583-589, (2003).
- [3]-F.R. Marciano, L.F. Bonetti, D.A. Lima-oliveira, C.B. Mello, M. Ueda, E.J. Corat, V.J. Trava-airoldi, *Diam. Relat. Mater.*,**19**, 1193-1143, (2010).

Acknowledgements

The authors want to acknowledge support from FAPESP (grant numbers 2017/08899-3 and 2012/15857-1).

EFFECT OF THE PLASMA IONIC NITRIDING PARAMETERS IN WEAR RESISTANCE OF SAE 1020 STEEL USED IN FORMING DIE

Miguel R. Danelon^{1*}, Marcos D. Manfrinato^{1,2}, Luciana S. Rossino^{1,2}

¹Sorocaba Technological College- FATEC, Sorocaba, SP, Brazil

²Federal University of São Carlos (UFSCar), Sorocaba Campi, Sorocaba, SP, Brazil

*Corresponding Author: miguelrdanelon@hotmail.com

1. Introduction

The plasma ionic nitriding is a thermo chemical treatment that improves metal wear, fatigue and corrosion properties, due a iron nitride layer, that forms on material's surface.[1]. The objective of this work is to analyze temperature, proportion and gas flow influence, to determinate the most effective parameter to increase wear resistance of plasma nitrided 1020 steel, used as aluminium forming die.

2. Experimental

The plasma ionic nitriding was carried out using a Pulsed-DC power supply, at a five hours treatment. The temperature was varied from 400, 450, 500, 550 and 600°C, to 80%N₂/20%H₂ proportion. For the 500°C fixed temperature, the proportion of %N₂/%H₂ was varied from 5/95, 20/80, 50/50 and 80/20, with a 500 sccm fixed gas flow and 1400 sccm of Ar. To 500°C temperature and 80%N₂/20%H₂ gas proportion, the gas flow was varied in 500 and 750 sccm. The materials were characterized by metallographic and Vickers micro hardness testing. The micro abrasive wear test by fixed ball, were realized in 600s with 8N charge.

3. Results and Discussions

The wear resistance temperature effect is presented in Figure 1. It is observed that the lowest wear volume was obtained to the 450° treated sample, due to the fine compound layer formed. The layer formed in 400°C, really thin, improves the wear resistance if compared to the material without treatment, but doesn't provides the better wear resistance. Higher treatment temperatures favor a thicker compound layer formation, hard and fragile, that, although increases studied material wear resistance, isn't more effective than 450°C treated sample. It can be observed, in Figure 2, that gas proportion utilized on treatment, also influences directly in the material wear resistance. The biggest wear resistance it was obtained by 20%N₂/80%H₂ nitrided sample, because the thickness is smaller compared to the other conditions. The sample treated in 5%N₂/95%H₂ proportion did not formed a compound layer, only forming a diffusion zone, which improved the material wear resistance without treatment, but presented the lowest wear resistance of the treated materials. It was observed that the increasing of gas flow from 500 sccm to 750 sccm, decreased the material wear resistance, wherein the 500 sccm treated sample obtained a 0,0008 mm³ wear volume and the 750 sccm treated sample obtained a 0,004 mm³ wear volume. This result could be related with the higher nitrogen potential present in treatment environment, which provides a thicker and harder compound layer formation, that breaks with facility, decreasing the material wear resistance. Thus, a less thick compound layer formation presented a better performance in wear, being directly influenced by the treatment parameters choice.

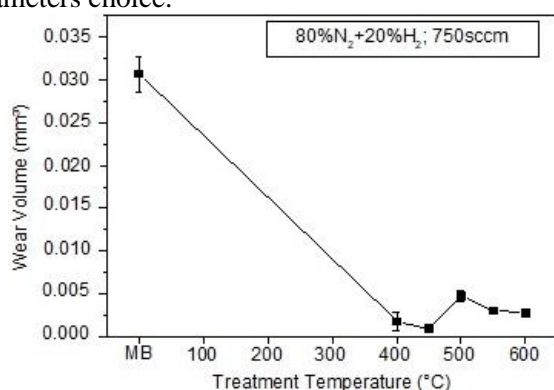


Fig. 1. Wear Volume as a function of treatment temperature

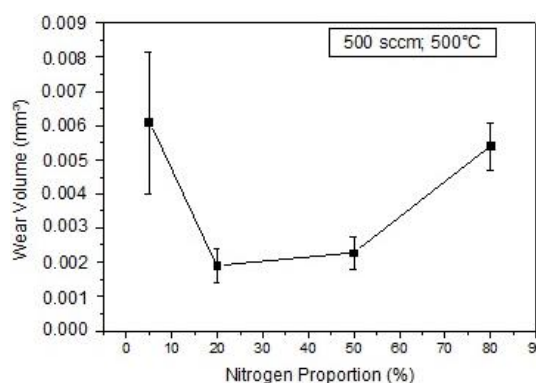


Fig. 2. Wear Volume as a function of nitrogen proportion, with 1400 sccm of Ar

4. References

[1]- Alves Jr. Nitretação a plasma: fundamentos e aplicações. Natal: UFRN, 2001.

Acknowledgments

We would like to thank CNPq (167181/2018-1)

MICROSTRUCTURAL DEVELOPMENT OF TITANIUM ALLOY TNTZ PRODUCED BY POWDER METALLURGY TECHNIQUE.

R. M. Pereira¹, R.F.Correia², V.A.R.Henriques^{1,3}¹ITA - Technological Institute of Aeronautics, Department of Aeronautical and Mechanical Engineering²INPE - National Institute for Space Research³IAE - Institute of Aeronautics and Space

*Corresponding Author: m_raissa@hotmail.com

1. Introduction

Titanium alloys are preferably used in industrial applications, once exceed the nonalloyed metal by many aspects including mechanical properties. The type and amount of each element combined with titanium will define different types of structures, which are classified in three categories: α alloys, $\alpha+\beta$ alloys and β alloys [1]. One of the main obstacles of obtaining titanium alloys is related to its high affinity with oxygen, which makes it very difficult to achieve finished products having desired microstructure and properties in high temperature. To overcome this issue, a vacuum or inert gas environment is introduced to remove O contents in the heating chamber [2]. Titanium alloys are usually obtained by vacuum melting process which has an elevated cost. The Powder Metallurgy (P/M) is an alternative technique with low cost that allows obtaining parts close to the final dimension [3]. This work aims to study the micro structural development of the Ti-29Nb-13Ta-4,6Zr alloy by powder metallurgy in order to establish processing parameters and to produce a homogeneous microstructure.

2. Experimental

TNTZ samples were produce from hydrided powders using blended elemental method. Initially, the mixture of the powders, at alloy stoichiometry, was cold and uniaxially compacted at 50MPa, followed by isostatic press at 400 MPa. Then, the samples were sintered under high vacuum condition (10^{-5} Torr) inside a niobium crucible from 800 °C up to 1600 °C at heating rates of 20 °C/min. The micro structural development of TNTZ was investigated by scanning electron microscopy, in the backscattered mode (BSE), to stress composition contrast. EDS analyses were performed to identify elements in dissolution.

3. Results and Discussions

The micro structural study of TNTZ during sintering showed the β phase development from the dissolution of Ta and Nb particles, according to figure 1. At 800 °C, it was noticed the uniform distribution of the elements in the matrix, where the white colour represents Ta, dark regions are Ti and light grey corresponds to Nb, according to EDS analysis. From 900 °C to 1300 °C it was possible to observe the formation of Widmanstätten like structures ($\alpha+\beta$) near to Ti particles from the dissolution of Zr particles. Increasing the temperature to 1400 °C, it was possible to observe the disappearance of the last Ta areas and from 1500 °C up to 1600°C, it was observed the establishment of β phase areas.

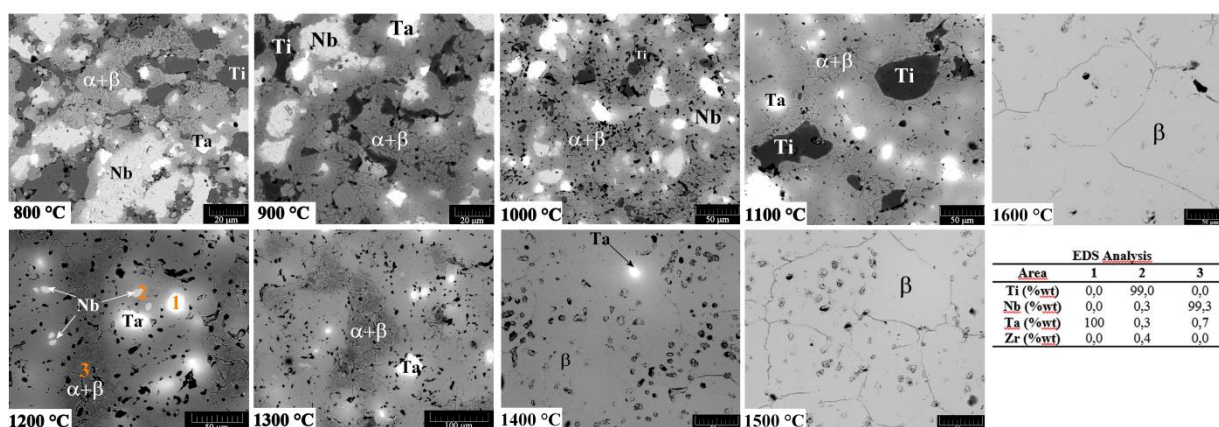


Fig. 1. Micro structural development of TNTZ alloy sintered from 800 °C up to 1600°C and EDS analysis at 1200 °C.

4. References

- [1]- V. N. Moiseyev "Titanium Alloys: Russian Aircraft and Aerospace Applications", Taylor & Francis, USA, (2006).
- [2]- A. K. M. Nurul Amin "Titanium Alloys - Towards Achieving Enhanced Properties for Diversified Applications", INTECHOPEN, Croatia, (2012).
- [3]- L. Bolzoni, E. M. Ruiz-Navas, and E. Gordo, *Mater. Sci. Eng. A*, **687**, 01, 47–53, (2017).

ON GROWING HOMOGENEOUS OXIDE-IRON LAYERS THROUGH ASYMMETRIC BIPOLAR PULSED PLASMA

Paula Fin, Abel A. Candido Recco, Juliano Sadi Sholtz, Luis César Fontana

1. Introduction

Oxidation of metals and alloys has several applications as insulating layers, electrical and electronic components. The main problem in metal oxidation through plasma DC is precisely the fact that oxide layers can be electrical insulating, which hinders the plasma maintenance during the process. The plasma electrolytic oxidation (PEO) process is the most studied process for metal oxidation, however, it presents some drawbacks as high porosity of the oxide layer formed on the surface and high-energy consumption [1]. The present paper proposes a modified voltage waveform for plasma-oxidation treatment, which ensures the plasma stability and enables the creation of dense and uniform oxide layers on metal surfaces in a controlled form.

2. Experimental

The experiments were performed in a 30cm diameter by 30cm height with grounded walls. The samples of AISI 1006 steel (polished with alumina 0.1 μ m) were oxidized through plasma during 2.0h and 0.5h at the temperatures of 300°C and 500°C, respectively. The oxidation parameters of samples were: base pressure of 4x10⁻² Torr; working gas: pure O₂; working pressure 0.5 Torr. The power supply used for the plasma generation was a bipolar pulsed source that generates positive pulses of high intensity and short period (1 μ s), adjustable in intensity and frequency, named ABiPPS (Asymmetric Bipolar Plasma Power Supply, [2]).

3. Results and Discussions

Figure 1-a and 1-b show SEM images of samples S300-2h and S500-0.5h, respectively. The samples treated in low temperature (S300-2h) presented layer thickness higher than 1 μ m. The samples treated at 500°C, during only 0.5h, presented even thicker oxide layers, higher than 6 μ m ($e_{500/0.5h} = 6.4\mu\text{m}$; $e_{300/2h} = 1.1\mu\text{m}$). We point out that the layers are compact, free of pores and show good adhesion, if compared to the layer spalling levels observed for other methods of iron oxidation [3]. By a XRD analyze was possible to determine that S300-2h samples have an oxide layer of a mono-phase Fe₃O₄ and that the S500-0.5h samples have the formation of two phases: Fe₃O₄ and α -Fe₂O₃.

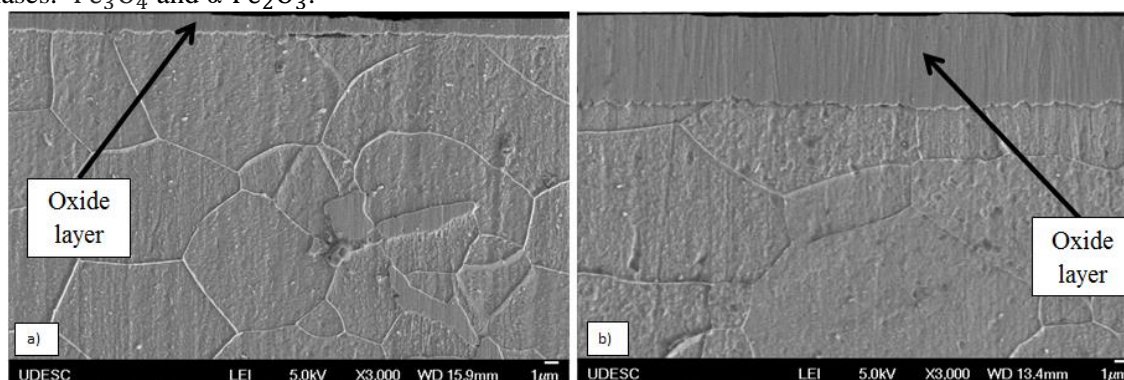


Fig. 1: Cross-section scanning electron microscopy images of ABNT 1006 steel oxidized samples: a) sample S300-2h; b) sample S500-0.5h.

4. References

- [1]- Lu, X., Mohedano, M., Blawert, C., Matykina, E., Arrabal, R., Kainer, K. U., & Zheludkevich, M. L. (2016). Plasma electrolytic oxidation coatings with particle additions—a review. *Surface and Coatings Technology*, 307, 1165-1182.
- [2]- Scholtz J. S., Fontana L. C., Plasma Densification Method, Patent N° US 9,999,118 B2, Jun. 12, 2018.
- [3]- Mitchell, T. E., Voss, D. A., & Butler, E. P. (1982). The observation of stress effects during the high temperature oxidation of iron. *Journal of Materials Science*, 17(6), 1825-1833.

Acknowledgments

This study was financed in part by the Coordenação de Aperfeiçoamento de Pessoas de Nível Superior- Brasil (CAPES)- Finance code 001.

INFLUENCE OF PLASMA IMMERSION ION IMPLANTATION ON THE FATIGUE BEHAVIOR OF AA 7050-T451 ALUMINUM ALLOY

Martin F. Fernandes^{1*}, Yara C. Bastos¹, Verônica M. O. Velloso¹ and Herman J. C. Voorwald¹
¹Department of Materials and Technology, Sao Paulo State University (Unesp), School of Engineering, Guaratinguetá. 12516-410. Sao Paulo, Brazil

*Corresponding Author: martin.fernandes@unesp.br

1. Introduction

The 7xxx aluminum alloy series is widely applied in the aeronautical industry due to high mechanical strength to weight ratio. The corrosive environment and friction forces imposed on aircraft components reduce the service life. Therefore, anodizing is frequently used to enhance resistance against corrosion and wear. However, anodizing has negative effects on the fatigue life of aluminum alloys [1]. Plasma immersion ion implantation (PIII) is an alternative surface treatment that can be used to improve hardness and reduce wear damage [1, 2]. Studies have shown that the PIII has less influence on the fatigue strength loss for low frequencies of treatment [1,2]. Shot peening (SP) is a cold working process used to increase the fatigue strength of a component. The present work aimed at investigating the fatigue behaviour of AA 7050-T451 aluminum alloy treated with a combination of both SP and PIII surface treatments.

2. Experimental

The material studied in this work is AA 7050-T451 aluminum alloy. Rotating bending fatigue tests were carried out in the base material and surface treated specimens. The surface treatment performed was SP followed by PIII. The SP parameters were Almen intensity of 0.41-0.49 mm A, coverage of 100% and shot of S 230, according to AMS 2430. The PIII treatment was performed in a vacuum chamber in which plasma containing the ions to be implanted was generated. Nitrogen implantation was realized by applying to the substrate negative high voltage pulses of 10.0 kV, pulse length of 50 μ s and repetition frequency equal to 0.1 kHz during 2 h. Scanning electron microscopy was used to observe the fracture surfaces. The residual stresses at the surface layer were measured using the X-ray diffraction method.

3. Results and Discussions

The fatigue tests results are shown in Fig. 1, where only the average points are presented for each stress level. The typical fracture surface for the surface-treated material is displayed in Fig. 2. The results show that the combination of SP and PIII treatments increases the fatigue strength of AA 7050 aluminum alloy compared to the base material. The surface treatment proposed is more advantageous regarding fatigue behaviour than chromic anodizing results from Minto *et al.* [1]. The combination of SP process and PIII treatment at a low frequency generated a compressive residual stress condition at the surface (-210 MPa), compared to -62 MPa for the base material, that was responsible for the retardation of the crack nucleation and propagation periods, which increased the fatigue life of the material.

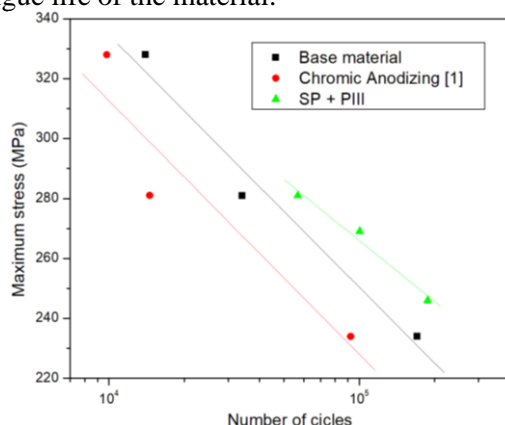


Fig. 1. S-N curves of the base material and surface treated conditions.

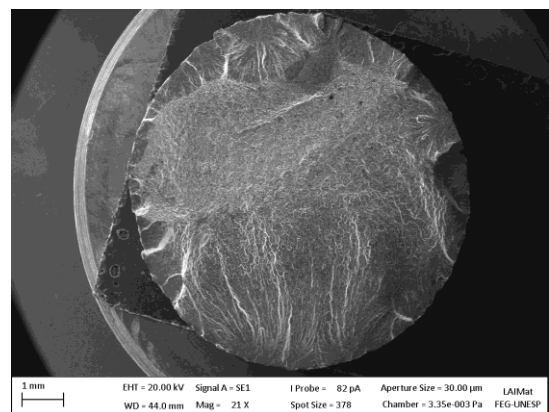


Fig. 2. Fracture surface of SP + PIII treatment condition tested at maximum stress of 281 MPa.

4. References

- [1]- T.A. Minto, V.M.C.A. Oliveira, H.J.C. Voorwald, Int. J. Fatigue, **103**, 17-27, 2017.
- [2]- V.M.C.A. Oliveira, M.O.H. Cioffi, M.J.R. Barboza et al., Int. J. Fatigue, **109**, 157-165, 2018.

Acknowledgments

This study was financed in part by the Coordenação de Aperfeiçoamento de Pessoal de Nível Superior - Brasil (CAPES) and São Paulo Research Foundation (FAPESP), grant # 2019/02125-1.

DEVELOPMENT AND CHARACTERIZATION OF CVD DIAMOND CUTTING TOOLS FOR PRECISION MICRO-TURNING OF MOLYBDENUM

Silva Neto, J. V.^{1*}, Andrade, A. E. N.², Trava-Airoldi, V.J.¹, Corat, E.J.¹

¹National Institute for Space Research, São José dos Campos, SP, Brazil

²ETEP Faculty of Technology, São José dos Campos, SP, Brazil

*Corresponding Author: jvneto.ifsp@gmail.com

1. Introduction

The machining of molybdenum is unconventional, usually performed by electrocorrosion or laser methods (1,2). However, one desirable use is the precision turning of thin Mo rods for posterior CVD diamond coating for application as dental tools (3,4). This process yield per tool insert is substantially impaired by the wear process by metal carbide particles formation (5). In order to obtain better results in turning procedures of Mo, we developed a modified insert geometry and coated these tools with a CVD diamond thin layer. Film quality was studied by FEG-SEM, EDS, Raman spectroscopy and turning tests.

2. Experimental

Tool inserts were cut to appropriate geometry by grinding wheel, sanded with sandpaper then polished with diamond abrasive paste with sequential grain sizes of 6, 3 and 1 μm . After this process samples were cleaned in isopropanol ultrasonic bath. Then took to the chemical corrosion of surface Cobalt by a two step chemical etching. After these preparation steps, samples were seeded with diamond nanoparticles, CVD diamond layer was applied in a HFCVD reactor, with the following set up: gas mixture of 2% methane in 98% hydrogen, 800 ± 5 °C process temperature, chamber pressure of 50 Torr. After etching and deposition steps samples were characterized by FEG-SEM and EDX. Film structured was studied by Raman spectroscopy. The machining performance was evaluated by turning of molybdenum rods with 2 mm diameter, cutting parameters were cutting depth 0.2 mm, cutting speed 2500 rpm and feed 11 mm/min.

3. Results and Discussions

The characterization by FEG-SEM can be seen at Figure 1 it was possible to obtain a homogenous and continuous CVD diamond coating over the entire surface. Figure 2 brings the Raman spectroscopy showing the diamond peak centered at 1339 cm^{-1} and the presence of G band, D band and a considerable luminescence.

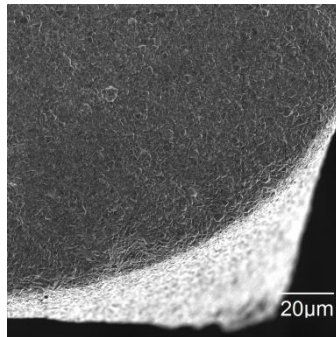


Fig. 1. (figure number in bold face times new roman 10 pt) Cutting tool tip with homogenous and continuous CVD diamond film.

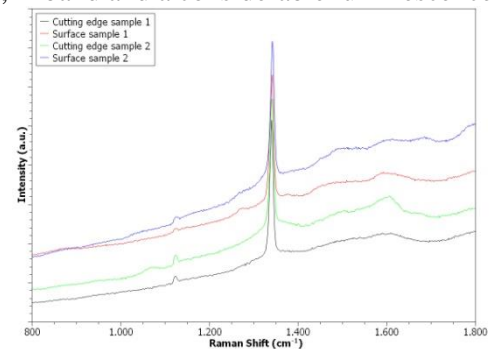


Fig. 2. Raman spectroscopy performed in 2 points of each sample, at rake surface lines in red and black for samples 1 and 2, and at cutting edges lines in blue and green for samples 1 and 2.

4. References

- [1]- Demellayer R, Richard J. High precision electro discharge machining of Molybdenum and Tungsten. *Procedia CIRP* [Internet]. 2013;6:89–94. Available from: <http://dx.doi.org/10.1016/j.procir.2013.03.030>
- [2]- Torres R, Kaempfe T, Delaigue M, Parriaux O, Hönninger C, Lopez J, et al. Influence of laser beam polarization on laser micro-machining of molybdenum. *J Laser Micro Nanoeng.* 2013;8(3):188–91.
- [3]- Trava-Airoldi VJ, Corat EJ, Del Bosco E, Leite NF. Hot filament scaling-up for CVD diamond burr manufacturing. *Surf Coatings Technol.* 1995;76–77(PART 2):797–802.
- [4]- Sein H, Ahmed W, Rego C. Application of diamond coatings onto small dental tools. *Diam Relat Mater.* 2002;11(3–6):731–5.
- [5]- Poulachon G, Moisan A, Jawahir IS. Tool-wear mechanisms in hard turning with polycrystalline cubic boron nitride tools. *Wear.* 2001;250–251(1–12):576–86.

Acknowledgments

This work was supported by FAPESP (process number 2012/15875-1) and CAPES.

DEVELOPMENT OF A CVD DIAMOND COATED MOLYBDENUM SUBSTRATE HOLDER FOR SINGLE CRYSTAL DIAMOND GROWTH IN MPACVD REACTOR

Da Silva Neto, J.V.^{1*}, Gomez, J. A.¹, Trava-Airoldi, V. J.¹, Corat, E. J.¹

¹National Institute for Space Research, São José dos Campos, Brazil

*Corresponding Author: jvneto.ifsp@gmail.com

1. Introduction

The growth of CVD single crystalline diamond is a topic that has attracted the interest of researchers worldwide for its properties in higher technologies as well as gemstones production (1). Final quality of the grown layer is of major importance for all of its applications (2). One of the problems that influence final film quality is the contamination by chamber materials, mainly the ones that are in contact with high temperature regions, which is the case for the substrate holder. This work proposes the solution by growing a polycrystalline CVD diamond layer in order to block the direct exposure of substrate holder material to the plasma region, that leads to the overheating and evaporation of holder material to sample surface.

2. Experimental

Molybdenum samples of 20 mm diameter and 2 mm thickness were cut from a molybdenum rod, sanded with sandpaper, and scratched with diamond paste in order to obtain better mechanical interlocking between film and substrate, then seeded with diamond nanoparticles. Diamond growth was performed in a Microwave Plasma Assisted Chemical Vapour Deposition (MPACVD) reactor at 190 Torr pressure and 4,2 kW of microwave input power.

3. Results and Discussions

Electronic Scanning Microscopy analysis (FE-SEM) shown a homogenous film, Raman spectroscopy reveals the diamond characteristic peak centred at 1332 cm^{-1} , for centre and edge regions and 1334 cm^{-1} for intermediate region. Figure 1 brings the top morphology observed in electron micrograph and Figure 2 is a comparative analysis between film regions, centre (blue), intermediate region (red) and edge (black). This inhomogeneity between structural quality is mainly due to differences in temperature of these regions.

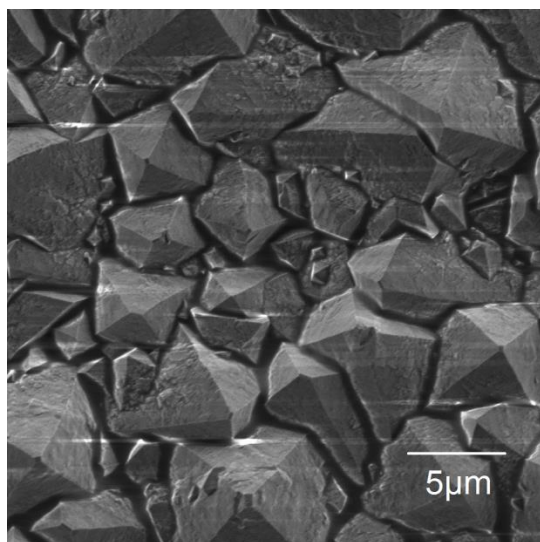


Fig. 1. Surface morphology at 10.000x magnification in FEG-SEM micrograph.

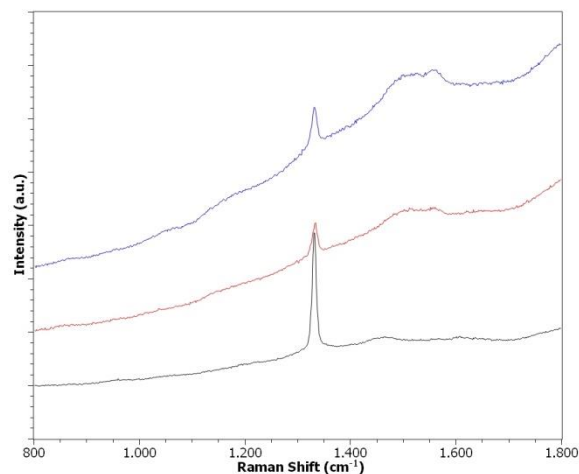


Fig. 2. Raman spectroscopy of different film regions. In blue, spectra taken from the center of the sample, in red in an intermediate region and in black at the edge of the sample.

4. References

- [1]- Tallaire A, Collins AT, Charles D, Achard J, Sussmann R, Gicquel A, et al. Characterization of high-quality thick single-crystal diamond grown by CVD with a low nitrogen addition. *Diam Relat Mater.* 2006 (10):1700–7.
- [2]- Linares R, Doering P. Properties of large single crystal diamond. *Diam Relat Mater.* 1999 (2–5):909–15.

Acknowledgments

This work was supported by FAPESP (process number 2012/15875-1) and CAPES.

EFFECTS OF LOW TEMPERATURE ATMOSPHERIC PRESSURE PLASMA ON *Escherichia coli*Kirchhof, E. S.^{1*}, Sampaio, A. G.¹, Rovetta, S. M.¹, Oliveira, M. A. C.¹, Kostov, K.², Koga-Ito, C. Y.¹¹ Institute of Science and Technology, São Paulo State University UNESP, São José dos Campos, Brazil.² Department of Physics and Chemistry, São Paulo State University UNESP, Guaratinguetá, Brazil.

*Corresponding Author: alinnsampaio@gmail.com

1. Introduction

Escherichia coli is a pathogen used as water quality control. Plasma is considered a promising alternative to eliminate this pathogen, as well as to neutralize organic pollutants an important resource to use to eliminate this pathogen, and neutralized organic polluted in water. The effect of plasma against antibiotic-resistance of *E. coli* in wastewater treatment was reported [1,2]. The aim of this study was to analyze the changes induced by plasma on bacteria cell.

2. Experimental

An aliquot of 40 µl of *E. coli* (ATCC 10799) inoculums (10^6 CFU/mL) was transferred to sterile glass slides. The suspensions were treated with low temperature atmospheric pressure plasma jet using set parameters described by Borges et. al. [1]. Suspensions were exposed to plasma for 1, 3, 5, 7 and 10 minutes. Subsequently, the number of viable cells were determined by plating method and results were expressed in colony forming units per millilitre (CFU/ml). The experiment was performed in three different occasions. Plasma treated and non-exposed bacterial cells (10^8 CFU/ml) were also analyzed by scanning electron microscopy (SEM). SEM micrographs was taken in magnification of 50.000x and HV of 5.0 kV in FEG MIRA 3, TESCAN. Cells were measured by Gwyddion 2.52 software. Statistical analyses were performed using Origin Pro 8.0. Data were submitted to normality test (Shapiro-Wilk) and ANOVA (post hoc Tukey's test). The level of significance was set in 5%.

3. Results and Discussions

Ten minutes of exposure to plasma was able to reduce *E. coli*. Control group showed 3.06×10^{10} CFU/ml ($\pm 6,89 \times 10^9$ CFU/ml) while plasma exposed group showed 1.64×10^{10} CFU/ml ($\pm 1.09 \times 10^{10}$ CFU/ml). It was an expressive and significant reduction of 54%. The effects of plasma could be also detected in SEM micrographs. Figure 1 shows regular rod-shaped cells. After exposition to plasma, cells with altered morphology and apparently severely damaged structure can be observed (Figure 2). White arrows point out cells images that suggest intracellular content loss. Significant reduction in the size of bacterial cells exposed to plasma was also detected ($284 \text{ nm} \pm 53 \text{ nm}$) in relation to control ($568 \text{ nm} \pm 92 \text{ nm}$). It can be concluded that 10 minutes exposure to low temperature plasma was effective in inactivating *E. coli*, causing morphologic alterations and intracellular content loss.

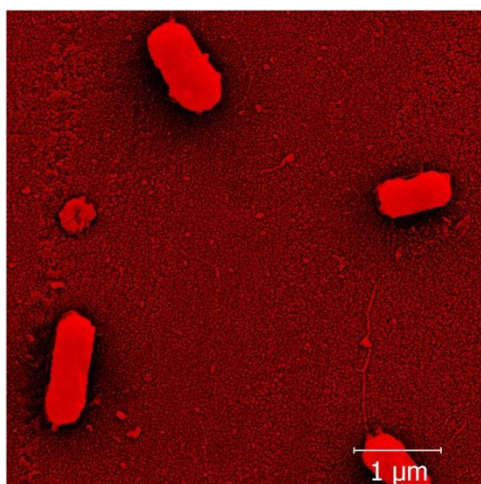


Fig. 1. SEM micrograph of non-exposed *E. coli* (control)

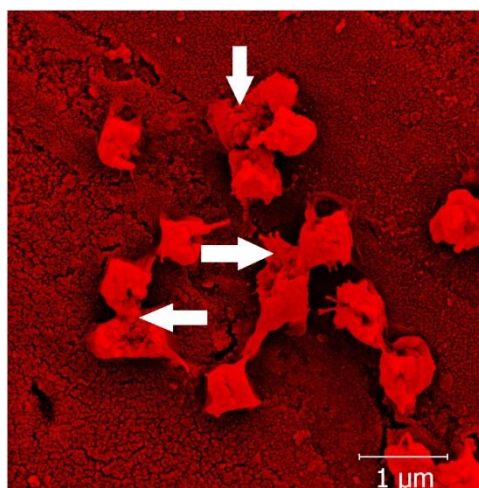


Fig. 2. SEM micrograph of *E. coli* exposed to low temperature plasma

4. References

[1]- A. C. Borges, et al., Clin Plasma Med. 2017, 7-8: 9-15.

[2]- Z. Rashmei, H. Bornasi, M. J. Ghoranneviss, Water Health. 2016, 14 (4):609-16.

Acknowledgments

To CNPq for the PIBIC/CNPq-UNESP scholarship.

CHARACTERIZATION OF POLYCRYSTALLINE CVD DIAMOND FILM DEPOSITED ON INTRINSIC SILICON WITH DIFFERENT CRYSTALLINE ORIENTATIONS.

Alexandre Marcello Cavalca de Almeida, Evaldo Chagas Gouvêa, Teófilo Miguel de Souza
Faculty of Engineering, UNESP – Univ Estadual Paulista, Guaratinguetá campus, Avenida Ariberto Pereira da Cunha, 333, CEP 12.516-410, Guaratinguetá, São Paulo State, Brazil
**Corresponding Author: marcello.cavalca@gmail.com*

1. Introduction

The CVD diamond is a synthetically produced material and has basically the same physical and chemical properties as natural diamond. Due to the properties of CVD diamond film and its potential as a material with many basic analyzes, several application possibilities have been evidenced, such as its use in metallurgical cutting tools, perforating drills, dental instruments, heat sinks, sample cells for analytical equipment, ceramic inserts, string musical instrument fuses, niobium and titanium alloy coating, electronic devices [1]. Therefore, the study of factors that influence the quality of the obtained diamond becomes important. Among the methods of production of artificial diamonds that exist today, two basic methods stand out: HPHT (High Pressure High Temperature) and Chemical Vapor Deposition (CVD) [2, 3], the latter being the methodology employed in the present work.

2. Experimental

The reactor installed and used in the proposed project is a large multifilament equipment that can work with an area up to 150 cm² (Fig 1, Fig 2). The hot tungsten filament deposition technique at high temperature (2000 to 2500 ° C) was applied. The process took place inside a low-pressure chamber (about 50 mmHg) in which a mixture of hydrogen-diluted methane gas is inserted. Diamond-CVD films were characterized for morphology, texture and thickness by Scanning Electron Microscopy (SEM) and assisted by Optical Microscopy (800X). X-ray diffraction analyzes and Raman scattering spectroscopy were performed to confirm and understand both the crystal structure and its interaction with the substrate.

3. Results and Discussions

The obtained films were characterized by analyzing the thickness of the formed film, in order to verify which type of doping favours the formation of the CVD diamond, and also the effect that the reaction time has on the films obtained, both in the formation and in the quality of the material. The project aims to analyze silicon with various crystalline orientations and verify the effects of time and crystalline orientation on the formation and quality of the obtained film. In this way a broader analysis was obtained on the effect that different doping and the reaction time of each obtained sample have on the formation, thickness and quality of the formed film.



Fig. 1. CVD Diamond Lab Interior.



Fig. 2. Reactor installed in the laboratory.

4. References

- [1]- J. Achard and F. Silva, *Diam. Relat. Mat.*, **20**, 145–152, (2011).
- [2]- Y. Manawi and A. Samara, *Materials*, **11**, 822, (2018).
- [3]- H. Li and M. Li, *Diam. Relat. Mat.*, **86**, 179–185, (2018)

Acknowledgments

To God, and also to professor Teófilo and lecturer Evaldo and my family.

CONSTRUCTION OF A REACTOR FOR TREATMENT OF MATERIALS THROUGH PLASMA NITRIDING

Danillo Duque T. B.*, Jean Maciel, Andreos Heller, Joel Stryhalski
Federal Institute of Education, Science and Technology of Santa Catarina - IFSC
 *Corresponding Author: *dandunque10@gmail.com*

1. Introduction

Plasma nitriding is a thermo chemical treatment that calls attention for its advantages, such as reducing waste and saving time and energy, becoming a considerable sustainable alternative in comparison to others nitriding processes and techniques [1]. The current work proposes the construction of a plasma nitriding reactor with a dome made of glass for a more didactic view of the physical phenomena involved in without losing the nitriding technical functionality.

2. Experimental

The project came out to continue the work started with the final paper (TCC) of [2] (see Fig. 1) and done based on the work of [3]. It have been done a research for the pieces needed to the fabrication of the reactor, machining at the laboratories of the campus the ones that were able to and buying the others. The reactor is at a test phase to avoid any air leakage so the pressure can be as low as possible, resulting in a low tension required to work.

3. Results and Discussions

As seen in Fig. 2, the reactor is already capable to generate the plasma. Despite that, there are still some adjustments to the electrical discharge to be made. After all, it will be possible to obtain some results like the reactor's characterization. Current-voltage curves will be obtain that is a macroscopic signature of the characteristics of plasma. Then, researches about morphology, materials resistance and tribological wear of the plasma-nitrided layer, plasma effects in different surfaces will be possible, opening the opportunity to conduct research in this area at the Institute.

In addition, due to the glass dome, the reactor can be used as a way to illustrate and teach some concepts like vacuum and plasma to students at regional events.



Fig. 1. SolidWorks sketch by [2].

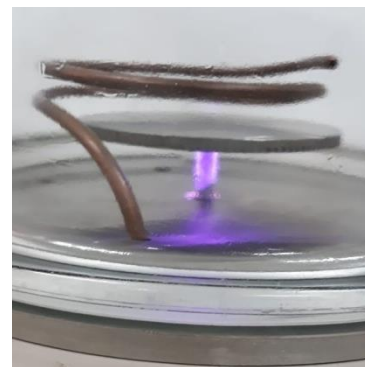


Fig. 2. One of the first attempts to turn on the reactor.

4. References

- [1]- Abdalla, A. J., and V. H. Baggio-Scheid. "Tratamentos termoquímicos a plasma em aços carbono." *Corrosão e Protecção de Materiais* 25.3 (2006).
- [2]- Lopes, Priscila Eduarda Kraft. "Projeto e construção de reator para tratamento termoquímico de superfície de nitretação por plasma." (2018).
- [3]- CORRÊA, Felipe Hilário, BECKER, Daniela, FONTANA, Luis César. Confinamento de elétrons em um sistema de plasma de tela ativa e geração de potencial flutuante extremo no interior da gaiola, *Rev. Bras. Apl. Vac., Campinas, Vol. 37, N°2, pp. 59-64, Maio - Ago., 2018*

Acknowledgments

A special thanks Federal Institute of Santa Catarina for the financial support in Edital nº 23/2018/PROPI/DAE

CHARACTERIZATION OF CLINKER USING FTIR AND XRD

Arthur Henrique do Nascimento Pereira, Filipe Leal Carvalho dos Santos¹,
 Felipe Werlick Velloso dos Santos, Antonio Renato Bigansolli*, Belmira Benedita de Lima-Kuhn
¹Department of Chemical Engineering, Institute of Technology, UFRRJ, Seropédica, RJ.
 *Corresponding Author: bigansolliarb@gmail.com

1. Introduction

"Portland clinker" is obtained from a sintering process. The "clinker" is produced by grinding and intimately mixing clay and lime-bearing minerals, and then heating the mixture to about 2550°F in a rotary kiln, producing physical and chemical changes in the raw materials [1].

2. Experimental

The Portland clinker cement sample was crushed in an agate mortar. After comminution, the sample was analysed with DRX and FTIR. FTIR spectra were recorded with a BRUKER VERTEX 70 spectrometer by applying the ATR PLATINUM. Powdered sample was recorded the from 4000 cm^{-1} to 500 cm^{-1} region. For the XRD experiments, the measurements were carried out at room temperature using Ni-filtered Cu-K α radiation in an diffractometer (Rigaku, Miniflex II). The conditions were $15^\circ < 2\theta < 55^\circ$, 0.05° step. The phases were identified based on Villars and Calvert crystallographic data [2] and the Powder Cell software [3].

3. Results and discussion

The results from the FTIR around 625 cm^{-1} may be related to Si-O-Si vibration. In the band between 750-958 cm^{-1} it show a possible vibration of carbonates or, most probably, Si-O stretching vibrations. Stretching vibrations of Si-O-Si and bending of Si-O are around and around 1000 cm^{-1} , and it is possible to find asymmetric stretching of CO_3 above 1500 cm^{-1} . In the XRD, the elements found are mostly calcium silicates (C_2S and C_3S), along with calcium aluminates (C_3A and C_4AF) [4].

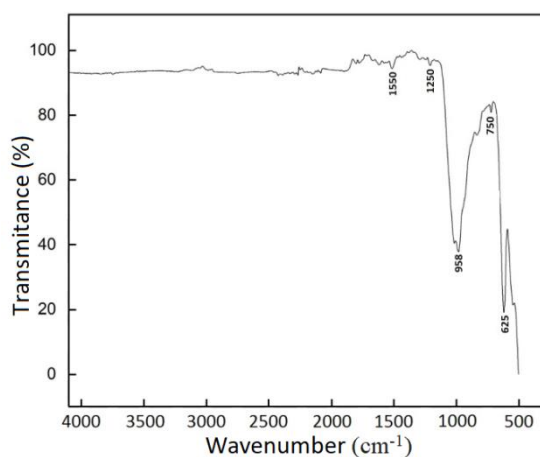


Fig. 1. Infrared Spectrum of Clinker (FTIR)

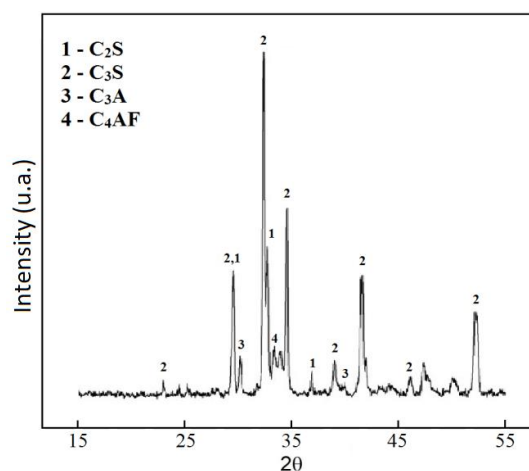


Fig. 2. X-ray Diffraction of Clinker (XRD)

4. References

- [1]-W. D. Callister, "Fundamentals of Materials Science and engineering", Sixth Edition, 426, (2001).
- [2]-P. Villars, L.D. Calvert, Pearson's Handbook of Crystallographic Data for Intermetallic Phases, second ed., 4 vols., ASM International, Materials Park, OH. (1991).
- [3]-W. Kraus, G. Nolze. PowderCell for Windows (version 2.3). Berlin: Federal Institute for Materials Research and Testing. (1999).
- [4]-F. L. C. Santos, "Caracterização e resistência à compressão do cimento Portland com adição de catalisador de equilíbrio (E-CAT)", Trabalho de Conclusão de Curso, UFRRJ, Seropédica, BR, (2018).

MICROSTRUCTURAL CHARACTERIZATION OF ALUMINA CORUNDUM USED AS A LOADING ELEMENT IN EPOXY RESIN

Louzada M. Z.^{1*}, Bigansolli A. R.² and Lima-Khün B. B.²

¹UFRJ – Universidade Federal do Rio de Janeiro, Rio de Janeiro, RJ, Brazil.

²UFRRJ – Universidade Federal Rural do Rio de Janeiro, Seropédica, RJ, Brazil.

*Corresponding Author: maurozamp94@gmail.com

1. Introduction

Recycling is one of the most used mechanisms in the industrial waste treatment system. One of the applications of this technique is the insertion of waste into polymer matrices. A suitable ratio and a combination of waste particles influence in a positive way mechanical properties of the material in which they are dispersed and they decrease its price [1]. The presence of reinforcing fillers in matrices is aimed to change the specific properties of the final product, which depends directly on the type of load and matrix used [1]. The aim of this work is to study the properties of polymer composite formed by an epoxy resin matrix reinforced with alumina filler. Then, this work presents the characterization of alumina waste by X-ray Diffraction (XRD) and the impact resistance of different blend compositions (5 wt% and 10 wt% alumina).

2. Experimental

The alumina waste was characterized by XRD, through a diffraction equipment, PANalytical, model Miniflex, using CuK α radiation at 30 kV, 15 mA, and scanning between 0° and 50°. The alumina identification from XRD data was done using the Powder cell [2] and FULLPROF [3] computer programs and crystallographic data from Villars and Calvert [4].

For the manufacture of the composite, silicone molds were made using polyethylene samples, which dimensions are standardized by ASTM D 256 [5]. The polymer Bisphenol A diglycidyl ether epoxy resin (DGEBA) and the hardener, Aradur 2963, were used in the proportions indicated by the manufacturer (Huntsman) in order to provide the best mechanical performance. The powders were weighed and manually mixed with Aradur 2963 in a beaker for 2 minutes using a glass stirring rod. Next, the Araldite GY 279 BR was added to the mixture, and mixed together for 10 minutes. Finally, the mixture (with 5 wt% or 10 wt% alumina corundum) was deposited into moulds. The specimens were removed from the moulds after 24 hours and, after 30 days (maximum time) of curing at room temperature, the impact tests were conducted.

3. Results and Discussion

The X-ray diffraction of the waste only shows reflections from the alumina corundum as observed in Figure 1. Figure 2 shows the impact test specimen with notch configurations such as V. The results of the IZOD Impact Testing indicated that the toughness reduced with increasing alumina loading in the composites associated with reduced interfacial bond between alumina and matrix.

Fig. 1. X-ray diffractogram of alumina

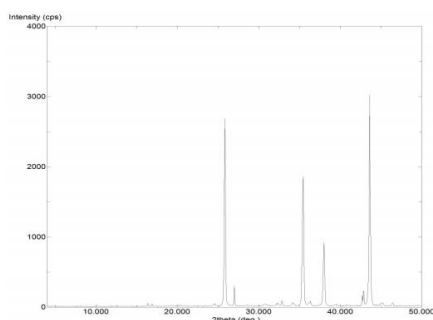
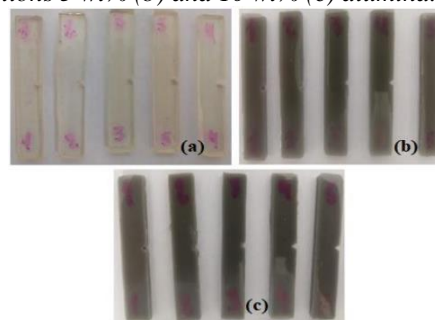


Fig. 2. Impact test specimen: pure epoxy resin (a), blend compositions 5 wt% (b) and 10 wt% (c) alumina.



4. References

- [1]- P. Valášek, M. Müller and S. Hloch. Technical Gazette, **22**, 567-572. (2015).
- [2]- W. Kraus, G. Nolze. PowderCell for Windows (version 2.3). Berlin: Federal Institute for Materials Research and Testing. (1999).
- [3]- J. Rodriguez-Carvajal, Physica B 192, 55–69. (1993).
- [4]- P. Villars, L.D. Calvert, Pearson's Handbook of Crystallographic Data for Intermetallic Phases, second ed., 4 vols., ASM International, Materials Park, OH. (1991).
- [5]- ASTM International D 256. Standard Test Methods for Determining the Izod Pendulum Impact Resistance of Plastics. (2004).

DLC THIN FILMS DEPOSITED IN BIOMATERIALS BY PIII&DN.M. Santos^{1,2*}, M. Ueda¹, B.M. Rueda² and F.V. Santos²¹*National Institute for Space Research, São José dos Campos, SP, Brazil*²*Federal University of Latin American Integration, Iguassu Fall, PR, Brazil***Corresponding Author: nazirmonteiro@gmail.com***1. Introduction**

Metal biomaterials, such as titanium and alloys, stainless steels and cobalt alloys, can be used to replace and repair plates, fracture plates, dental implants, fillers and pins, etc. These materials have good physical properties such as brightness, heat and electricity conductivity, high density and melting point, high toughness and high strength [1]. However, it has the ease of losing electrons; reactive surface and mass loss in interaction with the tissues in contact, with release of ions by dissolution, leakage or corrosion. It is essential to understand the role played by surfaces in the reactions that occur at the interfaces between different materials and between these materials and the biological environment. In addition, the surface modification possibilities allow changing the responses to various physical, chemical, mechanical, biological and functional performance stimuli. Formally surface treatments are divided into treatments involving the removal of layers of material and those in which there is deposition, i.e. the creation of coatings. Among the various methods of preparation of nanomaterials, we highlight the process of deposition of thin films [2]. To improve the properties of these materials and study their structural characteristics, thin carbon films were deposited on titanium alloy (Ti6Al4V) samples by Plasma Immersion Ion Implantation and Deposition (PIII&D) system [3]. The properties of the films deposited generally depend on the deposition conditions, which determine their microstructure, especially the respective proportions of sp^3 and sp^2 carbon site, therefore chemical structure of DLC films were analyzed by Raman Spectroscopy and the structural analysis were evaluated by optical microscopy and x-ray diffraction.

2. Experimental Procedure

DLC films were produced on Ti-6Al-4V (TAV) substrates by PIII&D using methane plasma. The films were prepared in a stainless-steel cylindrical vessel with a volume of 20 liters by driving Hollow Cathode (HC) discharges inside the tube attached to the top part of the chamber. The tubes used were titanium alloy, with 15 cm length and internal diameter of 11 mm, with one side closed configuration. Polished samples of TAV were fixed along the inner tube wall for subsequent analysis of the DLC coatings. Prior to each deposition, the substrates were further cleaned in argon plasma for 10 min (2.5 kV, 12 A, 20 μ s, 500 Hz). Methane plasma was generated by the application of pulses of 6.12 kV, 16 A, 20 μ s, 500 Hz rate, during 120 minutes, reaching temperatures of 780 °C.

3. Results and Discussions

The experimental results showed quite adhered films on the biomaterials. The typical Raman spectra of the DLC film presented two peak (D and G) characteristic of carbonaceous materials with crystalline and amorphous regions. The calculated ID/IG ratios suggest a homogeneous structure indicating the existence of DLC film. The study of the results indicate that PIII&D is a technique suitable for films deposition onto the surface of biomaterials.

4. References

- [1]-KELKAR, A. D; HERR, D.J.C; RYAN, J.C. Nanoscience and nanoengineering; Advances and applications. Ed. CRC Press, 2014.
- [2]- YASUDA H. Plasma Polymerization. Academic Press, 1995.
- [3]- LIERMERMAN M.A, LICHTENBERG A.J. Principles of Plasmas discharges and materials Processing, Willey Interscience, 2 ed. 2005.

STRUCTURAL ANALYSIS OF DLC FILMS DEPOSITED BY PIII&D IN AISI 304 STEEL

N. M. Santos^{1,2*}, M. Ueda¹, D. F. G. Silva², J. V. Ribeiro² and R. A. S. Lima²

¹*National Institute for Space Research, São José dos Campos, SP, Brazil*

²*Federal University of Latin American Integration, Iguassu Fall, PR, Brazil*

*Corresponding Author: nazirmonteiro@gmail.com

1. Introduction

The purpose of this work was the production of Diamond-like carbon (DLC) films inside metal tubes in order to increase the corrosion resistance of its inner surface and to investigate the properties of these films. DLC films have interesting properties for technological applications, such as high hardness, wear resistance, low friction coefficient and biocompatibility [1]. Using DLC films as protective coatings can increase the lifetime of the tubes used in propulsion of spacecrafts and thermal control systems of satellites and inhibit the permeation of corrosive species from the fuels and the cooling fluids through the film-metal interface. The properties of the films deposited by Plasma Immersion Ion Implantation and Deposition (PIII&D) system generally depend on the deposition conditions, which determine their microstructure, especially the respective proportions of sp³ and sp² carbon site [2, 3].

2. Experimental

DLC films were produced on AISI 304 steel substrates by PIII&D using methane plasma. The films were prepared in a stainless-steel cylindrical vessel with a volume of 20 liters by driving Hollow Cathode (HC) discharges inside the tube attached to the top part of the chamber. The two tubes used were titanium alloy (Ti6Al4V), with 15 cm length and internal diameter of 11 mm and 40 mm, with one side closed configuration. Polished samples of AISI 304 steel were fixed along the inner tube wall for subsequent analysis of the DLC coatings. Prior to each deposition, the tubes were further cleaned in argon plasma for 10 min (2.5 kV, 12 A, 20 μs, 500 Hz). Methane plasma was generated by the application of pulses of 6.12 kV, 16 A, 20 μs, 500 Hz rate, during 120 minutes, reaching temperatures of 780 °C for 11 mm tube and 450 °C for 40 mm tube. Chemical structure of DLC films were analyzed by Raman Spectroscopy and the structural analysis were evaluated by optical microscopy and x-ray diffraction.

3. Results and Discussions

The experimental results show an interesting change on the chemical structure of the as-deposited carbon films, when the diameter of tube varied from 11 mm to 40 mm, resulting in thicker and quite adhered films on the inner surface of tubes. The typical Raman spectra of the DLC film presented two peak (D and G) characteristic of carbonaceous materials with crystalline and amorphous regions. The calculated ID/IG ratios suggest a homogeneous structure indicating the existence of monocrystalline graphite on the film. The results indicate that PIII&D is suitable for carbon deposition onto the inner surface of three-dimensional structures and has commercial potential. The results showed that the inner surface of tube was completely coated by carbon films as demonstrated by analyzing the monitoring substrates fixed along the tube.

4. References

- [1]- S. F. M. Mariano, M. Ueda, R. M. Oliveira, E. J. D. M. Pillaca, N. M. Santos, "Magnetic-field enhanced plasma immersion ion implantation and deposition (PIII&D) of diamond-like carbon films inside tubes". *Surface & Coatings Technology*. v. 312, p. 47-54, 2017.
- [2]- Y. Lifshitz, "Diamond-like carbon present status", *Diamond and Rel. Mat.*, v.8, p. 1659-1676, 1999.
- [3]- J. Robertson, *Diamond-like amorphous carbon*. *Materials Science and Engineering R* v. 37, p. 129-281 (Reports: A review journal), 2002.

GALLIUM NITRIDE THIN FILM DEPOSITION BY REACTIVE MAGNETRON SPUTTERING: THE INFLUENCE OF RF POWER

R. S. de Oliveira¹, H. A. Folli¹, I. M. Horta¹, C. Stegemann¹, M. Massi²,
A. S. da Silva Sobrinho¹, D. M. G. Leite¹

¹Plasmas and Processes Laboratory – LPP, Technological Institute of Aeronautics - ITA,
São José dos Campos, SP, Brazil.

²Mackenzie Presbyterian University, School of Engineering-PPGEMN, São Paulo, SP, Brazil.

*Corresponding Author: regianasantana.oliveira@gmail.com

1. Introduction

Gallium nitride (GaN) has become the target of cutting-edge technology applications in optoelectronic devices, with frequent progress and improvements in growth techniques [1,2]. Several parameters present in the film deposition process by magnetron sputtering may influence the result observed later in the films. From this perspective, this work aims to study the influence of radiofrequency (RF) power applied to the gallium target for the growth of GaN thin films. X-ray diffraction technique was used to study the effects of RF power on the structural and morphological properties of the obtained films.

2. Experimental

GaN thin films were grown onto c-Si (100) substrates by reactive magnetron sputtering, using a pure (99.999%) Ga target in Ar + N₂ plasma atmosphere. The substrates were kept at nominally 600°C and a total working pressure of 3 mTorr. The RF power applied to the Ga target was then varied from 30 to 90 W. The total deposition time was 120 min for all films. Thickness data were obtained using a KLA-Tencor P7 mechanical profilometer. The XRD experiments were performed in Theta/2Theta geometry using a PANalytical Empyrean diffractometer, with CuK α 1.5418Å radiation. Due to Bragg's law and the Scherrer's equation [3], the lattice parameters *a* and *c* and the crystallite average size were determined and discussed in terms of the influence of the RF power applied during the deposition.

3. Results and Discussions

As preliminary results, in Fig. 1 we have the full diffractograms of the films. All the films have wurtzite structure, with (0002) peak preponderance, which indicates preferred growth orientation with c-axis perpendicular to the substrate surface. It is worth noting that this (0002) peak preference tends to decrease with increasing RF-power. Fig. 2 shows, respectively, the thicknesses of the samples obtained by mechanical profilometry (left), and the average crystallite size obtained from the FWHM of the (0002) (right). As expected, the film thickness presents a direct linear dependence with deposition power, while the crystallite size shows a quasi-linear decrease from ~23 to ~12 nm with the increase of RF power. All these results are then discussed in terms of the kinetic energy of the precursors and the surface diffusion length regimes considering the RF power and the deposition rate in each condition.

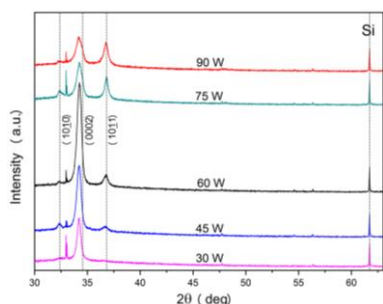


Fig. 1. XRD of GaN samples grown at different RF power.

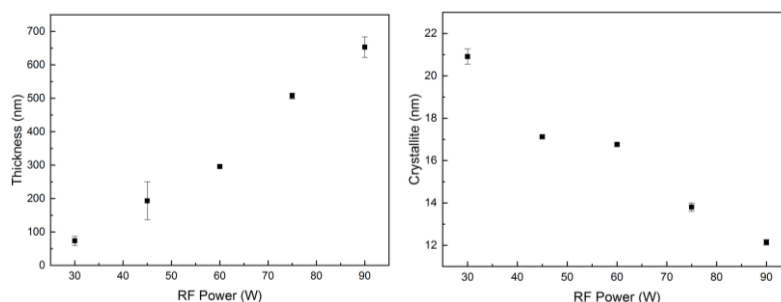


Fig. 2. Thickness (left) and average size of crystallites (right) of samples in relation to applied power.

4. References

- [1]- H. Jia, L. Guo, W. Wang, and H. Chen, *Adv. Mater.*, vol. 21, pp. 4641-4646, (2009).
- [2]- Y. Chen et. al., *Mater. Sci. Eng. R Reports*, vol. 138, pp. 60-84, (2019).
- [3]- B. D. Cullity, *Elements of x-ray diffraction*, Addison-Wesley Publishing Company, Inc. Philippines, (1978).

Acknowledgements

Fapesp (2015/06241-5, 2011/05772-0), CAPES (PG-FIS/ITA, 88881.122156/2016-01, 8887.157419/2017-00), CNPq (143273/2018-3), FINEP.

SODA-LIME GLASS: EFFECT OF MILLING TIME BY HIGH-ENERGY MILL

Juliana de Souza Oliveira Fonseca, Jônatas de Oliveira Sousa, Belmira Benedita de Lima-Kuhn,
Antonio Renato Bigansolli*

Departament of Chemical Engineering, Institute of Technology, UFRRJ, Seropédica, RJ.

**Corresponding Author: bigansolliarb@gmail.com*

1. Introduction

The glasses are noncrystalline silicates containing other oxides, a typical soda–lime glass consists of approximately 70 wt% SiO₂, the balance being mainly Na₂O (soda) and CaO (lime) [1]. Glass is one of the most popular storage and packaging products used today. It can be 100% recycled conserving both natural resources and landfill space [2]. One of the processes used in glass recycling is the milling, where the high-energy planetary mill can be used. In this equipment, milling time is directly related to the particle size distribution of the material, which is a fundamental for its application in several areas [3]. Therefore, the present work aims to study the effect of milling time on particle size distribution of the glass milled.

2. Experimental Procedure

Glass bottle commonly used for serving beer was washed to remove labels and then the glass bottle was fragmented to obtain particles between 1.7 and 2.2 mm. Then 50 g of the particles were grounded with high energy using a Retsch PM100 planetary ball mill. Grinding was performed at a speed of 400 rpm for 60 minutes with inversion for 5 minutes. Every 10 minutes, a sample was removed from the mill and characterized by a laser diffraction particle size analyzer (Mastersizer 2000. Malvern) for 6 times.

3. Results and Discussion

Fig. 1 presents the percentage share of particles of a given diameter in the course of the milling. The chart shows a decrease of particles size because of increasing milling time. Fig. 2 presents the particle size distribution after 60 minutes milling, an asymmetrical trimodal distribution is observed. The results from the characterization of samples have indicated this occurs due to the influence of the coefficient of friction of the average particles generated in the glass milling [4]. The sauter mean diameter of 1,960 μm was measured in sixth sample (milling by 60 minutes).

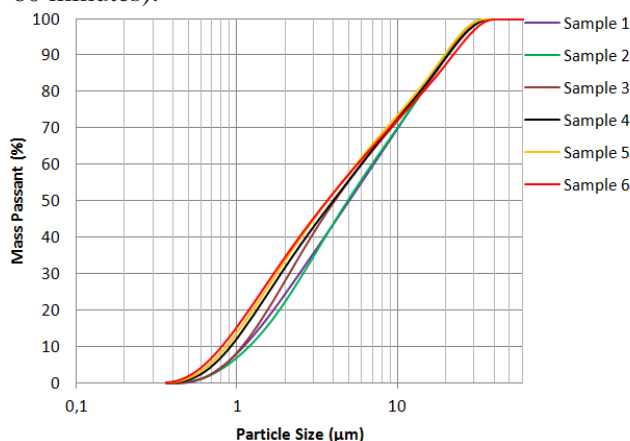


Fig. 1. Cumulative volume frequency of particles of a given diameter after different milling times.

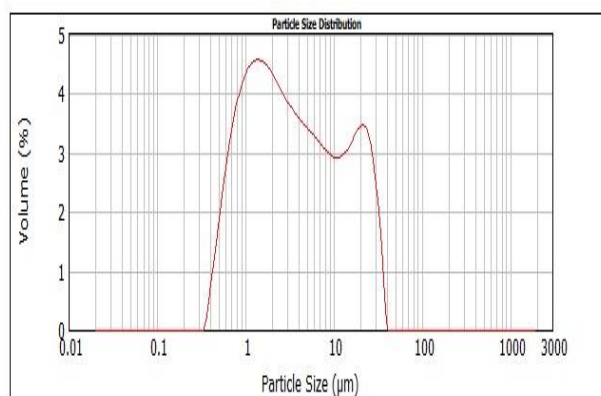


Fig. 2. Particle size distribution – milling by 60 minutes (sample 6)

4. References

- [1]- W. D. Callister, “*Fundamentals of Materials Science and engineering*”, **Sixth Edition**, 423, (2001).
- [2]- N. A. Padmalatha and S. Prabhish Shresta, BIMS International Journal of Social Science Research, ISSN 2455-4839.
- [3]- A. P. Spanholi “*Projeto de um moinho de alta energia*”, Trabalho de Conclusão de Curso, UTFPR, Pato Branco, BR, (2016).
- [4]- T. M. Mendes “*Influência do coeficiente de atrito entre os agregados e da viscosidade da matriz no comportamento reológico de suspensões concentradas heterogêneas*”, Dissertação, Escola Politécnica, USP, BR, (2008).

STUDY OF Ti-35Nb ALLOY OBTAINED BY POWDER METALLURGY USING HIGH PRESSURES

Hayka Cristina Vieira, Thailler Machado Nunes da Silva, Sergio Renato da Silva Soares,
Alexandra de Oliveira França Hayama*

Universidade Federal de Mato Grosso

*Corresponding Author: alexandra_hayama@ufmt.br

1. Introduction

Titanium alloys can be obtained by conventional melting or by powder metallurgy. The process of powder metallurgy can be divided into four main parts, being: obtaining the powders and their classification, mixing, compaction and sintering. After obtaining the powders and the classification, the mixing of the powders is done in proportions determined according to the chemical composition of the alloy. The compacting process is performed using presses and dies, and the compacting pressures vary with the different materials to be used, with the characteristics of the metallic powders and with the amount of the lubricant added to the powders mixture [1]. The last step is sintering which occurs at temperatures below the melting point of the base metal of the alloy [2]. In this context, the aim of this work is to evaluate the micro structural and mechanical behavior the Ti-35Nb alloy compacts produced under pressures of 1000, 1500 and 2000 MPa followed by sintering.

2. Experimental

Initially titanium and niobium elementary powders were classified by sieving using Tyler Series sieves mounted on a magnetic sieve shaker. After this classification, the powders were weighed on analytical balance following the chemical composition of Ti-35Nb (wt%) and then the powders were mixed in rotating cylinders for 48 h in order to allow homogenization of the alloy. After mixing, the uniaxial pressing of the powders was carried out under variable pressures, considering the pressures of 1000, 1500 and 2000 MPa, using a hydraulic press. Compacted samples were sintering under vacuum at temperature of 800°C for 30 and 60 min. Samples were characterized by optical light microscopy and Vickers Hardness measurements.

3. Results and Discussions

The principal results obtained shows that in the samples compacted at high pressure, the presence of porosity decrease as the compression pressure increases. High pressures favor the occurrence of mechanical twinning in the particles of the titanium powders and also their fracture, as well as changes in shape of the niobium particles, due to the plastic deformation of the powders occurred during the compacting. It was also verified that niobium powders have a tendency to connect by cold sintering at pressures from 2000 MPa (Fig. 1), these points being created during the cold compaction process. After sintering was verified that niobium and titanium grains were diffused separately (Fig. 2), with no noticeable diffusion between titanium and niobium, however, at the temperature and time studied there was no formation of Ti-35Nb alloy.

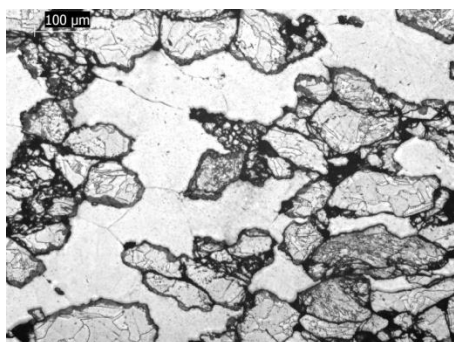


Fig. 1. Micrograph of Ti-35Nb alloy compacted uniaxially at 2000 MPa showing detail of cold sintering points of niobium powders.

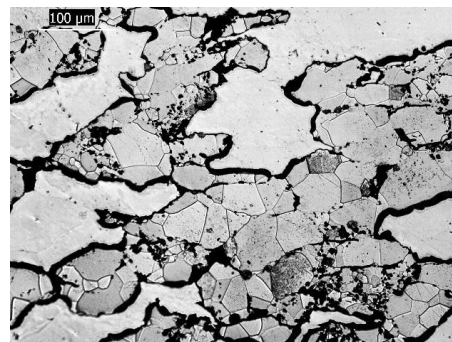


Fig. 2. Microstructure of Ti-35Nb alloy compacted at 2000 MPa and sintering at 800°C/60min.

4. References

- [1]-D. G. White, *History of Powder Metallurgy*. ASM Metals Handbook, Vol. 7 - Powder Metal Technologies and Application, 9th edition, 1998.
- [2]-V. Chiaverini, *Tecnologia Mecânica – Processos de fabricação e tratamento - Vol II*. McGraw-Hill, São Paulo, 2nd edition, 1986.

Acknowledgments

The authors are gratefully acknowledge the Instituto de Pesquisas Tecnológicas (IPT) for titanium powder and the Companhia Brasileira de Metalurgia e Mineração (CBMM) for niobium powder.

MICROSTRUCTURAL AND MECHANICAL EVALUATION OF THE Ti-35Nb ALLOY OBTAINED BY POWDER METALLURGY USING LOW PRESSURES

Thailler Machado Nunes da Silva, Hayka Cristina Vieira, Sergio Renato da Silva Soares,
Alexandra de Oliveira França Hayama*
Universidade Federal de Mato Grosso

*Corresponding Author: alexandra_hayama@ufmt.br

1. Introduction

Titanium β -type alloys are composed of non-toxic and biocompatible elements such as niobium and have properties suitable for use as a permanent implant in the human body such as corrosion resistance and biocompatibility. These materials can be obtained by inert atmosphere melting processes or by powder metallurgy processes, which is a viable alternative, because it allows the manufacture of parts with complex geometries and dimensions close to the final. In addition, the sintering temperatures used are low compared to other metallurgical processes and can be performed in simple design furnaces with lower energy consumption [1]. The powder metallurgy process can be divided into four main parts: obtaining the powders and their classification, mixing, compacting and sintering. The compaction process is performed using presses and dies, and the compaction pressures vary with the different materials to be used, the characteristics of the metal powders and the amount of lubricant added to the powder mixture [2]. Sintering occurs at temperatures below the melting point of the alloy base metal [1].

2. Experimental

Initially titanium and niobium elementary powders were classified by sieving using Tyler Series sieves mounted on a magnetic sieve shaker. After this classification, the powders were weighed on analytical balance following the chemical composition of Ti-35Nb (wt%) and then the powders were mixed in rotating cylinders for 48 h in order to allow homogenization of the alloy. After mixing, the uniaxial pressing of the powders was carried out under variable pressures, considering the pressures of 400, 600 and 800 MPa, using a hydraulic press. Compacted samples were sintering under vacuum at temperature of 800°C for 30 and 60 min. Samples were characterized by optical light microscopy and Vickers Hardness measurements.

3. Results and Discussions

The main results show that the titanium powders fractured during compaction and also presented deformation twins (Fig. 1). In the samples compacted at 800 MPa it was verified that the niobium powders showed more evident change, due to the plastic deformation caused by the higher compaction pressure. It was also found that niobium presented lower hardness than titanium, which explains its shape change during compaction, since it presents less hardness, thus being more ductile, corroborating the results presented. After sintering was verified that niobium and titanium grains were diffused separately (Fig. 2), with no noticeable diffusion between titanium and niobium, however, at the temperature and time studied there was no formation of Ti-35Nb alloy.

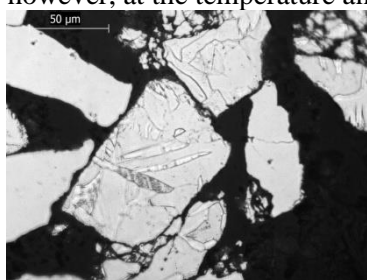


Fig. 1. Deformation twins in a sample of Ti-35Nb alloy compacted uniaxially at 400 MPa.

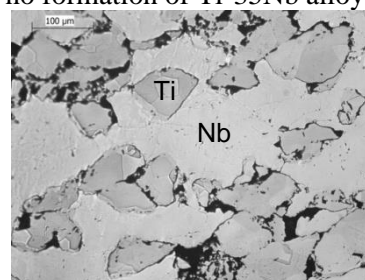


Fig. 2. Microstructure of Ti-35Nb alloy compacted at 800 MPa and sintering at 800°C/60min.

4. References

- [1]- V. Chiaverini, Tecnologia Mecânica – Processos de fabricação e tratamento - Vol II. McGraw-Hill, São Paulo, 2nd edition, 1986.
- [2]- D. G. White, History of Powder Metallurgy. ASM Metals Handbook, Vol. 7 - Powder Metal Technologies and Application, 9th edition, 1998.

Acknowledgments

The authors are gratefully acknowledge the Instituto de Pesquisas Tecnológicas (IPT) for titanium powder and the Companhia Brasileira de Metalurgia e Mineração (CBMM) for niobium powder.

ELECTRICAL AND STRUCTURAL PROPERTIES OF MPS COVERED BY PANI

AND DOPED WITH ERBIUM

Rosimara P. Toledo, Adhimar F. Oliveira and Danilo R. Huanca

¹*Institute of Physic and Chemistry from Federal University of Itajubá - Itajubá, MG, Brazil*

**Corresponding Author: rosimarap@yahoo.com.br*

1. Introduction

Porous silicon (PS) is a singular material due to its unique physical and chemical properties that make it suitable for different applications such as light emitting diodes [1]. In sensors field, it is desirable devices with high selectivity and sensitivity, but also, to insure the repeatability of these properties. This is the main reason by which it is necessary to passivate the porous structure to avoid its degradation by corrosion or phase formation. In this sense, different strategies have been employed to avoid the PS/analyte interaction [2]. The optimal performance of these sensors is also dependent on the functionalization features because it improves their selectivity and sensitivity [3]. Excellent material for this aim is PANI due to its highly stable chemical properties, even under ambient conditions [4]. In this work, we report the structural, electrical and optical characterization of the MPS/PANI:Er hetero-structure for photonic sensor applications.

2. Experimental

The samples are p-type crystalline Si (100) with $\rho \approx 10 \Omega \cdot \text{cm}$. For pore formation, silicon substrates were anodized in HF:DMF (1:9), applying 10 mA/cm^2 of current density for 20 min. After, PANI was deposited by cyclic voltammetry. It was made the optical characterization of them was made using the ATR-FTIR and Black Comet Spectro-radiometer for measuring the optical bandgap shift. The electrical characterization was made by Metrohm AUTOLAB potentiostat for measuring the impedance. This same equipment was employed for recording the current-potential curves. Finally, the structural analysis was made by means of a Scanning Electron Microscope (SEM).

3. Results and Discussions

Electrical properties of MPS/PANI:Er hetero-junctions were investigated. It was found that their electrical and optical properties become modified by the presence of Er, so that the OBG is shifted to high values in so far the Er concentration increases. The measurements show that PANI into MPS promotes the decrease of the forward current, because of the presence of oxide inside the structure. This I-V profile is changed after Er deposition so that the profile for the MPS/PANI:Er structure recovers its bare MPS like profile, in lowest cathodic current. According to impedance measurements, it could happen because of the modification of the electrical properties of the space charge region and the porous layer due to the presence of PANI:Er.

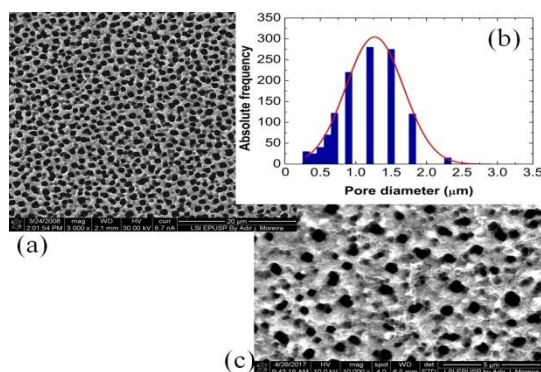


Fig. 1. Top-view SEM images of the (a) as-etched, and (b) histogram showing the pore diameter distribution. (c) PANI covered MPS.

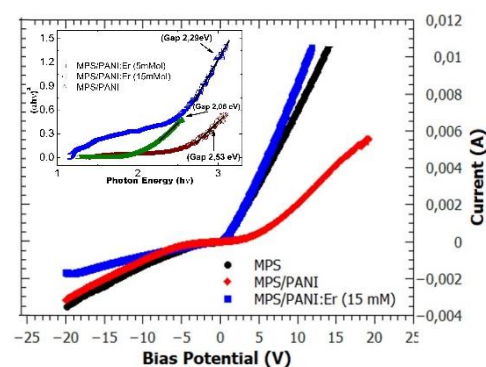


Fig. 2. (a) determination of the OBG, (b) IxV curves from MPS/PANI:Er

4. References

- [1] L. Pavesi, R. Chierchia, J. Appl. Phys., vol 86. pp. 6474-6476, 1999.
- [2] G. Mula, et. al, Thin. Sol. Film., vol. 556, pp. 8311-316, April 2014.
- [3] I. M. Antropov, et. al., Technical Physics Letters, vol. 37, pp. 213-215, March 2011.
- [4] I. Fratoddi, et. al, Sens. Act. B, vol. 220, pp. 534-548, 2015

Acknowledgments

The authors thank FAPEMIG (grant APQ-02492-16), CNPq (grant 425285/2016-2), and CAPES for scholarship financial support to R. P. Toledo.

STRUCTURAL CHARACTERIZATION AND GRANULOMETRIC ANALYSIS OF YELLOW CLAY AND AMBER GLASS

Felipe W. V. dos Santos, Lidiane A. Franco, Jônatas de O. Sousa,
 Belmira B. Lima-Kuhn, Antonio R. Bigansolli*
Departamento de Engenharia Química, Instituto de Tecnologia, UFRRJ, Seropédica,
**Corresponding Author: bigansolliarb@gmail.com*

1. Introduction

In Brazil, artisanal ceramics has an important economic and social role, however, a large part of clay deposits aren't adequately studied. Clays are classified as natural, earthy, fine-grained materials that, when moistened with water, exhibit plasticity [1]. Aiming to reduce the discarded waste in the environment the incorporation of waste glass in other materials seems a good method of reuse emphasizing the purpose of improving its properties [2]. Thus, we incorporate glass particles (from bottles commonly used in breweries) into clay. Therefore, this work aimed to obtain and characterize both clay and glass, using XRD laser diffraction and chemical analysis techniques.

2. Experimental

The material used to promote this work was the yellow clay extracted from the municipality of Seropédica (sample 2), processed in maromba in the pottery in Km42, from the municipality of Seropédica and the bottle Amber glass from breweries. The glass (Sample 2) was comminuted in the Restch model PM 100 high-energy mill for 8 minutes with a 4 minute inversion and 300 rpm rotation, thus being stored. The clay underwent a drying process, then was comminuted in a hammer mill, underwent a sieving process to obtain a uniform sample. The clay and glass samples were analyzed by chemical analysis techniques, XRD using a Rigaku Company model Miniflex II equipment and Laser Diffraction on a Malvern Mastersize 2000 equipment.

3. Results and discussion

The chemical analysis of clay presented in your composition Sodium, Potassium, Phosphorus, Zinc and little Cadmium with predominance of Potassium. In the glass analysis the same components were identified, but the predominance was Sodium. The results of the XRD analysis are shown in figures 1 and 2 featuring a crystalline phase for the clay sample showing peaks identified in the graph as M: Mica, Q: Quartz and K: Kaolinite and amorphous phase for the glass sample. Figures 3 and 4 represent the results of laser diffraction of the clay and glass samples respectively. In Fig. 3 the formation of an ascending bimodal distribution with a Sauter Diameter of 3,614 μm was observed while in Fig. 4 the distribution presented is a descending bimodal distribution with a Sauter Diameter of 19,884 μm .

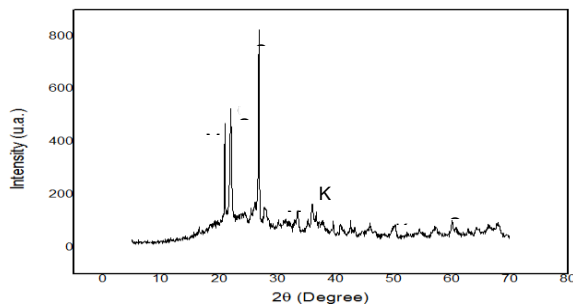


Fig. 1. Yellow clay Diffractogram

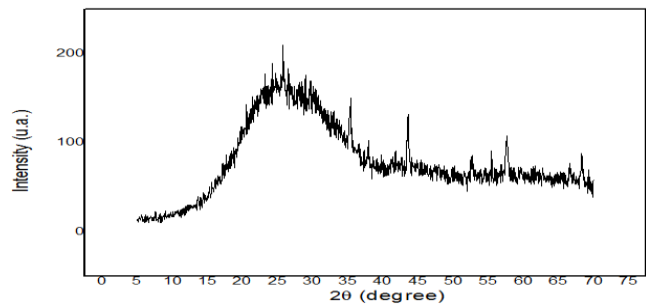


Fig. 2. Amber glass Diffractogram

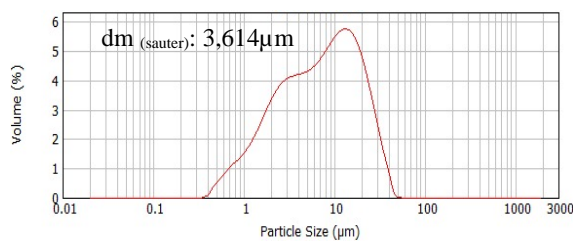


Fig. 3. Clay's Particle Size distribution

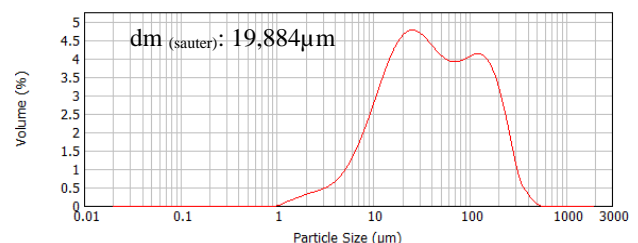


Fig. 4. Amber glass's particle size distribution

References

- [1] – ABCERAM – Associação Brasileira de Cerâmicas (www.abceram.org.br)
- [2] - M. C. Junior; J. F. M. Motta; A. S. Almeida and L. C. Tanno, CETEM. Rio de Janeiro. 2, 747-770. (2008).

WITH ADDITIONAL CATHODE.

Marco A Ramirez R^{1,2}, Funsho Kolawole^{2,3}, Luis Bernardo Varela², Vladimir Trava-Airoldi³,
Andre Paulo Tschiptchin²

¹ Instituto de Pesquisa e Desenvolvimento, Universidade do Vale do Paraíba UNIVAP, Sao Jose dos Campos. SP Brazil

² Departamento de Engenharia Metalúrgica e de Materiais, Universidade de São Paulo, Sao Paulo, Brazil

³ Department of Materials and Metallurgical Engineering, Federal University, Oye-Ekiti, Nigeria

⁴ INPE Laboratorio Associado de sensores e materiais. Sao Jose dos Campos. SP Brazil

1. Introduction

Diamond-like carbon (DLC) coatings has become very attractive for various industrial applications, such as cutting tools, automotive engines, biomedical implants, micro-electromechanical devices (MEMS). Due to their surface energies and ability to interact with lubricants to form surface protective films, good adhesion with substrate, increased wear resistance, improved electrical conductivity, decreased internal compressive stresses during deposition and thermal stability there are used in automobile components[1].

In the automobile industry, DLC coatings are usually applied on combustion engine components such as piston, tappet, camshaft, piston rings and gudgeon pin, valve stem and head and rocker arm. DLC coating helps in reducing friction and wear of the moving parts[2]. However, there are challenges facing the use of DLC coated components during service, which are; internal compressive stresses, low adhesion and low thermal stability leading to failures such as rolling contact fatigue, micro-pitting, delamination, oxidation and scuffing.

Hardness and internal compressive stress increase with increasing sp^3 content (sp^3/sp^2) ratio in DLCs. Internal compressive stress for DLC coatings in tribological applications is not good, due to the elastic strain energy that drives fractures along the coating/substrate interface, leading to delamination through blistering[3][4]. The addition of non-metals (Si, N, F or O) or metals (W, Cr, Ta, Ti, Mo or Cu) can improve thermal stability of DLC up to about 500 o C. Above, 500 o C transformation of sp^3 to sp^2 begins to occur leading to graphitization. The addition of metals increases the interfacial fracture toughness and moderates the internal stress by creating two (2) interface; substrate/adhesion layer interface and adhesion layer/functional coating interface

2. Experimental

This paper analyzes the morphological and structural characterization using SEM, and Raman spectroscopy to analyze atomic arrangement. The roughness analyze was made using optical profile. Tribological behaviour was analyzed by linearly reciprocating wear tests in high temperature around 500°C. Adhesion was tested according to the VDI3198 standard. The hardness was measured using nano-indentation.

3. Results and Discussions

This work will discuss the microstructure in their different deposition conditions, and the incorporation of different metallic nano-particles on the DLC films an their effect with high temperature exposure. The elevated coating hardness (higher than 25 GPa) promoted good wear resistance. These results suggest that the PECVD-DC Pulsed with additional cathode and methane as a precursor gas to grow DLC films on metallic substrates with incorporation of metallic nano-particles may represent a new alternative to improve the mechanical behavior in automotive applications.

4. References

- [1]- G. Capote, M. A. Ramírez, P. C. S. da Silva, D. C. Lugo, and V. J. Trava-Airoldi, "Improvement of the properties and the adherence of DLC coatings deposited using a modified pulsed-DC PECVD technique and an additional cathode," *Surf. Coatings Technol.*, 2016.
- [2]- A. Erdemir and C. Donnet, "Tribology of diamond-like carbon films: recent progress and future prospects," *J. Phys. D. Appl. Phys.*, vol. 39, no. 18, pp. R311–R327, 2006.
- [3]- M. A. Ramírez R, P. C. Silva, E. J. Corat, and V. J. Trava-Airoldi, "An evaluation of the tribological characteristics of DLC films grown on Inconel Alloy 718 using the Active Screen Plasma technique in a Pulsed-DC PECVD system," *Surf. Coatings Technol.*, 2015.
- [4]- P. C. S. da Silva, M. A. R. Ramos, E. J. Corat, and V. J. Trava-Airoldi, "DLC Films Grown On Steel Using An Innovator Active Screen System For PECVD Technique," *Mater. Res.*, 2016.

Acknowledgments

The authors would like to thank, São Paulo Research Foundation (FAPESP) for its financial support through grant # 2018/20721-8

EFFECT OF NITROCEMENTATION, DLC FILM AND DUPLEX TREATMENTS ON THE TRIBOLOGICAL PROPERTIES OF THE Ti6Al4V ALLOY

Larissa S. de Almeida^{1*}, Lucas A. P. de Campos¹, Marcos D. Manfrinato^{1,2}, Luciana S. Rossino^{1,2}

¹Universidade Federal de São Carlos – UFSCAR Campus Sorocaba, Sorocaba/SP, Brazil²Faculdade de Tecnologia José Crespo Gonzales – Fatec Sorocaba, Sorocaba/SP, Brazil

*Corresponding Author: solano.larissa@gmail.com

1. Introduction

The titanium and its alloys have increasingly been used for industrial, aeronautical and medical areas, due its properties of low density, high corrosion resistance and biocompatibility [1]. However, its low surface hardness and low wear resistance are limitation its used. The surface treatments are employed as alternatives to prolong the material life such as carbon and nitrogen diffusion hardening and deposition of DLC films [2]. The aim of this work is to compare wear resistance of the nitrocementation, DLC films and Duplex (nitrocementation + DLC) treatments in the Ti6Al4V alloy.

2. Experimental

The cleaning of the surface samples was carried out with the pressure of 2.0 torr and gases proportion of 80% Ar -20% H₂. The plasma ionic nitrocementation was carried out with the pressure of 5.86 torr and the gas proportion of 80% N₂ - 17% H₂ - 3% CH₄, at fixed time of 5 hours, and the temperature of ± 525° C. For the deposition of the DLC film, a SiC_x:H interface was deposited with the HMDSO as precursor, and then the DLC film was deposited by PECVD with CH₄ and Ar flow at 27 and 3 sccm respectively and power of 120W by 2 h. The analyses of metal surface after the treatments were obtained by the techniques of microabrasive wear test, hardness, metallography analysis and Energy Dispersive Spectroscopy (EDS) by Scanning Electron Microscopy (SEM).

3. Results and Discussions

In Fig 1 (a) is observed the light-colored compound layer formed in the nitrocemented treatment with approximately 1.3 μm of thickness. In fig. 1 (b) is observed a dark and light layer of approximately 1.7 μm thickness formed in duplex treatment. The fig. 2 show the influence of surface treatments on the wear resistance of Ti6AL4V, showing less wear volume to all treated samples compared to the untreated sample, significantly increasing the wear resistance, due to the increase in surface hardness, where the substrate, nitrocemented and duplex presented 255 HV, 396 HV and 2284 HV, respectively. Comparing the surface treatments, the DLC film was the most resistant to wear due to its high hardness and very low coefficient of friction. The Duplex treatment has been shown to improve wear resistance and its hardness has increased by 82% more over nitrocement only. The results are shown while the surface treatment was relevant to Ti6Al4V.

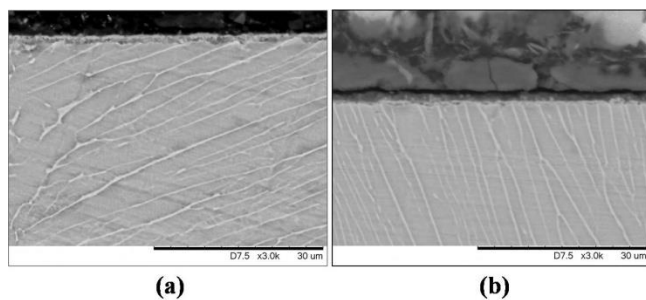


Fig. 1. Metallography of the sample (a) Nitrocemented (b) Duplex.

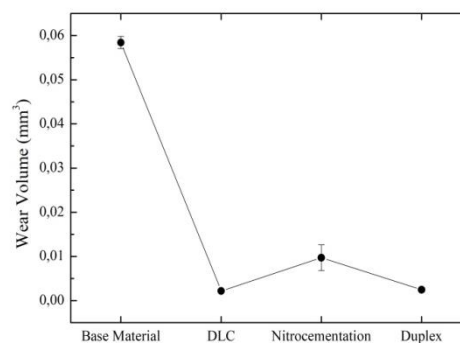


Fig. 2. Wear volume for untreated and treated samples.

4. References

- [1]- A. Samanta, M. Bhattacharya, I. Ratha, H. Chakraborty, S. Datta, J. Ghosh, A. K. Mukhopadhyay. Nano- and micro-tribological behaviours of plasma nitrided Ti6Al4V alloys. *Journal of the Mechanical Behavior of Biomedical Materials*, 77, 267–294 (2018). doi:10.1016/j.jmbbm.2017.09.013
- [2]- J. R. Sobiecki, T. Wierzchoń, Structure and properties of plasma carbonitrided Ti–6Al–2Cr–2Mo alloy. *Surface and Coatings Technology*, 4363–4367 (2006). doi:10.1016/j.surfcoat.2005.02.162

Acknowledgments

We would like to thank the Fatec Sorocaba and the LabTES for the infrastructure.

EVALUATION OF HYDROGEN EVOLUTION REACTIONS ON CARBON NANOTUBE FILMS TREATED BY O₂ OR N₂ PULSED-DC PLASMA

E. F. Antunes*, C. A. Escanio, C. A. O. Nunes, V. J. Trava Airoidi, E. J. Corat

1. Introduction

Low activity of hydrogen evolution reaction (HER) on carbon electrodes is a requirement to increase the lifetime of lead-carbon batteries. Although previous investigation has already pointed out [1] that we can make electrodes with an excellent interaction with aqueous electrolytes, just oxidizing their surface, the N-doping could provide, besides a high wettability, a lower HER activity [2-3]. Therefore, we present here a study about the incorporation of oxygen and nitrogen on carbon nanotubes (CNT) films by a DC-pulsed plasma system designed and built in our lab.

2. Experimental

To prepare the (CNT) films, we dropped 18 μ L of an ethanolic catalyst solution (based on iron nitrate and cobalt chloride) on pieces of 20mm diameter of graphite sheet. CNT growth followed by inserting the dried pieces into a 2" tubular furnace at 650°C. First, we purged the furnace with argon (200sccm/20min), and then inserted acetylene (30sccm) and the ethanol vapor (0.4 mL.L⁻¹/ 140°C) for 20 min. After growth, we treated the samples in a Pulsed-DC plasma reactor. The plasma discharges were performed with Ar/O₂ or Ar/N₂ (10sccm/40sccm), at 100mTorr, 700V, 2 min to attach O (or N) functional groups to the CNT surfaces. Subsequently, linear sweep voltammetry was performed on the samples in a potential ranging from -0.6 to 0, at 100 mV/s, to evaluate the hydrogen evolution potential with a 0.5 M H₂SO₄ electrolyte. By images of scanning electron microscopy (SEM/FEG-Tescan Mira3) and X-ray photo-electron spectroscopy (XPS-Thermo Scientific, Al-K-alpha – 1486.6 eV), we analyzed the changes incorporated to the CNT surface after each treatment.

3. Results and Discussions

We obtained dense and entangled CNTs films with diameter ranging from 20 to 30nm, and the plasma treatment did not provoke an observable erosion on them, as shown by SEM images (Fig.1a). The effectiveness of plasma treatment is evidenced by XPS measurements (Fig.1b) by the presence of the O1s and N1s peaks. To establish the HER activity trend of each sample, we calculate the Tafel plot from the voltammetry (Fig.2). The CNT films showed good stability in acidic electrolyte and the functional groups attached to their surface affected the interaction with H ions. Samples treated by N₂ plasma showed the highest overpotential in Tafel plot which indicates that our DC-pulsed plasma is efficient in producing Pyrrolic-N doping [3]

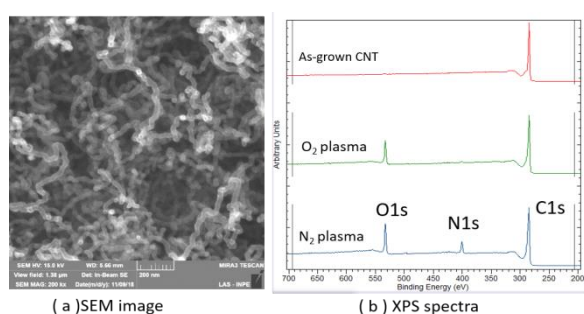


Fig.1: (a) Typical morphology of CNT films (image scale: 200nm), and (b) XPS spectra of as-grown CNTs, and after plasma treatments with O₂ and N₂

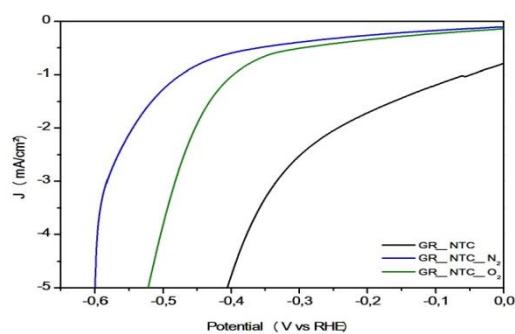


Fig. 2. Evaluation of HER activity by linear sweep voltammetry, for as-grown CNT, and treated samples.

4. References

- [1] A. O Lobo, et. Al *Materials Letters* 70 (2012) 89-93
- [2] R. Yadav et al. *Journal of Science: Advanced Materials and Devices* 2 (2017)141-149
- [3] Z. Jiang et al, *Journal of Materials Science: Materials in Electronics* 29 (2018) 10.1007/s10854-018-9550-x

Acknowledgments

This work was supported by FAPESP (Thematic Project: 2012/15857-1) and CNPq (PCI-DA 300273/2019-3). Special thanks to the UFABC Multiuser Center for the XPS measurements, and to the INPE Electrochemistry Lab, for sharing their potentiostat.

MECHANISM OF ACTION OF LOW TEMPERATURE ATMOSPHERIC PLASMA JET ON *Candida albicans*

Rovetta, S. M.^{1*}, Borges, A. C.¹, Nishime, T.C.², Kostov, K.G.², Koga-Ito, C. Y.¹

¹ Institute of Science and Technology, Sao Paulo State University/UNESP, São José dos Campos, Brazil.

1. Introduction

The increasing occurrence of antifungal resistance and high toxicity of conventional drugs are the main challenges in the treatment of infections caused by *Candida albicans*. Low temperature plasma is considered a promising agent against *C. albicans* [1]. However, its mechanism of action has not been elucidated so far. The objective of this study is to analyze the biochemical changes caused by plasma on fungal cells.

2. Experimental

An aliquot of 60 μl of *C. albicans* (SC5314 or clinical isolate) inoculum containing 10^8 cells/ml was transferred to sterile glass slides. The suspensions were treated with low temperature atmospheric pressure plasma jet using the following parameters: distance between the plasma source and sample 15 mm, voltage of 12 kV, 31 kHz frequency, jet power $\approx 0,6\text{W}$ and helium flow of 2 L/min. Samples were treated for 120 seconds. Biochemical evaluation of fungal cells was performed at ATR-FTIR by using Frontier Perkin Elmer 400. The spectra were recorded between 800 a 4000 cm^{-1} by OPUS software in 4 cm^{-1} resolution. A total of 32 scans per point was taken and 5 samples per group were evaluated. The spectra were baseline corrected and vector normalized. Second derivatives and fitting-curve were performed. The band areas were analyzed by ANOVA and post hoc Tukey's test. The level of significance was set in 5%.

3. Results and Discussion

Figure 1 shows the differences in the polysaccharides region at 980 and 1200 cm^{-1} . A decrease of 25.6% was observed after plasma treatment for reference strain and 30.5% for clinical isolate when compared to non-exposed controls. The spectra of second derivative of the bands centered at 1045 cm^{-1} (Figure 1) revealed that bands of β -glucans (1001 and 1022 cm^{-1}) had decreased intensities. Inversely, bands of mannans (978 and 1045 cm^{-1}) were increased [2] [3]. The protein region (1400 to 1700 cm^{-1}) had two peaks with increased intensities after treatment. The band at 1403 cm^{-1} increased in 28.1% for SC5314. The peak at 1543 cm^{-1} was 23% increased for reference strain and 3% for clinical isolate when compared to controls. The second derivative spectra of those bands showed that chitin was increased. Alterations in polysaccharides and protein bands after plasma treatment suggest that plasma acts on synthesis of β -glucans of *C. albicans* cell wall. The increase of chitin might be a cell protection mechanism in response to decrease of β -glucans.

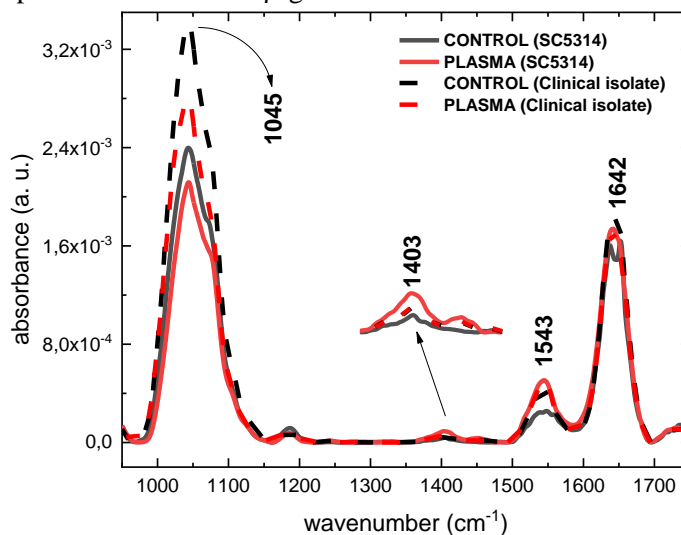


Fig. 1. ATR-FTIR spectra of *C. albicans* after plasma treatment

4. References

- [1]- A. C. Borges, et al., Clin Plasma Med., 7-8, 9-15, 2017.
- [2]- I. Adt, D. Toubas, J. M. Pinon, M. Manfait, G. Sockalingum, Arch Microbiol., 185, 277-285, 2006.
- [3]- F. Quilès, I. Accoceberry, C. Couzigou, G. Francius, T. Noël, S. El-Kirat-Chatel, Nanoscale, 9(36), 13731-13738, 2017.

PLASMA SIMULATION OF ARGON DISCHARGES AT DIFFERENT REDUCED ELECTRIC FIELDS

Gabriel Amâncio Hoerning* and Julio César Sagás

Laboratory of Plasmas, Films and Surfaces, Universidade do Estado de Santa Catarina. Joinville, Brazil

*Corresponding Author: gabriel.hoerning@gmail.com

1. Introduction

To understand plasma kinetics, it is necessary not only extensive experiments, but also numerical modelling to assess parameters that are hard to measure. Among the different approaches to simulate plasmas, hybrid models are highlighted due to the compromise between precision and computational cost [1]. In this work, argon plasmas generated by a stationary electric field in low pressure were studied to evaluate the role of different reactions to plasma density.

2. Methodology

To analyze the plasma chemistry, it was used the ZDPlasKin software [2] that incorporates the Bolsig+ solver [1] to obtain the electron energy distribution function (EEDF) at each condition. Using reactions and rate constants according to [3] and cross-sections according to [4], the discharge kinetics was simulated. By simulating discharges in pressures of 0.40 Pa, 1.3 Pa, 4.0 Pa e 6.7 Pa in a range of reduced electric field (ratio of electric field by gas density) from 10 Td to 100 Td, it was possible to verify how the species densities vary with these parameters. With QTPlasKin software, it was possible to analyze the relevance of each reaction to the plasma steady state.

3. Results and Discussions

Fig. 1 compiles the results and show that the plasma density increases with gas pressure due to a higher collision frequency. Among the reactions that contribute to plasma density grown up, ionization of different excited states affects less than 0.01% the steady state density (Fig. 2). For more complex systems this information is essential. Knowing the important reactions, it is possible to decrease the computational time required to do the calculations, but keeping accurate results.

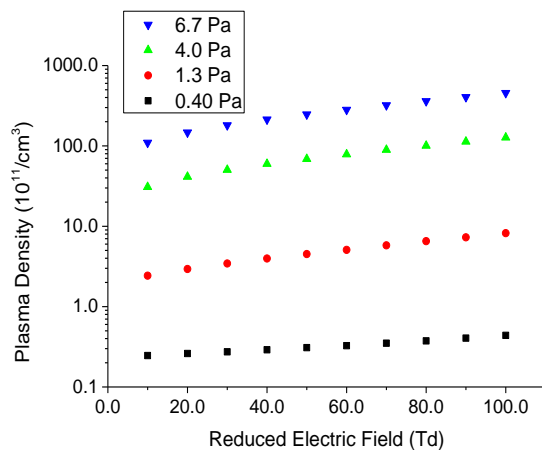


Fig. 1. Plasma density as a function of reduced electric field function at different pressures.

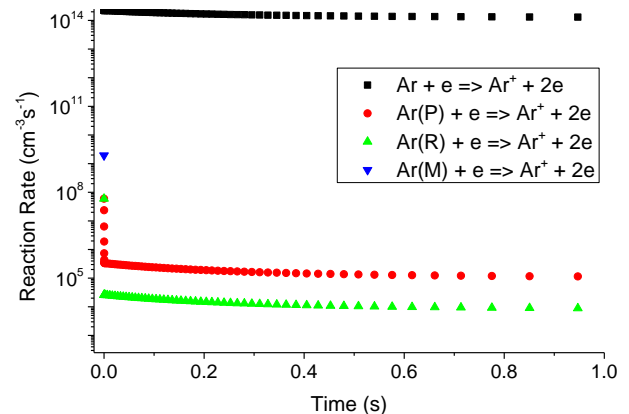


Fig. 2. Production of electrons by time. Ar(P) refers to the excited states 4p between 12.9 eV and 13.5 eV. Ar(R) refers to the resonance levels of 4s excited states of 11.5 eV and 11.7 eV. Ar(M) refers to the metastable levels of 4s excited states of 11.6 eV and 11.8 eV.

4. References

- [1]- G J M Hagelaar and L C Pitchford 2005 *Plasma Sources Sci. Technol.* **14** 722
- [2]- S. Pancheshnyi, B. Heisman, G.J.M. Hagelaar, L.C. Pitchford, Computer code ZDPlasKin (University of Toulouse, LAPLACE, CNRS-UPS-INP, Toulouse, France, 2008).
- [3]- M. H. Lee, S. H. Jang, and C. W. Chung, *Phys. Plasmas* **13**, 053502
- [4]- Hayashi database, www.lxcat.net, retrieved on July 3, 2019.

Acknowledgments

This project has been funded by the FAPESC through the program PAP in association with UDESC under contract PAP-TR 655. Gabriel Amâncio Hoerning thanks UDESC by the financial support through PROBIC grant.

AN STUDY OF THE MICROSTRUCTURE OF ADVANCED HIGH STRENGHT STEELS WELDS IN HIGH TEMPERATURE

Raquel Alvim de F Mansur^{1*}, Vagner Braga¹, Vinicius M. Mansur¹, Daolun Chen², Milton Sergio F de Lima¹

¹Instituto de Estudos Avançados – São Jose dos Campos-SP-Brazil

²Ryerson University- Toronto-Ontario-Canada

1. Introduction

The advancement of materials science and technology for developing materials that can be employed in the automotive and aerospace sectors, with high safety for the passengers, has obliged researchers to develop processing techniques that improve their properties. Currently, several research groups have studied the modifications of the properties through laser welding at high temperatures (Lima et al 2017). AHSS steels can be laser welded, but the rapid cooling can change the microstructure and the properties of the material and weaken it due to the formation of martensite. To overcome this issue, Lima et al (2017) studied laser welding using an induction furnace with temperatures within the bainitic region. The current paper proposes an in-situ austempering treatment subsequent to the laser welding of TRIP 750 steels by using an inductive furnace in the laser workstation. The aim is to produce bainite instead of martensite in the FZ grains. For comparison purposes, a standard procedure of annealing after the weld is also presented.

2. Experimental

The welds were realized in a fiber laser workstation doted of an IPG YLR-2000 laser, with maximum power 2000 W, minimum spot of 0.1 mm and almost Gaussian intensity profile. The moving in three-axis were coordinated by a CNC table. On the CNC table an induction furnace was constructed that heats the sample at a given predefined temperature (HT). Samples were heated to 487°C and kept 10 minutes at this temperature. For comparison purposes, room temperature (RT) samples were laser welded as well.

3. Results and Discussions

As presented in Figure 1a, RT samples are composed by martensite needles and some untransformed ferrite (rounded particles), as a result of fast cooling. The micro texture of the samples was also measured by means of the EBSD technique which allows identification of the texture changes associated with their distribution among the different microstructural constituents. Fig. 1(b) show an orientation map of the fusion zone weld cross-section at HT obtained via Oxford Aztec HKL software without performing any grain smoothing, along with its colour legend.

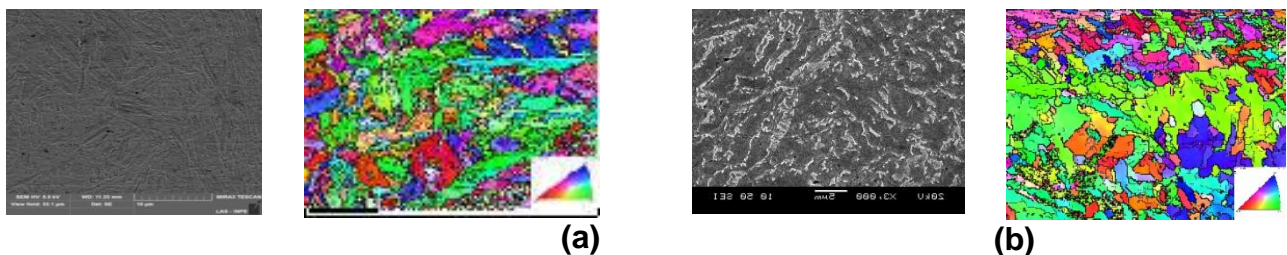


Figure 1 – (a) RT samples and (b) HT samples fusion zone optical and EBSD maps images.

4. References

- [1]-Correard GCC, Miranda GP, Lima MSF. Development of laser beam welding of advanced high-strength steels. International
- [2]-Lima MSF, Gonzales D, Liu S. Microstructure and mechanical behavior of induction-assisted laser welded AHS steels. *Welding Journal*. 2017;96(10):376-S

Acknowledgments

CAPES, IEAv, Ryerson University, Canada Government

